An Improved Stochastic Generation Approach for Assessing the Vulnerability of Water Resource Systems under Changing Streamflow Conditions

Masoud Zaerpour

A Thesis
in
the Department
of
Building, Civil & Environmental Engineering

Presented in Partial Fulfilment of the Requirements
For the Degree of
Doctor of Philosophy (Building Engineering) at
Concordia University
Montreal, Québec, Canada

November 2021

CONCORDIA UNIVERSITY
SCHOOL OF GRADUATE STUDIES

This is to certify that the thesis prepared

By: Masoud Zaerpour

Entitled: An Improved Stochastic Generation Approach for Assessing the Vulnerability of Water Resource Systems under Changing Streamflow Conditions and submitted in partial fulfillment of the requirements for the degree of

Doctor of Philosophy

complies with the regulations of the University and meets the accepted standards with respect to originality and quality.

Signed by the final examining committee:

_____ Chair
Dr. Tiberiu Popa

_____ External Examiner
Dr. Ahmad Shakibaeinia

_____ External to Program
Dr. Ali Akgunduz

_____ Examiner
Dr. Fariborz Haghighat

_____ Examiner
Dr. Luis Amador Jimenez

_____ Thesis Supervisor
Dr. Ali Nazemi

Approved by   _____
                   Dr. Mazdak Nik-Bakht, Graduate Program Director

November 25, 2021 _____
                   Dr. Mourad Debbabi, Dean,
                   Gina Cody School of Engineering and Computer Science

Abstract

An Improved Stochastic Generation Approach for Assessing the Vulnerability of Water Resource Systems under Changing Streamflow Conditions

Masoud Zaerpour, PhD
Concordia University, 2021

Water-related disasters such as floods and droughts highlight the urgent need for securing water resource systems for human and ecosystem utilizations. Increasing anthropogenic interventions along with climate variability and change have exacerbated the intensity and frequency of such water-related events, which will continue to increase in the future. Such pressures introduce substantial and unprecedented vulnerability to water resource management. Understanding the extent of potential vulnerabilities, however, is not trivial due to the uncertainty in current top-down impact assessments. To address current limitations, bottom-up frameworks have been proposed in the past decade to provide alternatives to top-down and scenario-led vulnerability assessments. The core idea behind bottom-up schemes is to analyze the potential impacts directly as a function of potential changes in streamflow conditions through a systematic stress testing scheme. To make such stress tests reliable, systematic methodologies are needed to synthesize streamflow, and other hydroclimatic variables, beyond the historical observations. Despite ongoing advances in stochastic streamflow generations under stationary conditions – with which the vulnerability assessment can be performed – little attention has been given to advancing the perturbation algorithms for altering the streamflow characteristics under nonstationary conditions; and in fact, only a few incorporate climate-related proxies into streamflow generation. This thesis aims to shed light on some limitations of bottom-up approaches and propose an improved stochastic streamflow generation framework for impact assessment in water resources systems under changing streamflow conditions. This takes place through: (1) Identifying uncertainties in current stochastic streamflow generation approaches as well as how and why these uncertainties matter to bottom-up impact assessment; (2) providing a guideline on the choice of the optimal scheme(s) for stochastic generation of streamflow series in various temporal and spatial scales; (3) proposing a methodology to incorporate the effect of large scale climate indices in stochastic streamflow generation; (4) identifying the types of changes in the streamflow regime through a systematic and globally-relevant approach; as well as (5) proposing a generic algorithm to shift a wide range of streamflow characteristics in streamflow time series, and to make a transient and non-stationary flow generation. This research results in an improved stochastic streamflow generation scheme capable of generating scenarios of change under nonstationary conditions. The skill of the proposed algorithm is assessed over multiple natural streams, showing good performance in representing the plausible changes required for the vulnerability assessment of water resource systems.

"Anyone who keeps learning stays young"

Henry Ford

Dedication

To my colleague, friend, and wife, Shadi

Statement of Contribution

Published and Submitted Journal Papers:

1. Nazemi, A., Zaerpour, M., & Hassanzadeh, E. (2020). Uncertainty in Bottom-Up Vulnerability Assessments of Water Supply Systems due to Regional Streamflow Generation under Changing Conditions. *Journal of Water Resources Planning and Management*, *146*(2), 04019071, https://doi.org/10.1061/(ASCE)WR.1943-5452.0001149.

2. Zaerpour, M., Hatami, S., Sadri, J., & Nazemi, A. (2021). A global algorithm for identifying changing streamflow regimes: Application to Canadian natural streams (1966-2010). *Hydrol. Earth Syst. Sci.*, 25, 5193–5217, https://doi.org/10.5194/hess-25-5193-2021.

3. Zaerpour, M., Papalexiou, SM., Nazemi, A. (2021). Informing Stochastic Streamflow Generation by Large-Scale Climate Indices at Single and Multiple Sites. *Advances in Water Resources*, https://doi.org/10.1016/j.advwatres.2021.104037.

4. Zaerpour, M., Nazemi, A. (2021). On Parametric Representations of Spatiotemporal Dependencies in Stochastic Streamflow Generation across Catchments, Timescales, and Flow Regimes. *Journal of Hydrology*. (Submitted on September 28th, 2021).

Working Papers:

1. Zaerpour, M., Nazemi, A. (2021). A generalized approach for synthetic streamflow generation under changing conditions. *Water Resources Research*. (In preparation).

Conference Papers and Presentations:

1. Zaerpour, M., Hatami S., Nazemi, A., (2019). A Fuzzy clustering approach to diagnosis of change in natural streamflow regime. *CSCE 2019 Conference Proceedings,* Montréal, Canada.
https://www.csce.ca/elf/apps/CONFERENCEVIEWER/conferences/2019/pdfs/PaperPDFversion_10_0513042005.pdf

Conference Presentations:

1. Masoud Zaerpour, Simon Papalexiou and Ali Nazemi. Advancing Stochastic Streamflow Prediction and Projection at Single and Multiple Sites by using Large Scale Climate Indices, *AGU Fall Meeting*, December 2020, Virtual.

2. Masoud Zaerpour and Ali Nazemi. Benchmarking Various Representations of Spatiotemporal Dependencies in Streamflow Series Using Copulas, *27th IUGG General Assembly*, July 2019, Montreal.

3. Masoud Zaerpour, Shadi Hatami, Javad Sadri, Ali Nazemi. A Fuzzy clustering approach to diagnosis of change in natural streamflow regime", *CSCE*, 2019.

4. Masoud Zaerpour, Shadi Hatami, Javad Sadri, Ali Nazemi. Diagnosing alteration in natural streamflow regime: A new look at an old problem, *CGU*, June 2018, Niagara Fall.

5. Masoud Zaerpour, Ali Nazemi. A fully spatiotemporal stochastic reconstruction framework for analysis of water resource system vulnerability to potential changes in streamflow regime, *CWRA*, June 2017, Lethbridge.

Contribution of the authors

This thesis is written in a manuscript-based format, in which Chapters 2 to 6 have been presented as standalone journal manuscripts. All these chapters are already published or in peer-review with the exception of Chapter 6, which is in the final stages of internal review.

Chapter 2 has been already published in the *ASCE's Journal of Water Resources Planning and Management*. I co-conceptualized the study and co-developed the methodology with my supervisor. I developed the computer codes, performed the analysis related to the proposed methodology, investigated and visualized the data, and drafted the first version of the manuscript with the help of my supervisor. My supervisor and Dr. Elmira Hassanzadeh did the vulnerability assessment. Dr. Nazemi wrote the revised version of the manuscript after it had been rejected in *Water Resources Research*.

Chapter 3 is currently under review for the *Journal of Hydrology* (extension for revisions is requested till the end of December 2021). I co-conceptualized the study and co-developed the methodology with my supervisor. I developed the computer codes, performed the analysis related to the proposed methodology, investigated and visualized the data, and wrote the first draft with the help of my supervisor. My supervisor and I then reviewed and edited the paper. I led the technical work during revisions.

Chapter 4 has been already published in *Advances in Water Resources*, I co-conceptualized the study and co-developed the methodology with my supervisor and Dr. Simon Papalexiou. I developed the computer codes, performed the analysis related to the proposed methodology, investigated and visualized the data, and wrote the first draft. My supervisor, Dr. Papalexiou and I then reviewed and edited the paper. I led the technical work during revisions.

Chapter 5 has been already published in *Hydrology and Earth System Sciences*, I co-conceptualized the study and co-developed the methodology with my supervisor and Shadi Hatami. I developed the computer codes, performed the analysis related to the proposed methodology, investigated and visualized the data, and wrote the first draft with the help of my supervisor with some inputs from Dr. Javad Sadri. My supervisor and I then reviewed and edited the paper with some inputs from Dr. Javad Sadri. I led the technical work during revisions.

Chapter 6 is aimed to be submitted in *Water Resources Research*. I co-conceptualized the study and co-developed the methodology with my supervisor. I developed the computer codes, performed the analysis related to the proposed methodology, investigated and visualized the data, and wrote the first draft with the help of my supervisor. My supervisor is currently reviewing the paper.

Acknowledgments

This thesis would not have been possible without the guidance and the support of my supervisor, Dr. Ali Nazemi. Thank you for your help, professional guidance, and support throughout my Ph.D. You were a great source of inspiration to me.

I am also grateful to all those with whom I have had the pleasure to work during this and other related projects. I especially would like to thank Dr. Elmira Hassanzadeh and Dr. Simon Papalexiou. I would also like to thank my committee members, Dr. Fariborz Haghighat, Dr. Luis Amador, Dr. Ali Dolatabadi, Dr. Ali Akgunduz, and Dr. Ahmad Shakibaeinia. Thank you to be part of my defense committee and for your valuable feedbacks.

I would like to show my gratitude to the staff at the BCEE Department of Concordia University, especially Jenny Drapeau and Tiberiu Cristian Aldea who have always been helpful during my Ph.D. program.

Nobody has been more important to me in the pursuit of this work than the members of my family. I would like to thank my parents, Safoura and Ahmad. Your love and guidance are with me now and forever. Thank you for everything. I am exceedingly grateful to my brothers Nima and Farzad. Thank you for always being there for me. Most importantly, I wish to thank my loving and supportive wife, Shadi. Thank you for your support, patience, encouragement, love, and thanks for being beside me during this journey.

Table of Contents

List of Figures

List of Tables

List of Abbreviations, Nomenclature, Greek and Math Symbols, and Subscripts

Frame I. Abbreviations

AMO	Atlantic Multidecadal Oscillation
ANOVA	ANalysis Of VAriance
AR	Auto Regressive
ARFIMA	Autoregressive Fractionally Integrated Moving Average
ARMA	Auto Regressive Moving Average
EAC	Exchangeable Archimedean Copula
ENSO	El Niño Southern Oscillation
FCM	Fuzzy C-Means algorithm
GCM	Global Climate Model
GCM	Global Climate Model
GEV	Generalized Extreme Value
HM	Hydrological Models
IHA	Indicators of Hydrologic Alterations
IPCC	International Panel of Climate Change
LSCI	Large Scale Climate Index
NAC	Nested Archimedean Copula
NAO	North Atlantic Oscillation
NQT	Normal Quantile Transformation
NSR	North Saskatchewan River
PCIS	Partial Correlation Input Selection
PDO	Pacific Decadal Oscillation
PMI	Partial Mutual Information
PNB	Provincial Net Benefit
RDM	Robust Decision Making
RHBN	Reference Hydrometric Basin Network
Sask-SRB	South Saskatchewan River Basin
SSR	South Saskatchewan River
SWC	Surface Water Coverage

Frame II. Nomenclature

$C(.)$	Copula function
BIC	Bayesian Information Criterion
$c(.)$	Copula density
CI	Confidence Interval
CRPS	Continuous Ranked Probability Score
$E(.)$	Long-term expected value over any ttime-episode
ES	Error Score
$F(.)$	Marginal CDFs of random variables
$f(.)$	Marginal PDFs of random variables
$H(.)$	Joint dependencies structure

Frame II. Continued.

KGE	Kling-Gupta Efficiency
MAE	Mean Absolute Error
NSF	Normalized Streamflow Features
PIT	Probability Integral Transform
POC	Percentage of Coverage
R^2	Coefficient of determination
RE	Relative Error
RMSE	Root Mean Squared Error
RMSEP	Root Mean Squared error in Probability
TDF	Cumulative Time Distribution

Frame III. Greek and Math Symbols

θ	Copula model parameters
τ	Kendall's tau dependence coefficient
Δ	Desired shift
∂	Partial derivative

Frame IV. Subscripts

AMJ	spring
JAS	summer
JFM	winter
max	maximum
mean	average
min	minimum
obs.	observed
OND	fall
pred.	prediction
proj.	projection
ref	reference
sim.	simulated
year	Annual scale

Chapter 1.
Introduction
 1.1. Water security threats to human society

Freshwater is one of the most vital natural resources on the Planet Earth, which accounts for only 2% of the total stored water molecules globally (Gleick et al., 1993; Eakins et al., 2010). Freshwater resources are crucial to human society, not only for drinking and sanitation, but also for irrigation, energy production, industrial uses and other socio-economic activities. Water quality and quantity crises, however, occur more frequently across the world in recent years (Shakibaeinia et al., 2016; Duran-Encalada et al., 2017; Kashyap et al., 2017; Dibike et al., 2018). These threats can include various sources, such as natural hydroclimatic variability (e.g. floods and droughts), global population growth, continued human interventions and intensive socioeconomic development (Vörösmarty et al., 2000; Meybeck, 2003; De Fraiture and Dennis, 2010). For instance, many floods happened recently in Austraila, Asia, Europe, and North America (e.g., 2019 Iran flood; 2019 Quebec flood; 2021 Turkey flood; 2020 China flood; 2021 India flood; 2021 Austraila flood; 2021 Germany flood) – see Merz et al. (2021) for review. On the other hand, recently the occurrence of drought, water shortages, and falling riverine water level events are getting higher. For instance, recent water shortages occurred in India (Shah and Mishra, 2020), South Africa (Haile et al., 2020), or an unexpected falling water levels on the St. Lawrence River in June 2021 (IJC, 2021), highlight just how crucial it is to secure regional water supplies for the human and environment (Villarini and Wasko, 2021). Furthermore, climate change and land-use alteration pose additional stress to water availability, which leads to significant changes in water supply in many regions (Milly et al., 2005; Barnett et al., 2005; Viviroli et al., 2011). Threats to freshwater resources therefore can limit development and endanger societal well-beings in many regions globally. Protecting water resources requires the diagnosis of threats.

It has been shown that large-scale climate variability has historically posed considerable impacts on water resources through changes in regional climate and hydrological cycles (Miles et al., 2000). Such variabilities are mainly influenced by major oceanic-atmospheric oscillations including, El Niño Southern Oscillation (ENSO), Pacific Decadal Oscillation (PDO), Atlantic Multidecadal Oscillation (AMO), and North Atlantic Oscillation (NAO). Large-scale climate patterns evolve over time spans of years (e.g., ENSO) to decades (e.g., AMO), affecting regional temperature and precipitation and shift central tendency of annual mean streamflow during seasons or over years in different regions (e.g., Lavers et al., 2010; Tamaddun et al., 2017; Nazemi et al., 2017; Lauro et al., 2019; Nalley et al., 2019; Wu et al., 2020; Zaerpour et al., 2021). Many prominent examples of regional multidecadal climate variability have been related to the AMO (Knight et al., 2006; Loaiza Ceron et al., 2020; Wu et al., 2020). A relevant example is the frequency of Atlantic hurricanes (Goldenberg et al., 2001; Trenberth and Shea, 2006; Enfield and Cid-Serrano, 2009). The AMO has also affected North American and European summer climate (Sutton and Hodson, 2005) and led to the occurrence of Sahel droughts, in which Sahel region of West Africa experiences multi-decadal decline in annual rainfall total (e.g., Rowell, 1996; Dai et

al., 2004; Evadzi et al., 2019). As a result, understanding the effects of natural variability on water resources is of paramount importance for regional water management, hydropower production, agriculture and other water-related socio-economic activities.

In addition, human interventions directly threaten freshwater resources by changing the dynamics of water cycle at the catchment and regional scale (Nazemi and Wheater, 2015a, b; Bosmans et al., 2017; Wada et al., 2017). This is manifested through operation of infrastructure related to water resource management (e.g. reservoirs, irrigation and other withdrawals) as well as changing in physical structure of the watershed (Meybeck, 2003; Vörösmarty et al., 2005; Haddeland et al., 2014). For instance, reservoir operation alters the timing of discharge, although it does not much change annual mean discharge. Due to human interventions, streamflow conditions can change not only over the course of annual and/or decadal, but also in a century or even a geological epoch (Ye et al., 2003; Huang et al., 2004; Scanlon et al., 2007; Magilligan and Nislow, 2005; Nazemi and Wheater, 2015a, b). A study by Fekete et al. (2010) showed that impact of human interventions, i.e., construction of dams and water consumptions, in some river basins is equal or greater than the impact of expected climate change over next 40 years. Moreover, population and industrialization have continued to increase over the last century, which results in more competition for available water resources between direct consumption (e.g., water supply for human and crops) and/or resource production (e.g., energy and industry). For instance, irrigation consumes around 70% of water withdrawals globally (Shiklomanov et al., 2004) and fuel-based energy production is directly dependent on regional water availability (Jones, 2008; Macknick et al., 2012).

Climate change is expected to additionally affect both water supply and water demand and can alter the elements of hydrological cycle, due to changes in hydroclimate variables such as temperature and precipitation (Nijssen et al., 2001; Fu et al., 2008; Sun et al., 2018; Guermazi et al., 2019; Luo et al., 2019). It has been shown climate change can greatly impact natural streamflow regime (Vörösmarty et al. 2000; Barnett et al., 2005; Dey and Mishra, 2017; Ficklin et al., 2018) and introduces a new set of management challenges, particularly in water scarce regions (Middelkoop et al., 2001; Hagemann et al., 2013; Grafton et al., 2013; Arnell et al., 2014; Schiermeier, 2014; Döll et al., 2015; Didovets et al., 2017). Schellnhuber et al. (2014) indicated that climate warming by just 2°C over the present level would greatly affect human and different sectors of water resources. Harmonized studies have shown that warming climate has triggered in number and strength of the extreme weather and climate events, such as heat waves, flood and droughts (Meehl et al., 2004; Hirabayashi et al., 2013; Kundzewicz et al., 2014; Mann et al., 2015; Mazdiyasni et al., 2015; Cheng et al., 2016; Arnell et al., 2016). These are potential risk events that entail developing and implementing long-term water management and plan practices (Stoutenborough et al., 2014). For instance, drought conditions are likely to become more frequent and severe in some parts of South America, western and central Europe, central Africa, Australia and East Asia (Peñuelas et al., 2001; Hisdal et al., 2001; Prudhomme et al., 2014; Yu et al., 2014). While, the north and northeast of Europe and some parts of U.S. are the regions prone to an

increase in flood frequencies (Lehner et al., 2006; Hodgkins et al., 2017; Musselman et al., 2018; Brunner et al., 2020). Despite all efforts, there is a growing concern about the effects of climate change on water resources systems and infrastructure. U.S. federal agencies are now required to review the potential impacts of climate change on their assets and missions. Herman et al. (2020) and Fletcher et al. (2019) showed that necessity of adapt infrastructure to changing climate conditions. This study demonstrated that how thawing permafrost, increased flooding, and coastal erosion can affect public infrastructure. Similar considerations are also in place in the United Kingdom for key infrastructure providers (Defra, 2011). In 2009, a project arranged by UK Government to examine and improve the resilience of national infrastructures including water sectors to long-term impacts of climate change. In Canada, studies showed the necessity of updating the intensity-duration-frequency (IDF) curves as a result of climate change (Alam et al., 2015; Elshorbagy et al., 2015; Simonovic et al., 2017). Another study by Kemp et al. (2018) indicated potential impact of sea-level rise on Canadian coast. They illustrated that global climate change particularly in vulnerable regions including Maritime Provinces may result in sea-level rise. Climate change may also affect the infrastructure in cold regions (Melvin et al., 2017; Streletskiy et al., 2019). In Canada, around half of ground surface is within permafrost regions. Performance of infrastructure, including roads, pipelines, embankments, typically relies on the stability of the frozen ground in these regions. However, climate change may exacerbate permafrost warming especially in discontinuous permafrost areas (Couture et al., 2003; O'Neill et al., 2020).

1.2. Challenges for Engineering and management

As noted above the threats to human water resources are many, which can introduce a new set of challenges to engineering and management practices by posing substantial stress on water resource systems. Considering that the processes determining water availability are massively interconnected and under different causes of change across a range of scales, the underlying dynamics and drivers of hydroclimatic variability and change are not fully known. Filling this gap is critical for bringing forward new methodologies for water resources planning and management. In addition to stationarity, which is the concept of unchanged variability in natural systems, has long been compromised by human interventions, climate change and heightened climate variability (Milly et al., 2008; Milly et al., 2015). Conventional water resource management, however, is based on the stationarity assumption. As a result, there are no longer valid as they are unable to fully account for dynamics within water resources systems.

Although different methodologies have been adopted to address vulnerability of water resource system to the effects of human interventions, climate change and variability separately (Conway, 1996; Dessai and Mike, 2007; Sheffield et al., 2009; Seiller and Anctil, 2014; Cayan et al., 2016), there is no methodology that is widely accepted (Herman et al., 2015; 2020). For instance, methods that implement climate models, limits the risk analysis only to climate factors that is captured by uncertain climate models (Ahmed et al., 2013; Hagemann et al., 2013; Gosling et al., 2016). On the other hand, majority of alternative approaches still limit the assessment to climate (Brown et

al. 2012; Moody and Brown, 2013). Hence, to craft a more workable water resources management, improved tools are needed to facilitate better understanding of system vulnerability to the combined effects of human interventions as well as climate variability and change.

1.3. Paradigms for assessing water resource systems vulnerability to changing condition

1.3.1. Top-down approach

The most widely-used approach to assess climate change impacts typically relies on the use of Global Climate Model (GCM) projections (Pandey et al., 2019; Gebrechorkos et al., 2020) – see Figure 1.1a. However, raw climate variables from GCMs have biases which must be corrected before their use (Piani et al., 2010; Teutschbein et al., 2012; Brown et al., 2012). In addition, GCMs outputs are produced at coarse spatial scales while the study areas are usually small. Commonly, output from GCMs is downscaled prior to their use in hydrological models (Wilby et al., 1998; Wilby et al., 1999; Wilby et al., 2002). In this framework, Hydrological Models (HMs) are used to estimate streamflow, conditioned to downscaled climate projections. Water resources system models are then used to estimate the resultant effects of projected streamflow series on water resource system performance (Wiley and Palmer, 2008; Brekke et al., 2009a,b; Vano et al., 2010; Vicuna et al., 2010).

Various limitations, however, are associated with this framework (Mote et al., 2011; Beven, 2011; Pielke and Wilby, 2012; Her et al., 2019). For instance, due to climate model uncertainty which is widely accepted in literature (Jekins and Lowe, 2003; Wilby and Harris, 2006) and different assumptions of greenhouse gas emissions (New and Hulme, 2000), GCMs often have uncertain outputs. These uncertainty cascade into even larger uncertainties in downscaled climate change scenarios (Webster et al., 2002; Stainforth et al., 2005; Smith et al., 2009). This is due to the inability of downscaling methods to simulate second- or higher-order moments of climate variables on the regional and local scales (Wilby and Wigley, 1997; Wilby et al., 1998; Salathe, 2005). In addition, natural external climate forcings, such as large volcanic eruptions or long-term variations in solar energy irradiance cannot be seen in the GCMs, which can be an undeniable source of uncertainty (e.g., Myhre and Myhre, 2003; Matsui and Pielke, 2006; Davin et al., 2007). Moreover, global climate model predictions are unable to skillfully simulate major atmospheric circulation patterns (Pielke Sr., 2010; Annamalai et al., 2007) that are the main cause of natural climate variability as noted above (e.g., Otterman et al., 2002; Chase et al., 2006). Another problem with top-down approach is the fact that understanding different responses of water resource system to changes in hydroclimatic variables is very limited (Stainforth et al., 2007). Even using a large ensemble of GCMs, a limited range of change in a climate variable can be captured (Borgomeo et al., 2015). In parallel, current hydrological models cannot translate the climate projections to streamflow without large uncertainties. They also suffer from the assumption that the models developed based on the historical data can be applied for projecting future conditions (Beven, 2011). Later, these uncertainties propagate into the impact assessment of water resource system (Nazemi and Wheater, 2014). Therefore, there is a need to critically think over the top-down approach and move toward more flexible assessments that are capable to formally test the response

of water resource system to much wider range for feasible climate and/or streamflow conditions (Steinschneider and Brown 2013, Brown and Wilby, 2012, Nazemi et al. 2013).
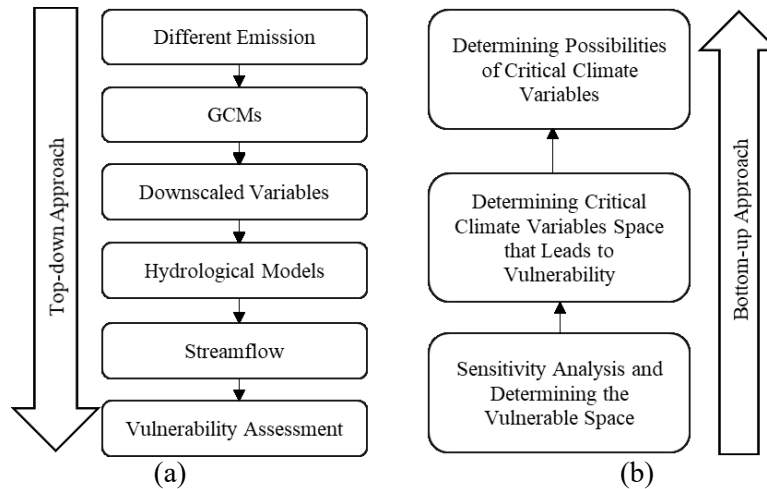
Figure 1.1. (a) The Top-down framework showing the conventional forward propagation approach and (b) the bottom-up approach, which starts by defining vulnerability ranges for hydrologic indicator.

1.3.2. Bottom-up approach

Another approach to assess vulnerabilities of water resource systems is to analyze response of the system without direct use of downscaled GCMs projections (e.g., Wilby and Dessai, 2010; Bryant and Lempert, 2010; Prudhomme et al., 2010; Knighton et al., 2017; Broderick et al., 2019). Such approaches can be classified under the umbrella of "bottom-up" frameworks, in which vulnerabilities of water resource systems are determined without focusing only on the future states of the systems, captured by climate projections. As a result, bottom-up approaches differ from more traditional top-down framework (Christensen et al., 2004; Wiley and Palmer, 2008; Borgomeo et al., 2018; Conway et al., 2019; Quinn et al., 2020). In fact, bottom-up framework changes the purpose of vulnerability assessment from predicting the future risks to identifying critical conditions under which the water resource system is vulnerable (see Brown and Wilby, 2012). The assessment starts with a set of critical climate variables to which the water resource system is most sensitive. Each critical variable is then associated to a feasible range, reflecting various possibilities for future climate change. This range can be identified whether by using a large sets of climate projections (Stainforth et al., 2007) or by considering stakeholders' needs (Brown et al., 2011). The identified domain should be further translated to corresponding streamflow ensembles using hydrological models. Later, simulated streamflows can be input to water resource system models and quantify the system's stress within the feasible climate change envelope (see Figure 1.1b).This approach results in a better understanding of possible system responses through generating much wider range of scenarios of changes that can test potential decision options and system vulnerabilities (Lempert et al., 2004; Brown and Wilby, 2012; Steinschneider and Brown 2013; Turner et al., 2014; Singh et al., 2014; Herman et al., 2015).

1.3.2.1. Decision scaling approach

Decision scaling approach are being used increasingly for climate impact assessments. They are considered as bottom-up approach as they provide a basis for evaluating water resource system performance to changes in hydroclimatic information (Brown et al., 2012, 2019; Kim et al., 2019). Later, these approaches try to add values to the impact assessment using the projections of climate models (Brown and Wilby, 2012). These approaches focus on a system of interest (e.g., agriculture, an ecosystem, etc.) and systematically identify its vulnerabilities to climate through obtaining response of system to some scenarios of change.

An important aspect of decision scaling approach is the generation of perturbed series of climate variables that form the inputs to hydrologic and water resource assessment models. These series collectively referred to as an 'exposure space', and represent the range of conditions of interest that a system may be exposed to under a future climate (Guo et al., 2016). The common steps in this method are (1) identifying the problem, defining objectives and performance measures; (2) using a stress test to identify the hazard and evaluate the performance of the system under a wide range of nonclimatic and climatic variability and change; and (3) evaluating the risk using climate information. A schematic diagram of decision scaling approach is shown in Figure 1.2. The information generated can be used to assess system vulnerability under alternative climate change scenarios, and to calculate climatic thresholds at which system is sensitive (Brown et al., 2011; Steinschneider et al., 2015; Poff et al., 2016).
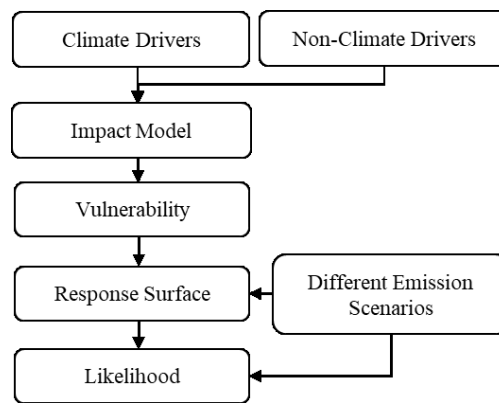
Figure 1.2. Decision scaling framework for climate risk assessment of water resource system.

Decision scaling approach is based on the premise that uncertainties associated with climate change is inevitable, and estimating the true probabilities is not possible through climate models (Stainforth et al., 2007; Brown et al., 2012). However, the skill of the climate models may be informative for estimating the relative probabilities, whether one climate state is more likely than others in the future. In addition, it should be noted that the results of decision scaling do not attempt to provide "optimal" solutions in the traditional decision analytic sense. Instead, the approach identifies the best decision conditional on the weight of the evidence obtained by climate projection. This approach tries to find how hydroclimatic variables make the system vulnerable and understand the critical thresholds for which new management option should be taken.

However, recent studies extend decision scaling approach to include hydro-economic factors in vulnerability assessment of water resource system (Ghile et al., 2014; Lownsbery 2014; Ray et al., 2019), considering the fact that demand may put great pressure on water resource system (Vorosmarty et al., 2000; Fekete et al. 2010).

Despite an interest in decision-centric approaches, technical methods for vulnerability assessment (i.e., generating perturbed climate scenarios to test system vulnerability) are relatively underdeveloped. Till now, a few methods have been utilized for perturbation of climate variables. The most popular approach has been to apply simple change factors to the historical values of precipitation and temperature data, and explore system sensitivity to mean climate shifts (Johnson and Weaver, 2009; Gober et al., 2010; Lempert and Groves, 2010; Brown et al., 2012). Some studies have considered other forms of change, including shifts in intra-annual climate (Prudhomme et al., 2010) and high-order statistics (e.g., variance, serial correlation) of annual hydroclimate data (Moody and Brown, 2013). Other studies adopt a stochastic weather generator, which provides a long synthetic time series of weather variables (Forsythe et al., 2014; Glenis et al., 2015; King et al., 2015). While all of above-mentioned approaches are appropriate for their specific application, they exhibit limited ability to perturb the entire distribution of climate variables at multiple temporal scales (Steinschneider and Brown, 2013). However, different concurrent temporal scales changes are possible under climate change (Timmermann et al., 1999; Collins, 2000; IPCC, 2007). Such combined patterns of change are indeed important in climate sensitivity analysis. Thus, there is a need for more generalized and comprehensive tools to conduct climate vulnerability assessments for systems sensitive to different climate variables across multiple temporal scales.

1.3.2.2. Robust decision making

Robust Decision Making (RDM) is based on sampling multiple climate conditions stochastically from observed records or GCM projections, which provides a tool to assess vulnerability of water resource system to a wider range of climate conditions (Lempert et al., 2006; Groves and Lempert, 2007; Lempert and Collins, 2007; Groves et al., 2008; Bartholomew and Kwakkel, 2020). This approach provides decision makers with information about adverse thresholds in climate and land use change that may cause a system vulnerable. It differs from decision scaling, in which the stress reflects the overall performance of system without using climate projections (Brown et al., 2011) and the critical thresholds can directly be used to inform policy decisions. For example, if a system quickly becomes vulnerable (small changes in climate or land use causing vulnerability), it provides decision makers with the insight that a very robust policy or drastic action will be needed to avoid potentially large damages. The steps in RDM include (1) considering ensembles of large plausible scenarios, (2) search for robust decision options that do "well enough" for an extensive range of possible futures, (3) apply adaptive strategies to achieve robustness.

As noted above, the primary challenge in applying decision analysis under climate change is the uncertainty associated with GCM projections. In order to make decisions, instead of first

predicting the uncertain future, using RDM a systematic understanding of long-term future can be obtained considering many plausible climate projections (Lempert et al., 2010). This can be described by some methodologies, such as the Bayesian decision model with imperfect information, in which the information from GCMs can be later tailored to the vulnerabilities identified (Richards et al., 2013; Sperotto et al., 2017; Landis et al., 2017). Although, RDM provide a decision support to inform decision makers about the robustness of alternative decision options, but it does not provide explicitly any information about ranking of alternative decisions (Hall et al., 2012). Despite the development in the context of RDM, there are still major challenges. Current RDM framework mainly accounts for climate-related risk assessment, which is obtained using available climate projections. However, this approach cannot consider multiple sources of risks in future system performance. For instance, RDM has limited skill in addressing the effect of human interventions or different policy options on water resource system. Also, it still requires hydrological models to convert the realized climate futures into estimated water availability conditions.

1.4. State-of-the-Art: Fully bottom-up approach

As previously mentioned, top-down approaches are highly uncertain. Besides, bottom-up approaches have several limitations including addressing only climate-related risk and using uncertain hydrological models to translate climate variables into hydrological indicators. Hence, there is a need for more reliable methods to assess the potential impact of changing conditions on water resource systems. More recent contributions, therefore, have moved towards fully bottom-up approaches to generate future water availability conditions without incorporating any climate and/or hydrological models. Accordingly, vulnerability can be directly mapped as a function of feasible changes in streamflow conditions. The advancement of such fully bottom-up framework requires the development of methodologies to address some limitations of these approaches with which the vulnerability of water resources systems under changing conditions can be assessed. For this purpose, stochastic modeling of streamflow has a key role in hydrology. Conventional methods typically implement autoregressive and their variants to linearly model the streamflow series (Pegram, 1980; Stedinger and Taylor 1982; Salas et al., 1985). Non-parametric models have been proposed as an appealing alternative to linear parametric methods for stochastic simulation of streamflow series (Lall, 1995). However, these methodologies have some limitations, e.g., the limited skill in representing the nonlinear behavior of streamflow series, or the ability to go beyond the range of historical data. Recently, copula-based methodologies have been extensively used for stochastic simulation of hydrological data (Bardossy and Pegram, 2009; Hao and Singh, 2012; Jeong and Lee, 2015; Lall et al., 2016; Lei et al., 2018; Pereira and Veiga, 2018). It is mainly due to their capability to model any sort of association between random variables. In addition, in copula-based simulation, marginal behavior of each random variable can be modeled independent from the dependence structure that governs the relationship between variables (Genest and Favre, 2007; Nazemi and Elshorbagy 2012; Pereira et al., 2017). Furthermore, any arbitrary distribution can be chosen as the marginal distribution (Chen et al., 2015). Several copula-based methodologies

have been developed for stochastic simulation of streamflow (Lee and Salas, 2011; Hao and Singh, 2012; Kong et al., 2015), but they have some limitations which will be discussed further in detailed.

1.5. Gaps in Knowledge and Technics

In response to limitations of top-down approaches, alternative approaches based on bottom-up impact assessments have been suggested by focusing on analyzing the vulnerability using various forms of stress tests (Lempert and Collins 2007; Prudhomme et al. 2010; Brown et al. 2012; Steinschneider and Brown 2013; Mateus and Tullos 2017; Roach et al. 2016; Whateley et al. 2016; Danner et al. 2017; Ray et al. 2018; Guo et al. 2018; Spence and Brown 2018; Van Tra et al. 2018). In such approaches, future climate projections can be incorporated as one of the potential sources for identifying possible changes in streamflow, but the assessment can be performed without using GCM-based projections (Wilby and Dessai 2010; Brown and Wilby 2012; Herman et al. 2015, 2016; Steinschneider et al. 2015; Knighton et al. 2017; Shortridge and Zaitchik 2018). The results of such stress tests provide a basis to map critical thresholds for system vulnerability under a wide range of feasible future climate conditions. Although the majority of bottom-up assessments avoid the uncertainties resulted from climate projections, there are recent examples of fully bottom-up approaches in which the uncertainties from hydrological models are also avoided (Nazemi and Wheater 2014b). In such approaches, a large ensemble of synthetically generated streamflow realizations is used to directly map system vulnerability as a function of changes in long-term streamflow characteristics (see Nazemi et al. 2013; Borgomeo et al. 2015).

Although bottom-up frameworks can address some of the uncertainties in top-down impact assessments, they include other forms of uncertainty. Most importantly, despite methodological differences, all bottom-up assessments use systematic approaches, with which realizations of perturbed climate or streamflow conditions can be generated. For the case of streamflow, stochastic approaches have been widely used for generating synthetic series at single and multiple sites (Prairie et al. 2007; Hao and Singh 2011; Chen et al. 2015). However, due to various simplifications and/or assumptions in producing synthetic streamflow realizations, the effects of changing water availability conditions on system performance may be misrepresented, potentially further misleading the decision-making process. One important context for such uncertainties is when streamflow is generated at the regional scale and needs to represent spatiotemporal dependencies between multiple tributaries. In such cases, misrepresenting the spatial dependencies between tributaries may result in underestimating the concurrence of streamflow events under current and changing conditions, in particular, high and low extremes (e.g., AghaKouchak et al. 2014; Leonard et al. 2014; Mazdiyasni and AghaKouchak 2015; Zscheischler and Seneviratne 2017).

Additionally, with respect to the representation of spatiotemporal dependencies in synthetic streamflow realizations, existing methodologies can be categorized under two strains of linear and nonlinear approaches. Applications of linear stochastic models can be traced back to more than half a century ago (see Salas, 1980). In particular, variations of auto-regressive-moving-average models fusioned with other linear and nonlinear techniques have been frequently used for

streamflow generation at single site (Nowak et al. 2011; Serinaldi and Kilsby 2017; Tsoukalas et al. 2018a; Papalexiou 2018). Having said that, water resources systems often consist of multiple streams that are highly dependent on one another across a range of spatiotemporal scales, requiring the use of multisite stochastic streamflow generation models. Such multisite streamflow generation schemes enable assessment of vulnerability of water resource systems to simultaneous changes in streamflow such as analysis of regional flood events at multiple locations (e.g., Keef et al., 2009; Quinn et al., 2019; Brunner et al., 2020). For this purpose, multisite linear models have been developed in hydrology (e.g., multisite AR/ARMA; Salas and Pegram, 1977; Salas et al., 1985; Bartolini et al., 1988).

In contrast to linear models that consider representing the dependence structure using the Pearson correlation coefficient, nonlinear models are mainly developed based on the representation of rank correlation statistics (e.g., Spearman's rho and Kendall's tau; see Genest and Favre 2007). Recently, copula-based methodologies have been extensively used for stochastic simulation of hydrological data, including streamflow (Bardossy and Pegram, 2009; Hao and Singh, 2012; Madadgar and Moradkhani. 2011; Borgomeo et al., 2015; Pereira and Veiga, 2018; Chen et al., 2019; Nazemi et al., 2020). Copulas are favorable in hydrology for their capability in modeling *nonlinear* association between random variables using rank correlation statistics (i.e., Spearman's rho, or Kendall's tau – see Genest and Favre, 2007), as well as decomposing the modeling the joint relationships from marginal representations (Wang et al., 2009; Nazemi and Elshorbagy 2012; Pereira et al., 2017). Several copula-based methodologies have been developed for stochastic simulation of streamflow at a single site (Lee and Salas, 2011; Hao and Singh, 2012; Kong et al., 2015). Having said that, in the context of copula-based approaches in the multisite setting, a variety of methods have been proposed for representation of spatial dependency in multisite streamflow generation schemes (Nazemi et al., 2013, 2020; Hao and Singh, 2013; Chen et al., 2015, 2019; Pereira et al., 2017; Serinaldi and Kilsby, 2017).

1.6. Research Statement

Despite the developments noted above, there is not a consensus yet on the best representation for spatiotemporal dependencies in single and multisite generation of streamflow series. This is a major concern as capturing the sequencing of extreme events (i.e., low/high flows) as well as capturing their regional co-occurrence is of high interest for engineering applications (Quinn et al., 2019; Brunner et al., 2020; Wing et al., 2020). This is because streamflow process is governed by various mechanisms acting on different temporal and spatial scales, affecting the dependence structure of streamflow (Fleming and Dahlke, 2014; Konapala and Mishra, 2016; Lee et al., 2018). There have been some evidences arguing more nonlinearity in streamflow dependence structure in smaller catchments (Pilgrim, 1976; Wang et al., 1981) and/or finer timescales (e.g., Rao and Yu, 1990; Chen and Rao, 2003; Wang et al., 2005), although contracting evidences are also available (Robinson et al., 1995; Goodrich et al., 1997). Despite the fact that such clues may be available in some circumstances, it is not yet clear how linear or nonlinear representations of

spatiotemporal dependencies in stochastic streamflow generation can lead to a better or worse simulations of flow characteristics in single and multiple sites.

In addition to the choice of linear/non-linear models required for streamflow generation for vulnerability assessment of water resource systems, little attentions have been given on the inclusion of impact of climate variability on streamflow generation. Previous studies have made it clear that considering the effects of climate variability through Large Scale Climate Indices (LSCIs) directly on streamflow or indirectly through affected hydroclimate variables, e.g., temperature and precipitation, may improve the predictability of streamflow particularly at seasonal to interannual scales (e.g., Kiem et al., 2021; Kwon et al., 2008; Steinschneider et al., 2019; Wasko and Sharma, 2017). The indirect incorporation of LSCI in the generation of streamflow is in fact very common in the context of process-based models, in which variables such as temperature and precipitation are the basis of simulating streamflow (Eisner et al., 2017; Shrestha et al., 2013; Su et al., 2017). Process-based models, however, are deterministically formulated by implementing physically-based and/or conceptual equations without explicitly considering the distributional and/or joint properties of observed data (Montanari and Koutsoyiannis 2012; Farmer and Vogel, 2016). Past studies showed that although dependence between precipitation and LSCIs can be low (e.g., Westra and Sharma, 2010), LSCIs have more consistent impacts on streamflow and/or temperature (Bonsal and Shabbar, 2011; Nalley et al., 2016; Nazemi et al., 2017). In particular, the direct dependencies between streamflow and LSCIs in coarser spatial and temporal scales are rather strong. This has motivated a strain of modeling attempts to explicitly incorporate the effect of LSCIs in streamflow generation through stochastic approaches (Lee et al., 2018a; Liu et al., 2015; Wang et al., 2009).

Furthermore, streamflow regimes, traditionally, have been considered stationary in time (Milly et al. 2008). However, the looming effects of climate change along with human interventions through land and water management have raised fundamental questions regarding stationarity of streamflow regime during the current "Anthropocene" (Arnell and Gosling, 2013; Nazemi and Wheater, 2015a, 2015b). Even in undisturbed streams, recent literature is full of evidence, indicating major alterations induced by heightened climate variability and change (Barnett et al., 2005; Stahl et al., 2010; Rood et al., 2016; Hodgkins et al., 2017; Dierauer et al., 2018). As a result, assessing how streamflow regime is changing as a result of alterations in natural and anthropogenic drivers is currently one of the imminent questions in the field of hydrology.

Despite the extensive body of knowledge already gathered around assessing the effects of climate change on altering streamflow regimes, there are still rooms for methodological developments. Most importantly, among many potential flow characteristics that can constitute and describe streamflow regime, often only a few are taken into account (Whitfield and Cannon, 2000; Hall et al., 2014; Vormoor et al., 2015). This is a limitation because climate change impacts are often manifested in the entire streamflow hydrograph, and not only around a unique set of streamflow characteristics (Olden and Poff, 2003). This is particularly the case in cold regions as at the watershed scale, multiple processes contribute to the streamflow generation, each behaving

differently in response to climate variability and change (Whitfield and Pomeroy, 2016). As a result, alterations in streamflow regimes are not only significant (e.g., Déry and Wood, 2005; MacDonald et al., 2018; Islam et al., 2019; Champagne et al., 2020); but also they are complex, due to compound impacts of changes in temperature, shifts in forms and magnitude of precipitation, as well as alterations in snow/ice accumulation and melt (DeBeer et al., 2016; Hatami et al., 2018; Rottler et al., 2020). At this stage of development, it is not yet possible to systematically quantify streamflow regimes and their alterations to one another using a large set of simultaneously changing streamflow characteristics (Burn et al., 2016; Burn and Whitfield, 2018).

Regardless of methodological differences, these decision-centric frameworks are mainly developed based on an ensemble of synthetic streamflow series generated under current and changing conditions, to which the system response is assessed. For this purpose, stochastic modeling of streamflow has a key role in hydrology. Conventional methods typically implement autoregressive models and their variants to linearly model the streamflow series (Pegram, 1980; Stedinger and Taylor 1982; Salas et al., 1985). Such approaches, however, cannot represent the marginal streamflow distribution, especially in the case of asymmetric and/or multimodal conditions (Papalexiou, 2018; Papalexiou and Serinaldi, 2020). To address these issues, Non-parametric approaches have been developed as an appealing alternative (Lall and Sharma, 1996); however, they can only generate the streamflow realizations within the range of observed data and are limited in extrapolation (Papacharalampous et al., 2019; Quilty and Adamowski, 2020). More recently, copula-based models have gained lots of attention in hydrolclimatology (Nazemi and Elshorbagy, 2012; Aghakouchak, 2014) and in stochastic streamflow generation in single- (Hao and Singh 2012; Nazemi et al., 2013) and multiple sites (Pereira and Veiga, 2018; Chen et al., 2015, 2019; Nazemi et al., 2020). This is mainly due to the capability of copula-based approaches in capturing the nonlinear spatiotemporal dependence structure observed within streamflow (Bardossy and Pegram, 2009; Hao and Singh 2012; Worland et al., 2019; Wang et al., 2019).

Despite ongoing advances in stochastic streamflow generations with which the vulnerability assessment can be performed, little attention has been given on advancing the perturbation algorithms for altering the streamflow characteristics (Nazemi et al., 2013; Borgomeo et al., 2015; Feng et al., 2017). Some studies focus on developing algorithms for perturbing only few streamflow characteristics such as annual volume or timing of annual peak developed by Nazemi et al. (2013) and later applied in Feng et al. (2017), or the work of Herman et al. (2016) for perturbing only the frequency of low flow. Perhaps, the most general approach for perturbing the streamflow characteristics is developed by Borgomeo et al. (2015) in which any desired shift in streamflow characteristics can be provided by rearranging of annual hydrographs to generate a set of desired properties while such characteristics are treated as a combinatorial optimization problem. Such approaches, however, is a very time-consuming task, and similar to other optimization techniques may converge to local optimum. Additionally, such algorithms are based on reshuffling the observed annual hydrograph and cannot generate the streamflow realizations beyond the observed data. Furthermore, for generation of streamflow realization, different

characteristics of flow regime have been considered in the one objective function. Nonetheless, these characteristics are not explicitly independent of each other.

1.7. The Scope of this thesis

The research presented in this thesis is focused on providing a comprehensive stochastic framework to generate streamflow series at single and multiple sites under changing conditions. This thesis tries to improve the stochastic streamflow generation scheme required for vulnerability assessment of water resource system by addressing limitations summarized as follows:

(i)   As mentioned earlier, with respect to the representation of spatiotemporal dependencies in synthetic streamflow realizations, existing methodologies can be categorized under two strains of linear and nonlinear approaches. There is, however, no general consensus on how spatiotemporal dependencies between multiple river reaches should be represented under changing condition. Additionally, it is not clear how and to what extent the results of an impact assessment depend on the scheme used for generating streamflow at regional scales.

(ii)   There have been some lines of evidence arguing linearity/nonlinearity in the streamflow dependence structures changing with the timescales, sizes of streamflow catchment, and types of flow regime. Despite the fact that such clues may be available in some circumstances, it is not yet clear how linear or nonlinear representations of spatiotemporal dependencies in stochastic streamflow generation can lead to a better or worse simulations of flow characteristics in single and multiple sites across different timescales, sizes of basin, and various flow regimes.

(iii)   Streamflow has been often represented as a function of other hydroclimatic processes such as temperature, precipitation, and evapotranspiration at the catchment scale. These variables are affected by large-scale climate patterns, which can consequently impact streamflow generation globally. Despite ongoing advances in streamflow generation methodologies, only a few incorporate climate-related proxies in streamflow generation; and none – to the best of our knowledge – explicitly incorporate the influence of multiple LSCIs in the procedure of stochastic streamflow generation.

(iv)   Assessing how streamflow regime is changing as a result of alterations in natural and anthropogenic drivers is currently one of the imminent questions in the field of hydrology. Identifying how streamflow regimes are changing is required for developing perturbation methodologies to represent the desired shift under future changing condition. Despite the extensive body of knowledge already gathered around assessing the effects of climate change on altering streamflow regimes, there are still rooms for methodological developments. Most importantly, among many potential flow characteristics that can constitute and describe streamflow regime, often only a few are taken into account. This is a limitation because climate change impacts are

often manifested in the entire streamflow hydrograph, and not only around a unique set of streamflow characteristics.

(v)   Regardless of methodological differences, these decision-centric frameworks are mainly developed based on an ensemble of synthetic streamflow series generated under current and changing conditions, to which the system response is assessed. For this purpose, stochastic modeling of streamflow has a key role in hydrology. Despite ongoing advances in stochastic streamflow generations with which the vulnerability assessment can be performed, little attention has been given on advancing the perturbation algorithms for altering the streamflow characteristics. Some studies focus only on developing algorithms for perturbing only few streamflow characteristics such as annual volume or timing of annual peak. Some other methods implement any desired shift in streamflow characteristics by rearranging of annual hydrographs to generate a set of desired properties while such characteristics are treated as a combinatorial optimization problem which is a very time-consuming task and rely only on reshuffling the observed annual hydrograph.

1.8. Thesis Layout

The thesis follows a manuscript-based format including a collection of five manuscripts that are published, submitted, or in preparation. This PhD thesis aims at providing an improved stochastic streamflow generation approach for assessing the vulnerability of the water resources system to changing streamflow conditions. The driving questions in each parts of our study can be summarized into: (1). What are the uncertainties in the status-quo methodologies? (2). How can we improve the preservation and perturbation of streamflow regime during stochastic generation? (3). How can we incorporate the effect of natural variability manifested through Large Scale Climate Indices (LSCIs) into vulnerability assessments? (4). What are the emerging types of changes in various streamflow regimes in Canada? (5). How can we represent the various types of changes in the flow regime?

The five journal papers compose Chapters 2 to 6, each aims to address one of the above questions. Some papers are slightly edited to unify the format of the thesis.

(i)   Chapter 2 identifies the gaps in the fully bottom-up framework and showcase the uncertainty in an impact assessment as a result of the ambiguity in the choice of streamflow generation scheme. By focusing on an important regional water resource system in Western Canada, this thesis examines how alternative regional generation schemes can result in different reproduction of the historical stream- flow regime and explore whether there is a particular scheme that can outperform others in terms of reproducing a range of observed streamflow conditions.

(ii)   Chapter 3 sheds light on the various forms for characterizing the key feature exhibited by the observed streamflow data, i.e., spatiotemporal dependence structure, and to

develop a set of guidelines for choosing the right spatiotemporal representation in the right circumstances. By considering a wide range of spatiotemporal representations for stochastic streamflow generation, this chapter investigates the performance of each scheme in reproducing the long-term characteristics of streamflow series and annual flood peak in a number of case studies and across a range of scales and flow regimes.

(iii)   Chapter 4 proposes a generic approach based on vine copula method to explicitly incorporate LSCIs as exogenous covariates in stochastic streamflow generation at the monthly scale both in prediction and projections modes and at single and multiple sites. We hypothesize that the explicit representation of LSCIs improves both prediction and projection skills, particularly in terms of representing seasonality and inter-annual variability. We showcase the application of the proposed scheme for the prediction and projection of three mountainous headwaters in southern Alberta, Canada. To benchmark the performance of the proposed algorithm, we compare the skills of our model with already existing reference algorithms.

(iv)   Chapter 5 proposes a new methodology to systematically quantify streamflow regimes and their alterations to one another using a large set of simultaneously changing streamflow characteristics. In line with some recent suggestions in the literature, this chapter conceptualizes streamflow regimes as continuous spectrums rather than distinct states. This conceptualization requires a methodology that can formally deal with subjectivity in the definition of streamflow regimes. This provides a methodological basis to classify streamflow regimes as intersecting clusters. Accordingly, the chapter highlights how such regime shifts are attributed to changes in streamflow characteristics using a formal dependence analysis. This algorithm is applied in Canada, where the rate of warming is twice the global average, and changes in streamflow characteristics are significant in time and space.

(v)   Chapter 6 proposes a general approach to synthesize a large ensemble of perturbed streamflow, with which the vulnerability of water resource systems to the plausible changes in streamflow hydrograph can be analyzed. The proposed framework first identifies the main types of shifts in the streamflow hydrographs happening across different flow regime types and then implement the shifts in the marginal distribution of flow at the subannual time scale as well as in the expected timing of annual peak. The new algorithm can systematically alter various streamflow characteristics alone or simultaneously, depending on the types of changes in different flow regimes. The practical utility of the new perturbation algorithm is demonstrated in single- and multisite settings using a number of natural streams with different flow regime types across Canada.

(vi)   Finally, Chapter 7 summarizes the main contributions of this thesis and future research needs.

Uncertainty in Bottom-Up Vulnerability Assessments of Water Supply Systems due to Regional Streamflow Generation under Changing Conditions[1]

The contents of this chapter have been published in "Nazemi, A., Zaerpour, M., & Hassanzadeh, E. (2020). Uncertainty in Bottom-Up Vulnerability Assessments of Water Supply Systems due to Regional Streamflow Generation under Changing Conditions." in Journal of Water Resources Planning and Management. The contents are slightly modified from the submitted article.

Synopsis

Changing natural streamflow conditions apply pressure on water supply systems globally. Understanding potential vulnerabilities using IPCC-endorsed top-down impact assessments, however, is limited due to uncertainties in climate and/or hydrological models. In recent years, bottom-up stress tests have been proposed to avoid some of the uncertainties in top-down assessments, but the uncertainty in bottom-up approaches and its impact on vulnerability assessments are poorly understood. Here, we aim at addressing uncertainties that originate from synthetic realizations of regional streamflow with which the system vulnerability is mapped and assessed. Four regional streamflow generation schemes are used to form alternative hypotheses for performing a bottom-up impact assessment in a large-scale water supply system under changing conditions. Our findings suggest that despite having different levels of realism, none of the schemes can dominate others in terms of reproducing all historical streamflow characteristics considered. There can also be significant differences in the results of impact assessments, particularly in terms of variability in long-term streamflow characteristics and system performance. These differences cause uncertainty in assessing risk in system performance and stress-response relationships under changing conditions.

2.1. Introduction

Mountainous headwaters are important sources of freshwater supply globally. As a result, it is not surprising that human activities, downstream of mountainous headwaters, have been formed around certain characteristics of incoming streamflow, collectively known as the natural streamflow regime. Although natural streamflow regimes have been historically considered to be stable over time, the effects of climate change (Barnett et al. 2005; Milly et al. 2005) and increasing anthropogenic interventions through land and water management (Vörösmarty et al. 2000; Nazemi and Wheater 2015a, b) have challenged the legitimacy of the stationarity assumption in streamflow characteristics (Milly et al. 2008, 2015). As such pressures on natural streamflow are increasing (Haddeland et al. 2014; Prudhomme et al. 2014), nonstationarity should be considered the new normal for natural streamflow regimes during the Anthropocene (see Mallakpour et al. 2018).

Alterations in the streamflow regime can translate into vulnerabilities in water resource systems. Various methodologies have been suggested to assess the impact of changing streamflow regimes on the planning and management of water supply systems (Salas et al. 2012; Eisner et al. 2017; Sunde et al. 2017; Khatri   et al. 2018). These frameworks are mainly based on a top-down, scenario-led (in short and top-down) approach, which uses downscaled projections of global climate models (GCMs) as the basis for impact assessments. In the case of assessing the vulnerability of water resource systems to changes in streamflow regime, downscaled GCM projections are passed through hydrological models with which changes in streamflow conditions can be quantified (Wiley and Palmer 2008; Gizaw et al. 2017; de Oliveira et al. 2017; Wang et al. 2018). The projected streamflow series are then used to identify the system response to changing conditions using an integrated impact assessment model. Although this approach is endorsed by the International Panel of Climate Change (see IPCC 2014), this approach is subject to large uncertainty due to the limitations in both downscaled climate projections and hydrological models (Wilby and Harris 2006; Stainforth et al. 2007; Beven 2011; Pielke and Wilby 2012; Wilby et al. 2014; Pina et al. 2017; Maraun et al. 2017; Jaramillo and Nazemi 2018). In response to these limitations, alternative approaches based on bottom-up impact assessments have been suggested that focus on analyzing vulnerability using various forms of stress tests (Lempert and Collins 2007; Prudhomme et al. 2010; Brown et al. 2012; Mateus and Tullos 2017; Roach et al. 2016; Whateley et al. 2016; Danner et al. 2017; Ray et al. 2018; Guo et al. 2018; Spence and Brown 2018; Van Tra et al. 2018). In such approaches, future climate projections can be incorporated as one of the potential sources for identifying possible changes in streamflow, but the assessment can be performed without using GCM-based projections (Wilby and Dessai 2010; Brown and Wilby 2012; Herman et al. 2015, 2016; Steinschneider et al. 2015; Knighton   et al. 2017; Shortridge and Zaitchik 2018). The results of such stress tests provide a basis to map critical thresholds for system vulnerability under a wide range of feasible future climate conditions. Although the majority of bottom-up assessments avoid the uncertainties resulted from climate projections, there are recent examples of fully bottom-up approaches in which the uncertainties from hydrological models are also avoided (Nazemi and Wheater 2014b). In such approaches, a large ensemble of synthetically generated streamflow realizations is used to directly map system vulnerability as a function of changes in long-term streamflow characteristics (see Nazemi et al. 2013; Borgomeo et al. 2015).

Although bottom-up frameworks can address some of the uncertainties in top-down impact assessments, they include other forms of uncertainty. Most importantly, despite methodological differences, all bottom-up assessments use systematic approaches, with which realizations of perturbed climate or streamflow conditions can be generated. For the case of streamflow, stochastic approaches have been widely used for generating synthetic series at single and multiple sites (Prairie et al. 2007; Chen et al. 2015). However, due to various simplifications and/or assumptions in producing synthetic streamflow realizations, the effects of changing water availability conditions on system performance may be misrepresented, potentially further misleading the decision-making process. One important context for such uncertainties is when streamflow is generated at the regional scale and needs to represent spatiotemporal dependencies

between multiple tributaries. In such cases, misrepresenting the spatial dependencies between tributaries may result in underestimating the concurrence of streamflow events under current and changing conditions, in particular, high and low extremes (e.g., AghaKouchak et al. 2014; Leonard et al. 2014; Mazdiyasni and AghaKouchak 2015; Zscheischler and Seneviratne 2017).

With respect to the representation of spatiotemporal dependencies in synthetic streamflow realizations, existing methodologies can be categorized under two strains of linear and nonlinear approaches. Applications of linear stochastic models can be traced back to more than half a century ago (see Salas, 1980 for review). In particular, auto-regressive-moving-average models along their variations and fusion with other linear and nonlinear techniques have been frequently used for streamflow generation at single and multiple sites (Nowak et al. 2011; Serinaldi and Kilsby 2017; Tsoukalas et al. 2018a; Papalexiou 2018). In contrast to linear models that consider representing the dependence structure using the Pearson correlation coefficient, nonlinear models are mainly developed based on the representation of rank correlation statistics (e.g., Spearman's rho and Kendall's tau; see Genest and Favre 2007). Copulas provide a flexible methodology to the nonlinear representation of joint characteristics of multiple dependent random variables (e.g., Genest and Favre 2007; Nazemi and Elshorbagy 2012; Sadegh et al. 2017). Using copulas, streamflow at every pair of time and space can be stochastically generated through conditional resampling (see e.g., Appendixes S1–S3). For stationary streamflow generation, copulas are already applied at single (Lee and Salas 2011; Hao and Singh 2012) and multiple sites (Hao and Singh 2013; Pereira and Veiga 2018). However, algorithms that are used to generate synthetically altered streamflow regimes have mostly been developed for a single site (e.g., Nazemi et al. 2013). To overcome this, linear spatial regressions have been proposed that transfer locally generated streamflow to multiple sites (e.g., Nazemi and Wheater 2014a). Such schemes, however, are limited due to the inability of regression models to represent all modes of association between multiple river reaches (e.g., Hassanzadeh et al. 2016b, 2017; Tsoukalas et al. 2018b).

At the current stage of development, there is no general consensus on how spatiotemporal dependencies between multiple river reaches should be represented under changing conditions. In addition, since the results of existing algorithms for spatial streamflow generation under changing conditions are not yet intercompared, it is currently unknown whether there is a scheme that can dominate other competing alternatives in terms of reproducing the observed regional streamflow regime. Moreover, it is not clear how and to what extent the results of an impact assessment depend on the scheme used for generating streamflow at regional scales. To highlight these gaps and to showcase the uncertainty in an impact assessment as a result of the ambiguity in the choice of streamflow generation scheme, we use four alternative schemes (two existing and two new) for multisite streamflow generation under changing conditions. These schemes differ from one another only in terms of how spatiotemporal dependencies between river reaches are represented and incorporated within the streamflow generation procedure. We examine how alternative regional generation schemes can result in different reproduction of the historical streamflow regime and explore whether there is a particular scheme that can outperform others in terms of

reproducing a range of observed streamflow conditions. By implementing these schemes in the context of a bottom-up vulnerability assessment, we then show how different schemes can result in different long-term characteristics under changing conditions and how the different characteristics can produce uncertainties in the understanding of impacts of changing streamflow conditions on the water resource system.

2.2. Case Study

The Saskatchewan River Basin in Western Canada is the most important water supply in the Canadian Prairies, which is home to the country's irrigated agriculture. The part of the river basin in the Saskatchewan Province (hereafter Sask-SRB), exemplifies a water resource system with complex interactions between natural and human processes—see Fig. 2.1. The incoming streamflow to the province is provided by two major tributaries, i.e., the North and the South Saskatchewan Rivers (hereafter NSR and SSR, respectively). Having expected annual discharges of 213 and 215 m3/s at the Alberta/Saskatchewan border, respectively, NSR and SSR together account for approximately 80% of the total streamflow availability in the Saskatchewan (Pomeroy et al. 2005). Both rivers initiate from the Canadian Rockies, where the annual streamflow regime can be adequately characterized by the annual volume and timing of the annual peak (Fleming and Sauchyn 2013; Nazemi et al. 2017). Both tributaries, in particular, SSR, serve multiple water demands in Alberta before reaching the Saskatchewan border. After entering the province, SSR is stored in the Lake Diefenbaker, a large multipurpose reservoir. Although irrigation currently accounts for the majority of water withdrawal in the province, hydropower provides the highest net benefit of the water use (Martz et al. 2007), and the hydropower is generated at three locations, namely, Lake Diefenbaker's Gardiner dam as well as the Nipawin and E.B. Campbell dams, downstream of Fork, where SSR and NSR join and form the Saskatchewan River. The Saskatchewan River then feeds the Saskatchewan River Delta (SRD), the largest inland delta in North America (Hassanzadeh et al. 2017). The outflow from Sask-SRB is subject to the 1969 inter-provincial Master Agreement on Apportionment, requiring Saskatchewan to pass half of the natural streamflow to Manitoba annually (Pomeroy et al. 2005). The Sask-SRB is faced with major water security threats (Wheater and Gober 2013, 2015). Most importantly, increasing climate variability and change has affected the characteristics of streamflow in headwaters, where most of the regional streamflow originated. These changes are due to alterations in regional precipitation patterns and snow/melt processes (Shook and Pomeroy 2012; Chun et al. 2013; Harder et al. 2015; Hatami et al. 2019). In addition, in-stream human interventions, through redistribution and consumption of river flows, have contributed to significant changes in the key streamflow regime indicators in the region, namely, annual streamflow volume and timing of the annual peak (Nazemi et al. 2017). Meanwhile, Saskatchewan is considering a proposal for expanding its irrigation area 4-fold. This expansion can result in an increased provincial net benefit (PNB) and increased current changes in streamflow regime downstream from Lake Diefenbaker. These changes, in conjunction with hydropower production, can significantly affect the ecological functioning of the SRD and accordingly limit the essential life resources for both humans and ecosystems in the delta.

Few impact assessments have been performed in the Sask-SRB to quantify potential system vulnerabilities under changing streamflow, demand, and operational policies (Hassanzadeh et al. 2016a,b, 2017). All these assessments use a fully bottom-up approach based on an integrated simulation-based water resource system model named SWAMPSK (see Hassanzadeh et al., 2014 for more details on the model). These impact assessments, however, use different schemes for synthetic streamflow generation at the regional scale. In Hassanzadeh et al. (2016a, b), a regression-based scheme was used to extend the stochastically generated streamflow at the NSR to SSR, using the scheme suggested in Nazemi and Wheater (2014a). Further investigations, however, revealed in limitations of the regression-based scheme in representing low and high flow quantiles at the SSR. As a result, in the later work of Hassanzadeh et al. (2017), the incoming flows at the NSR and SSR were generated independently using the single-site reconstruction algorithm of Nazemi et al. (2013) without considering the spatial dependence between reaches. This independent generation was to ensure that low and high inflows to the SRD could be well represented. Here, we revisit this case study and reassess the vulnerability of the Sask-SRB using the two previously developed methods, along with two new schemes for regional streamflow generation (in total, four schemes). The four schemes were considered different from each other only in the way spatiotemporal dependencies between and within the SSR and NSR are represented. We are particularly interested in understanding (1) how skillful these four schemes are in reproducing a historical streamflow regime and whether there is a scheme that can dominate others with respect to capturing a range of observed streamflow characteristics; (2) how different the generated streamflow series are under changing water availability conditions; and (3) how sensitive the results of an impact assessment are to the scheme used for streamflow generation. In the following section, we briefly introduce the applied schemes for generating the incoming regional streamflow to the Sask-SRB.

2.3. Copula-Based Stochastic Streamflow Generation at Single and Multiple Sites

The stochastic reconstruction approach (see Nazemi et al. 2013) uses copulas for streamflow generation under changing streamflow conditions. The algorithm was originally proposed for single-site streamflow generation for regions like Sask-SRB, where the annual streamflow regime can be sufficiently described by annual streamflow volume and timing of the annual peak. In brief, the algorithm is built upon the fact that empirical probability distributions of sub-annual streamflow can provide a theoretical basis for generating multiyear streamflow series with identical expected annual characteristics. The algorithm combines this theoretical basis with two heuristic schemes based on multiplicative and additive quantile mapping (Panofsky and Brier 1958; Wood et al. 2002) to represent shifts in annual volume and timing of the peak—see Nazemi et al. (2013) for detailed formulation.
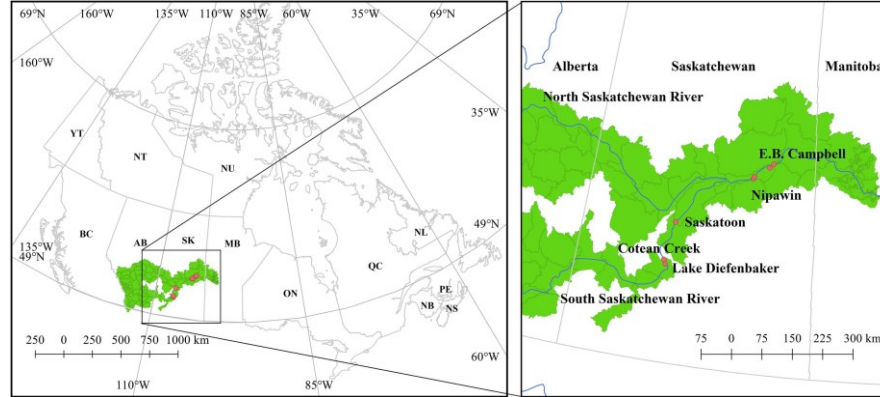
Figure 2.1.The extent and key components of Sask-SRB, the water resource system developed around the Saskatchewan River Basin in Saskatchewan, Canada.

To generate random realizations of streamflow, the algorithm uses a conditional sampling strategy in which parametric copulas provide a basis for representing lag-1 temporal dependencies in streamflow series (i.e., the dependence between consecutive weeks at a given site)—see Appendix A1 for the formulation of the copula-based temporal sampling strategy. We consider four schemes for generating regional incoming streamflow to Sask-SRB: (1) ignoring the spatial dependence between the two reaches—M1, implemented before in Hassanzadeh et al. (2017); (2) representing the spatial dependence using a regression-based spatial extension scheme—M2, implemented before in Hassanzadeh et al. (2016a, b); (3) representing the spatial dependence using a bivariate spatial copula models— M3; and (4) representing the full spatiotemporal dependence using a system of nested bivariate copula models—M4. To generate regional streamflow using M1, streamflow series can be first generated independently at the two reaches using the single-site algorithm (see Section S1 for the sampling procedure) and then randomly mixed-and-matched with one another to form random realizations of regional streamflow series, in which spatial dependencies are not represented. M2, M3, and M4 are based on generating streamflow series at a reference or a donor tributary (hereafter primary site) and transferring the generated realizations to other reaches (hereafter secondary sites) using different representations. M2 uses a set of linear regression models to transfer the generated streamflow series from a primary to a secondary reach at the same time step—see Nazemi and Wheater (2014a) for methodological details. In M3, linear regression models are replaced by lag-0 spatial copulas (i.e., the dependence between corresponding weeks in the primary and secondary reaches). Both M2 and M3 focus only on representing the spatial dependence and ignore explicit representation of temporal dependencies at the secondary reach. To overcome this gap, M4 is developed based on the guidelines of Chen et al. (2015) for representing the full spatiotemporal dependence at the secondary reach using a system of three mutually independent bivariate copulas—see Appendixes A2 and A3 for the formulations of M3 and M4, respectively.

2.4. Experimental Setup and Benchmarking Procedure

Before any intercomparison among schemes, the best copula structure and parametric sets for each scheme need to be identified. We considered three common parametric copula functions, namely,

Frank, Clayton, and Gaussian copulas for setting up the four schemes—see Nelsen (2006) for formulations of these copulas. We used each copula function in conjunction with empirical representations of marginal distributions (i.e., weekly flows in NSR and/or SSR reaches); therefore, any difference between various setups of one scheme can be attributed to the choice of copula functions. Accordingly, we identified the best parametric copulas for preserving lag-1temporal and lag-0 spatial dependencies between the two tributaries during the baseline period of 1980–2010. The Kendall's tau (Genest and Favre 2007) was used to quantify temporal and spatial dependencies (see Appendix A4 for observed versus simulated Kendall's tau). The maximum likelihood density method was used to estimate the copula parameters (see Shojaeezadeh et al. 2018). The results show that Frank copula can consistently outperform Clayton and Gaussian copulas in reproducing the observed temporal and spatial dependencies at the NSR and SSR—see Appendix A4. Frank copula was therefore selected for setting up the four schemes and performing the other experimentations. As the copula function is common among all schemes, any difference between generated series can be attributed only to the procedure with which spatiotemporal dependencies between the two reaches were represented. Here, we attempted to make an intercomparison between M1 and M4 to understand the quality of generated long-term streamflow characteristics and to shed light on uncertainties in understanding system response due to uncertainties in synthetic streamflow series. We first intercompared the performance of the four schemes in reproducing the long-term streamflow characteristics during a common historical baseline. For this purpose, we implemented a resampling approach and rigorously inspected the expected values for performance and associated uncertainty in reproducing the long-term historical characteristics from 1980 to 2010.

In brief, for each scheme, we once chose the NSR and once chose the SSR as the primary was reached (hereafter, NSR → SSR and SSR → NSR paths, respectively), for which 100 realizations of the historical streamflow series with the length of 31 years were generated with no shift in annual streamflow volume or timing of the peak. For each realization, we then generated the corresponding streamflow series at the secondary site using the four spatial extension schemes. For each regional realization (i.e., pairs of streamflow series at the primary and secondary reaches), we calculated the error in reproducing 10 key long-term streamflow characteristics. These error measures include mean and root mean square errors in representing long-term observed values of the annual volume (V_{hist}); annual peak (P_{hist}); annual timing of the peak (T_{Phist}); annual flow quantiles at 10%, 50%, and 90% non-exceedance percentiles ($Q10_{hist}$, $Q50_{hist}$, and $Q90_{hist}$, respectively); as well as the lag-1 temporal dependence and the annual temporal dependence structure (i.e., lagged dependencies among 52 weekly streamflow in 1 year) at the secondary reach. We only focused on the secondary tributary, because the generated flows at the primary reach for all schemes were the same. We also considered two regional characteristics related to preserving the lag-0 spatial dependence and the annual spatial dependence structure (i.e., pairwise dependencies between all combinations of weekly flows in the two tributaries). Considering 100 realizations in each ensemble, the expected values of the calculated errors for all realizations were considered as *representative ensemble score* in reproducing the long-term streamflow

characteristics using a particular scheme. We repeated the aforementioned ensemble sampling 100 times, resulting in each scheme comprising 100 samples, with which the *representative scheme score* and the associated sampling uncertainty were empirically quantified using the sample estimates of the mean and standard deviation, respectively. By using this multi ensemble approach, it is possible to formally address the differences in the scheme scores in light of the sampling uncertainties. For this, we used the single-factor analysis of variance (ANOVA) with Bonferroni correction (Bland and Altman 1995) to perform multiple pairwise comparisons between the scheme scores. In brief, ANOVA used the samples of 100 representative ensemble scores for M1, M2, M3, and M4 and tested whether the schemes resulted in statistically different scores. This, however, does not provide knowledge on how the four schemes can be compared pairwise. Bonferroni correction adjusts the *p*-value of the ANOVA test to compensate for multiple pairwise comparisons—see Stuart and Jones (2006), Dauwalter et al. (2006), and Shoda et al. (2012) for the procedure and application examples. Second, to address how the four schemes can lead into different long-term streamflow characteristics under changing conditions, we first identified a set of feasible changes in annual flow volume and timing of annual peak based on previous studies in the region (i.e., Martz et al. 2007; Pomeroy et al. 2009; Hassanzadeh et al. 2016b). In total, we considered 154 scenarios of change by mixing and matching 25% to 25% shifts in annual volume (perturbation step: 5%) with 5 to 8 weeks for the timing of annual peak flow (perturbation step: 1 week). Each scenario of change can be accordingly represented by a regime, for which an ensemble including 100 weekly realizations of regional streamflow with a length of 31 years can be generated using each of the four schemes. The generated streamflow realizations were then intercompared among the four schemes based on two differences: (1) representations of the expected long-term changes in streamflow characteristics; and (2) variabilities in long-term streamflow characteristics that were captured. We estimated the difference between the expected value of long-term characteristics obtained through 100 realizations and the corresponding observed value during the baseline period as an empirical proxy for the expected change in long-term streamflow characteristics. We also considered the coefficient of variation in long-term characteristics obtained through 100 realizations as a proxy for measuring the variability in long-term streamflow characteristics. In addition, the ANOVA test with Bonferroni correction was implemented to measure the significance of the pairwise differences between generated long-term streamflow characteristics among the four schemes. Third, it is also important to address the uncertainties in a bottom-up impact assessment due to the method used to generate streamflow series under changing conditions. As a result, we introduced the generated streamflow ensembles obtained by M1–M4 under 154 changing conditions to the SWAMPSK to provide the projected response of the Sask-SRB water system under changing conditions. We considered three performance measures: annual PNB (in Canadian $M); annual surface water coverage (SWC; in km2) area in the SRD during the ice-free season, a proxy for measuring overall ecosystem health in the delta (see Sagin et al., 2015 for the formulation); and the ratio of Manitoba apportionment to the available streamflow in Saskatchewan (hereafter, APP; dimensionless). These measures represent the economic, ecologic, and socio-politic responses of the Sask-SRB to changing

streamflow conditions, respectively. Similar to the experimentation performed for generated streamflow characteristics under changing conditions, we compared the results of vulnerability assessments obtained using M1–M4 based on two criteria: (1) how differences between the expected changes in the long-term system performance were captured; and (2) how variability in long-term system performance was represented under changing conditions. The ANOVA test with Bonferroni correction was also implemented to measure the significance of the pairwise differences between long-term system responses identified by the use of different schemes for regional streamflow generation.

Table 2.1 also presents the limited performance of spatial extension schemes in reproducing the streamflow characteristics at the secondary site. For instance, M2, M3, and M4 did not reproduce the expected lag-1 temporal dependence or the expected annual temporal dependence structure at the secondary reach with the same skill as M1, in which the spatial dependence between the two reaches are ignored. Moreover, although M4 can better reproduce the temporal dependence at the secondary reach comparing to M3, it fails in reproducing the expected lag-0 spatial dependence with the same performance as M3. These observations reveal the existence of trade-offs in the performance of spatial extension schemes and the fact that the considered spatial extension schemes are incomplete. Finally, by comparing the corresponding error measures between the two paths of spatial extension, NSR $\rightarrow$ SSR provides slightly better results compared to SSR $\rightarrow$ NSR, which confirms the previous findings of Hassanzadeh et al. (2016b). The NSR $\rightarrow$ SSR path is considered for the other c in this study—see Figs. A4–A9 in Appendix A5 for various comparisons between the four schemes in reproducing the historical observed characteristics.

2.5. Results

2.5.1. Generated Ensembles of Streamflow Characteristics under Changing Conditions

As noted previously, the generated streamflow ensembles obtained by the four schemes provide significantly different long-term streamflow characteristics in more than 90% of comparison cases, and there is no single scheme that can dominate others with respect to all performance scores in reproducing observed characteristics during a common baseline period. As a result, all schemes can be considered as competing alternatives with which the streamflow series under changing conditions can be generated for the purpose of bottom-up impact assessments. Fig. 2.2 summarizes the results in terms of the changes in expected long-term streamflow characteristics at the secondary site (i.e., SSR) in comparison with corresponding values during the baseline period. Top to bottom rows show the results for M1 to M4, respectively. From left to right, columns respectively refer to expected change in timing of the peak [ΔT_p], relative changes in the expected annual volume [$1-(V/V_{hist})$], peak [$1-(P/P_{hist})$], as well as flow quantiles [$1-(Q10/Q10_{hist})$] , [$1-(Q50/Q50_{hist})$], and [$1-(Q90/Q90_{hist})$] under 154 feasible changing conditions. According to this figure, changes in the expected long-term streamflow characteristics generated by the four schemes can diverge from one another, and the differences between the long-term changes captured depend on the streamflow characteristics and the scenario of change considered— see Table A2 in

Appendix A6 for a detailed empirical analysis of the differences between error characteristics at the SSR. In brief, in the case of representing the changes in the timing of the annual peak, the divergence between the schemes was more profound under positive shifts in the timing of the annual peak. In addition, M2 could not track the imposed changes, particularly near the lower and upper ends of the feasible range of change. Regarding the representation of the annual streamflow volume, the difference between the four algorithms was more highlighted under positive shifts in annual streamflow volume. In terms of the annual peak, the four algorithms provided significantly different results for the majority of flow regimes. With regard to annual Q10 and Q90, the divergence between the schemes was more vivid under positive shifts in annual streamflow volume, combined with negative shifts in the timing of the annual peak. This is rather different for Q50, in which the differences between the schemes were more obvious under positive shifts in the timing of the annual peak, combined with positive shifts in annual streamflow volume. We also compared the variability in generated long-term streamflow characteristics (i.e., within 100 realizations) at each regime using the coefficient of variation. Fig. 2.3 summarizes the result for the six local characteristics at the secondary reach under the 154 feasible scenarios of change. Similar to Fig. 2.2, top to bottom rows depict the results for M1–M4, respectively, and the columns from left to right refer to simulated coefficients of variation in long-term annual timing of the peak, volume, peak, and three flow quantiles. Again, there are significant differences between the variability in long-term streamflow characteristics generated using the four schemes. As a general observation, M2 generates the least variability in the long-term characteristics compared to other schemes. The M4, in contrast, reproduces the corresponding variability obtained by the M1 in the majority of flow regimes. Note that we are not making a statement for the suitability of any method for vulnerability assessment; rather, we emphasize the differences between alternative streamflow generation schemes in representing the variability in long-term streamflow characteristics under changing conditions.
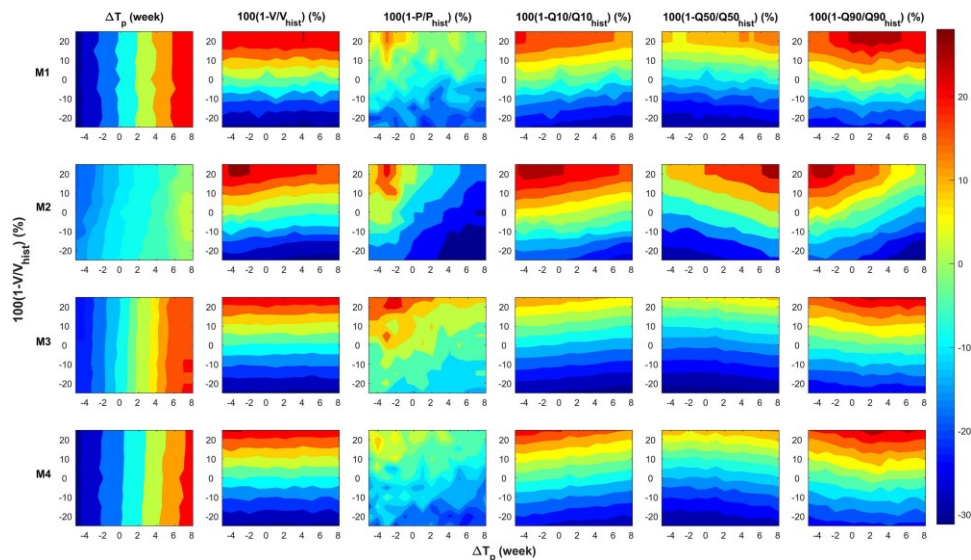
Figure 2.2. Relative changes in expected long-term streamflow characteristics under changing conditions compared to the corresponding historical values.

25

Table 2.1. Estimated expected means and standard deviations of first- and second-order errors in reconstructing key characteristics of streamflow regime to Saskatchewan during the period of 1980–2010.

Streamflow characteristics	Scheme	NSR				SSR			
		Expected mean error	STD of mean errors	Expected RMSE	STD of RMSEs	Expected mean error	STD of mean errors	Expected RMSE	STD of RMSEs
Timing of the peak (week)	M1	**0.24**	**0.10**	1.16	0.08	**0.04**	**0.11**	0.98	0.06
	M2	0.60	0.09	1.14	0.06	0.32	0.05	**0.55**	**0.04**
	M3	0.50	0.10	1.16	0.07	0.68	0.07	1.04	0.07
	M4	0.40	0.10	**1.09**	**0.06**	0.55	0.08	1.13	0.08
Volume (MCM)	M1	**4.40**	**21.87**	268.23	18.88	55.40	43.00	409.30	26.80
	M2	26.94	16.20	**164.99**	**11.67**	**-5.40**	**24.90**	**238.50**	**15.90**
	M3	33.48	21.88	221.93	14.46	11.60	36.00	345.50	24.60
	M4	127.29	28.90	308.88	18.64	95.50	40.80	426.70	28.30
Peak (CMS)	M1	-20.62	5.34	63.42	3.76	**1.50**	**9.30**	**94.30**	**6.40**
	M2	-159.96	3.04	162.81	2.90	-98.90	6.60	116.50	5.90
	M3	14.48	5.46	**55.47**	**3.68**	104.20	9.60	135.20	8.80
	M4	**5.12**	**5.95**	58.61	4.00	50.00	9.80	111.10	7.70
Q10 (CMS)	M1	1.24	0.20	2.44	0.14	**-2.70**	**0.30**	**3.90**	**0.20**
	M2	9.91	0.06	9.92	0.06	10.20	0.10	10.30	0.10
	M3	**-0.27**	**0.17**	**1.49**	**0.10**	-5.40	0.20	5.70	0.20
	M4	-0.62	0.23	2.26	0.16	-6.00	0.20	6.60	0.20
Q50 (CMS)	M1	**0.05**	**0.40**	4.92	0.35	2.50	0.70	6.80	0.50
	M2	6.21	0.36	7.24	0.34	11.70	0.40	12.50	0.40
	M3	0.19	0.41	**3.99**	**0.32**	-1.40	0.50	**4.60**	**0.30**
	M4	0.76	0.62	5.93	0.41	**0.00**	**0.50**	5.40	0.30
Q90 (CMS)	M1	6.20	2.16	26.44	1.71	10.90	4.90	45.50	2.80
	M2	**-1.64**	**1.68**	**17.38**	**1.09**	-16.20	2.60	**30.30**	**1.90**
	M3	5.89	2.05	21.67	1.38	**0.60**	**4.00**	38.60	2.90
	M4	22.96	2.59	35.08	2.32	22.50	4.80	51.60	3.50
Expected lag-1 temporal dependence (-)	M1	**0.01**	**0.01**	**0.07**	**0.00**	**0.00**	**0.01**	**0.07**	**0.00**
	M2	0.10	0.01	0.26	0.01	0.01	0.01	0.25	0.00
	M3	0.35	0.02	0.39	0.01	0.31	0.02	0.36	0.01
	M4	0.10	0.01	0.14	0.00	0.07	0.01	0.12	0.00
Expected annual temporal dependence (-)	M1	**0.07**	**0.03**	**0.18**	**0.01**	0.03	0.03	**0.17**	**0.00**
	M2	0.10	0.03	0.21	0.01	**0.00**	**0.03**	0.18	0.00
	M3	0.15	0.02	0.24	0.00	0.06	0.02	0.21	0.00
	M4	0.11	0.03	0.20	0.01	0.02	0.03	0.17	0.00
Expected lag-0 spatial dependence (-)	M1	0.37	0.05	0.42	0.03	0.37	0.05	0.42	0.04
	M2	-0.60	0.00	0.65	0.00	-0.60	0.00	0.65	0.00
	M3	**-0.01**	**0.02**	**0.10**	**0.00**	**-0.01**	**0.02**	**0.10**	**0.00**
	M4	-0.24	0.02	0.22	0.01	-0.24	0.02	0.22	0.01
Expected annual spatial dependence (-)	M1	0.13	0.03	0.24	0.01	0.13	0.03	0.24	0.01
	M2	**-0.01**	**0.03**	0.21	0.00	**-0.01**	**0.03**	0.21	0.00
	M3	0.02	0.02	**0.19**	**0.00**	0.02	0.02	**0.19**	**0.00**
	M4	**0.01**	**0.03**	0.20	0.00	**0.01**	**0.03**	0.20	0.00

Note: The streamflow series are generated through random resampling of 100 ensembles, each with 100 realizations using M1–M4. Both NSR and SSR are considered once as a secondary reach. For each error characteristic, the statistics of the best scheme is bold.

2.5.2. Impact Assessment under Changing Streamflow Regime

The aforementioned analyses shed light on the differences among the four schemes in terms of the expected values and variability in long-term streamflow characteristics generated under changing conditions. The next step is to analyze whether the differences in streamflow characteristics lead to differences in the results of the impact assessment.
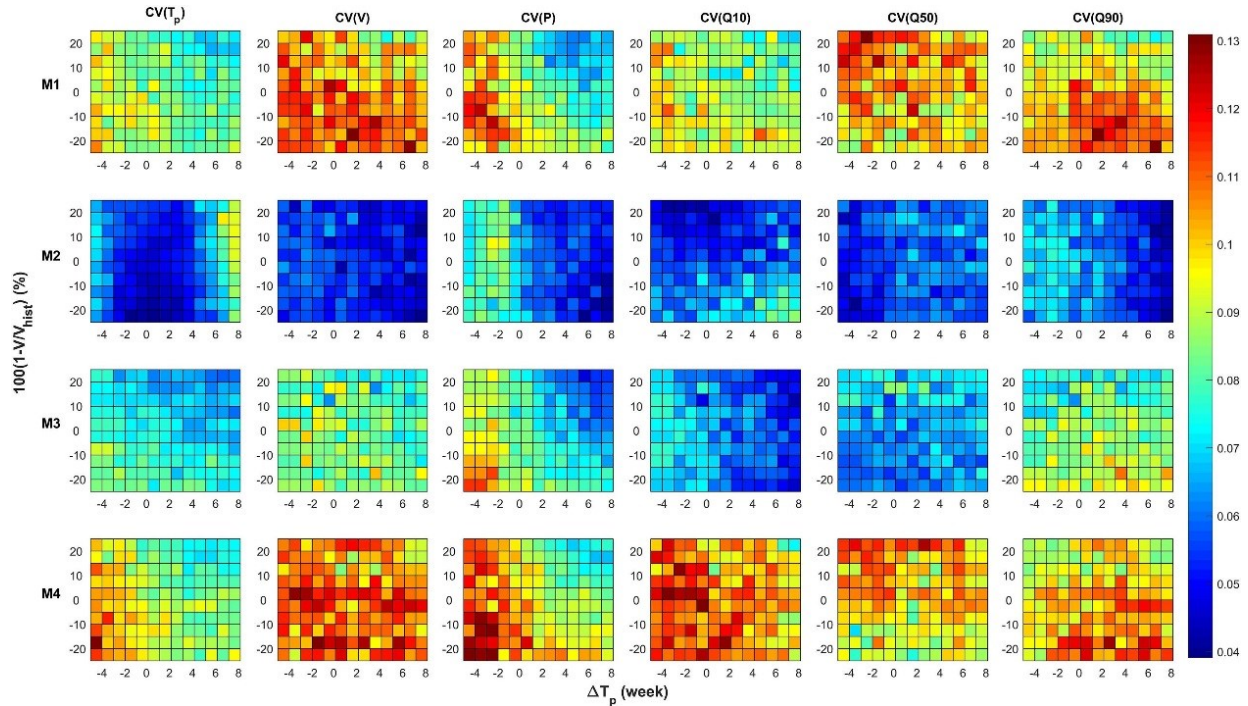
Figure 2.3. Coefficient of variation in ensembles of long-term streamflow characteristics reconstructed under changing conditions.

By feeding the SWAMPSK with generated streamflow ensembles obtained by M1–M4, we focus here on comparing the following: (1) changes in the expected long-term values of PNB, SWC, and APP under changing streamflow conditions with respect to the corresponding values during the historical period; and (2) coefficients of variations in PNB, SWC, and APP under changing conditions. Fig. 2.4 summarizes the findings with respect to the differences in estimated changes in the expected values of long-term system performances—see also Table A3 in Appendix A6. Top to bottom rows in Fig. 2.4 correspond to relative changes in the expected long-term values of PNB, SWC, and APP (i.e., 1-(PNB/PNB_{hist}), 1-(SWC/SWC_{hist}), and 1-(APP/APP_{hist}) under 154 scenarios of change. The relative variations were assessed by the streamflow ensembles of M1–M4, sorted from left to right columns, respectively. The four individual assessments show the sensitivity of the performance measures to changes in the annual incoming flow to Saskatchewan; however, each assessment can describe this sensitivity differently. Note that Table A3 reveals that the differences between the results of impact assessments are less noticeable compared to the differences revealed for streamflow characteristics reported in Table A2. Still, the differences between the results for PNBs were more highlighted under positive shifts in the annual streamflow

27

volume. For the SWC, divergences were more highlighted under positive shifts in annual streamflow volume and timing of the peak. With respect to the APP, the impact assessment conducted by M2 provides very different images for changes in the system performance compared to the other three schemes. In addition, the differences between assessments made by M1, M3, and M4 become more obvious under positive shifts in the annual streamflow volume; however, these differences are clearly less significant compared to those reported for streamflow characteristics.
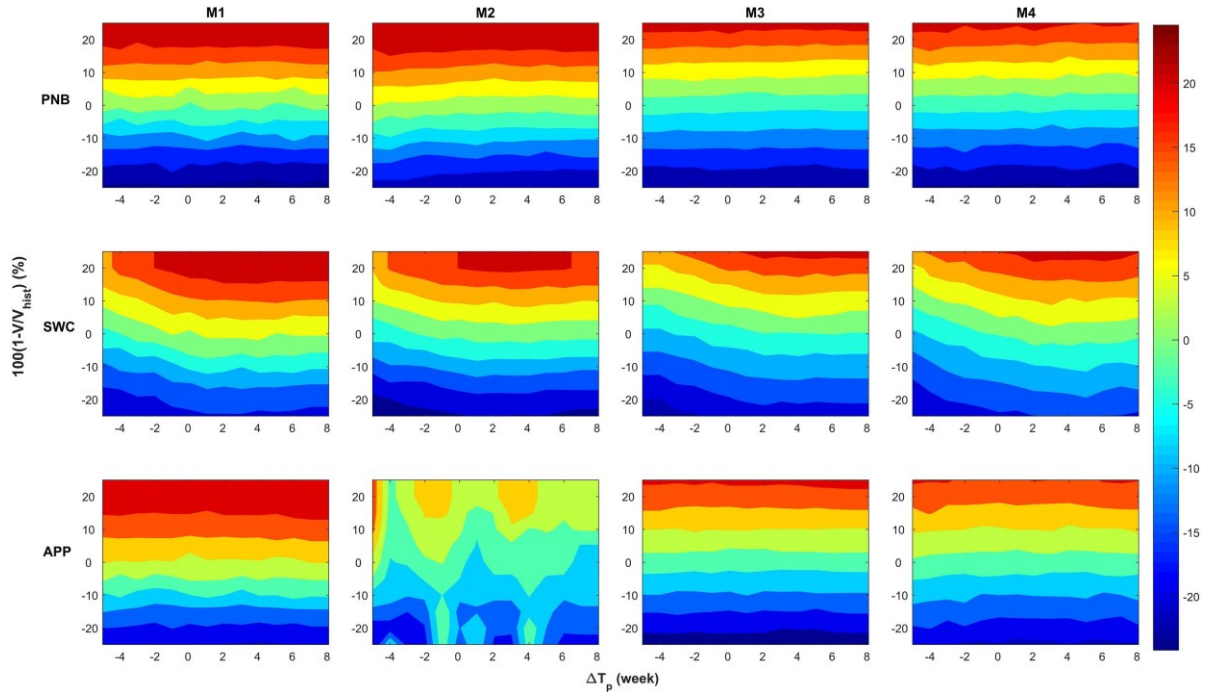
Figure 2.4. Relative changes in the expected long-term performance of the Sask-SRB with respect to the corresponding historical values.

We also inspected the variability in the long-term system performances at each flow regime, conditioned to ensemble streamflow series obtained by the four schemes. The coefficients of variation were used to measure the variability in long-term performances. Fig. 2.5 summarizes the results, in which top to bottom rows depict the results for PNB, SWC, and APP, simulated by forcing the SWAMPSK model with streamflow realizations obtained by M1 to M4 (sorted from the left to the right, respectively). The figure reveals substantial differences between the variability in long-term performance measures. For the case of PNB and SWC, assessments made by M4 show the largest variability in long-term performance under changing conditions, followed by M3. For the case of APP, however, the assessment made by M2 shows the largest variability with a significantly different pattern compared to the other three schemes.
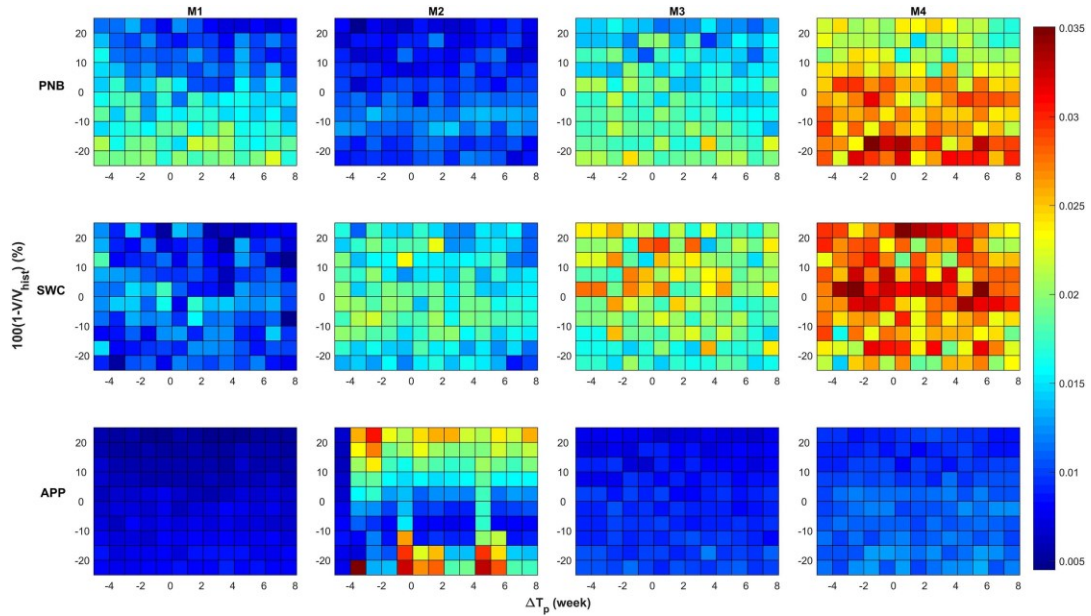
Figure 2.5. Coefficient of variation in long-term performances of the Sask-SRB under changing conditions.

2.6. Discussion

The results provided reveal that even with the same realizations of the streamflow at the primary site, the corresponding spatial extensions to the secondary site, made by the four schemes, can be quite different under changing conditions. Further impact assessment shows that the differences in the long-term streamflow characteristics in some cases result in the long-term impact assessments diverging in terms of both the expected values and variability of the considered performance measures. The propagation of uncertainty from streamflow ensembles to the impact assessment, however, is complex and depends on the performance measures and the scenario of change considered. In addition, larger variability in long-term streamflow characteristics does not necessarily result in larger variability in the performance measures. For instance, while M1 and M4 produce comparable ranges of variability in the considered streamflow characteristics, the results of impact as assessments made by the two schemes are significantly different in terms of the estimated variability in long-term system performance. These findings highlight the sensitivity of the bottom-up assessment to the methodology used to generate regional streamflow series. In the following section, we explore how this sensitivity can result in uncertainty in understanding the risk and stress-response relationships.

2.6.1. Uncertainty in Identifying the Risk in System Performance

To better picture the differences between the results of impact assessments obtained by the four schemes, we compared the risk profiles of the performance measures under three specific streamflow conditions—see Fig. 2.6. In simple terms, risk profiles show the probabilistic characteristic of long-term system performances obtained by multiple realizations (see Hassanzadeh et al. 2016a). The three specific flow regimes exemplify the warm/dry condition, the scenario with (4, 0.25) change; historical condition, the scenario with (0, 0) change; as well as

cold/wet condition, the scenario with (4, 0.25) change. In each panel, the risk profiles generated based on M1, M2, M3, and M4 are shown by dashed dot, dashed, solid, and dotted lines, respectively. Red, green, and blue profiles refer to the warm/dry, historical, and cold/wet conditions, respectively. The solid black lines show the historical performances simulated using the observed data. In terms of PNB, there can be differences in the risk profiles, particularly under representative warm/dry (e.g., between M2 and others) and historical conditions (e.g., M1 and M2 compared to M3 and M4).
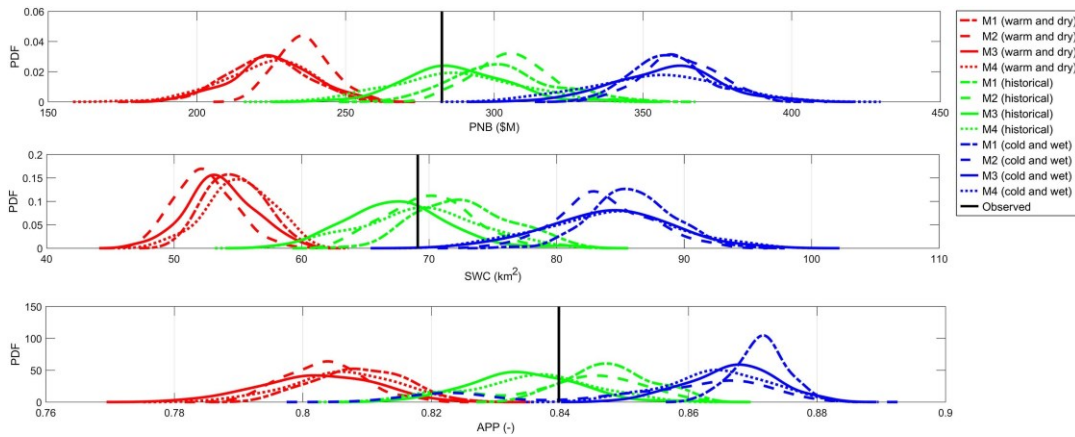
Figure 2.6. Probabilistic risk profiles for PNB (first row), SWC (second row), and APP (third row) obtained for three specific flow conditions. In all panels the risk profiles under historical, warm/dry and cold/wet conditions are shown in green, red, and blue colors respectively; dashed dot, dashed, solid and dotted lines refer to the risk profiles obtained by M1, M2, M3, and M4, respectively. The black solid line shows the performance under observed streamflow.

For the SWC, the differences between the risk profiles were more highlighted under the historical and representative cold/wet conditions. This is similar to the case of APP; in particular, the range of the risk profile obtained using M2 was substantially larger than what was obtained by other schemes under wet/cold conditions. Moreover, while the assessments made by the synthesized streamflow series can capture observed responses (solid black lines) within the range of risk profiles, none of the schemes can provide an unbiased estimation for all performance measures considered. For instance, the expected long-term performance obtained by M3 under no-change condition can provide an unbiased estimation of the observed long-term PNB; however, it underestimates the observed long-term SWC and APP. Similarly, while the expected long-term performance obtained by M4 under the no-change condition can closely match the observed long-term performance for SWC, it underestimates the APP.

2.6.2. Uncertainty in Understanding the Stress-Response Relationships

One key issue in the vulnerability assessment of water supply systems is to understand how variability and change in long-term streamflow characteristics translate into variability and change in long-term performance measures in water supply systems. To address this, we considered the expected changes in the timing of the peak along with relative changes in the expected annual

volume, peak, as well as flow quantiles under 154 feasible changing conditions and paired them with the corresponding values related to relative changes in expected annual performance measures. For each pair, we then compared the significance of dependence (characterized using Kendall's tau) between flow characteristics and performance measures. Table 2.2 summarizes the corresponding Kendall's tau coefficients in which significant values (p-value 0.05) are bolded (see also Fig. A10 in Appendix A7). By considering the dependencies between expected changes in streamflow characteristics and expected changes in system performance, M1, M3, and M4 provide comparable stress-response relationships within the pairs of streamflow characteristics and performance measures. M2, however, portrays different pictures on the existing dependencies between change in streamflow characteristics and the system response. Most importantly, while M1, M3, and M4 show insignificant dependence between changes in the timing of the peak and changes in the performance measures, M2 shows strong dependence between changes in the timing of the peak and changes in PNB and APP. In addition, the magnitudes of pair dependencies are subject to change if the method used for streamflow generation varies. For instance, while M2 suggests that an increase in the incoming streamflow quantiles has minimal effect on increasing apportionment ratio to Manitoba, M1 and M3 show much stronger impacts. This variation introduces conflicting insights on system responses under changing conditions.

We performed similar analyses to understand the dependence between the coefficients of variation of long-term streamflow characteristics and long-term system response. The results summarized in Table 2.3 present significant differences in the way pair dependencies are mapped by each scheme (see also Fig. A11 in Appendix A7). For instance, while M1, M3, and M4 portray significant positive dependency between the variabilities in long-term annual peak flow and long-term PNB, M2 suggests that this dependency is insignificant and negative.

Table 2.2. The dependencies between expected long-term changes in long-term streamflow characteristics and expected long-term changes in system performance characterized by the Kendall's tau.

Expected change in system performance	scheme	Expected change in streamflow characteristics					
		ΔT_p	$1 - \dfrac{V}{V_{hist}}$	$1 - \dfrac{P}{P_{hist}}$	$1 - \dfrac{Q10}{Q10_{hist}}$	$1 - \dfrac{Q50}{Q50_{hist}}$	$1 - \dfrac{Q90}{Q90_{hist}}$
$1 - \dfrac{PNB}{PNB_{hist}}$	M1	-0.02	**0.96**	**0.67**	**0.89**	**0.91**	**0.91**
	M2	**-0.13**	**0.92**	**0.47**	**0.90**	**0.73**	**0.75**
	M3	-0.08	**0.98**	**0.67**	**0.94**	**0.90**	**0.91**
	M4	-0.07	**0.98**	**0.66**	**0.93**	**0.90**	**0.90**
$1 - \dfrac{SWC}{SWC_{hist}}$	M1	0.10	**0.85**	**0.60**	**0.78**	**0.90**	**0.92**
	M2	-0.03	**0.81**	**0.37**	**0.80**	**0.83**	**0.64**
	M3	0.06	**0.86**	**0.57**	**0.80**	**0.90**	**0.93**
	M4	0.08	**0.85**	**0.59**	**0.79**	**0.89**	**0.94**
$1 - \dfrac{SWC}{SWC_{hist}}$	M1	0.03	**0.94**	**0.65**	**0.85**	**0.94**	**0.90**
	M2	**-0.14**	**0.69**	**0.43**	**0.70**	**0.59**	**0.63**
	M3	-0.06	**0.97**	**0.65**	**0.91**	**0.92**	**0.93**
	M4	-0.05	**0.96**	**0.64**	**0.91**	**0.92**	**0.89**

Note: The significant dependencies (p-values ≤ 0.05) are bold.

Table 2.3. The dependencies between expected variability in long-term streamflow characteristics and expected variability in long-term changes in system performance characterized by the Kendall's tau.

Variability in system performance	Scheme	Variability in streamflow characteristics					
		$CV(T_P)$	$CV(V)$	$CV(P)$	$CV(Q10)$	$CV(Q50)$	$CV(Q90)$
$CV(PNB)$	M1	**0.33**	**0.64**	**0.40**	**0.37**	0.01	**0.66**
	M2	**-0.12**	0.24	-0.05	**0.39**	0.08	0.09
	M3	**0.34**	**0.62**	**0.31**	**0.28**	-0.07	**0.62**
	M4	**0.34**	**0.62**	**0.31**	**0.28**	-0.07	**0.62**
$CV(SWC)$	M1	**0.23**	**0.47**	**0.25**	**0.16**	**0.23**	**0.35**
	M2	**-0.19**	**0.56**	**0.24**	-0.01	0.04	**0.43**
	M3	-0.11	**0.50**	0.01	**0.16**	**0.40**	**0.17**
	M4	0.02	**0.60**	0.01	**0.17**	**0.42**	**0.30**
$CV(APP)$	M1	**0.24**	**0.48**	**0.27**	**0.28**	-0.13	**0.64**
	M2	-0.01	**-0.13**	-0.06	**-0.18**	0.09	**-0.12**
	M3	**0.41**	**0.51**	**0.28**	**0.15**	**-0.19**	**0.71**
	M4	**0.25**	**0.53**	**0.21**	**0.19**	**-0.14**	**0.66**

Note: The significant dependencies (*p*-values ≤ 0.05) are bold.

For the case of variability in the SWC, M1, and M2 show strong dependencies between variabilities in long-term annual peak flow and SWC, whereas M3 and M4 do not suggest this strong dependence. Similarly, M1, M2, and M3 show strong dependencies between SWC and Q10 as well as SWC and Q50, while M2 marks these pairs as independent at the considered significance level. This discussion can be extended to the uncertainty in understanding the causes of change in the variability of long-term APP: while M1, M3, and M4 suggest that the variability in long-term APP is dependent on the variability in long-term annual peak, peak timing, and Q50; M2 marks these dependencies as insignificant.

2.7. Conclusions and Further Remarks

Bottom-up approaches to the impact assessment under changing conditions are proposed to address some of the uncertainties in top-down approaches; however, they may include other sources of uncertainty. One important source of uncertainty in bottom-up frameworks originates from synthetic climate and/or streamflow realizations, with which the vulnerability in system performance is assessed. Mathematical schemes for generating synthetic time series, however, are numerous and are based on different assumptions and/or simplifications. Accordingly, the long-term characteristics of generated realizations may be different from one another; hence, the results of impact assessments based upon them also may be different. Through a set of experimentations, our study demonstrates the existence of such uncertainties in the bottom-up impact assessment of large-scale water supply systems that require generating regional streamflow series at multiple tributaries. We use four different spatial extension schemes that differ from one another only in the way the spatiotemporal dependencies between regional streamflow reaches are represented. Through a rigorous intercomparison, it is shown that despite having different degrees of realism, none of the schemes can dominate others with respect to reproducing streamflow characteristics during a common historical period. As a result, they can be considered alternative hypotheses for

bottom-up impact assessment under changing conditions. The results of vulnerability assessment show that there can be substantial differences between the four schemes in terms of representing expected values and coefficients of variations in long-term streamflow characteristics, and to a lesser extent in system performance, under changing conditions. The range of such differences depends on the streamflow characteristic, performance measure, and the changing water availability conditions considered and is more evident in terms of the variability than the expected values. This issue can introduce uncertainty in understanding the risk in system performance and the causal relationships between changing streamflow conditions and changing system performance.

Our findings demonstrate further evidence for deep uncertainty in assessing the impact of changing streamflow conditions on water resource systems, particularly originated from having multiple non-falsified hypotheses for changing regional regimes. Surprisingly, guidelines for representing streamflow characteristics in non-stationary conditions, while maintaining spatiotemporal dependencies between multiple tributaries, are largely overlooked in the literature and current approaches are still incomplete, as we show for the case of copula-based sampling schemes. We, therefore, suggest further efforts toward improved methodologies for synthetic regional streamflow generation under changing conditions. In addition, we believe that building improved algorithms would be rather impossible before making a set of comprehensive intercomparison studies that can address the pros and cons of multiple methodologies, including reshuffling strategies (e.g., Borgomeo et al. 2015), across a range of spatial and temporal scales that are relevant to the impact assessment. Up to the time when such improved schemes become available, we suggest considering multiple weather and/or streamflow generators for informing the impact assessment and/or weighing their results according to their performance in reproducing historical conditions. In addition, the results of top-down approaches can be merged with the findings of bottom-up assessments to associate likelihood values to vulnerabilities identified under changing conditions (see e.g., Ashraf et al. 2019; Mallakpour et al. 2018). Lastly, another source of uncertainty, apart from input to the system, is in the system models, with which the impact of changing conditions on the performance of water resource systems are assessed (see Brunner et al., 2019). Addressing/handling this source of uncertainty requires a set of standalone experimentations that should correspond with the efforts we suggest here.

On Parametric Representations of Spatiotemporal Dependencies in Stochastic Streamflow Generation across Catchments, Timescales, and Flow Regimes[2]

The contents of this chapter are submitted as "Zaerpour, M., Nazemi, N., (2021). On Parametric Representations of Spatiotemporal Dependencies in Stochastic Streamflow Generation across Catchments, Timescales, and Flow Regimes" in Journal of Hydrology. The contents are slightly modified from the submitted article.

Synopsis

Several applications in water resource planning and management require synthetic streamflow series that can represent modes of variability beyond historical observations. A prominent way to address this need is through using stochastic streamflow generators. While so far, several parametric approaches are introduced to represent spatiotemporal dependencies in stochastic streamflow generation using linear or nonlinear schemes; there is still not a consensus on how these dependencies can be optimally represented. This has relevance in capturing cascade, simultaneous and compound streamflow events across a range of spatial and temporal scales. Here, we perform a comprehensive benchmarking study to assess various parametric representations of spatiotemporal dependencies in terms of their skills and uncertainty in reconstructing long-term characteristics of historical streamflow across a range of time scales, catchment areas, and hydrologic regimes. We highlight that when reconstructing flow characteristics at a local stream is sought, linear and nonlinear representations of temporal dependence result in statistically undistinguishable reconstructions in most comparison cases. At the spatial scale, in contrast, the optimality of a given representation is largely dependent on the flow regime, catchment area, modeling timescale, and even long-term characteristics considered for reconstruction. We show that in nival and/or mixed streams, nonlinear representations, particularly through vine copulas, outperform linear schemes; while in pluvial streams, linear representations demonstrate higher skills compared to nonlinear schemes. Our study provides a set of guidelines for selecting stochastic streamflow generators, depending on the application in hand.

3.1. Introduction

The livelihood, prospect, and wellbeing of human societies are largely dependent on the availability of freshwater resources (Palmer et al., 2015; Villarini and Wasko, 2021; Zaerpour et al. 2021a). During the current "*Anthropocene*", the water availability and human water need do not fully match (Savenije et al., 2014; Zandmoghaddam et al., 2019). On the one hand, climate change and human interventions through land and water management have transformed the

---

availability of surface and groundwater reserves (see Nazemi and Wheater, 2015a, 2015b; Aghakouchak et al., 2021; Ashraf et al., 2021). On the other hand, both population and water demand per capita are increasing, putting an ever-increasing pressure on declining water resources, which elevates competition over remaining water resources (Nazemi and Madani, 2018). The inevitable result of the mismatch between water availability and water demand is water insecurity, revealing itself across scales. Examples can vary from drying lakes and wetlands (Aghakouchak et al., 2015; Alborzi et al., 2018), to the unavailability of water for irrigation and drinking (Nazemi et al., 2013), and to regional and political tensions over water (Wheater and Gober, 2013). These new conditions falsify the stationarity assumption, used traditionally for water resources planning and management (Milly et al., 2008, 2015; Nazemi and Wheater, 2014a; Lehner et al., 2017); and therefore, future decisions cannot be supported solely based on historical records (Prairie et al., 2008; Nowak et al., 2011; Koutsouris and Lyon, 2018). One way to fill this data gap is through stochastic simulations of water availability and demand that can provide synthetic data support for long-term planning and management under changing conditions (Rajagopalan et al., 2010; Feng et al., 2017; Lamontagne and Stedinger, 2018; Guo et al., 2019).

Streamflow is arguably the most critical water resource. As rivers roll downstream, they become widely and freely accessible to communities that are developed around them and benefit human activities often in an inexpensive, durable, and reliable manner (see Amir Jabbari and Nazemi, 2019). Having said that, not only lack of streamflow, but also a surplus of streamflow can be also a source of water insecurity as it causes flooding. Due to the importance of streamflow in water resource planning and management and the fact that streamflow observations are sparse and limited in both time and space, stochastic simulation of streamflow has a long tradition in hydrology (Fiering, 1967; Matalas, 1967), as it provides synthetic sets of plausible, yet unobserved streamflow realizations (Papalexiou, 2018; Rajagopalan et al., 2019; Brunner et al., 2019). Stochastic streamflow generation, however, involves several complexities. Most importantly, the streamflow process is governed by various runoff generation mechanisms, acting on different temporal and spatial scales, and can affect the dependence structure of streamflow differently (Fleming and Dahlke, 2014; Konapala and Mishra, 2016; Lee et al., 2018; Hatami et al., 2019). In addition, surface water resources systems often consist of multiple streams that are highly dependent on time and space. As a result, representing such dependencies matters for capturing sequential, simultaneous, and compound events across a range of temporal and spatial scales (Keef et al., 2009; Quinn et al., 2019; Wing et al., 2020; Brunner et al., 2020).

Classic stochastic streamflow models can be seen as timeseries models in various forms of combination between Auto-Regressive (AR) and Auto-Regressive Moving Average (ARMA) models, or their variants (see Pegram, 1980; Stedinger and Taylor, 1982). Such stochastic models were initially developed at a single site, and essentially represent the spatiotemporal dependency "*linearly*" (Lawrance and Lewis 1981; Fernandez and Salas, 1986). They have been also extended to multiple sites (e.g., Salas and Pegram, 1977; Salas et al., 1985; Bartolini et al., 1988); however, they become parametrically heavy and therefore can entail large uncertainties. To address this

issue, contemporaneous linear models are developed, which avoid modeling the joint spatiotemporal dependencies by decoupling the dependence structure. This enables separate modeling of spatiotemporal dependencies; and there, univariate models can be fitted to each site separately (Salas and Pegram, 1977; Stedinger et al., 1985).

In parallel to linear models, Non-Parametric (NP) models have been proposed as an alternative to traditional timeseries models (see Lall, 1995). Generally speaking, NP models work based on resampling from observed streamflow; as a result, empirical characteristics of streamflow are persevered (Lall and Sharma, 1996; Sharma and O'Neill, 2002; Marković et al., 2015). Unlike linear models, NP models avoid any prior assumptions on marginal distributions and/or the dependence structure within observed data; and therefore, they are suitable to reproduce nonlinearities along with asymmetric margins that are common features in streamflow data. A wide variety of NP models have been developed for single site generation of streamflow, including moving block bootstrap (Vogel and Shallcross, 1996), k-nearest neighbor bootstrap (Rajagopalan and Lall, 1999; Kumar et al., 2000), as well as kernel-based methods and their variants (Tarboton et al., 1998; Kumar et al., 2000; Sharma and O'Neill, 2002). NP models in their original form, however, are often unable to extrapolate beyond observations (Srinivas and Srinivas, 2005), and accordingly, modified approaches have been developed (Prairie et al., 2005, 2006; Srinivas and Srinivas, 2001; Souza Filho and Lall, 2003) that are further extended to multisite (Prairie et al., 2007; Sapin et al., 2017); however, they are computationally complex, particularly at regional scales with multiple streams (Rajagopalan et al., 2010). NP models are not discussed in this paper.

Recently, copula-based models have been used numerously for stochastic simulation of hydroclimatic data, including streamflow (Bárdossy and Pegram, 2009; Madadgar and Moradkhani, 2011; Borgomeo et al., 2015; Pereira and Veiga, 2018). Copulas are favored for their ability in representing the *nonlinear* association between random variables using rank-based statistics, i.e. Spearman's rho and Kendall's tau (see Genest and Favre, 2007; Hatami and Nazemi, 2021), as well as decomposing joint relationships from marginal representations (Wang et al., 2009; Nazemi and Elshorbagy 2012; Pereira et al., 2017). Several copula-based algorithms have been developed for stochastic generation of streamflow at single sites based on representing the temporal dependence structure through conditional probability distributions, inferred from streamflow samples in consecutive time steps (Lee and Salas, 2011; Hao and Singh, 2012; Kong et al., 2015). Extending single site methods to multisite algorithms is rather trivial; and a variety of multisite approaches have been developed based on different assumptions (Nazemi et al., 2013, 2020; Hao and Singh, 2013; Chen et al., 2015, 2019).

Despite all mentioned developments, there is still a lack of consensus on how dependence structures in time and space should be represented within the stochastic streamflow generation. This is a relevant question across a range of temporal and regional scales, as well as flow regimes and in both single and multisite settings. There have been some evidence for inclined nonlinearity in dependence structures across smaller catchments (Pilgrim, 1976; Wang et al., 1981) and/or finer

timescales (e.g., Rao and Yu, 1990; Chen and Rao, 2003; Wang et al., 2006), although contracting evidences are also available (Robinson et al., 1995; Goodrich et al., 1997).

The objective of this study is to perform a comprehensive benchmarking, in which the effects of different parametrizations of spatiotemporal dependencies are seen in the skills and uncertainty in reconstructing observed streamflow characteristics. This results into a set of guidelines for choosing the right representations in the right circumstances. For this purpose, we consider a wide range of possible representations of spatiotemporal dependencies as parallel hypotheses and investigate the performance of each scheme in a number of case studies and across a range of timescales, catchment sizes, and flow regimes. The remaining of the paper is organized as the following. Section 3.2 briefly outlines the methodological elements for parametric representations of temporal and spatial dependencies in streamflow. In Section 3.3, we present our case studies, specific modeling hypotheses, and the benchmarking approach. We provide our results at a reference timescale in Section 3.4 and then discuss the sensitivity of our findings across various timescales in Section 3.5. Finally, Section 3.6 concludes our study and provides some further remarks.

3.2. Methodology

Depending on how spatiotemporal interdependencies are represented within stochastic streamflow generation, different parametric representations can be positioned within a spectrum identified by fully linear and fully nonlinear representations. In time, linear representation of temporal dependence is often based on AR models. In contrast, nonlinear approaches mainly involve copula-based models (see Section 3.2.1). In space, the decoupling hypothesis is often employed, when linear models are considered for temporal representations.

This enables representing spatial and temporal dependencies separately (see Serinaldi and Kilsby, 2017). If linear representation for temporal dependence is considered, the spatial dependence between residuals of local AR models can be then represented either through linear (i.e. Linear Regression; LR) or nonlinear (i.e. bivariate copulas) representations. If a nonlinear representation is chosen for temporal dependence, then the spatial dependence is either represented implicitly without direct representation of temporal dependencies between two or more sites, or explicitly through a full representation of regional spatiotemporal dependencies (see Section 3.2.2). In this study, we set up different modeling hypotheses on the basis of mixing-and-matching different linear and nonlinear representations together. Below, we briefly outline the methodological elements for developing such parametric representations. The specific modeling hypotheses and the details of benchmarking procedure used in this study are discussed in Section 3.3 below.

3.2.1. Linear and nonlinear representations of temporal dependencies

The linear representation of temporal dependence starts with standardization and deseasonalization of the streamflow time series. The standardized and deseasonalized streamflow data are then modeled using an AR(1) model. In multisite settings, the residuals of AR(1) developed at each site and time step are temporally independent but spatially dependent. These residuals can further be modeled using LR or multivariate copulas, which will be discussed in Section 3.2.2.

The lag-1 temporal dependence can be also represented using bivariate copulas that can characterize the joint streamflow distribution between consecutive time steps in a "nonlinear" (more accurately, not necessarily linear) manner. Based on Sklar's theorem (Sklar, 1959), if u and v are two continuous random variables (here streamflow at two consecutive time steps) with marginal Cumulative Distribution Functions (CDFs) of $F(u)$ and $F(v)$, the joint cumulative distribution of $F_{U,V}(u, v)$ can be described as:

$$F_{U,V}(u, v) = C(u, v) \tag{3.1}$$

where C denotes the copula function. u and v are two random variables, sampled from marginal streamflow distributions at two consecutive time steps at the reach p, i.e., $u = F(Q_t^p)$ and $v = F(Q_{t+1}^p)$. Having the CDF of flow at the time step t and the joint copula function estimating the dependence between flows at time steps t and $t + 1$, the probability distribution of flow at the next time step $t + 1$ can be calculated by (Nazemi et al., 2013, 2020):

$$C(v|u = u^*) = P\{F(Q_{t+1}^p) \leq v | F(Q_t^p) = u^*)\} = \frac{\partial}{\partial v} C_{t,t+1}(u, v) \tag{3.2}$$

where $C_{t,t+1}$ is the bivariate copula function between consecutive $CDFs$ at time steps t and $t + 1$, Q_t^p is the sampled flow at time step t in the reach p, Q_{t+1}^p is the sampled flow at time step $t + 1$, P is the conditional CDF and $C(v|u = u^*)$ is the conditional copula. Having the conditional bivariate copula, the flow at the time step $t + 1$ can be calculated as:

$$Q_{t+1}^p = F^{-1}\left\{C^{-1}(v|u = u^*)\right\} \tag{3.3}$$

Despite the variety of parametric copula functions (see Plackett, 1965; Clayton, 1978; Genest 1987; Joe, 1997; Nelsen, 2007; Renard and Lang, 2007), the procedure described above provides a generic scheme for single-site streamflow stochastic streamflow generation. Note that for each consecutive sub-annual time step, a specific bivariate copula should be identified to represent intra-annual variability in the temporal dependence structure.

3.2.2. Linear and nonlinear representations of spatial dependencies

Representing spatial dependence particularly matters for multisite stochastic streamflow generation. Spatial dependence between two streams can be represented either through the dependence between the residuals of AR models developed at each stream, or through a direct transformation of streamflow from a donor stream (hereafter a *primary*) to a receiver reach (hereafter a *secondary*). Both conceptualizations can be represented using linear and non-linear parametric models. In linear representation, the residual of AR models in the primary site is used to estimate the residual of the AR model at a secondary site using a LR scheme. If the direct transformation is sought, then the streamflow generated at a primary site is directly transferred to the secondary site using a set of LR models identified at each sub-annual time step – see Nazemi and Wheater (2014b) for details.

Similar to representing temporal dependence using copula, the spatial dependence can be reconstructed based on conditional resampling from the joint distribution of streamflow at primary and secondary sites. Two assumptions can be made for building up the joint distributions. First, it can be assumed that the flow at the secondary site and at each time step can be adequately simulated using the joint distribution of flow at primary and secondary sites and the flow in the primary site. This requires implementing bivariate copulas without direct representation of lag-1 temporal dependencies at the secondary site. Here we term this representation as the *implicit* approach as the temporal dependence in the secondary site is not directly represented. Implementing bivariate copulas for representing spatial dependence is very similar to the lag-1 temporal dependence outlined above. In this case, bivariate copulas can describe the joint spatial dependence as:

$$F_{U,W}(u,w) = C'(u,w) \tag{3.4}$$

where $u = F(Q_t^p)$ and $w = F(Q_t^s)$ are the corresponding $CDFs$ at the primary and secondary reaches at time step t, respectively. Knowing the marginal CDF of the flow at the primary site and the copula function $C'(u,w)$, the flow quantile at secondary site can be sampled as:

$$C'(w|u = u^*) = P\{\left(F(Q_t^s \leq w \big| \left(F(Q_t^p) = u^*\right)\right\} = \frac{\partial}{\partial u} C'_{t,t}(w,u) \tag{3.5}$$

where $C'_{t,t}$ is the bivariate copula function between flow $CDFs$ at the identical time step t, Q_t^p is the sampled flow at time step t in the primary site p, Q_t^s is the sampled flow at time step t in the secondary site s, P is the conditional CDF and $C'(w|u = u^*)$ is the conditional copula. Accordingly, flow at time step t can be calculated from inverse function as follows:

$$Q_t^s = F_{s,t}^{-1}\{C'^{-1}(w|u = u^*)\} \tag{3.6}$$

which means that by having the marginal flow CDF u at each time step t in the primary site, the flow at the identical time step t at the secondary sites can be calculated using the conditional probability distribution, inferred from the bivariate copula function.

More appealing representation can be based on the joint distribution of flows at the primary and secondary site at the same time step and streamflow at the secondary site at the previous time step using trivariate copulas. We call this representation the *explicit* approach as the temporal dependence in the secondary site is directly represented. In order to establish trivariate joint distributions, two distinct methodologies can be used. The first approach is based on Vine copulas, which is a generic approach to construct high-dimensional joint distribution by using a cascade of parametric bivariate copulas as building blocks (see Bedford and Cooke, 2001; Joe, 1997; Aas et al., 2009). This approach is further used by Chen et al. (2015; 2019) for streamflow reconstruction. In this case, a trivariate copula is decomposed into a product of three bivariate copulas, in which parameters of each bivariate copula structure can be estimated separately. Having flow distributions at the primary site at time $t + 1$, $v = F(Q_{t+1}^p)$, and the flow at time step $t + 1$, $w = F(Q_t^s)$, and flow at a secondary site at time $t + 1$, $z = F(Q_{t+1}^s)$ then the joint distribution between v, w, and z can be described as:

$$f(v, w, z) = f_1(v)f_{2|1}(w|v)f_{3|1,2}(z|v, w) \tag{3.7}$$

where the subscripts 1, 2, and 3 correspond to Q_{t+1}^p, Q_t^s, and Q_{t+1}^s, respectively. Based on the Sklar's theorem and applying the joint distribution for C-vine copula as described in Bedford and Cooke (2001), we can express the conditional distributions in Eq. (7) as:

$$f_{2|1}(w|v) = \frac{f(w, v)}{f(v)} = \frac{c_{1,2}\big(F_1(v), F_2(w)\big)f_1(v)f_2(w)}{f_1(v)} = c_{1,2}\big(F_1(v), F_2(w)\big)f_2(w) \tag{3.8}$$

and

$$\begin{aligned} f_{3|1,2}(z|v, w) &= \frac{f(w, z|v)}{f(w|v)} = \frac{c_{2,3|1}\big(F(w|v), F(z|v)\big)f(w|v)f(z|v)}{f(w|v)} \\ &= c_{2,3|1}\big(F(w|v), F(z|v)\big)c_{1,3}\big(F_1(v), F_3(z)\big)f_3(z) \end{aligned} \tag{3.9}$$

Consequently, the three dimensional joint density in Eq. (7) can be represented in terms of three bivariate copulas $C_{1,2}$, $C_{1,3}$, and $C_{2,3|1}$ with densities $c_{1,2}$, $c_{1,3}$, and $c_{2,3|1}$ as below:

$$f(v, w, z) = f_1(v)f_2(w)f_3(Q_t^A)c_{1,2}\big(F_1(v), F_2(w)\big)c_{1,3}\big(F_1(v), F_3(z)\big)$$
$$c_{2,3|1}\big(F(w|v), F(z|v)\big)$$

(3.10)

Having the joint distribution from Eq. (10), the conditional distribution function of $(z|v, w)$ can be obtained by applying the h-function recursively (Aas et al., 2009; Czado et al., 2012) as:

$$h = F(z|v, w) = \frac{\partial C_{2,3|1}\big(F(z|v), F(w|v)\big)}{\partial F(w|v)}$$

(3.11)

In which $F(z|v) = h(z|v) = \frac{\partial c_{3,1}(F(z),F(v))}{\partial F(v)}$ and $F(w|v) = h(w|v) = \frac{\partial c_{2,1}(F(w),F(v))}{\partial F(v)}$. Consequently, the Eq. (11) can be rewritten as:

$$h = F(z|v, w) = h[h(z|v)|h(w|v)]$$

(3.12)

Accordingly, knowing the states of $v = F(Q_{t+1}^p)$, and $w = F(Q_t^s)$, flow at secondary site s at time step $t + 1$ can be calculated. This can be achieved by estimating the inverse of h-function, given uniform random numbers of ε as follows:

$$Q_{t+1}^s = F^{-1}\left\{h^{-1}\left[\left(h^{-1}\big(\varepsilon|h(w|v)\big)\right)|v\right]\right\}$$

(3.13)

Another way to represent the dependence in higher dimensions is using multivariate Archimedean copulas, most notably the Exchangeable Archimedean Copula (EAC; Nelsen, 1999; Joe, 1997), for which the copula function has the form:

$$C^{"}(v, w, z) = \phi\{\phi^{-1}(v) + \phi^{-1}(w) + \phi^{-1}(z)\},$$

(3.14)

$$\phi: [0, \infty] \to [0, 1] \quad and \quad v, w, z \in [0, 1]^3$$

where the $\phi(.)$ is a generating function of copula defined in the range of zero to one, is monotonically decreasing and $\phi(1) = 0$. $\phi(.)$ is a copula generator of a copula function in a particular dimension d (here $d = 3$) if any only if $(-1)^k \phi^k(t) \geq 0$ for all $k \in \{0, ..., d-2\}$, $t \in (0, \infty)$, and $(-1)^{d-2}\phi^{d-2}(t)$ is decreasing and convex on $(0, \infty)$ – see McNeil and Nešlehová (2009) for more details. Similar to Eq. (7), the joint distribution between CDF of flows, v, w, and z can be expressed by $C^{"}$ in Eq. (14) and the flow each time step $t + 1$, Q_{t+1}^s can be sampled from the copula space by getting the inverse function in Eq. (14) – see Whelan (2004) for the sampling procedure over the copula space.

Besides many useful properties such as an explicit functional form and different types of tail dependence, one main drawback of EACs is their symmetry. To overcome this shortcoming, Nested Archimedean Copulas (NACs; a.k.a. Hierarchical Archimedean Copulas) are suggested, allowing for asymmetry in the dependence structure. Introduced by Joe (1997), NACs are

favourable as they are structurally simple and are easy to interpret (see Embrechts et al., 2001; Savu and Trede, 2006). Having the marginal CDF of flows, v, w, and z, NAC can be defined as:

$$C'''(v, w, z) = \psi_0 \left(\psi_0^{-1}(v) + \psi_0^{-1} \left(\psi_1 \left(\psi_1^{-1}(w) + \psi_1^{-1}(z) \right) \right) \right) = \tag{3.15}$$

$$C'''(v, C(w, z; \psi_1); \psi_0)$$

where ψ_0 and ψ_1 are the generators of copulas with two levels of hierarchies. w and z are first coupled through ψ_1, and then w and z with v through ψ_0. Having the joint distribution described by copula function C in Eq. (15) the flow at time step $t + 1$ can be obtained from the inverse function as explained in Eq. (10) – see Whelan (2004) and Berg and Aas (2007) for further details on sampling procedure using EACs and NACs.

3.3. Experimental setup and case study

To generate different hypotheses for representing dependencies, we mix-and-match different linear and nonlinear models. In total, seven schemes are considered, ranging from a fully linear to a fully nonlinear representation. Table 1 introduces these schemes, labeled from M1 (the fully linear scheme) to M7 (the fully nonlinear scheme). In M1 and M2, an AR(1) model is employed to represent the temporal dependence. For the spatial dependence, M1 uses an LR to model the residual, whereas M2 implements a bivariate copula on the residuals of the AR(1) model. Both M1 and M2 have been widely used for stochastic generation of hydroclimatic variables (see e.g., Salas and Pegram, 1977; Salas et al., 1985; Bárdossy and Pegram, 2009; Serinaldi and Kilsby, 2017). M3 is the combination of a bivariate copula for representation of temporal dependency and a series of LR for spatial extension scheme, developed by Nazemi et al. (2013) and implemented in Hassanzadeh et al. (2015, 2017). Similarly in M4 to M7, bivariate copulas are used for modeling the temporal dependency at a primary site, and their differences are in the ways that the spatial extension to a secondary site takes place. M4 is after the scheme developed in Nazemi et al. (2020), in which a bivariate copula transfers the flow from each time step of a given primary stream to a secondary reach. Both M3 and M4 focus on representing spatial dependence and ignore the explicit representation of temporal dependence in secondary sites. In M5 to M7, representations of temporal and spatial dependencies in secondary sites are coupled. M5 uses vine copulas after the scheme suggested by Chen et al., (2015, 2019). M6 and M7 employ EAC and NAC, respectively.

To benchmark the skills of the considered representations, we focus on 12 natural streams, located in six catchments across southern Canada – see Figure 3.1. Each catchment includes two natural streams, for which the daily flow data from 1981 to 2010 are obtained from Water Survey of Canada's Canadian Reference Hydrometric Basin Network (RHBN; Brimley et al., 1999). These streams are characterized by relatively pristine and stable land use conditions, and therefore, can provide ideal testbeds for assessing how different representations can portray the "*hydrologic reality*" in the absence of major anthropogenic interventions. Each catchment is chosen in a way

that represents a particular flow regime (nival, mixed, and pluvial) and catchment size (large and small) in Canada – see Zaerpour et al. (2021a) for a comprehensive reflection on Canadian natural streamflow regimes and their recent changes.

Table 3.1. The seven parametric hypotheses considered for modeling spatiotemporal dependencies in streamflow series along with their notation and source M1 to M7.

Single site	Multisite (Secondary site)		Notation	Reference
Temporal dependence	Temporal dependence	Spatial dependence		
Autoregressive (lag-1)	Autoregressive	Linear Regression	M1	Salas and Pegram (1977)
	Autoregressive	Bivariate copula	M2	Serinaldi and Kilsby (2017)
Bivariate copula	Implicit (not represented parametrically)	Linear Regression	M3	Nazemi et al. (2013)
		Bivariate copula	M4	Nazemi et al. (2020)
	Explicit (coupled with spatial dependence)	Vine copula	M5	Chen et al. (2019)
		Exchangeable Archimedean copula	M6	Aas and Berg (2013)
		Nested Archimedean copula	M7	Grimaldi and Serinaldi (2006) Wang et al. (2018)

Table 2 introduces these stations based on their location, size, and regime types according to the classification of Burn and Whitfield (2017). Each station is identified by a pair number *Cxy*, in which *x* represents the catchment type (i.e. 1 to 6; see Table 2) and *y* whether the stream is primary or secondary (i.e. 1 or 2). Temporal dependencies in primary streams are stronger and explicit representations in these streams are essential. Our benchmarking exercise attempts to address (1) how the skills of different representations vary across flow regimes, i.e. nival, mixed and pluvial; (2) how the skills of different representations vary across catchment sizes, i.e. large *vs.* small; and (3) how the skills of different representations vary across time scales, i.e. daily, weekly and monthly. The performance of different parametric representations across each condition are assessed in terms of reconstructing long-term streamflow characteristics, including annual volume, annual peak volume and timing, low-, mid-, and high-flow quantiles, proxied by Q10, Q50, and Q90, along with the short-term temporal (lag-1) and instantaneous spatial (lag-0) dependencies.
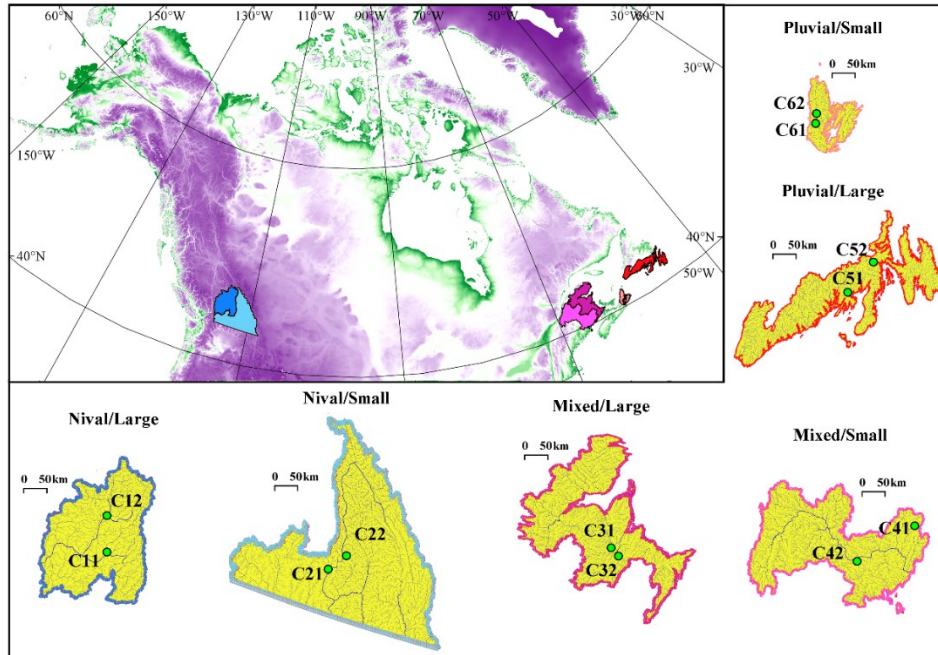
Figure 3.1. The locations of the six Canadian catchments and the two streams considered in each catchment. Catchments are picked according to flow regimes (three types of nival, mixed, and pluvial)) and catchment sizes (two types of small and large); see Table 2 below for the information related to the considered streams.

Table 3.2. Hydrometric stations considered, along with their formal identifiers and notations in this study.

Catchment type		Station ID	RHBN ID	Station Name (and province)	Area (km²)	Lat (N)	Long (W)
Regime	Size						
Nival	Large	C11	08LD001	Adams River near Squilax (BC)	3,210	50.9	119.7
		C12	08LA001	Clearwater River near Clearwater (BC)	10,300	51.7	120.1
	Small	C21	08NE077	Barnes Creek near Needles (BC)	204	49.9	118.1
		C22	08NE006	Kuskanax Creek near Nakusp (BC)	330	50.3	117.7
Mixed	Large	C31	01BP001	Little Southwest Miramichi River at Lyttleton (NB)	1,340	46.9	65.9
		C32	01BO001	Southwest Miramichi River at Blackville (NB)	5,050	46.7	65.8
Mixed	Small	C41	01AP002	Canaan River at East Canaan (NB)	668	46.1	65.4
		C42	01AK001	Shogomoc Stream near Trans Canada Highway (NB)	234	45.9	67.3
Pluvial	Large	C51	02ZF001	Bay Du Nord River at Big Falls (NS)	1,170	47.8	55.4
		C52	02ZH001	Pipers Hole River at Mothers Brook (NS)	764	48.0	54.3
Pluvial	Small	C61	01FB003	Southwest Maragaree River near Upper Maragaree (NL)	357	46.2	61.1
		C62	01FB001	Northeast Maragaree River at Margaree Valley (NL)	368	46.4	61.0

We consider three commonly used copulas, namely Frank, Clayton, and Gaussian copulas for setting up different schemes presented in Table 1 – see Nelsen (2007) for more information on these copula functions. These three parametric copulas are chosen as they can represent a wide

range of statistical dependencies (Genest and Favre, 2007). We use empirical distributions for marginal representations for both primary and secondary sites; therefore, any difference between various schemes can be attributed to the choice of copula function. All copula functions are parameterized using the maximum pseudo-likelihood (e.g. Dupuis 2007; Wang et al., 2009). We also perform some initial experiments to choose the best copula structure at the weekly time scale. In this particular timescale, it is found out that Frank copula is the best copula among the three considered copulas in capturing the observed temporal and spatial dependencies. We, therefore, implement Frank for setting up all schemes and across all timescales; so that any potential due to changing the copula function is canceled. Considering each scheme, we generate 100 ensembles each include 100 realizations to account for uncertainty in both skills and sampling according to the procedure presented in Nazemi et al. (2020). The expected value of each ensemble is the representative scheme skill, and the range of 100 expected values produced by 100 ensembles is the representative uncertainty related to each scheme. The differences in the skills of different schemes can be formally assessed using the Analysis of Variance (ANOVA) with Bonferroni correction test (Bland and Altman, 1995).

3.4. Results

We first assess the effect of different representations of temporal dependence on the skill in reconstructing flow characteristics at primary sites. Table 3 summarizes the results in which the expected mean errors in reconstructing different flow characteristics by AR(1) and Frank copula models in the primary stream across the six catchments and the three timescales considered. Significant differences between the skills of AR and copula models are formally addressed using the ANOVA test with Bonferroni correction. Note that significant pairwise differences at p-value=0.05 are bolded in Table 3. The result shows that in ≈92% of comparison cases, linear and nonlinear representations of temporal dependencies result in similar skills in reconstructing long-term streamflow characteristics. No significant difference between linear and nonlinear representations is seen in the monthly timescale across all catchments. In the finer weekly and daily scales, there is also no significant difference in terms of reconstructing temporal dependencies as well as flow quantiles in all streams. Considering annual flow volume, few differences can be seen at weekly and daily timescales, in which AR(1) model consistently outperforms the skill of bivariate Frank copula. Considering the timing of the annual peak, differences are seen at the daily scale across two catchment types, in which copula-based representations consistently provide a better skill. Similar conclusions can be made for the skill in representing the annual peak, in which Frank copula consistently provides better performance than the AR model.

Table 3.3. Comparison between the skills of linear and nonlinear representations of temporal dependencies, delivered by AR(1) and Frank copula models, in terms of the expected mean errors in reconstructing key characteristics of primary streams during the period of 1981 to 2010. For each error characteristic, the significant differences between AR(1) and copula models are bolded.

Expected mean error in	Timescale	C11 (Nival/Large)		C21 (Nival/Small)		C31 (Mixed/Large)		C41 (Mixed/Small)		C51 (Pluvial/Large)		C61 (Pluvial/Small)	
		AR	Copula	AR	Copula	AR	Copula	AR	Copula	AR	Copula	AR	Copula
Volume (MCM)	monthly	0.11	1.28	0.00	0.11	0.00	0.56	0.00	-0.09	0.00	1.42	0.00	0.10
	weekly	**0.12**	**6.42**	0.00	-0.82	**0.00**	**9.03**	0.00	0.55	0.81	1.48	0.00	-0.68
	daily	**1.78**	**9.42**	0.14	2.00	1.16	3.68	**0.13**	**8.90**	**-0.16**	**5.56**	0.12	1.79
Timing of Peak (Timescale)	monthly	0.05	0.06	-0.10	-0.05	-0.07	-0.04	0.11	0.14	-0.25	-0.12	-0.12	0.12
	weekly	-0.02	0.03	0.25	0.10	0.45	0.72	-0.92	-0.30	-2.26	-2.40	0.53	0.92
	daily	-0.44	0.41	4.28	5.15	**-2.27**	**0.45**	-7.15	-8.87	-10.25	-10.67	**1.93**	**-2.44**
Peak (CMS)	monthly	0.48	1.24	-0.45	0.02	-3.69	2.63	-0.22	-0.16	-3.33	-1.57	-1.06	-0.73
	weekly	-4.16	4.04	-3.30	-1.79	**-11.28**	**-2.05**	-2.32	-1.13	**-11.59**	**-4.35**	-1.75	-1.04
	daily	-3.48	3.45	-4.84	-2.04	**-8.15**	**0.56**	-4.74	-3.17	8.54	9.04	-1.67	0.05
Q90 (CMS)	monthly	-1.79	-0.47	0.13	0.06	2.45	1.25	0.00	-0.09	-0.21	0.12	-0.56	-0.51
	weekly	0.62	1.07	0.69	0.27	4.00	2.87	0.41	0.14	1.85	1.68	-0.30	-0.45
	daily	0.33	0.52	0.72	0.54	2.73	4.07	0.59	0.63	1.42	1.72	-0.02	-0.18
Q50 (CMS)	monthly	0.18	-0.41	0.05	0.04	-0.91	-0.73	0.05	0.05	0.16	0.27	0.09	0.18
	weekly	-0.40	-0.76	0.06	0.04	-0.64	-0.28	0.06	0.09	0.56	0.59	0.24	0.28
	daily	-0.30	-0.50	0.04	0.04	-0.44	-0.45	0.09	0.17	0.26	0.94	0.10	0.32
Q10 (CMS)	monthly	-0.44	0.19	-0.04	-0.01	-0.25	-0.08	-0.05	-0.05	0.29	0.89	0.07	0.04
	weekly	-0.29	0.54	-0.06	-0.02	-0.29	-0.04	-0.07	-0.04	0.05	0.43	0.12	0.16
	daily	-0.24	0.33	-0.08	-0.05	-0.35	-0.02	-0.06	-0.01	-0.22	0.12	0.04	0.09
Lag-1 temporal dependence (-)	monthly	-0.05	-0.01	-0.02	0.00	-0.01	0.01	0.01	0.01	-0.02	0.00	-0.03	0.00
	weekly	-0.04	-0.02	-0.04	-0.02	-0.03	-0.01	-0.03	-0.01	-0.03	-0.01	-0.03	-0.02
	daily	-0.02	-0.02	-0.03	-0.02	-0.04	-0.02	-0.04	-0.02	-0.04	-0.03	-0.03	-0.03

As the results of the linear and nonlinear representations of temporal dependencies at the primary sites are quite comparable, from now on we only focus on the intercomparison of skills in different schemes at secondary sites. Below, we only intercompare the results in a weekly timescale. We then address the deviations in our findings in case the timescale becomes finer (i.e. daily) or coarser (i.e. monthly) in the Discussion section.

Figure 3.2 summarizes the results for reconstructing the annual volume across the six catchments considered. From the left to the right, columns are related to nival, mixed and pluvial regimes, respectively. The top and bottom rows correspond to the large and small basins, respectively. In each panel, relative deviations from the expected annual volume are shown for the considered seven schemes, ordered counterclockwise. Perfect, underestimated, and overestimated fits are identified by relative deviation of 1, <1 and >1, respectively. Blue boxes show the interquartile ranges obtained from 100 ensembles, each with 100 realizations. The interquartile range is a robust measure of sampling uncertainty (Lee and Salas, 2011). Dark blue lines are the expected skill calculated by the mean of the boxplots.

In the Nival/Large (N/L) stream, all seven models can capture the expected relative volume within the interquartile range with less than 1% mean expected Relative Error (RE). Having said that, M1 and M2 can reconstruct the observed expected annual volume with much less uncertainty. A similar conclusion can be considered in the Nival/Small (N/S) reach, although the mean expected REs can be slightly higher than the N/L stream. In streams with a mixed regime, i.e., Mixed/Large (M/L) and Mixed/Small (M/S), M1 to M5 can capture the expected annual volume with REs less than 2%. M6 and M7 however consistently underestimate the expected annual volume and the rate of bias is more in the M/S stream. A similar conclusion can be made for pluvial streams, i.e. Pluvial/Large (P/L) and Pluvial/Small (P/S). Again, M1 to M5 can capture the observed long-term annual volume with REs less than 2% in both large and small basins. M6 and M7 are not able to provide unbiased estimates of the long-term annual volume, and the rate of bias is slightly more in the small compared to the large basin.

We also investigate the performance of the seven considered schemes in reconstructing the expected peak characteristics, i.e., the expected timing and magnitude of the annual peak. Figure 3.3 summarizes the results at the secondary reaches across the considered six basins. Green and grey lines show the interquartile ranges of expected errors for magnitude and timing of the peak, respectively and black dots depict mean expected errors. The red dots are the centers of the origin, showing the location of an ideal model with zero errors. The closer the black dots are to the red dots, the better the skill is in capturing the expected peak characteristics. The results in general show the relative dominance of M5. In the N/L reach, the absolute error in capturing the expected timing of peak using all schemes are less than 0.5 week. Associated REs in capturing the expected magnitude of the annual peak is also low, i.e. less than 5%, with M5 showing a better skill, i.e. $RE \approx 0.5\%$. The same conclusion can be made in the considered N/S reach, and M5 shows better skills in reconstructing the expected timing and magnitude of the annual peak flow. In the considered M/L reach, M1 to M5 can

represent the timing of peak with less than 0.5 week error, but M5 outperforms others both in terms of reconstructing the timing and magnitude of the annual peak. In the considered M/S reach, M5 is the only scheme that can represent the peak characteristics within it interquartile range, with less than 0.5 week expected error in representing the timing and RE of 1.2% in representing the magnitude of the expected annual peak. In the P/L reach, only M1, M2, M6, and M7 can capture the expected timing of peak within their interquartile range; however, when looking at the magnitude of the peak, M5 shows a better skill with RE of 5.7%. In the P/S reach, again M5 outperforms other schemes and can capture both peak timing and magnitude within its interquartile range, with an expected error less than 0.5 week in the timing of the peak and REs of 6.7% in representing the magnitude of the expected annual peak.
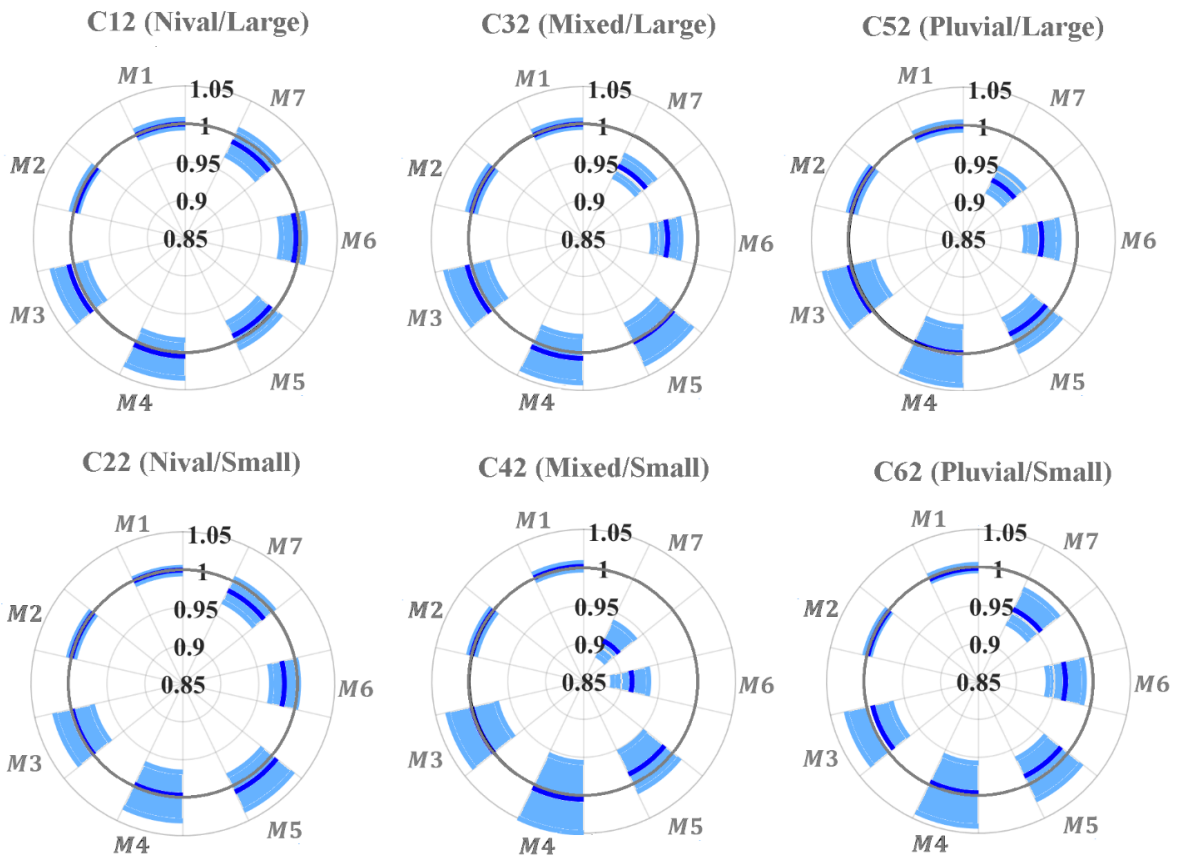
Figure 3.2. The expected deviations from reconstructing the observed long-term annual volume using the seven schemes (M1 to M7) and across secondary sites of the six catchments types considered. The streamflow series generated through random resampling of 100 ensembles, each with 100 realizations Each box represents the interquartile range of expected error obtained from 100 ensembles. The mean expected error is shown in dark blue line. The closer the box to 1, the better performance in capturing the expected volume.

In parallel, we assess the skill of each scheme in capturing the expected annual low (Q10), mid (Q50), and high (Q90) flow quantiles. Figure 3.4 summarizes the findings with respect to the differences in the three expected quantiles using seven models across the secondary sites in the six catchment types considered. The solid lines are the non-exceedance probability of the observed flow.

In each panel, the left, the middle, and the right boxplots refer to the expected reconstructed values of Q90, Q50, and Q10 respectively obtained through 100 ensembles. The corresponding observed values are shown with black dots.
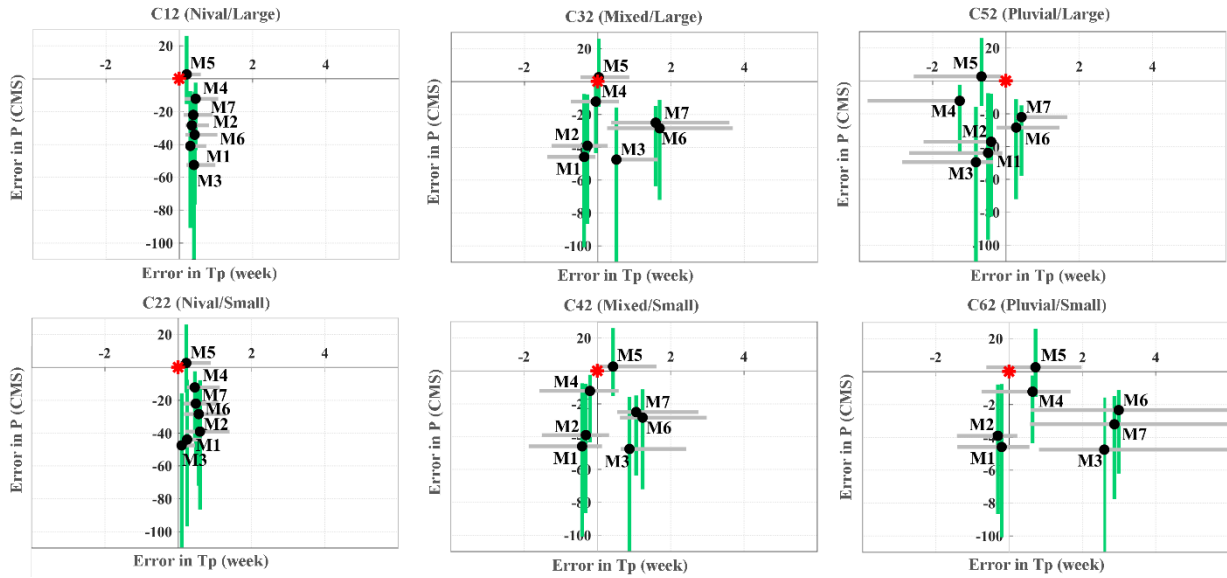
Figure 3.3. The error in representing expected annual peak flow characteristic, i.e., timing and magnitude of peak. The streamflow series generated through random resampling of 100 ensembles, each with 100 realizations using M1 to M7 schemes. Each pairs of grey and green lines represent interquartile ranges for expected errors in capturing timing and magnitude of the peak, respectively; and the black dots show the mean of expected errors. The closer the mean expected errors are to centers of origin identified by red dots, the better the skills of models are in capturing expected peak characteristics.

In the N/L stream, all settings can capture the observed long-term Q50 within their interquartile range. Having said that, only M5 captures the long-term Q10 with $RE \leq 5\%$. In terms of Q90, M5 dominates other copula-based representations with $RE \approx 1\%$. In the N/S stream and for Q50, again copula-based schemes are able to represent the observed value in the interquartile range, but M6 and M7 dominate other models due to lower REs. For high and low flow quantiles, M4 (with REs of 2% and 0.4% respectively). In the considered M/L reach, only M6 and M7 are able to reconstruct the long-term quantiles with REs of 3% and 1% for Q50, as well as 2% and 1% for Q90, respectively. Having said that, none of the considered schemes are able to capture the observed Q10 within their interquartile range. In the M/S stream, M4 and M5 can represent the observed Q90 value in the interquartile range with REs of $\approx$1.3% and $\approx$2.4%; however, for Q50 and Q10, none of the schemes are able to capture the observed value within their interquartile ranges, although M5 still provides a relatively higher skills compares to others, particularly with regard to Q50. In the P/L stream, M1 and M2 show better skills in capturing the flow quantiles with REs being 1% and 3%, and 6% for Q90, Q50, and Q10, respectively. This is the case in the P/S stream, where M1 and M2 outperform other schemes with REs of around 1%, 2.5%, and 4.6% regarding high, mid, and low flow quantiles.
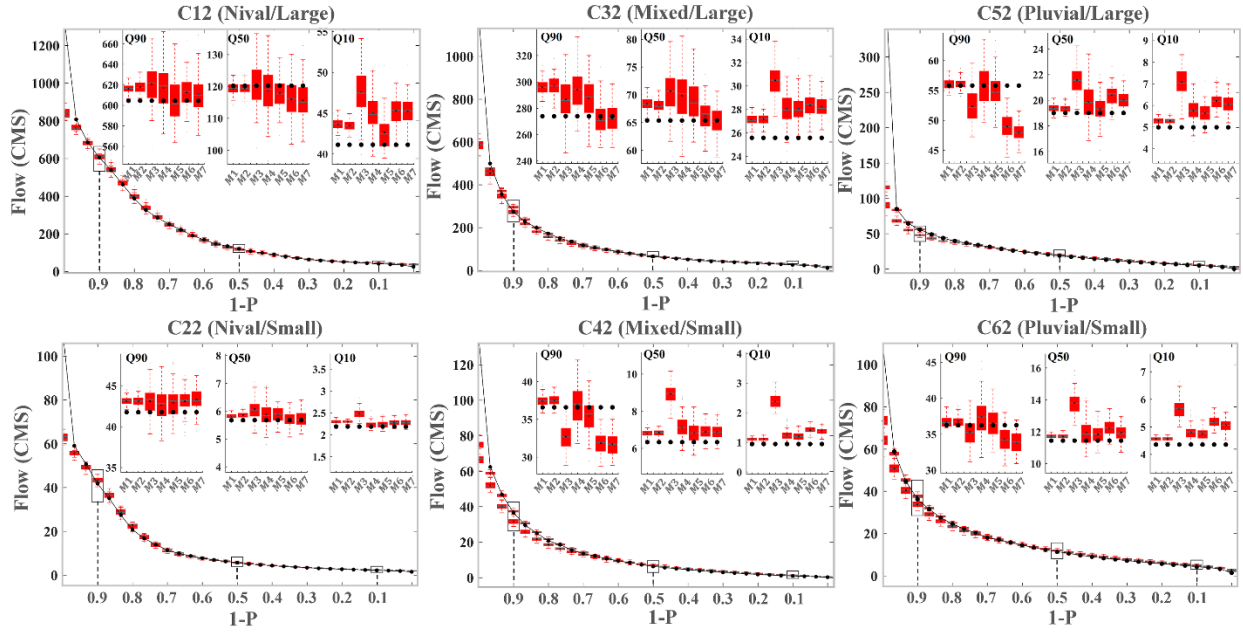
Figure 3.4. Errors in representing low, mid and high flow quantiles (i.e. Q10, Q50 and Q90 at the secondary streams across the six catchment types considered. Boxplot show the expected flow quantiles reconstructed by resampling of 100 ensembles, each with 100 realizations using M1 to M7 schemes. The historical values are shown in black dots.

In order to evaluate the skills in preserving the dependence structure, the performance in capturing the lag-1 temporal dependence in the secondary sites as well as the lag-0 spatial dependence between primary and secondary sites are evaluated. Figure 3.5 summarizes these analyses by measuring Kendall's tau, shown by red and blue boxplots, respectively. In the N/L reach, M1 outperforms other schemes in terms of temporal dependence. In terms of spatial dependence, copula-based schemes show better skills in capturing the observed dependence. In the N/S reach, only M5 can capture the observed lag-1 dependence within the interquartile range. Another copula-based model, i.e. M4, shows better skills in representing the spatial dependence. In the considered M/L stream, only M3 and M4 can respectively capture observed temporal and spatial dependencies within their interquartile range. In the M/S basin, M1 and M4 can capture the lag-1 and lag-0 dependencies within their interquartile range. In the P/L and P/S stream, M1 again outperforms other models in terms of lag-1 temporal dependence. Regarding lag-0, only M2 and M4 are capable to capture observed values in their interquartile range.
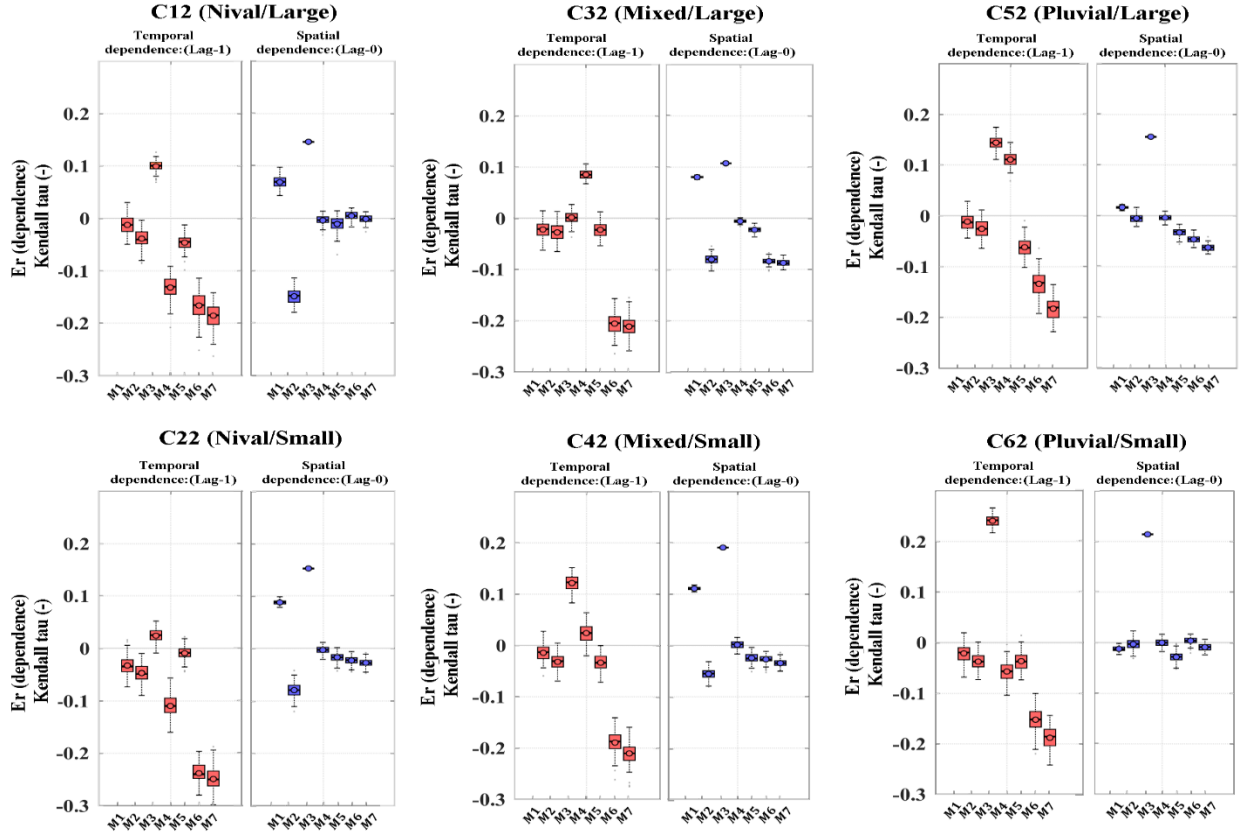
Figure 3.5. The error in representation of lag-1 temporal and lag-0 spatial dependencies, shown by red and blue boxplots respectively. The streamflow series, from which the temporal and spatial dependencies retrieved, are generated through random resampling of 100 ensembles, each with 100 realizations using M1 to M7 schemes across six catchment types.

3.5. Discussion

The results provided in Section 3.4 are only relevant at the weekly scale and therefore it is necessary to investigate the sensitivity of our findings in other temporal scales. Here we repeat the above experimentations in coarser (monthly) and finer (daily) scales and explore the expected accuracy and uncertainty in reconstructing the streamflow characteristics across the six catchments types considered. The findings of these analyses are summarized in Figs. B1 and B2 in the Appendix B. Similar to the experimentation made at the weekly scale, we generate 100 ensembles, each including 100 realizations using all seven schemes at the daily and monthly scales. We estimate the skill and uncertainty using the mean and standard deviation of the expected error obtained from the expected error estimates of 100 ensembles. In both figures, the green, red and blue lines represent the monthly, weekly, and daily statistics, respectively. In terms of expected annual volume, M1 to M5 schemes can capture the expected annual volume with RE of less than 3% in all timescales considered, while M6 and M7 are only skillful at the monthly scale. Looking at the standard deviation, however, M1 and M2 show significantly lower uncertainty than other schemes. In terms of the expected timing of the peak, M5 shows a better skill in capturing the observed value with less than 2 days absolute error

in N/L and N/S reaches regardless of the timescale considered. In the mixed and pluvial reaches, however, the skill of M1 and M2 outperforms other schemes, except in the considered P/S basin in which M6 and M7 show better skills. Uncertainty in estimating the timing of the peak increases, as the timescale gets finer. In terms of the magnitude of the peak, M5 shows the best skill on the monthly and weekly scales with the average RE of respectively 1% and 3.4% across the six catchments considered. M6, however, shows better skill in N/L in the daily scale with a RE of 3.1%. In N/S, mixed, and pluvial reaches, M4 outperforms other models with a RE of 4%. Similar to the expected timing of the peak, the uncertainty bounds expand at finer timescales.

Regarding flow quantiles, the skills of considered schemes are variant in different timescales, flow quantiles, and catchment types. In terms of expected Q90, M5 outperforms other schemes at the monthly scale and across all catchments. At the weekly and daily timescales, M5 shows better skill in the N/L reach with RE ≤ 2.1%. In N/S, M4 outperforms other schemes at the weekly and daily timescale with an average RE of 3.1%. In the M/S and pluvial reaches, M1, M2, and M4 show better performance with average RE of less than 2.4%, 2.1%, and 2.0%, respectively. The uncertainty bounds in representing expected Q90 expand at the finer timescales. For Q50 again M5 outperforms other models at monthly, weekly, and daily scales with expected REs of 1.6%, 1.9%, and 2.1% across the considered scales, respectively. For the Q90 and in the N/L reach, the uncertainty bounds expand as the timescale gets finer. In other reaches, a mixed pattern can be observed with the least uncertainty in the monthly scale across different reaches. For Q50 and in the N/L, the least uncertainty is observed at the monthly scale. In other reaches, however, a mixed pattern is observed. For Q10 as well, M5 outperforms other schemes with average REs of less than 2%, across daily, weekly and monthly scales. The largest uncertainty bounds in estimating low flow quantiles are in contrast observed at the monthly scale except in the considered N/L reach. The least uncertainty bounds are related to the M1 and M2 across different reaches. In terms of lag-1 temporal dependence and at monthly scale, M1, M2, and M5 outperform other schemes with less than 0.05 absolute errors across all timescales. In terms of lag-0 spatial dependence and in the monthly scale, M4, and M5 can well capture the observed value with less than 0.01 absolute error. The uncertainty bounds for the lag-1 temporal and lag-0 spatial dependencies mostly increase at coarser timescales. M3 and M5 exhibit the lowest uncertainty for lag-1 temporal dependence. M3 also has the lowest uncertainty for the lag-0 spatial dependence.

The divergent results seen across different timescales and catchment types are mainly due to various mechanisms that dominate streamflow generation across timescales, catchment sizes, and regime types; and hence, the suitability of different schemes changes. As a result, the choice of the appropriate scheme becomes somehow case dependent. However, to provide a general guideline on the choice of model in each specific condition, we rank the models based on their expected skills using the results provided in Fig. B1 in the Appendix B. Fig. 3.6 displays the ranking of the seven considered schemes in capturing the eight long-term characteristics of streamflow series across the six different catchment types and the three timescales considered. Long-term streamflow characteristics are placed counterclockwise, and schemes are identified with colored dots. Linear-based schemes (i.e., M1 and M2) are shown with shades of red; nonlinear schemes with the implicit

representation are depicted with shades of green (i.e., M3 and M4); and the nonlinear models with explicit representations are displayed in shades of blue (i.e., M5, M6, and M7). The scheme with the best skill in reconstructing each specific error measure stands in the outermost circle with rank 1, and the worst locates in the innermost circle with rank 7.
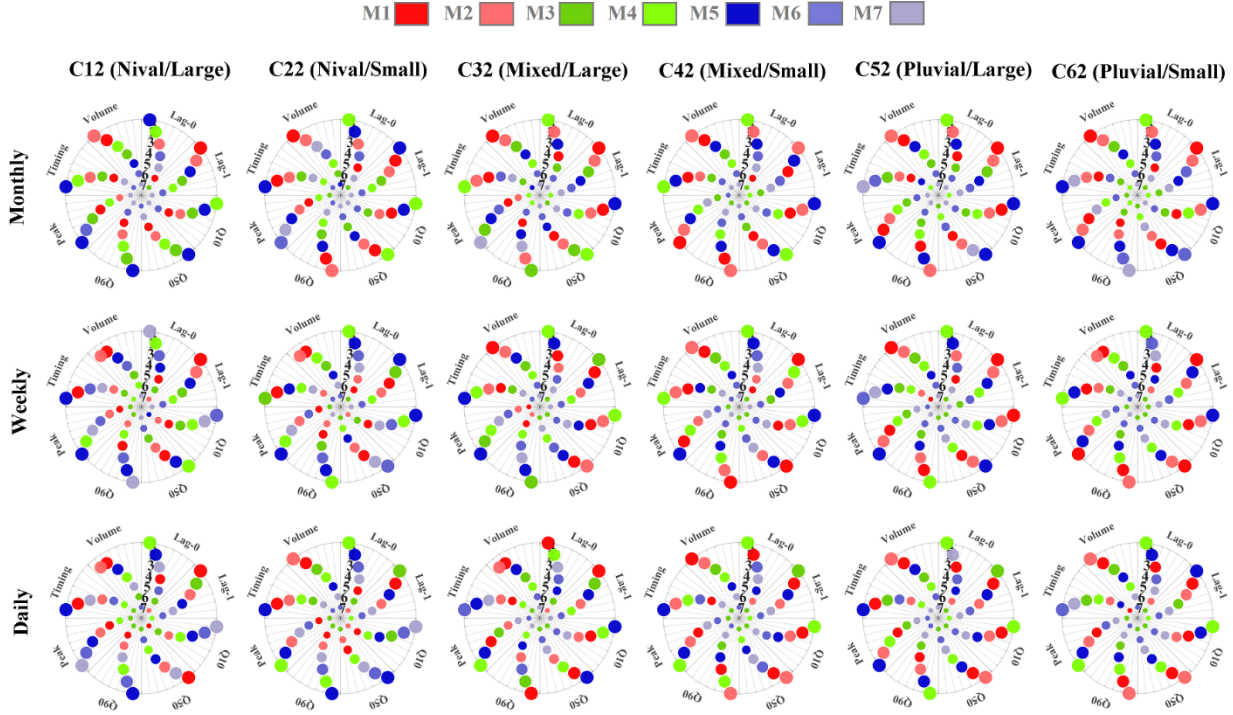
Figure 3.6. The ranking of the seven considered schemes based on their skills in reconstructing the eight streamflow characteristics. The schemes are ranked from 1 to 7 based on their performance in capturing each long-term streamflow characteristics. In each circle, the characteristics are ordered counterclockwise. The model with the highest skill is shown with the biggest dot size and located in the outermost circle.

In general, at the monthly timescale, M2 and M5 are ranked among the top two schemes in 50% and 48% of comparison cases. In the nival regime, M5 is the best choice as outperforms other schemes in 62.5% of comparison cases. In the mixed regime, however, M2 is the rank 1 in around 69% of the comparison cases. At the weekly timescale, M5 with 50% and M1 with 46% chance of being rank 1 dominate other schemes in capturing various streamflow characteristics across different flow regimes. In nival and mixed regimes, M5 outperforms other schemes in 56.3% of comparison cases at the weekly timescale. In the pluvial regime, however, M1 with a 50% chance of being rank 1 shows a more reliable scheme. At the daily timescale, M1 with 54.2% and M5 with 43.8% of cases surpass the skill of other schemes. Similarly, the performances vary across flow regimes. In the nival and mixed regimes, M5 in 50% and 56.3% of chance for being rank 1 dominates other schemes; whereas, in the pluvial regime, M1 with a 62.5% chance of becoming rank 1 outperforms other modeling schemes.

3.6. Summary and concluding remarks

Accurate representations of spatial and temporal dependencies in streamflow data matter to various applications within the territory of water resource planning and management, from assessing regional extremes to quantifying the risk of cascade, simultaneous and/or compound events. While various parametric schemes, extending from fully linear to fully nonlinear stochastic models are available, a consensus on how the spatial and temporal dependencies should be best represented is currently lacking. After a brief overview of theoretical aspects of the parametric representation of dependence, we design a comprehensive experiment to benchmark the skill and uncertainty of various representations across a range of timescales, catchments, and streamflow regimes. We have taken a pragmatic approach to benchmark the performance of various representations and assess their ability in reconstructing long-term streamflow characteristics that matter most to planning and management. For this purpose, we select six catchments across southern Canada, portraying three regime types (i.e., nival, mixed, and pluvial) in catchments with large and small contributing areas, and consider representing temporal and spatial dependence at daily, weekly and monthly timescales. We then observe the skills and uncertainty in reconstructing eight long-term streamflow characteristics.

As far as temporal representation of dependence at a local stream is concerned, our study reveals that in most comparison cases, differences between linear and nonlinear representations are rather statistically indistinguishable. Having said that, when representing the spatial dependence structure among multiple sites is sought, then the skills and uncertainty of various representations depend on the catchment size, timescale, regime type, and even the streamflow characteristics considered. In terms of annual volume, linear schemes show better skills and less uncertainty across all streams and timescale considered. In contrast, when representing timing and magnitude of annual peak flow matters, coupled representations of spatiotemporal dependence through vine copulas dominate other schemes in nival and mixed regimes. In pluvial catchments though, linear approaches outperform nonlinear copula-based schemes. Regardless of regime type, the timing of the peak is better reconstructed in streams with smaller contributing areas. In terms of flow quantiles, nonlinear approaches can represent extreme high and low quantiles better than the linear approaches in nival and mixed catchments, whereas, the linear approaches dominate others in pluvial streams. In terms of lag-1 temporal dependence, linear representations and the scheme based on vine copulas outperform others. In terms of spatial dependence, vine copula representation dominates other schemes. When moving toward coarser time scales, differences in the skills and uncertainty of different schemes become less significant.

Our study provides a practical guideline for choosing an optimal representation depending on the context of application considered. Few points, however, are remained and should be put in perspective. First, as it was shown in Nazemi et al. (2020), even when the skills in reconstructing long-term streamflow characteristics are similar, it does not necessarily mean that the results of stress tests made with the generated synthetic streamflow series would be similar too. This delineates a problem, which is more relevant to water resource planning and management than stochastic

hydrology; yet it must be addressed. Second, in some of the comparison cases, none of the schemes are able to capture certain flow quantiles. The recent study of Zaerpour et al. (2021b) provides the hope that with consideration of large-scale climate indices, the skills in representing high and low quantiles can be improved. Last but not the least, streamflow regime is evolving rapidly due to climatic changes and/or anthropogenic interventions. At this juncture, effective approaches for stochastic streamflow generation under multiple changes in streamflow characteristics are deemed necessary. We hope to soon present a generalized algorithm for representing gradual and/or abrupt regime shifts within stochastic streamflow generation.

Informing Stochastic Streamflow Generation by Large-Scale Climate Indices at Single and Multiple Sites[3]

The contents of this chapter have been published as "Zaerpour, M., Papalexiou, S. M., & Nazemi, A. (2021). Informing Stochastic Streamflow Generation by Large-Scale Climate Indices at Single and Multiple Sites." in Advances in Water Resources. The contents are slightly modified from the submitted article.

Synopsis

Despite the existence of several stochastic streamflow generators, not much attention has been given to representing the impacts of large-scale climate indices on seasonal to interannual streamflow variability. By merging a formal predictor selection scheme with vine copulas, we propose a generic approach to explicitly incorporate large-scale climate indices in ensemble streamflow generation at single and multiple sites and in both short-term prediction and long-term projection modes. The proposed framework is applied at three headwater streams in the Oldman River Basin in southern Alberta, Canada. The results demonstrate higher skills than existing models both in terms of representing intra- and inter-annual variability, as well as accuracy and predictability of streamflow, particularly during high flow seasons. The proposed algorithm presents a globally relevant scheme for the stochastic streamflow generation, where the impacts of large-scale climate indices on streamflow variability across time and space are significant.

4.1. Introduction

Streamflow has been often represented as a function of other hydroclimatic processes such as temperature, precipitation, and evapotranspiration at the catchment scale (Blöschl et al., 2007). These variables are affected by large-scale climate patterns (Merz et al., 2014; Steirou et al., 2017; Tan and Gan, 2017), which can consequently impact streamflow generation globally (Kisi et al., 2019; Konapala et al., 2018; Ward et al., 2014). For instance, various evidences show that Large-scale Climate Indices (LSCIs), most notably El Niño–Southern Oscillation (ENSO), Interdecadal Pacific Oscillation (IPO), and Pacific Decadal Oscillation (PDO) influence the streamflow in Australia (McGowan et al., 2009; Murphy and Timbal, 2008; Pui and Sharma, 2011; Pui et al., 2012). ENSO, North Atlantic Oscillation (NAO), and Atlantic Multidecadal Oscillation (AMO) affect European streamflow (Giuntoli et al., 2013; Steirou et al., 2017). Similarly, ENSO, PDO, AMO, and NAO impact streamflow in North America (Asong et al., 2018; Nazemi et al., 2017; Rajagopalan et al., 2000; Tamaddun et al., 2017, 2019; Wu et al., 2020).

Previous studies have made it clear that taking into account the effects of LSCIs directly on streamflow or indirectly through affected hydroclimate variables, e.g., temperature and precipitation, may improve the predictability of streamflow particularly at seasonal to interannual scales (e.g., Kiem et al., 2021; Kwon et al., 2008; Steinschneider et al., 2019; Wasko and Sharma, 2017). The indirect incorporation of LSCI in the generation of streamflow is in fact very common in the context of process-based models, in which variables such as temperature and precipitation are the basis of simulating streamflow (Eisner et al., 2017; Shrestha et al., 2013; Su et al., 2017). Process-based models, however, are deterministically formulated by implementing physically-based and/or conceptual equations without explicitly considering the distributional and/or joint properties of observed data (Montanari and Koutsoyiannis 2012; Farmer and Vogel, 2016). Past studies showed that although dependence between precipitation and LSCIs can be low (e.g., Westra and Sharma, 2010), LSCIs have more consistent impacts on streamflow and/or temperature (Bonsal and Shabbar, 2011; Nalley et al., 2016; Nazemi et al., 2017). In particular, the direct dependencies between streamflow and LSCIs in coarser spatial and temporal scales are rather strong. This has motivated a strain of modeling attempts to explicitly incorporate the effect of LSCIs in streamflow generation through stochastic approaches (Lee et al., 2018a; Liu et al., 2015; Wang et al., 2009).

One way to represent the impact of LSCIs on stochastic streamflow generation is to transform the original data into a Gaussian process that can be then described using multivariate joint distributions (Bennett et al., 2014; Papalexiou, 2018; Wang and Robertson, 2011). The simplest representation of such kind can be formed by assuming a symmetric and linear teleconnection between streamflow and LSCIs. Linear models such as autoregressive (AR) and its variants have been widely used for streamflow simulation (Matalas 1967; Salas et al., 1985; Lee et al., 2010; Prairie et al., 2008), however, they are unable to adequately represent marginal streamflow distributions, especially in the case of asymmetric, nonlinear and multimodal conditions (Papalexiou, 2018; Papalexiou and Serinaldi, 2020; Rajogopalan et al., 2019), which is the case in many regions and/or finer timescales (Fleming and Dahlke, 2014; Hlinka et al., 2014; Khan et al., 2006; Konapala and Mishra, 2016; Lee et al., 2018b). Nonparametric resampling schemes can address some of the issues in linear models (Lall and Sharma, 1996; Sharma and O'Neill, 2002); however, the generated flows may end up being too close to the reshuffling of historical sequences (e.g., Grantz et al., 2005; Lee et al., 2010).

Over the last two decades, copula-based models (see Genest and Favre, 2007; Nelsen, 2007) have gained popularity in hydroclimatology (Aghakouchak, 2014; Nazemi and Elshorbagy, 2012) and have been applied in various contexts, including stochastic streamflow generation (Salvadori and De Michele, 2004; Worland et al., 2019; Zhang and Singh, 2019). Copulas offer a generic solution to multivariate probabilistic sampling, particularly with respect to quantifying the risk (Chen et al., 2015; Hao and Singh 2013; Serinaldi and Kilsby, 2017). Application of copulas in streamflow generation can provide an opportunity for preserving dependence structures in time and space and/or between streamflow and other relevant variables. Copula-based stochastic streamflow generations have been used at the single site quite extensively and are able to capture nonlinear responses

observed in streamflow time series (Bardossy and Pegram, 2009; Hao and Singh 2012; Nazemi et al., 2013; Wang et al., 2019). More recently methods based on multidimensional copulas, in particular Vine copulas, have been used for multisite streamflow generation (Chen et al., 2019; Nazemi et al., 2020; Pereira et al., 2017; Pereira and Veiga, 2018). Despite ongoing advances in copula-based streamflow generations, only a few incorporate climate-related proxies in streamflow generation (Slater and Villarini, 2018; Wang et al., 2019); and none – to the best of our knowledge – explicitly incorporate the influence of multiple LSCIs in the procedure of stochastic streamflow generation.

Here, we propose a generic approach based on vine copulas to explicitly incorporate LSCIs as exogenous covariates in stochastic streamflow generation at the monthly scale both in prediction and projections modes and at single and multiple sites. We hypothesize that the explicit representation of LSCIs improves both prediction and projection skills, particularly in terms of representing seasonality and inter-annual variability. We recognize that this is a challenging problem. First, the proposed model should be able to capture both symmetric and asymmetric relationships between LSCIs and streamflow in time and space (see Hoerling et al., 1997). In addition, as the statistical dependence between streamflow and LSCIs can change in both time and space, the proposed model should have a dynamic structure (Wang et al., 2019; Nguyen-Huy et al., 2020). For this purpose, we use vine copulas in conjunction with a formal predictor selection algorithm to identify the best common set of LSCIs for streamflow generation at a monthly scale.

We showcase the application of the proposed scheme for the prediction and projection of three mountainous headwaters in southern Alberta, Canada. To benchmark the performance of the proposed algorithm, we compare the skills of our model with already existing reference algorithms. At the single site, we compare the performance of our proposed algorithm with the copula model, proposed by Lee and Salas (2011), which has been used frequently in the literature (e.g., Chen et al., 2015; Nazemi et al., 2013) and extended into multisite mode using regression models (Nazemi and Wheater, 2014). Both single and multisite versions of this existing copula-based algorithm were previously implemented in the same case study (see Nazemi et al., 2013; Nazemi and Wheater, 2014). Vine copulas were also used to represent asymmetric and nonlinear spatial relationships among multiple streams (Chen et al. 2015, 2019; Nazemi et al., 2020).

These models provide a benchmark to discuss the added value of incorporating LSCIs in the process of streamflow generation. The remainder of this paper is organized as the following: Section 4.2 presents the methodological basis of the proposed algorithm. Section 4.3 briefly introduces our case study. Section 4.4 discusses the model development, experimental setup, and benchmarking procedures. Section 4.5 presents the results, compares the proposed model with existing reference models, and discusses the added value of incorporating LSCIs in stochastic streamflow generation. Finally, Section 4.6 concludes the study.

4.2. Methodology

The core of our proposed algorithm is a vine copula, linked to a formal input selection scheme for selecting a set of LSCIs as exogenous covariates that influence the streamflow at the considered

timescale – monthly throughout this paper. We show below that the proposed algorithm is generic and can be applied in both single and multisite settings and in both prediction and projection modes. By prediction, we refer to short-term (precisely one-step-ahead) probabilistic estimates of streamflow conditioned to a known initial state. Prediction mode has relevance to real-time applications such as flood forecasting or operational planning of water resource systems. By projection, in contrast, we refer to long-term estimates of streamflow conditioned to a range of possible initial states. Projection mode is relevant to long-term planning and management of water resource systems as well as scenario analysis particularly under changing climate and land-use conditions. Below we illustrate the elements of the proposed algorithm and its procedure.

4.2.1. Vine copulas

Consider a d-dimensional copula function $C: [0, 1]^d \rightarrow [0, 1]$, in which C is a multivariate Cumulative Distribution Function (CDF) of a random vector $(U_1, U_2, .., U_d)$, defined on the unit hypercube $[0, 1]^d$, where U_i denotes uniform marginal distributions $U(0,1)$ – see Joe (1997). The fundamental work of Sklar (1959) shows that for any multivariate CDF, such as $F(x_1, x_2, ..., x_d)$ of d random variables $(X_1, X_2, ..., X_d)$, there is a copula function C, that can describe $F(x_1, x_2, ..., x_d)$ using marginal CDFs $F_1(x_1), F_2(x_2), ..., F_d(x_d)$ as the following:

$$F(x_1, x_2, ..., x_d) = C\big(F_1(x_1), F_2(x_2), ..., F_d(x_d)\big) \tag{4.1}$$

denoting that the original d-dimensional CDF is decomposed into (1) a dependence structure between uniform random variables, and (2) marginal CDFs that are defined independently from the dependence structure. If the marginal distribution functions are continuous, then the copula function C is unique, and the joint Probability Density Function (PDF) can be calculated as (Joe, 1997):

$$f(x_1, ..., x_d) = c(F_1(x_1), ..., F_d(x_d)) \prod_{j=1}^{d} f_j(x_j) \tag{4.2}$$

where $c(\cdot)$ is the d-dimensional copula PDF and $f_j(x_j)$ is the marginal PDFs of the X_j; $j = 1,2, ..., d$. Vine copulas provide a generic approach to construct high-dimensional joint distributions by using bivariate copulas as building blocks as any high-dimensional copula can be decomposed into a product of $d(d - 1)/2$ bivariate copulas ordered as a sequence of $(d - 1)$ nested trees with nodes joined by edges (see Bedford and Cooke, 2001; Joe, 1997; Aas et al., 2009; Czado, 2010). Here we focus on a particular form of vine copulas, i.e. canonical vines (hereafter C-vines), which are based on ordering the variables by importance. Considering a multivariate density function as a product of conditional densities, a C-vine can be constructed by:

$$f(x_1, \ldots, x_d) = f_1(x_1) \prod_{j=2}^{d} f_{j|1:j-1}(x_j | x_1, \ldots, x_{j-1}) \tag{4.3}$$

where $1:j-1 = 1,2,\ldots,j-1$. Based on the Sklar's theorem and Eq. (2), we have:

$$f_{j|1:j-1}(x_j | x_{1:j-1}) = c_{j-1,j|1:j-2}\left(F(x_{j-1}|x_{1:j-2}), F(x_j|x_{1:j-2})\right) f(x_j|x_{1:j-2}) \tag{4.4}$$

where $F(\cdot \,|\, \cdot)$ and $f(\cdot \,|\, \cdot)$ denote conditional CDFs and PDFs, respectively. By applying Eq. (4.4) recursively, the joint density in Eq. (4.3) can be expressed as (Bedford and Cooke, 2001):

$$f(x_1, \ldots, x_d) = \prod_{k=1}^{d} f_k(x_k) \prod_{i=1}^{d-1} \prod_{j=1}^{d-i} c_{i,j+i|1:i-1}\left(F(x_i|x_{1:i-1}), F(x_{j+i}|x_{1:i-1})\right) \tag{4.5}$$

The C-vine copula construction in Eq. (4.5) involves marginal conditional distributions in the form $F(x|\boldsymbol{v})$, which can be obtained recursively using the h-function derivative (Joe, 1997, 2014):

$$h = F(x|\boldsymbol{v}) = \frac{\partial C_{x,v_j|\boldsymbol{v}_{-j}}\left(F(x|\boldsymbol{v}_{-j}), F(v_j|\boldsymbol{v}_{-j})\right)}{\partial F(v_j|\boldsymbol{v}_{-j})} \tag{4.6}$$

where $\boldsymbol{v}$ is a d-dimensional multivariate space with v_j, is one arbitrary component chosen from $\boldsymbol{v}$, and $\boldsymbol{v}_{-j}$ denotes the vector $\boldsymbol{v}$ excluding v_j and $C_{x,v_j|v_{-j}}$ is the bivariate copula.

4.2.2. Selecting large-scale climate indices to inform streamflow generation

While C-vine copulas provide a theoretical framework for conditioning streamflow generation to LSCIs, several LSCIs may influence streamflow at a given lead time and the relevant LSCIs in one time step may be irrelevant in others. As a result, there is a need for a systematic and rather dynamic identification of appropriate LSCIs at a given lead time (Quilty et al., 2016, 2019; Robertson and Wang, 2012). Statistical methods such as Principal Component Analysis (Barnston and Ropelewski, 1992), Independent Component Analysis (Aires et al., 2000), Partial Mutual Information Selection (PMI; Sharma, 2000; Sharma and Mehrotra, 2014; Sharma et al., 2016), and Partial Correlation Input Selection (PCIS, May et al., 2008, 2011) have been developed and already used in the literature for predictor selection. Here, we use PCIS, an iterative forward-looking input selection algorithm, which chooses one LSCI at a particular lag during each iteration (Brown et al., 2012; Quilty et al., 2016, 2019; Tran et al., 2016). The selected LSCI is the one that has the largest dependence score with the streamflow at a given monthly time step. Similar to Amir Jabbari and Nazemi (2019), we apply Kendall's tau (Kendall, 1976) to measure the dependence between lagged monthly LSCIs and monthly streamflow. The Kendall's tau is more compatible for selecting LSCIs, as there can be strong nonlinear dependence between LSCIs and the monthly streamflow (Hlinka et al., 2014; Konapala et al., 2018). The algorithm terminates when adding new predictors causes no improvement in the Bayesian Information Criterion (BIC), estimated from the predictand residuals. As we apply the PCIS

for each month separately, the selected monthly LSCIs can change. For more details on PCIS see May et al., (2008, 2011) and Hatami et al. (2019).

4.2.3. Proposed streamflow generation scheme

By choosing the relevant LSCIs, C-vine copulas can be used to allow conditioning streamflow at each time step to previous values of streamflow as well relevant LSCIs as exogenous covariates. Previous studies showed that at coarser time scales (e.g. weekly, monthly), the lag-1 dependence is sufficient for streamflow generation (Chen et al., 2015; Nazemi and Wheater, 2014; Wang et al., 2019). Fig. 4.1 summarizes the proposed streamflow generation scheme at single site considering the lag-1 temporal dependence. No need to mention that this framework can be extended to consider more lags and/or to cover finer timescales. For the sake of simplicity, we only consider one LSCI in the schematic and formulations are given below. In the case of more LSCI, this formulation can be extended to higher dimensions following the procedure explained in section 2.1.

In single site setting, the task is to generate streamflow at any site A (Fig. 4.1a), where C-vines are used to decompose the dependence structure between monthly flows at time t (i.e. Q_t^A), $t-1$ (i.e. Q_{t-1}^A), as well as a relevant LSCI at time $t-\tau$ (i.e. $L_{t-\tau}$), where τ is the lag between the monthly flow at time t and the selected LSCI. Following the Eqs. (3) and (4) the joint distribution between Q_{t-1}^A, Q_t^A and $L_{t-\tau}$ can be established as:

$$f(Q_{t-1}^A, L_{t-\tau}, Q_t^A) = f_1(Q_{t-1}^A)f_{2|1}(L_{t-\tau}|Q_{t-1}^A)f_{3|1,2}(Q_t^A|Q_{t-1}^A, L_{t-\tau}) \tag{4.7}$$

where the subscripts 1, 2, and 3 correspond to Q_{t-1}^A, $L_{t-\tau}$ and Q_t^A, respectively. Using Eq. (4), the conditional distributions in Eq. (7) can be estimated as:

$$\begin{aligned} f_{2|1}(L_{t-\tau}|Q_{t-1}^A) &= \frac{f(L_{t-\tau}, Q_{t-1}^A)}{f(Q_{t-1}^A)} = \frac{c_{1,2}\big(F_1(Q_{t-1}^A), F_2(L_{t-\tau})\big)f_1(Q_{t-1}^A)f_2(L_{t-\tau})}{f_1(Q_{t-1}^A)} \\ &= c_{1,2}\big(F_1(Q_{t-1}^A), F_2(L_{t-\tau})\big)f_2(L_{t-\tau}) \end{aligned} \tag{4.8}$$

and

$$\begin{aligned} f_{3|1,2}(Q_t^A|Q_{t-1}^A, L_{t-\tau}) &= \frac{f(L_{t-\tau}, Q_t^A|Q_{t-1}^A)}{f(L_{t-\tau}|Q_{t-1}^A)} \\ &= \frac{c_{2,3|1}\big(F(L_{t-\tau}|Q_{t-1}^A), F(Q_t^A|Q_{t-1}^A)\big)f(L_{t-\tau}|Q_{t-1}^A)f(Q_t^A|Q_{t-1}^A)}{f(L_{t-\tau}|Q_{t-1}^A)} \\ &= c_{2,3|1}\big(F(L_{t-\tau}|Q_{t-1}^A), F(Q_t^A|Q_{t-1}^A)\big)c_{1,3}\big(F_1(Q_{t-1}^A), F_3(Q_t^A)\big)f_3(Q_t^A) \end{aligned} \tag{4.9}$$

As a result, the three dimensional joint density in Eq. (7) can be represented in terms of bivariate copulas $C_{1,2}$, $C_{1,3}$, and $C_{2,3|1}$ with densities $c_{1,2}$, $c_{1,3}$, and $c_{2,3|1}$ as the following:

$$\begin{aligned} &f(Q_{t-1}^A, L_{t-\tau}, Q_t^A) \\ &= f_1(Q_{t-1}^A)f_2(L_{t-\tau})f_3(Q_t^A)c_{1,2}\big(F_1(Q_{t-1}^A), F_2(L_{t-\tau})\big)c_{1,3}\big(F_1(Q_{t-1}^A), F_3(Q_t^A)\big) \\ &\quad c_{2,3|1}\big(F(L_{t-\tau}|Q_{t-1}^A), F(Q_t^A|Q_{t-1}^A)\big) \end{aligned} \tag{4.10}$$

The graphical representation of the proposed three-dimensional C-vine copula is depicted in Fig. 4.1b and includes two trees. In the first tree T_1, the circled nodes 1 to 3 represent respectively the three PDFs of flows at time step $t-1$, LSCI signal with lag τ, i.e. $L_{t-\tau}$, and the flow at time step t. The dependencies between nodes (i.e., edges) are modeled using bivariate copulas formed for each pair. The edges in the first tree become nodes for the second level. Accordingly, the conditional distribution function of $F(Q_t^A|Q_{t-1}^A, L_{t-\tau})$ can be obtained by recursive use of Eq. (6) as (Aas et al., 2009; Czado et al., 2012):

$$h = F(Q_t^A|Q_{t-1}^A, L_{t-\tau}) = \frac{\partial C_{2,3|1}\big(F(Q_t^A|Q_{t-1}^A), F(L_{t-\tau}|Q_{t-1}^A)\big)}{\partial F(L_{t-\tau}|Q_{t-1}^A)} \tag{4.11}$$

Note that $F(Q_t^A|Q_{t-1}^A) = h(Q_t^A|Q_{t-1}^A) = \frac{\partial c_{3,1}(F(Q_t^A), F(Q_{t-1}^A))}{\partial F(Q_{t-1}^A)}$ and $F(L_{t-\tau}|Q_{t-1}^A) =$

$h(L_{t-\tau}|Q_{t-1}^A) = \frac{\partial C_{2,1}\big(F(L_{t-\tau}), F(Q_{t-1}^A)\big)}{\partial F(Q_{t-1}^A)}$. As a result, Eq. (11) can be rewritten as:

$$h = F(Q_t^A|Q_{t-1}^A, L_{t-\tau}) = h[h(Q_t^A|Q_{t-1}^A)|h(L_{t-\tau}|Q_{t-1}^A)] \tag{4.12}$$
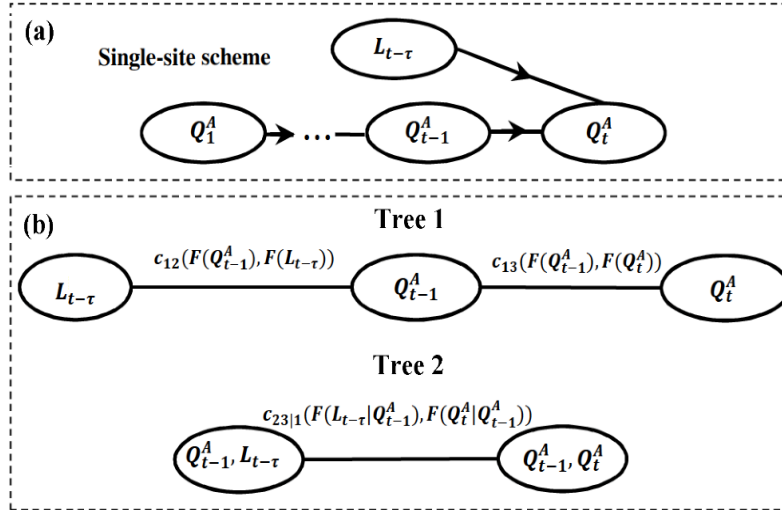
Figure 4.1. The schematic pathway for single site generation of streamflow with consideration of large-scale climate indices (panel a) along with the corresponding C-vine copula representation proposed (panel b). $Q_1^A,\ldots,$ Q_{t-1}^A, Q_t^A denote the monthly flows at a given site A. In panel b, the variables 1 to 3 indicate Q_{t-1}^A, $L_{t-\tau}$ and Q_t^A shown in nodes of the Tree 1.

In the multisite setting, the streamflow generation is based on selecting a primary site, which is used as a reference to realize streamflow in other reaches (hereafter secondary sites) using the temporal and spatial dependencies within and between streamflow series (see Nazemi et al., 2013, 2020; Nazemi and Wheater, 2014). These dependencies are usually not the same and require asymmetric copulas to be handled (e.g., Chen et al., 2015; Grimaldi and Serinaldi, 2006). Fig. 4.2a shows the multisite streamflow generation schematically. Let Q_t^B and Q_{t-1}^B be the monthly flows at

time step t and $t-1$ at the secondary site B. Note that we consider a unique LSCI at time $t-\tau$, i.e., $L_{t-\tau}$, relevant to both stations. This has a physical relevance as the effect of LSCIs on streamflow regime is manifested regionally (Bonsal and Shabbar, 2008; Nalley et al., 2016; Nazemi et al., 2017). The extension of the proposed vine copula to a multisite setting is shown schematically in Fig. 4.2b. Based on Eqs. (4.4) and (4.5), the joint dependence can be constructed as:

$$f(Q_{t-1}^B, Q_{t-1}^A, L_{t-\tau}, Q_t^B) = f_1 \cdot f_2 \cdot f_3 \cdot f_4 \cdot c_{1,2} \cdot c_{1,3} \cdot c_{1,4} \cdot c_{2,3|1} \cdot c_{2,4|1} \cdot c_{34|21} \tag{4.13}$$

where $c_{1,2}$ is $c_{1,2}\big(F_1(Q_{t-1}^B), F_2(Q_{t-1}^A)\big)$ and $c_{1,3}$ and $c_{1,4}$ being defined similarly; $c_{34|21}$ is $c_{34|21}(F(L_{t-\tau}|Q_{t-1}^A, Q_{t-1}^B), F(QB_t|Q_{t-1}^A, Q_{t-1}^B)$ – see also Eqs. (4.5) and (4.10). Having the joint distribution function from Eq. (4.13), the conditional CDF, $F(Q_t^B|Q_{t-1}^B, Q_{t-1}^A, L_{t-\tau})$, can be obtained recursively by applying the appropriate h-function from Eq. (4.6):

$$\begin{aligned} h &= F(Q_t^B|Q_{t-1}^B, Q_{t-1}^A, L_{t-\tau}) \\ &= h\{h[h(L_{t-\tau}|Q_{t-1}^B)|h(Q_{t-1}^A|Q_{t-1}^B)]|h[h(Q_t^B|Q_{t-1}^B)|h(Q_{t-1}^A|Q_{t-1}^B)]\} \end{aligned} \tag{4.14}$$
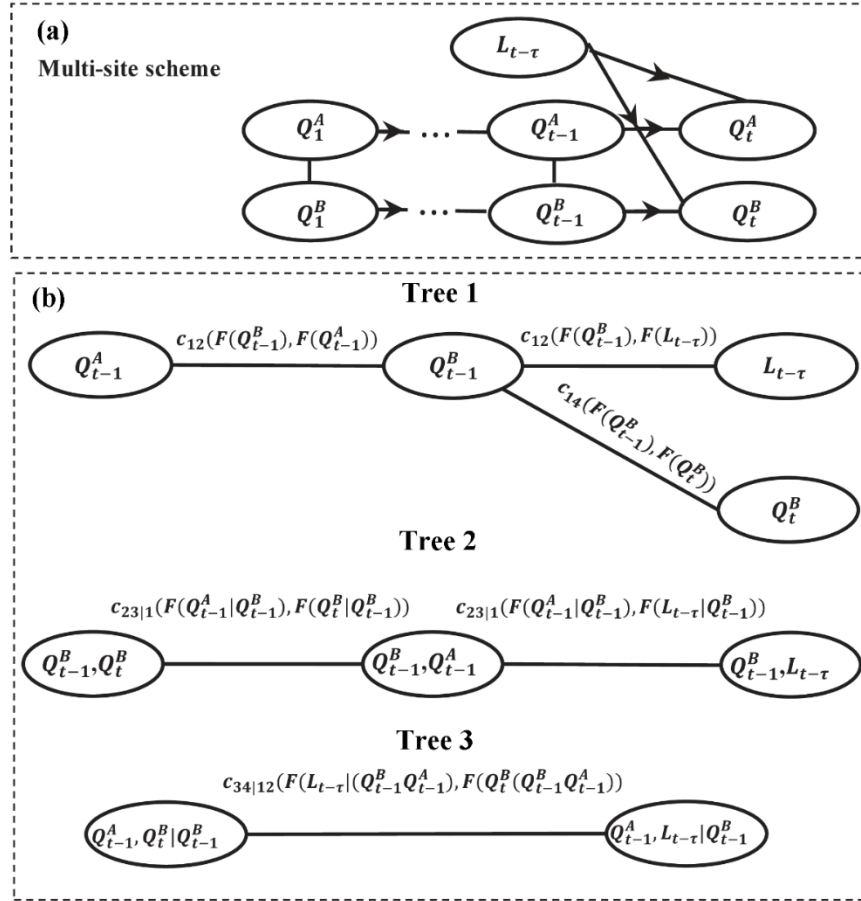
Figure 4.2. The schematic pathway for multisite generation of streamflow with consideration of large-scale climate indices (panel a) along with the corresponding C-vine copula representation proposed for multisite streamflow generation (panel b). $Q_1^A, \dots, Q_{t-1}^A, Q_t^A$ denote the monthly flows at the primary site A. $Q_1^B, \dots, Q_{t-1}^B$, Q_t^B denote the monthly flows at the secondary site. In panel b, the variables 1 to 4 indicate $Q_{t-1}^B, Q_{t-1}^A, L_{t-\tau}$ and Q_t^B, respectively.

We apply the inverse forms of h-functions given in Eqs. (12) and (14) for streamflow generation at single and multiple sites, respectively. In the prediction mode and single-site setting, the aim is to obtain $F(Q_t^A)$ based on the known states of $F(Q_{t-1}^A)$ and $F(L_{t-\tau})$. This is achieved by estimating the inverse of h-function, given uniform random numbers of ε:

$$Q_t^A = F^{-1}\left\{h^{-1}\left[\left(h^{-1}\left(\varepsilon|h(L_{t-\tau}|Q_{t-1}^A)\right)\right)|Q_{t-1}^A\right]\right\} \tag{4.15}$$

The ensemble generation is obtained by synthesizing a large number of uniformly distributed random numbers (10,000 throughout this paper) to realize corresponding scenarios of Q_t^A. This large number of realizations is needed to account for sampling uncertainty and to come up with confidence bounds (Roy and Gupta, 2020). The mean value of these realizations is considered as the best prediction at each time step. Similarly in the multisite mode, the procedure of streamflow generation is also based on Monte Carlo simulations using the information available for Q_{t-1}^B, Q_{t-1}^A, and $L_{t-\tau}$ using the inverse h-functions:

$$Q_t^B = F^{-1}\left\{h^{-1}\left[h^{-1}\left(h^{-1}\left(\varepsilon|h(h(L_{t-\tau}|Q_{t-1}^B)|h(Q_{t-1}^A|Q_{t-1}^B))\right)\right)|h(Q_{t-1}^A|Q_{t-1}^B)\right)Q_{t-1}^B\right]\right\} \tag{4.16}$$

The process of ensemble generation in the projection mode is very similar to the prediction mode, with the exception that the conditioning is not based on known antecedent quantities of streamflow. For this purpose, having the appropriate predictors (i.e., LSCIs) at each month, flows can be generated at the following month conditioned to the given LSCIs.

4.3. Case study and Data

The Oldman River and its tributaries form a large basin (27600 km^2) and provide around 40% of the total annual streamflow in southern Alberta, Canada (Alberta Environment, 2010). The Oldman River originates from mountainous headwaters in the eastern slopes of the Rocky Mountains and joins the Bow River before rolling downstream toward the province of Saskatchewan. The basin is located in a semi-arid cold region, where snowmelt from the Rocky Mountains headwaters is the main source of the annual water supply, providing between 70% to 90% of the total annual flow volume (Nazemi et al., 2017). The water resource system in this basin is complex, including several sectors of water demand, some with competing interests (e.g., environmental *vs.* irrigation water demands). Irrigation is the largest water consumption in the basin and includes 88% of the total water demand (Zandmoghaddam et al., 2019). The basin is currently under pressure due to rapid socio-environmental changes that intensify water demand and/or loss (e.g., inclined evapotranspiration due to warming). This has created a regional water security concern, where natural streamflow cannot meet additional water demand (Gober and Wheater, 2014; Martz et al., 2007). This concern will be even more in the future and under heightened climate variability and change as the natural streamflow

is also under rapid changes (Zaerpour et al., 2020), mainly due to the decline in the winter snowpack in the Rocky Mountains (Prowse et al., 2006).

We have chosen three headwater rivers, upstream of the Oldman Reservoir namely the Oldman River near Waldron's Corner, Crowsnest River near Lundbreck, and Castle River near Beaver Mine. Together, they provide 95% of the natural inflow to the Oldman River (Nazemi et al., 2017). Fig. 4.3 shows the map of the Oldman River, in which the three considered headwater streams are identified. Table 4.1 shows the key information about these streams. For each stream, we extract the monthly streamflow values for the period of 1967 to 2008 from the Water Survey of Canada's Hydrometric Database (HYDAT; Water Survey of Canada, 2017, http://www.wsc.ec.gc.ca/).

We consider six large-scale climate indices including PDO, ENSO, NAO, AMO, Arctic Oscillation (AO), and Pacific North American (PNA) as potential LSCIs for streamflow generation. These LSCIs are the main ocean-atmospheric patterns that affect hydroclimatological variables in Canada (Bonsal et al., 2006; Coulibaly and Burn, 2004; Nalley et al., 2019; Rasouli et al., 2020; Whitfield et al., 2010). In brief, the PDO is a large-scale climate pattern of sea-surface temperature fluctuations in the Pacific with the periodicity of inter-decadal to multi-decadal scales (Mantua et al., 1997). PDO data for the considered period is obtained from the Joint Institute for the Study of the Atmosphere and Ocean, University of Washington (http://jiasao.washington.edu/pdo/ PDO.latest). The NAO is represented by the atmospheric pressure at sea level between the Icelandic Low and the Azores High with a periodicity of around 3-6 years and is pronounced during the cold season. The AO is characterized by atmospheric circulation patterns over the extra-tropical Northern Hemisphere where sea-level pressures over the polar vary in opposition to middle latitudes at around $45°N$ (Thompson and Wallace, 1998). NAO and AO data are obtained from National Center for Environmental Information (http://www.ngdc.noaa.gov/). The AMO is an atmospheric-oceanic phenomenon with a periodicity of 50-70 years that arises from the variations in sea-surface temperature in the Atlantic Ocean (Enfield et al., 2001). AMO data are obtained from Earth System Research Laboratories center (http://www .esrl.noaa.gov/psd/data/correlation/amon.us.long.data). The PNA pattern features a sequence of high and low-pressure anomalies stretching from the subtropical West Pacific to the east coast of North America. PNA data are extracted from Physical Sciences Laboratory (https://www.psl.noaa.gov/data /correlation/pna.data). ENSO represents large-scale ocean-atmosphere oscillations in the tropical Pacific influencing climatic conditions around the globe including Canada. (Trenberth, 1997). ENSO data is obtained from the Climate Prediction Center (http://www.cgd.ucar.edu/cas/catalog/climind/). Regarding ENSO, we consider four indices including NINO3, NINO3.4, NINO4, and NINO1+2 anomalies, selected using the predictor selection method based on the level of dependence to monthly flows.
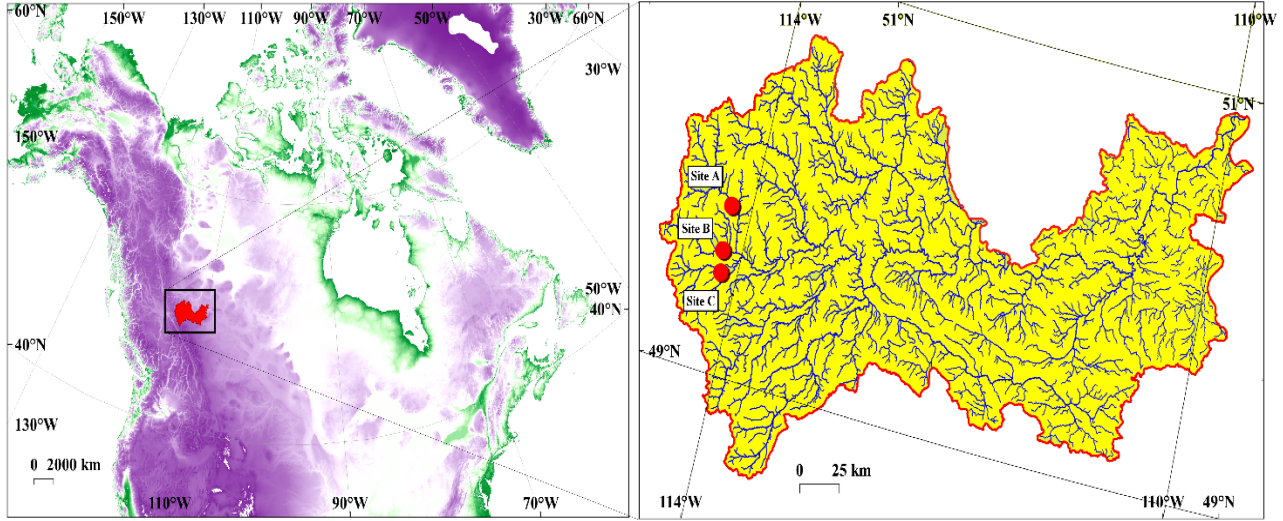
Figure 4.3. The Oldman River Basin along with its three main headwater streams, namely Oldman River near Waldron's Corner (Site A), Crowsnest River near Lundbreck (Site B), and Castle River near Beaver Mine (Site C).

Table 4.1. The three rivers used in this study along with their names, coordinates, drainage areas, and gauging IDs.

Name	Description	Lat.	Long.	Drainage area (km^2)	HYDAT ID
Inflow 1 (site A)	Oldman River near Waldron's Corner	49.813	−114.183	1446.1	05AA023
Inflow 2 (site B)	Crowsnest River near Lundbreck	49.594	−114.171	658	05AA002
Inflow 3 (site C)	Castle River near Beaver Mines	49.488	−114.144	820.7	05AA022

4.4. Experimental setup and benchmarking approach

We apply the proposed algorithm in the three considered streams in single and multisite settings and in both prediction and projection modes. In the single site setting, streamflow is generated at each site independently. In the multisite setting, however, one stream should be chosen as the primary site, from which streamflow is realized regionally in other locations. Here we follow the generation pathway used by Nazemi and Wheater (2014). They performed a rigorous experiment to choose the best pathway for streamflow generation and concluded that the Oldman River near Waldron's Corner (Site A) can be considered as the primary reach for the other two reaches. Most essentially, the performance of our proposed algorithm is benchmarked with observed streamflow characteristics. We also compare the performance of our proposed scheme at the single site with an existing reference model proposed by Lee and Salas (2011) and applied in the Oldman River Basin by Nazemi and Wheater (2014). The basic idea in such a model is to conditionally resample flow at the lead time of one month from the antecedent streamflow conditions without considering the effect of LSCIs.

Similarly in the multisite setting, we compare the performance of our proposed algorithm with the multisite algorithm based on vine copula developed by Chen et al. (2015, 2019) and used in Nazemi et al. (2020). Table 4.2 shows the notation used for proposed and reference algorithms in prediction and projection modes.

Table 4.2. Notations for the proposed and reference models in single and multiple site settings and in prediction and projection modes.

Experimental setup		Proposed algorithm (LSCI considered)	Reference algorithms (no LSCI considered)	
Algorithm setting	Simulation mode	Notation	Notation	Reference
Single site	Short-term (Prediction)	PS1	RS1	Nazemi and Wheater (2014)
	Long-term (Projection)	PS2	RS2	
Multisite	Short-term (Prediction)	PM1	RM1	Nazemi et al. (2020)
	Long-term (Projection)	PM2	RM2	

The first step in our proposed algorithm is to select a set of relevant LSCIs at each monthly timestep. The pool of LSCIs, from which relevant indices at each timestep are selected, consists of the six named LSCIs up to 24 months lags. We initially considered more lag times up to 48 months (see Nalley et al., 2016); however, inline with several other studies in western Canada (e.g., Shabbar et al., 1997) or globally (Chiew and McMahon, 2002), the analysis of Kendall's tau rank dependence showed that the memory of LSCIs on streamflow in the three considered streams does not go beyond 24 months. We then use the PCIS algorithm to select the best set of LSCIs predictors at each month from a pool of options. As the three streams are located in close proximity and are under the influence of similar LSCIs, we aim at finding a common set of predictors at the three sites – see Hatami et al. (2019) for the details of using the PCIS algorithm for global input selection in multiple locations. We also compare the results with PMI to ensure that a robust set of LSCI is selected. Finally, we select the structure of vine copulas by the Maximal Spanning Tree algorithm as described by Czado et al. (2013) and considering empirical distributions in margins for both monthly streamflow and the selected LSCIs. In this context, a fast sequential estimation procedure for parameter estimation is suggested (Dissmann et al., 2013). In brief, the first bivariate copula families and parameters for the first tree are identified before calculating the weights for the second tree and so on. We consider a set of well-known parametric copula functions, including Gaussian, Student t, Clayton, Gumbel, Frank, Joe, and their rotated forms for setting up the vine copulas – see Nelsen (2006) and Pereira and Veiga (2018) for the formulation of these copulas. The copula identification and parameterization are

performed by applying the Maximum log-Likelihood Method and considering the Bayesian Information Criteria (BIC; Akaike, 1979) as the Goodness of Fit (see also Sadegh et al., 2017). The modeling is implemented in the *R* platform by utilizing the *VineCopula* (Nagler et al., 2019; Schepsmeier et al., 2016), *CDVine* (Brechmann and Schepsmeier, 2013), *copula* (Hofert et al., 2014), *CDVineCopulaConditional* (Bevacqua, 2017), and *NPRED* packages (Sharma and Mehrotra, 2014; Sharma et al., 2016).

The performance of the proposed algorithm is evaluated in the prediction and projection modes and compared with reference models using a set of metrics. In the projection mode, we generate 10,000 synthetic historical streamflow realizations with the same length as the observed data. To demonstrate the performance of projected streamflow ensembles, basic statistics including long-term monthly mean value, standard deviation, skewness, as well as the lag-1 temporal and lag-0 spatial dependencies are calculated. To measure the relative improvement in the performance of the proposed method in representing persistence in the historical streamflow, we adopt the interannual variability metric (Johnson and Sharma, 2011; Taylor, 2001):

$$S = \frac{4(1+r)^4}{(\hat{\sigma}_f + 1/\hat{\sigma}_f)^2(1+r_0)^4} \tag{4.17}$$

where r is the correlation coefficient between observed and simulated streamflow, $\hat{\sigma}_f$ is the ratio of the expected standard deviation of ensemble projections to the standard deviation of the observed streamflow, and r_0 is the maximum theoretical correlation which is taken as 1. The range of S varies between 0 and 1. The score of 1 happens when both $\hat{\sigma}_f$ and r are equal to one and there is no error in capturing the interannual variability. The relative improvement in the performance of the proposed model in capturing the interannual variability over the reference model is given by the interannual variability skill score as (Wang and Robertson, 2011):

$$\text{SS}_{\text{Proj.}} = \frac{S - S_{\text{ref}}}{1 - S_{\text{ref}}} \times 100\% \tag{4.18}$$

where S and S_{ref} represent the interannual variability metric values for the proposed and the reference model, respectively.

In the prediction mode, we similarly generate 10,000 realizations of streamflow series with the same length as observed data in both single and multisite settings. We calibrate and validate the predictions using the buffered-leave-one-out cross-validation method (Le Rest et al., 2014; Roberts et al., 2017). For prediction in each year, the corresponding year and the two years ahead are excluded, while the remaining years are used for predictor selection and model building procedures. The predicted monthly flow is then compared with the observed data. We present the overall skill of predictions as a skill score, which is the relative improvement in Error Scores (ESs) of the prediction over a set of reference predictions (Wang et al., 2009):

$$SS_{\text{pred.}} = \frac{ES_{\text{ref}} - ES}{ES_{\text{ref}}} \times 100\% \tag{4.19}$$

where ES and ES_{ref} represent the five considered error metrics calculated for the proposed and the reference model, respectively. Each skill measure assesses different aspects of the forecast distribution. A higher SS value indicates better performance in the proposed model, with a score of 0 representing the same performance as the reference model.

The first skill score used is SS_{MAE}, which is based on expected Mean Absolute Error (MAE) of the predicted mean. MAE measures the expected mean absolute error of predicted monthly streamflow ensemble and is defined as:

$$MAE = \frac{\sum_{t=1}^{T} |\bar{x}_{\text{sim}} - x_{\text{obs}}|}{T} \tag{4.20}$$

where T is the total number of years. The second score, SS_{RMSE}, is based on expected Root Mean Squared Error (RMSE) of the predicted mean. RMSE assesses the standard deviation of predicted error applied to the ensemble mean:

$$RMSE = \sqrt{\frac{\sum_{t=1}^{T} (x_{\text{sim}} - x_{\text{obs}})^2}{T}} \tag{4.21}$$

The third skill score, SS_{RMSEP}, is based on the expected Root Mean Squared error in Probability (RMSEP; Bennett et al., 2014; Wang and Robertson, 2011) of the predicted mean. The RMSEP measures predicted error on a probability scale, giving the predicted events similar opportunity to contribute to the overall assessment of predicted skill:

$$RMSEP = \sqrt{\frac{1}{T} \sum_{t=1}^{T} [F_{\text{sim}}(x_t) - F_{\text{obs}}(x_t)]^2} \tag{4.22}$$

where $F_{\text{obs}}(x_t)$ is the CDF of the historical streamflow data, $F_{\text{sim}}(\bar{x}_t)$ is the CDF of the expected predicted streamflow. RMSEP is less sensitive to events with large errors (Wang and Robertson, 2011). The fourth score, SS_{CRPS}, is based on the expected Continuous Ranked Probability Score (CRPS; Harrigan et al., 2018; Kaune et al., 2020; Wang and Robertson, 2011) of the predicted mean. Unlike RMSEP, CRPS metric measures the error of the whole predicted probability distribution, and can be sensitive to just a few (usually very high flow) events with large prediction errors:

$$CRPS = \frac{1}{T} \sum_{t=1}^{T} \int [F_{\text{sim}}(x_t) - H(x_t - x_{\text{obs}})]^2 \, dx \tag{4.23}$$

where $F_{\text{sim}}(x_t)$ is the predicted CDF and $H(x_t - x_{\text{obs}})$ is the Heaviside step function defined as (Wang and Robertson, 2011):

$$H(x_t - x_{\text{obs}}) = \begin{cases} 0, & x_t < x_{\text{obs}} \\ 1, & x_t \geq x_{\text{obs}} \end{cases} \tag{4.24}$$

Finally, the fifth score (SS_{KGE}) is based on the expected Kling-Gupta efficiency (KGE; Gupta et al., 2009). The KGE focuses on three criteria including correlation between observations and simulations, the bias, and the relative variability in the simulated and observed values expressed as:

$$\text{KGE} = 1 - \sqrt{(r-1)^2 + \left(\frac{\sigma_{\text{sim}}}{\sigma_{\text{obs}}} - 1\right)^2 + \left(\frac{\mu_{\text{sim}}}{\mu_{\text{obs}}} - 1\right)^2} \tag{4.25}$$

where r is the correlation between observations and simulations, σ_{obs} and σ_{sim} are the standard deviations of observed and simulated values, μ_{obs} and μ_{sim} are the means of observed and simulated values. KGE values close to 1 represent perfect model performance. Note that unlike the previous four scores where zero indicates the best performance, $\text{KGE} = 1$ indicates the perfect agreement between simulations and observations. To allow homogeneous comparison between all score, we scale the KGE to skill score as (Knoben et al., 2019):

$$\text{SS}_{\text{KGE}} = \frac{\text{KGE} - \text{KGE}_{\text{ref}}}{1 - \text{KGE}_{\text{ref}}} \times 100\% \tag{4.26}$$

Apart from accuracy, we also measure the reliability of predicted ensembles, by assessing the statistical consistency of the predicted probability distributions and the associated observed events (Jolliffe and Stephenson, 2011; Toth et al., 2003). In this study, we use histograms of Probability Integral Transforms (PIT; Dawid, 1984; Gneiting et al., 2007) to assess the average reliability of the prediction distributions. The PIT of the observed value is given as:

$$\text{PIT} = F_{\text{sim}}(x_{\text{obs}}) \tag{4.27}$$

where F_{sim} denotes the CDF of simulated flow, and $F_{\text{sim}}(x_{\text{obs}})$, therefore, is the non-exceedance probability of the observed streamflow based on the CDF of the simulated streamflow. The PIT values are then assigned to different histogram bins and the frequency of each bin is calculated. The predictive distribution is said to be reliable if the PIT values are distributed uniformly. U-shaped histograms usually indicate that the probabilistic predictions have under-dispersion. On the contrary, if the PIT histogram is hump-shaped, then the probabilistic predictions indicate over-dispersion. The deviation metric D quantifies the deviation from uniformity in PIT. This measure, which is introduced by Nipen and Stull (2011) and later used in Bourdin et al. (2014), can be defined as:

$$D = \sqrt{\frac{1}{B}\sum_{i=1}^{B}\left(\frac{b_i}{\|T\|} - \frac{1}{B}\right)^2} \tag{4.28}$$

where B is the number of bins, b_i is the number of observations in bin i, and $\|T\|$ is the size of the dataset. Lower variability in bin frequency is indicative of a flatter PIT. Sampling limitations, however, can cause a reliable prediction not generate a perfectly flat PIT histogram, leading to an expected value of the deviation $E(D_p)$ for perfect prediction (Brocker and Smith, 2007; Pinson et al., 2010) given by:

$$E(D_p) = \sqrt{\frac{1 - B^{-1}}{\|T\| B}} \tag{4.29}$$

Note that apart from the given metrics, we also look at the 95% Confidence Interval (CI) of generated ensembles both in terms of probabilistic characteristics as well projected/predicted timeseries.

4.5. Results and discussions

4.5.1. Influential Large Scale Climate Indices in upper Oldman

We initially analyze the dependence between lagged LSCIs and monthly streamflow in the three considered headwaters. Considering 1 to 24 months lags for six considered LSCIs, a pool of 144 LSCIs is formed for each month, from which the relevant LSCIs for a given month are chosen using the global version of PCIS presented in Hatami et al. (2019). Results are summarized in Fig. 4.4. Each panel includes the results at one site, in which rows are months ordered from October to September from the top to the bottom. Columns show the six considered LSCIs. In each month, the relevant LSCIs that are selected through the PCIS algorithm are numbered and shaded. Numbers identify relevant lags and colors indicate values of Kendall's tau dependencies between selected LSCIs and the corresponding monthly flows. As it can be observed, the dependencies between LSCI and monthly streamflow are dynamic within a year and there can be months in which more than one LSCIs to which streamflow is significantly dependent. This is particularly the case in high flow months (e.g. April's flow), in which the fully extended version of C-vine mentioned in Section 2.1 should be implemented. Among the considered LSCIs, PDO is the most frequent LSCI selected across different months and demonstrates the strongest dependence with spring and summer flows. This empirical evidence is in line with previous findings, showing that the PDO is the dominant LSCIs in this region (e.g., Fleming et al., 2007; Nazemi et al., 2017). NAO and ENSO are the other two key LSCIs, which is in line with findings of Gobena and Gan (2006) for streamflow in southwestern Canada. Additionally, AO and PNA are among LSCIs selected more than once. These results are inline with previous findings over western Canada (e.g., Bonsal and Shabbar, 2008; Gobena and Gan, 2006).
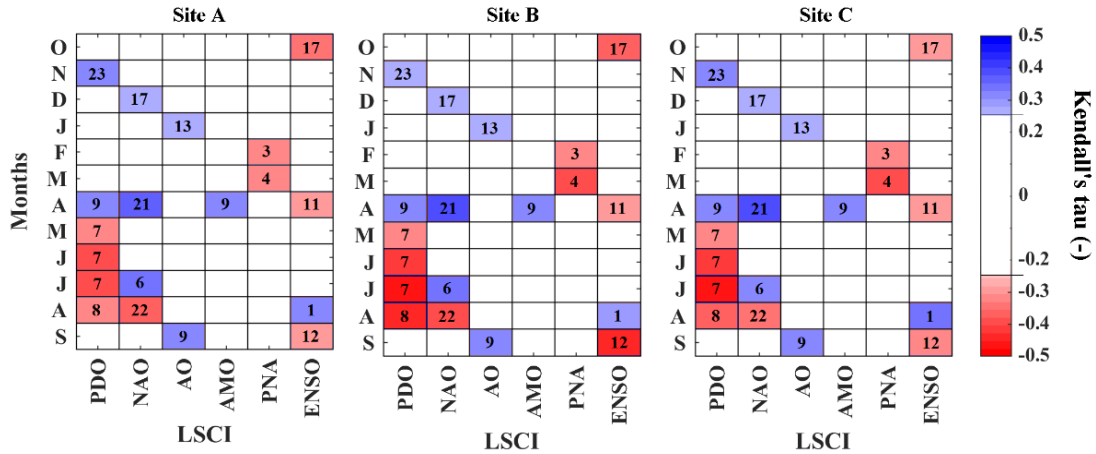
Figure 4.4. Influential LSCIs with their respective monthly lags, chosen collectively at sites A, B, and C using PCIS algorithm. Shades of blue and red in the first row show positive and negative dependencies between lagged LSCIs and streamflow at the monthly scale, which are significant at *p*-value< 0.05. Numbers inside significant cells identify relevant lags in month between LSCIs and monthly flows.

To address the uncertainty in the selected predictors, we repeat the input selection using the PMI algorithm. PMI uses mutual information as oppose to the Kendall's tau used in the modified PCIS, used in this study. Results are presented in Fig. C1 in the Appendix C, showing a considerable match between the results of PCIS and PMI. In 7 out of 12 months, including all wet months, the results of PMI and PCIS are fully identical. In months January, April, and August, PMI chooses some LSCI that PCIS does not identify. Similarly in May, PCIS can identify a LSCI that PMI has missed. Only in February, which is a dry month, PMI and PCIS result into fully divergent sets of relevant LSCIs. This intercomparison certifies the selection of relevant LSCIs.

4.5.2. Benchmarking the skill of the proposed model in the projection mode

By identifying the influential LSCI, the proposed model can be setup and evaluated using the procedure explained in Section 4. We first evaluate the results in the projection mode. Fig. 4.5 shows the long-term expected statistics of the first three moments of the monthly streamflow, i.e., mean, standard deviation, and skewness, obtained from 10,000 realizations with the same length as the historical data. In each panel, pink and gray lines depict the results obtained by the reference and proposed models, respectively. Black lines indicate the observed values. In general, both the reference and proposed algorithms are able to preserve the observed statistics very well. Considering the single site generation and in site A, Relative Errors (REs) in projecting the expected long-term monthly flow for both models is less than 5% across all months. Although reconstructing observed values of monthly standard deviation and skewness entails more error, the REs remain less than 10% for both the reference and proposed models, except for the skewness of monthly flow in February reconstructed by the proposed model (RE = 21%). In site B, both the reference and proposed models can represent the long-term expected statistics of the three moments in all months with REs less than 10% in both single and multisite settings, except for the single site generation in months of August and September in which REs in the representation of standard deviation and skewness obtained by the reference model is higher than 20%. In site C, the REs in the representation of long-term expected

statistics of monthly flows by the reference and proposed models are less than 5% in the single site setting. While in the multisite reconstruction of site B, both proposed and reference models show similar performance, the REs in the representation of the long-term expected mean and standard deviation of monthly flows are marginally higher for the reference model in site C, yet remain below 10%. The REs in the multisite generation of long-term expected skewness of monthly flows in site C is lower for the proposed model, particularly in the low flow season.

We also assess the performance of our proposed algorithm in preserving the lag-1 temporal dependencies within each site as well as lag-0 spatial dependence between primary (here site A) and secondary sites (here sites B and C). Fig. 4.6 summarizes findings in the representation of (a) lag-1 temporal, and (b) lag-0 spatial dependencies, respectively. Black lines show the observed lag-1 and lag-0 dependencies. Pink and gray colors illustrate the results obtained by the reference and proposed models in single and multisite settings, respectively.
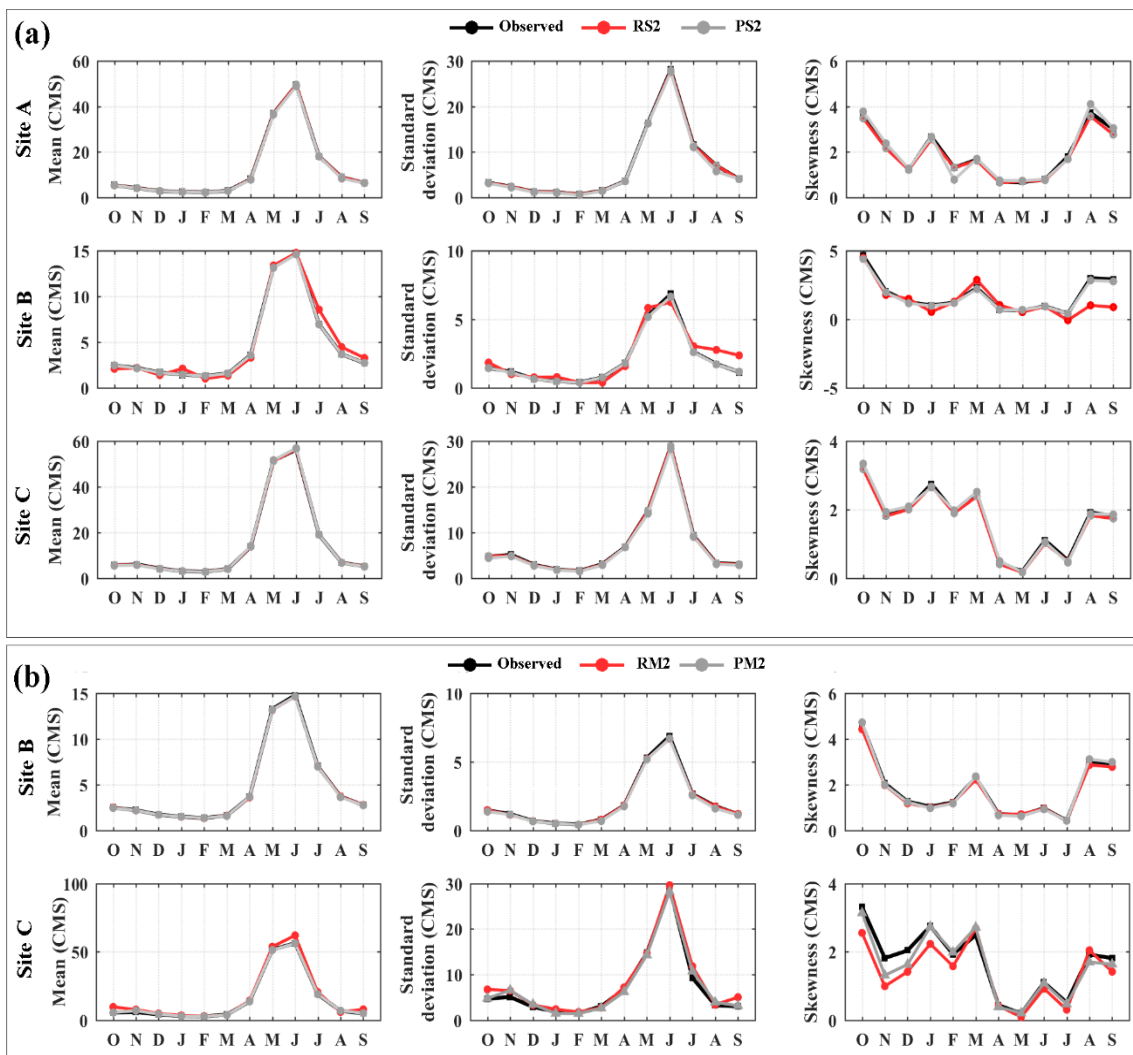
Figure 4.5. Performance of the reference and proposed algorithms in capturing long-term statistics of three first moments of monthly streamflow, i.e. mean (left panels), standard deviation (middle panels), and skewness (right panels) at the three sites in (a) single site and (b) multisite settings. Black lines show is observed statistics. Pink and gray lines show the simulated results obtained by the reference and proposed algorithms.

In summary, both reference and proposed algorithms are able to preserve temporal and spatial dependencies quite well. In the single-site setting, the reference and proposed algorithms are able to preserve the lag-1 temporal dependencies with an absolute error of less than 0.1. In the multisite setting, the proposed model can preserve lag-1 temporal dependence with absolute error values of less than 0.1, except few cases during the low flow season in site C. The reference model, however, show better performance in capturing the temporal dependence in those months. The interesting point is that the lag-1 dependence in site B is preserved better in multisite setting, when streamflow in site B is conditioned based on the generated flow in site A. This, however, is not the case in site C. Regarding the spatial dependencies, both the reference and proposed models can capture the spatial dependencies with less than 0.1 absolute error in multisite scheme.
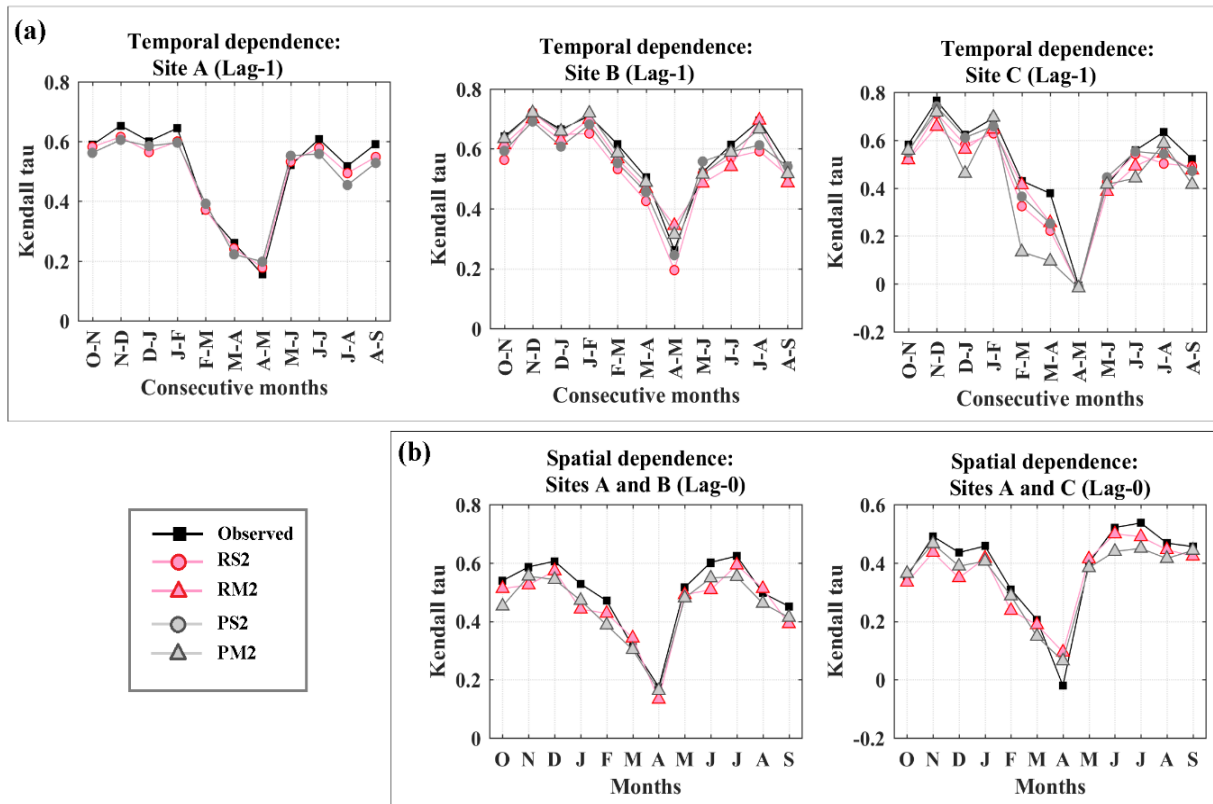
Figure 4.6. Performance of the reference and proposed algorithms in capturing (a) the observed lag-1 monthly temporal dependence and, (b) monthly lag-0 spatial dependencies between primary and secondary sites. Observed dependencies are shown in black lines. Results related to the reference and proposed models are shown in pink and gray colors, respectively.

We assess the performance of the reference and proposed models in capturing the interdependencies between lagged LSCIs and the flows at a monthly scale. Fig. 4.7 depicts the expected MAE in representing observed interdependencies between influential LSCIs and monthly flows, demonstrated in Fig. 4.4. Panel (a) is related to the reference algorithm and panels (b) and (c) are related to the performance of the proposed algorithm in single and multisite settings, respectively.

In general, the expected MAE in the representation of interdependencies for the reference model is high (MAE > 0.25). This is due to the fact that the reference model does not explicitly represent

the interdependencies between lagged LSCI and monthly streamflow. The performance of the proposed model in contrast is significantly better, showing an expected MAE of below 0.1 for high flow season and below 0.15 for low flow season in single site setting. The expected MAE in multisite setting is below 0.15 for both low and high flows.
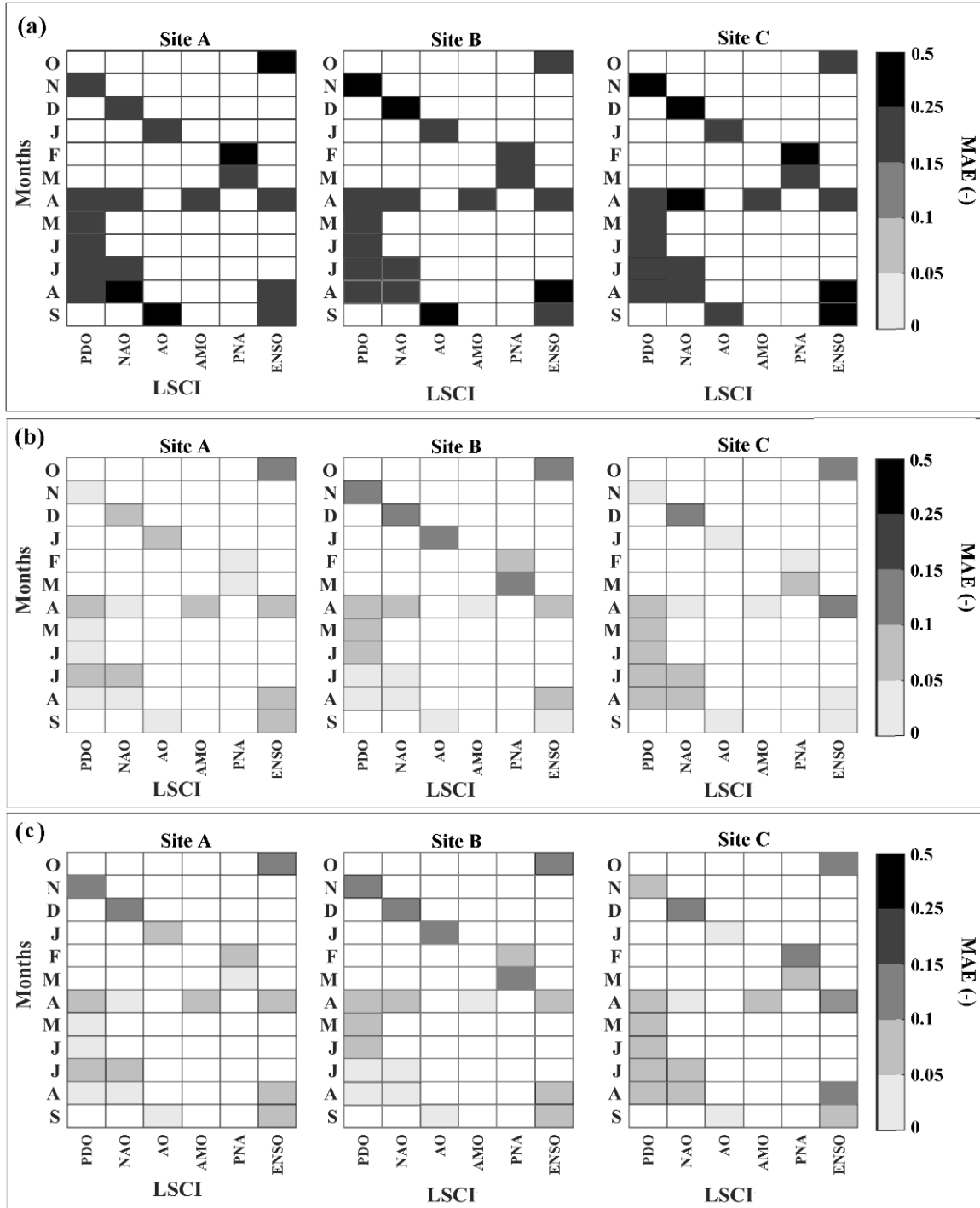
Figure 4.7. The expected Mean Absolute Error in representing the interdependencies between influential LSCIs and streamflow at monthly scale. The result related to the reference model is shown in the top row. The

results related to the proposed model are shown in the middle and bottom rows for the single and multisite settings, respectively.

The projected streamflow ensembles generated by proposed and reference models in both single and multisite settings are investigated in the form of hydrographs for the driest year (1977-78), a normal year (i.e. near long-term average; 2008-2009), and the wettest year (1995-96), as illustrated in Fig. 4.8. For simulations during the entire data period see Figs. C2 to C6 in the Appendix C. The pink and gray ensembles are the 95% CI obtained by the reference and proposed models, respectively. The black lines show the observed time series. This figure clearly shows that proposed and reference models can capture the observed time series within the 95% CIs. Having said that, the seasonality can be much better represented by the proposed model than the reference model. This can be supported by significantly narrower CI is in the case of the proposed model. Considering single site generation and in the dry year, the expected reduction in the CI across the three sites is 45% and 54.9% during low and high flow seasons, respectively.
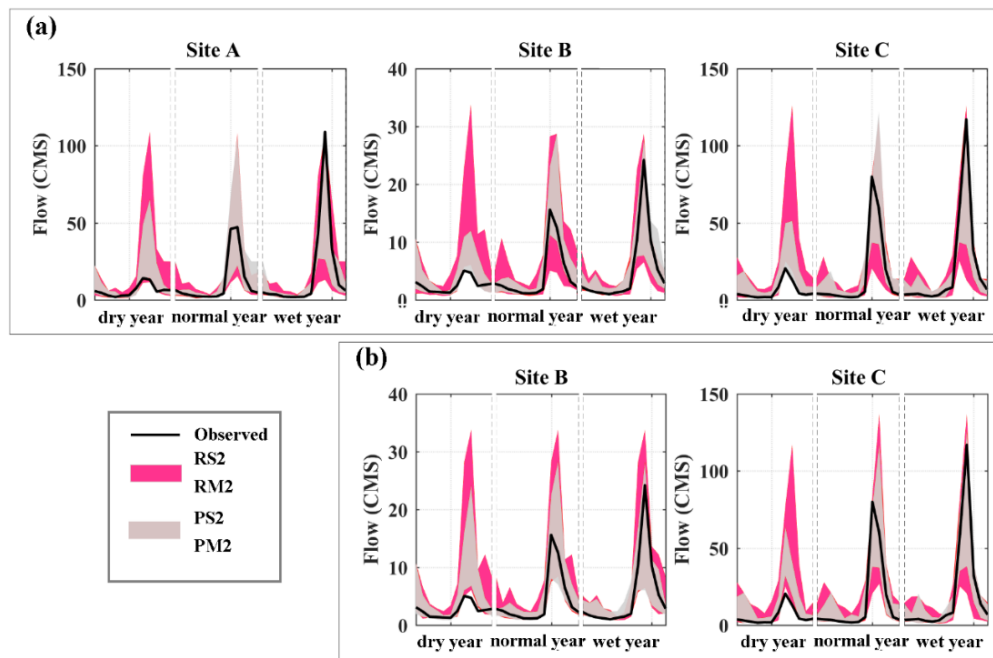
Figure 4.8. Streamflow ensembles generated through (a) single site and (b) multisite setting of the reference and proposed models for the driest (1977-78), a near average (2008-2009) and the wettest year (1995-96) at the three headwaters. Pink and gray ensembles show the 95% confidence intervals of the reference and the proposed models, respectively, obtained by 10,000 realizations. The black lines are the observed streamflow at the three sites.

The expected reduction in projected CI in the multisite setting is slightly lower and marks 40.6% and 51.3% in low and high flow seasons, respectively. In the normal year, the expected reduction in the CI across the three sites in the single site setting are 30.6% and 22% during low and high flow seasons, respectively. In contrast to dry year, the expected reduction in multisite setting is more than single site and marks 38.8% and 23.3% during low and high flow seasons, respectively. In the wet year and through single site generation, the average reduction in the proposed model is 26.8% and

35% during low and high flow seasons, respectively. Similar to the dry year the improvements in predictive uncertainty are slightly less in multisite setting, and marks 21.3% and 28.8% reduction compared to the reference model during low and high flow seasons, respectively.

We also analyze the performance of the proposed model in representing the extremes. For this purpose, we fit a Generalized Extreme Value (GEV) distribution to the annual low and high flows, enabling the extrapolation beyond the range of observed data. Figure 9 shows the uncertainty bounds of ensembles of 10,000 GEVs fitted to simulated annual low and high flows in single (Fig. 4.9a) and multisite settings (Fig. 4.9b). Fig. 4.9 includes two rows, showing the ensembles of fitted GEVs for the simulated annual low (top rows) and high flows (bottom rows). The dots are the observed extremes, and the black lines are the fitted GEV distribution to the observed extremes. The skill is assessed by the percentage of reduction in CI of generated streamflow (10,000 realizations) as the Percentage of Coverage (POC), which is the percentage of observed data falling within the CI of generated streamflow. In general, both reference and the proposed model demonstrate high skills in capturing the observed extremes within the CI. In the single site setting and for the low flows, the proposed and reference models are expected to capture 88.9% and 92.9% of extremes within their CI, respectively. Regarding the high flows, proposed and reference models show POCs of 95.2% and 96.0%, respectively. Similar skills can be seen in the multisite setting, where both POCs are 90.5% and 91.7% for proposed and reference models in representing the annual low flows, respectively. These POCs changes in the case of high flows to 94.0% and 96.4%, respectively.

While the POC statistics are slightly better in the case of the reference models, CIs are substantially reduced, providing less uncertainty in the projected flow. In single site setting and for low flows, the average range of CI of the proposed model is reduced by 11.7% compared to the reference model; whereas, this value is 3.1% in the multisite setting. Regarding the high flows, the range of CI of the proposed model is much reduced compared to the reference model, reaching to average of 15.5% and 31.1% reduction in single and multisite settings, respectively.

Finally, we investigate the performance of the proposed model in representing of interannual variability. Fig. 4.10 represents percentages of improvement in interannual skill scores at single (panel a) and multiple sites (panel b). The average improvement in this skill score in the single site setting is 10.2% across the three considered sites. The lowest and highest improvements occur in site A and site B with average improvements of 3.6% and 14.1%, respectively. The proposed model demonstrates improvements in capturing interannual variability during high flow season with an average improvement of 16.0% in single site generation and across the three sites. In the multisite setting, the average improvement in the interannual variability skill score is slightly lower, with expected improvements of 13.5% and 10.1% in sites B and C, respectively. Having said that during the high flow season, considering relevant LSCI in the multisite generation results in more improvements compared with the single site generation. The expected improvement in capturing the interannual variability during the high flow season is 23.5% in sites B and C.
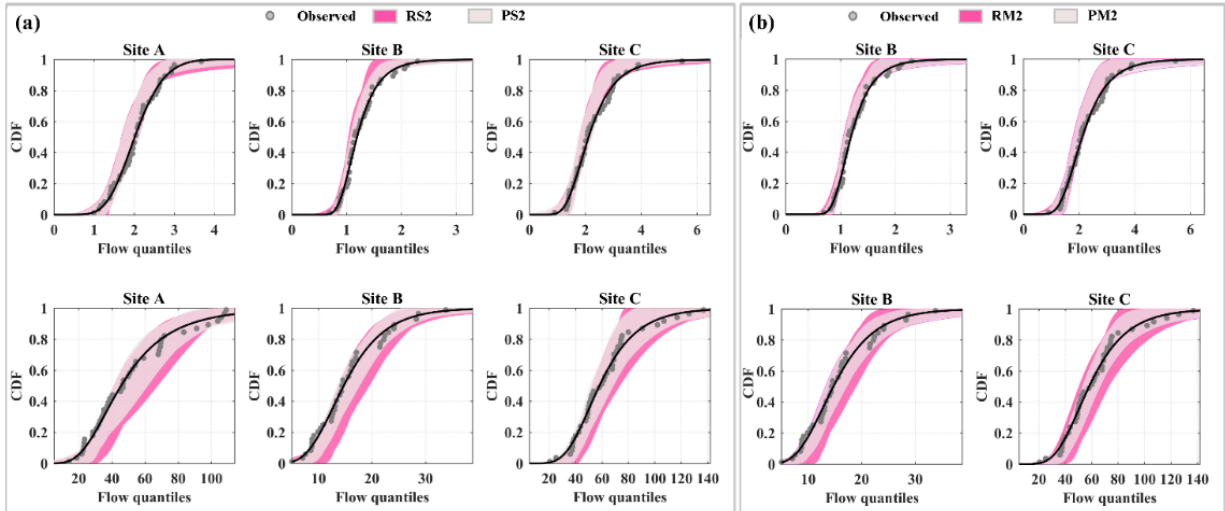
Figure 4.9. Reduction in the uncertainty bounds of projected extremes obtained by the proposed model at (a) single site and (b) multiple sites, in comparison with the reference models. In each panel, the top and bottom rows are related to the fitted GEV distribution fitted to the annual low and high flow values. The darker and lighter pink envelopes are related to the proposed and the reference models, respectively. The dots are the observed annual low and high flows. The solid black lines are the fitted GEV distribution.
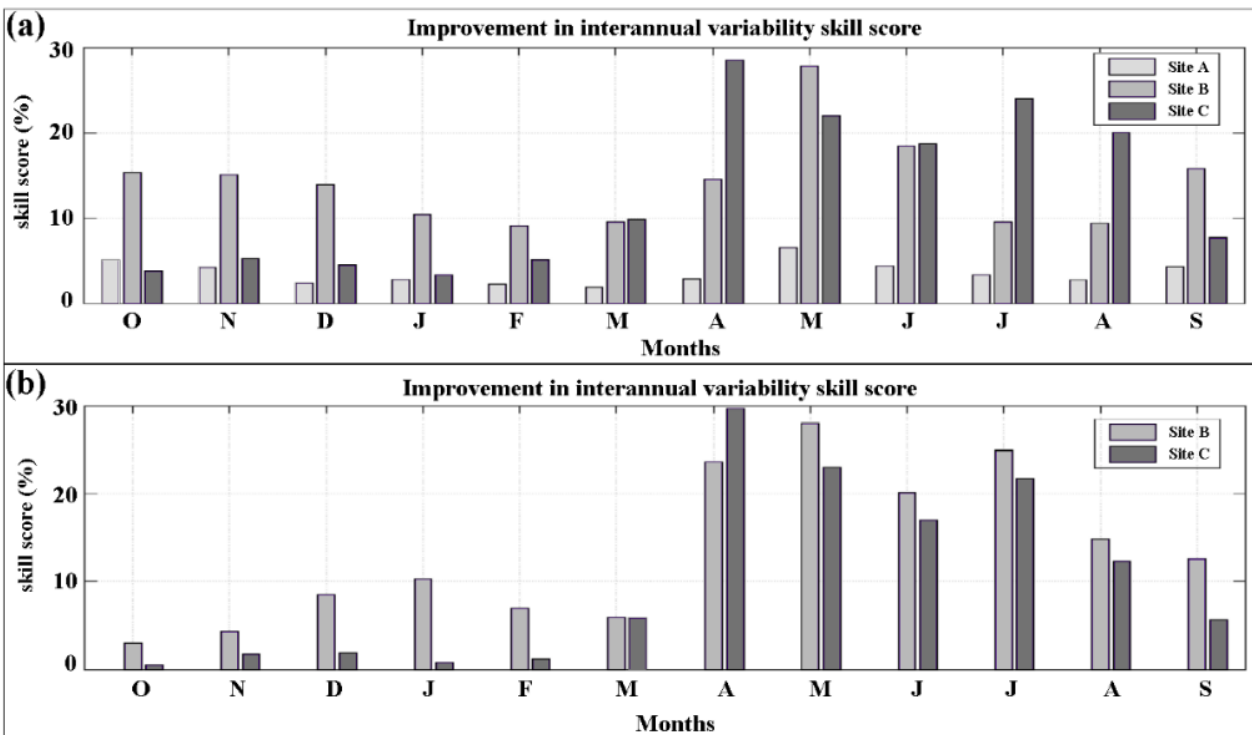
Figure 4.10. Improvements in capturing interannual variability obtained by the proposed model in single-site (panel a) and multisite settings (panel b) compared with the corresponding reference models.

4.5.3. Benchmarking the skill of the proposed model in the prediction mode

In the prediction mode, five skill scores including SS_{MAE}, SS_{RMSE}, SS_{RMSEP}, SS_{CRPS}, and SS_{KGE} are reported for single (Fig. 4.11a) and multisite (Fig. 4.11b) settings at the three considered sites. Generally speaking, predictions made by the proposed algorithm exhibit better skills than reference models. The average improvement in single site predictions is $\overline{SS}_{MAE} = 5.3\%$, $\overline{SS}_{RMSE} = 4.5\%$, $\overline{SS}_{RMSEP} = 5.8\%$, $\overline{SS}_{CRPS} = 6.2\%$, and $\overline{SS}_{KGE} = 14.3\%$. The range of changes in skill scores varies largely across different months and extends from -15% to $+35\%$. The greatest improvement in skill scores in the single site generation occurs in high flow season with average increases of $\overline{SS}_{MAE} = 15.3\%$, $\overline{SS}_{RMSE} = 12.8\%$, $\overline{SS}_{RMSEP} = 13.4\%$, $\overline{SS}_{CRPS} = 14.1\%$, and $\overline{SS}_{KGE} = 27.1\%$. In the multisite prediction of streamflow in secondary sites B and C, a similar pattern can be seen except few discrepancies in low flow season. In general, simulation made by the proposed model exhibits improvement in almost all months with average improvements of $\overline{SS}_{MAE} = 5.4\%$, $\overline{SS}_{RMSE} = 3.1\%$, $\overline{SS}_{RMSEP} = 6.4\%$, $\overline{SS}_{CRPS} = 4.9\%$, and $\overline{SS}_{KGE} = 15.4\%$. The most encouraging result is the improvement in the skill scores during the high flow season reaching to $\overline{SS}_{MAE} = 16.4\%$, $\overline{SS}_{RMSE} = 14.9\%$, $\overline{SS}_{RMSEP} = 14.1\%$, $\overline{SS}_{CRPS} = 15.8\%$, and $\overline{SS}_{KGE} = 28.3\%$. These skills vividly show the value gained by incorporating LSCIs into streamflow prediction, particularly in high flow seasons.

In addition to the improvement in the prediction errors, we assess the reliability of streamflow predictions. Figure 12 presents histograms of the PITs related to the prediction using the proposed scheme against its reference counterparts in single (Fig. 4.12a) and multisite settings (Fig. 4.12b). Each panel includes two rows, showing the PIT histograms for the low and high flow seasons (winter and spring; top and bottom rows, respectively). The gray and pink envelopes show the PIT histograms obtained by 10,000 realizations generated by the proposed and reference schemes, respectively. The deviations from uniformity in PIT histograms can be quantified using the measure of degree of uniformity, D, with lower values indicating better reliability. Perfectly reliable predictions produce a PIT histogram with a uniform distribution. The expected value of perfect prediction, D_p, is 0.0267. Regarding the low flow season, although the predictions made by both the reference and proposed schemes exhibit slight overdispersion, but in general both models show average deviation from PIT uniformity close to the perfect prediction. In low flow season and in single site, the proposed model shows slightly better reliability in prediction of observed values with average $D = 0.0251$ compared to $D = 0.0267$ for the benchmark scheme. Similarly, in multisite setting the average deviation related to PIT of the proposed scheme is 0.0242 compared to 0.0262 for the benchmark scheme, indicating slightly better reliability of the proposed scheme. Regarding the high flow season, similar to low flow, both models exhibit slight overdispersion. In single site setting, the average deviation of PIT related to the proposed model is 0.0214 compared to 0.0262 for the benchmark model, demonstrating slightly better reliability of the proposed model. In multisite setting, these values are 0.0163 and 0.0211 for the proposed and benchmark models, respectively.

Additionally, to further assess the reliability of predictions in single and multisite settings particularly in terms of the extremes, we evaluate the improvement in the 95% CIs of the proposed scheme against its reference counterparts in single (Fig. 4.13a) and multisite settings (Fig. 4.13b).

Each panel includes two rows, showing the CIs in the low and high flow seasons (i.e., winter and spring; top and bottom rows, respectively). The gray and pink envelopes show the 95% CI obtained by 10,000 realizations generated by the proposed and reference algorithms, respectively. Black dots are the observed flow qsuantiles and the solid lines are the best predictions (mean ensembles) obtained either in single site (panel a) or multisite (panel b) settings. For each flow season, the uncertainty intervals during dry (flows with percentile level of 0.1 or lower) and wet conditions (flows with percentile level of 0.9 or higher) are separated from the rest of the flow conditions by the dashed red lines.
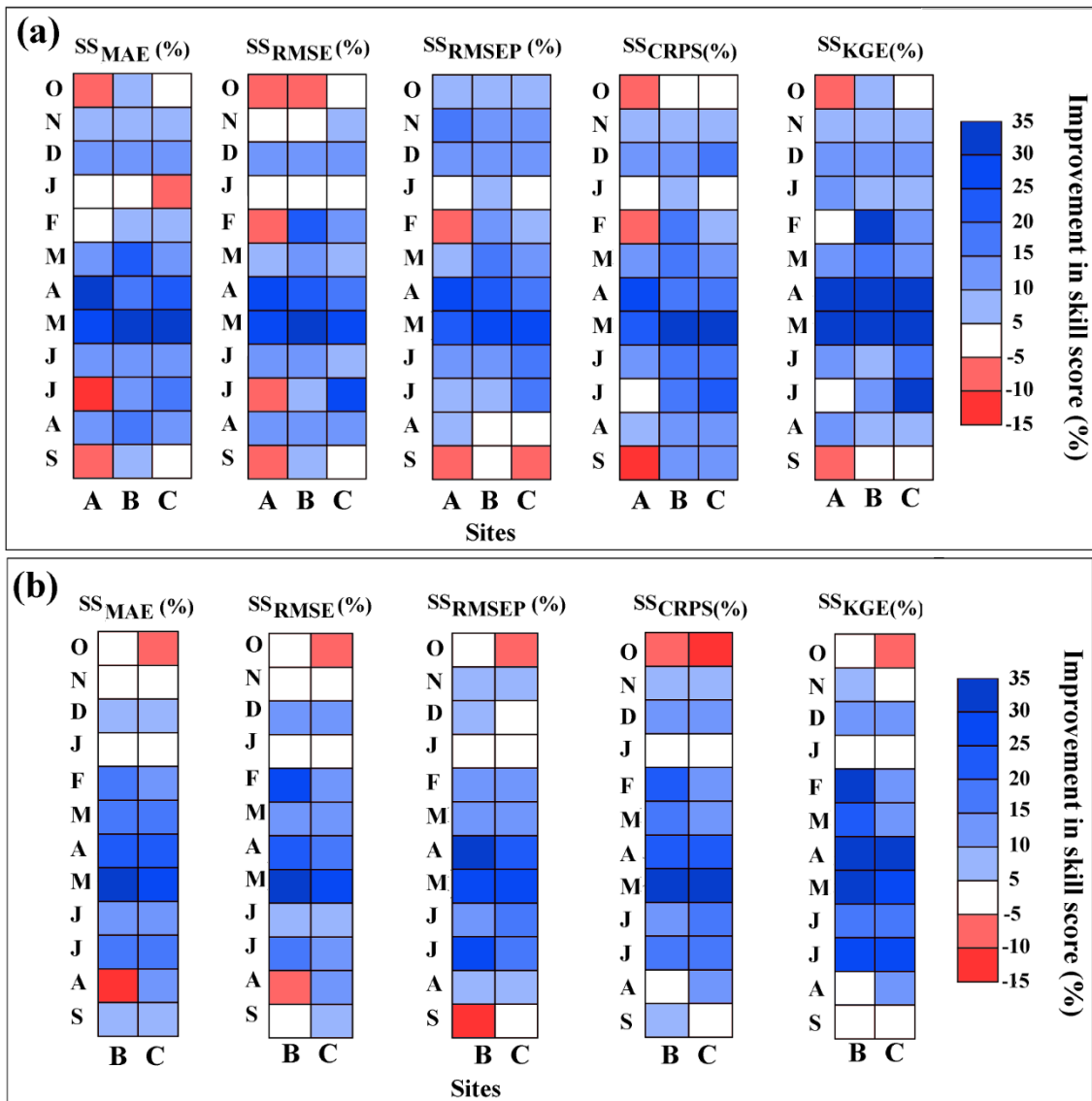
Figure 4.11. Improvements in the five considered predictive skill scores by informing the stochastic streamflow generation with LSCIs at single (panel a) and multiple sites (panel b)
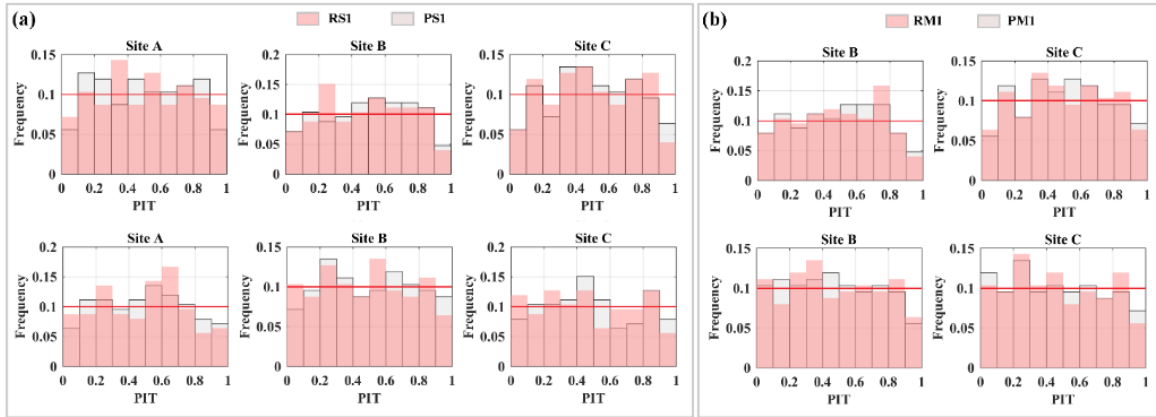
Figure 4.12. Probability Integral Transform histograms obtained by the proposed model at (a) single site and (b) multiple site settings, compared to the corresponding reference models. In each panel, the top and bottom rows are related to the low and high flow seasons, respectively. The gray and pink bars show PIT histograms of the proposed and the reference models, respectively.
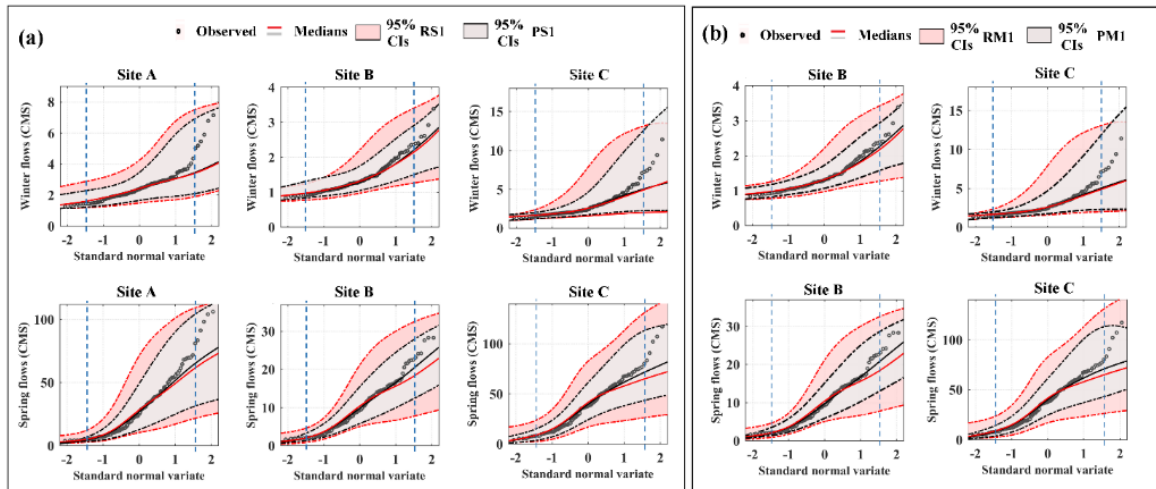
Figure 4.13. Improvements in the uncertainty bounds of the predictions obtained by the proposed model at (a) single site and (b) multiple sites compared with the corresponding reference models. In each panel, the top and bottom rows are related to the low and high flow seasons, respectively. The gray and pink envelopes show the 95% CIs related to the proposed and the reference models, respectively. The solid lines are the mean of predicted ensembles, taken as the best prediction. The black dots are the observed flows. Dashed lines separate the dry, normal, and wet flow conditions in each season.

Based on Fig. 4.13, empirical distributions of the observed high and low flows fall within 95% CI of both the reference and proposed models in all sites and through single and multisite settings. Having said that, the proposed model can estimate the flow with much less uncertainty. The average reduction in CI during the low flow season is 18.3% and 21.1% in single and multisite settings. Reductions in the uncertainty bounds during the high flow season, however, are much larger with expected reductions of 41.3% and 45.1% through the single and multisite settings, respectively. In the low flow season, the highest reductions in the uncertainty bounds occur in the normal flow conditions (between 0.1 to 0.9 percentile) with expected reductions of 26.3% and 31.4% in CI through single and multisite settings, respectively. In the high flow season, the largest improvements in the

uncertainty bounds happen during dry conditions with average reductions of 68.3% and 64.5% in CI through single and multisite settings, respectively.

4.6. Summary and conclusion

Skillful and reliable streamflow prediction and projection capabilities are of urgent needs for water resource planning and management. Here we aim at improving the skills of stochastic streamflow generation at single and multiple sites by explicit incorporation of LSCIs through a stochastic generator. In particular, we suggest a sampling scheme based on using C-vine copulas, in which the structure and parameters of the model change at each time step. This is due to the variation of the influential LSCIs and the type of dependencies, which can change across different timesteps, here monthly. To accommodate this, we use a global input selection algorithm to pick the most significant LSCIs from a pool of potential predictors at each month and consider the selected LSCIs as influential predictors, to which the streamflow is conditioned.

To showcase the application of this model in practice, we demonstrate the use of the proposed algorithm at single and multiple sites, and in both prediction and projection modes in three headwaters of the Oldman River Basin, Alberta, Canada. The performance of the proposed algorithm is rigorously compared with the observed data as well as reference models that are essentially identical to proposed models, yet do not use any information about LSCIs within stochastic streamflow generation. The results of our study show that while simulation performances of the reference and proposed models are very similar in representing the first three moments of monthly streamflow as well as lag-1 temporal and lag-0 spatial dependencies within and between streamflow reaches, the explicit consideration of LSCIs can significantly reduce simulation uncertainty and improve simulation skills in projection and predictive modes and in both single and multisite settings, particularly in high flow seasons. In projection mode and considering the single site setting, the expected reductions in CI in the three sites are 34.1% and 37.1% in low and high flow seasons, respectively. In multisite setting, these values are 33.6% and 34.5% in low and high flow seasons, respectively. The average improvement in the interannual variability skill score in single and multisite settings is over 10% across the three considered sites. Having said that during the high flow season, considering relevant LSCI in the multisite streamflow generation results in expected improvement in capturing the interannual variability by more than 23%. In terms of observed annual extremes, both reference and proposed models can capture the observed values within the range of CI with high POC values of greater than 90% in most cases. The proposed model, however, demonstrates less uncertainty in capturing the observed extremes, particularly regarding high flows for which the ranges of CI are decreased by 15.5% and 31.1% in single and multisite settings, respectively.

In prediction mode, both reference and proposed models show slight overdisperision in PIT histograms in single and multisite settings, but with expected deviation from uniformity close to perfect reliability value $D_p = 0.0267$. The expected deviations from the uniformity of PIT histograms of the proposed model are 0.0233 and 0.0203 in single and multisite settings; whereas, these values are 0.0265 and 0.0237 for the benchmark model, indicating slightly better reliability of the proposed model. In terms of CI, the average reduction during the low flow season is 18.3% and 21.1% in single

and multisite settings. Reductions in the uncertainty bounds during the high flow season, however, are much larger with expected reductions of 41.3% and 45.1% through the single and multisite settings, respectively. Within the high flow season, the largest improvements in the uncertainty bounds happen during dry conditions with average reductions of 68.3% and 64.5% in CI through single and multisite settings, respectively.

Although the method is developed for lead time of one month the proposed algorithm is generic and can be applied in other basin. Our proposed method can be also extended by including more conditioning variables such as precipitation and/or temperature, whether observed or simulated. This can provide a versatile and comprehensive model to inform water management models for better planning under current and future conditions. We hope that our contribution here can inspire more efforts toward improved stochastic generation of streamflow in prediction and projection modes.

A Global Algorithm for Identifying Changing Streamflow Regimes: Application to Canadian Natural Streams (1966-2010)[4]

The contents of this chapter are published as "Zaerpour, M., Hatami S., Sadri J., & Nazemi, A. (2021). A global algorithm for identifying changing streamflow regimes: Application to Canadian natural streams (1966-2010)." in Hydrology and Earth System Sciences. The contents are slightly modified from the submitted article.

Synopsis

Climate change affects natural streamflow regimes globally. To assess alterations in streamflow regimes, typically temporal variations in one or few streamflow characteristics are taken into account. This approach, however, cannot see simultaneous changes in multiple streamflow characteristics, does not utilize all the available information contained in a streamflow hydrograph, and cannot describe how and to what extent streamflow regimes evolves to one another. To address these gaps, we conceptualize streamflow regimes as intersecting spectrums that are formed by multiple streamflow characteristics. Accordingly, the changes in a streamflow regime should be diagnosed through gradual, yet continuous changes in an ensemble of streamflow characteristics. To incorporate these key considerations, we propose a generic algorithm to first classify streams into a finite set of intersecting fuzzy clusters. Accordingly, by analyzing how the degrees of membership to each cluster change in a given stream, we quantify shifts from one regime to another. We apply this approach to the data, obtained from 105 natural Canadian streams, during the period of 1966 to 2010. We show that natural streamflow in Canada can be categorized into six regime types, with clear hydrological and geographical distinctions. Analyses of trends in membership values show that alterations in natural streamflow regime vary among different regions. Having said that, we show that in more than 80% of considered streams, there is a dominant regime shift that can be attributed to simultaneous changes in streamflow characteristics, some of which have remained previously unknown. Our study not only introduces a new globally relevant algorithm for identifying changing streamflow regimes, but also provides a fresh look at streamflow alterations in Canada, highlighting complex and multifaceted impacts of climate change on streamflow regimes in cold regions.

5.1. Introduction

Natural characteristics of streamflow are critical to ecosystem livelihood and human settlements around river systems (Poff et al., 2010; Nazemi and Wheater, 2014; Hassanzadeh et al., 2017). Historically, humans have considered seasonality, variability, and magnitude of natural streamflow as key factors for determining potentials for socio-economic developments (Knouft and Ficklin, 2017). Streamflow characteristics are diverse and can contain different information. While some

---

[4] Zaerpour, M., Hatami, S., Sadri, J., & Nazemi, A. (2021). A global algorithm for identifying changing streamflow regimes: application to Canadian natural streams (1966–2010). Hydrology and Earth System Sciences, 25(9), 5193-5217, https://doi.org/10.5194/hess-25-5193-2021.

streamflow characteristics determine potentials for agriculture and energy production (Hamududu and Killingtveit, 2012; Amir Jabbari and Nazemi, 2019; Nazemi et al., 2020), some others proxy the consequences of devastating disasters such as floods or droughts (Arheimer and Lindström, 2015; Burn and Whitfield, 2016; Zandmoghaddam et al., 2019).

A set of streamflow characteristics, collectively defining the overall flow behavior in a river reach, is called the streamflow regime (Poff et al., 1997). Traditionally, streamflow regimes have been considered stationary in time (Milly et al. 2008). However, the looming effects of climate change along with human interventions through land and water management have raised fundamental questions regarding stationarity of streamflow regime during the current "*Anthropocene*" (Arnell and Gosling, 2013; Nazemi and Wheater, 2015a, 2015b). Even in undisturbed streams, recent literature is full of evidence, indicating major alterations induced by heightened climate variability and change (Barnett et al., 2005; Stahl et al., 2010; Rood et al., 2016; Hodgkins et al., 2017; Dierauer et al., 2018). As a result, assessing how streamflow regime is changing as a result of alterations in natural and anthropogenic drivers is currently one of the imminent questions in the field of hydrology.

Despite the extensive body of knowledge already gathered around assessing the effects of climate change on altering streamflow regimes, there are still rooms for methodological developments. Most importantly, among many potential flow characteristics that can constitute and describe streamflow regime, often only a few are taken into account (Whitfield and Cannon, 2000; Hall et al., 2014; Vormoor et al., 2015). This is a limitation because climate change impacts are often manifested in the entire streamflow hydrograph, and not only around a unique set of streamflow characteristics (Olden and Poff, 2003). This is particularly the case in cold regions as at the watershed scale, multiple processes contribute to the streamflow generation, each behaving differently in response to climate variability and change (Whitfield and Pomeroy, 2016; Zaerpour et al., 2019). As a result, alterations in streamflow regimes are not only significant (e.g., Déry and Wood, 2005; MacDonald et al., 2018; Islam et al., 2019; Champagne et al., 2020); but also they are complex, due to compound impacts of changes in temperature, shifts in forms and magnitude of precipitation, as well as alterations in snow/ice accumulation and melt (DeBeer et al., 2016; Hatami et al., 2018; Rottler et al., 2020; Hatami and Nazemi, 2021). At this stage of development, it is not yet possible to systematically quantify streamflow regimes and their alterations to one another using a large set of simultaneously changing streamflow characteristics (Burn et al., 2016; Burn and Whitfield, 2018).

Here, we propose a new methodology to address this challenge. First, by considering more streamflow characteristics, the distinctions between regime types and their alterations become more fuzzy and relative. Accordingly, in line with some recent suggestions in the literature (see e.g., Ternynck et al., 2016; Burn and Whitfield, 2017; Knoben et al., 2018; Brunner et al., 2018, 2019; Aksamit and Whitfield, 2019; Jehn et al., 2020), we conceptualize streamflow regimes as continuous spectrums rather than distinct states. This conceptualization requires a methodology that can formally deal with subjectivity in the definition of streamflow regimes. For this purpose, we use elements of fuzzy set theory (see Zadeh, 1965; Nazemi et al., 2002) to provide a methodological basis to classify streamflow regimes as intersecting clusters. We then measure the gradual departure from one fuzzy

cluster to others using significant monotonic trends in membership degrees and use this information as an indicator for a regime shift in a given stream. Accordingly, we highlight how such regime shifts are attributed to changes in streamflow characteristics using a formal dependence analysis.

We apply this algorithm in Canada, where the rate of warming is twice the global average (Bush and Lemmen, 2019), and changes in streamflow characteristics are significant in time and space (e.g., Buttle et al., 2016; O'Neil et al., 2017; Dierauer et al., 2020). By considering more than 100 natural streams, we provide – for the first time – a homogeneous, pan-Canadian view on recent alterations in natural streamflow regimes. The remainder of this paper is as the following: Section 5.2 describes our three-step methodology related to (i) clustering regime types, (ii) detecting regime changes, and (iii) attributing regime changes to alterations in streamflow characteristics. Section 5.3 introduces our case study and the data. The results and discussions are presented in Sects 5.4 and 5.5. Finally, Sect. 5.6 concludes our work and provides some further remarks.

5.2. Methodology

5.2.1. Rationale and proposed algorithm

From both conceptual and computational perspectives, quantifying changes in streamflow regimes is not a trivial task due to the relativity in the definition of streamflow regime and how a change can be identified. On the one hand, the flow regime at a given stream is defined by a large number of streamflow characteristics, some of which have conflicting trends in time and space. On the other hand, the flow regime is often identified based on similarity/dissimilarity of characteristics in a set of benchmarking streams with known regimes. Accordingly, regime shifts are not only defined based on alterations in streamflow characteristics relative to the past, but also with respect to relative changes with respect to other streams with known regime types. This creates a complex mathematical problem due to the "*curse of dimensionality*" (see e.g., Trunk 1979), meaning that the complexity of the problem increases exponentially by increasing the number of streams and/or streamflow characteristics, with which the streamflow regime is defined. To solve this problem, the general tendency in the literature is to reduce the dimensionality of the problem through the use of methodologies, such as Multi-Dimensional Scaling, Empirical Orthogonal Functions, and Principal Component Analysis (e.g., Maurer et al., 2004; Johnston and Shmagin, 2008). Despite methodological differences, all these approaches try to provide a parsimonious representation of a hyperdimensional space by creating a much simpler space that can preserve the sample variability in the original domain (Guetter and Georgakakos, 1993). Although these methodologies are able to substantially reduce the dimensionality and give valuable insights into changes in hyperdimensional data sets, the results are hard to interpret, particularly when attribution to some physical characteristics are concerned (Matalas and Reiher, 1967; Overland and Preisendorfer, 1982; Hannachi et al., 2009 and references therein). In the case of quantifying changes in streamflow regimes, this limitation translates into an inability to attribute the formation and transition in regime types directly to a set of specific streamflow characteristics.

Here, we aim at addressing this problem through a new methodology that does not rely on dimension reduction; rather, it tries to embrace the inherent high dimensionality of the problem. Below we suggest an integrated approach to (1) classify natural streamflow regimes into a set of interpolating regime types, (2) diagnose the gradual evolution in regime types and their shifts in time, and (3) attribute changes in streamflow regimes to alterations in streamflow characteristics. Fig. 5.1 shows the proposed procedure. We use MATLAB® Programming platform for the implementation of this procedure.
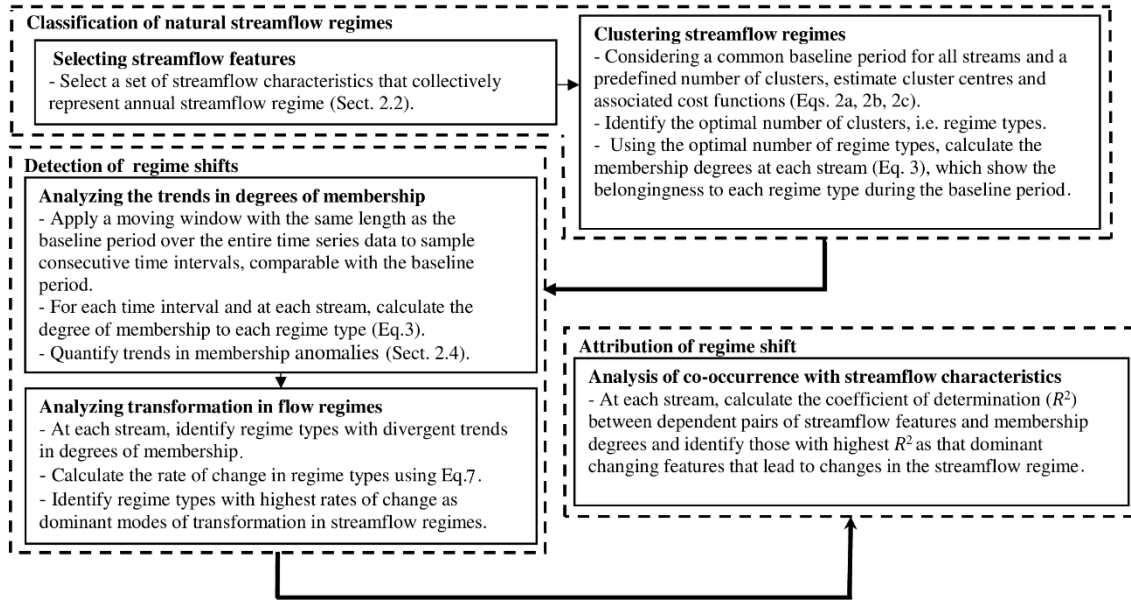
Figure 5.1. The workflow of the proposed three-step algorithm for classifying streamflow regime, diagnosing shift in streamflow regime, and attributing the regime shift to the changes in streamflow characteristics.

Our approach is built upon two fundamental considerations. First, we acknowledge that streamflow regimes are constituted by several streamflow characteristics, and therefore changes in streamflow regimes are manifested through changes in a large ensemble of streamflow characteristics. Second, we recognize that there are soft as oppose to hard distinctions between streamflow regimes; and, regime shifts occur gradually rather than abruptly. We select a large set of streamflow characteristics – or features – to collectively characterize the streamflow regime. We then use the Fuzzy C-Means algorithm (FCM) to classify streams into a set of overlapping regime types during a common initial data period. We accordingly quantify changes in degrees of association to each regime type during the entire data period using a moving trend analysis. By monitoring the co-occurrence of divergent trends in membership values, the transitions of regime types to one another can be identified. Finally, we monitor the co-evolution of regime shifts with the alterations in streamflow characteristics through a formal dependency analysis.

5.2.2. Feature selection

Indicators of Hydrologic Alterations (IHAs; Richter et al., 1996) are commonly applied as *features* to characterize changes in natural streamflow regimes (e.g., Wang et al., 2018). Different sets of IHAs can be considered to constitute streamflow regimes. Here we consider 15 IHAs, including annual mean flow, monthly mean flows as well as timings of the annual low and high flows that together can represent the shape of the annual hydrograph. At each stream, we use the mean (first moment) and variance (second moment) of these 15 indicators during a multi-year timeframe to come up with 30 features that together can capture the shape of the expected annual hydrograph and the variability around it. Table 5.1 shows the name and notation of the features used, where $x_{j=1:15}$ and $y_{j=1:15}$ denote the mean and the variance of the 15 considered IHAs.

Table 5.1. The thirty streamflow features used for clustering natural streamflow regime in Canada.

Feature	Notation	Feature	Notation	Feature	Notation	Feature	Notation	Feature	Notation
October mean flow	mean: x_1 variance: y_1	November mean flow	mean: x_2 variance: y_2	December mean flow	mean: x_3 variance: y_3	January mean flow	mean: x_4 variance: y_4	February mean flow	mean: x_5 variance: y_5
March mean flow	mean: x_6 variance: y_6	April mean flow	mean: x_7 variance: y_7	May mean flow	mean: x_8 variance: y_8	June mean flow	mean: x_9 variance: y_9	July mean flow	mean: x_{10} variance: y_{10}
August mean flow	mean: x_{11} variance: y_{11}	September mean flow	mean: x_{12} variance: y_{12}	Annual flow	mean: x_{13} variance: y_{13}	Timing of the annual low flow	mean: x_{14} variance: y_{14}	Timing of the annual high flow	mean: x_{15} variance: y_{15}

5.2.3. Fuzzy C-means clustering

Clustering is the process of arranging data into a finite set of classes, so that members in the same class have similar characteristics. Various statistical methodologies are used for clustering in hydrology (see Tarasova et al., 2019; Brunner et al., 2020), often to non-overlapping (i.e. hard) classes (Olden et al., 2012). Recent theoretical developments have alternatively considered a set of overlapping (i.e. soft) classes, in particular in the form of fuzzy clusters (e.g., Knoben et al., 2018; Wolfe et al., 2019). The association to each fuzzy cluster can be quantified using a degree of membership (see Bezdek, 1981; Sikorska et al., 2015). The process of clustering streamflow regime using FCM can be summarized as the following: Assume that streamflow data from N hydrometric gauges during a common timeframe w with the length of l years are available. For each stream, the first and second moments of n IHAs (here $n = 15$), i.e. $\mathbf{X} = [x_{ij}]$, $\mathbf{Y} = [y_{ij}]$; $i \in \{1, \ldots, N\}$, $j \in \{1, \ldots, n\}$, can be extracted during the initial timeframe w. Before going forward, extracted features are normalized to avoid scale mismatches:

$$\bar{x}_{i,j} = \frac{x_{i,j} - \mathbf{min}\{x_{i=1:N,j}\}}{\mathbf{max}\{x_{i=1:N,j}\} - \mathbf{min}\{x_{i=1:N,j}\}} \quad \forall j \in \{1,\ldots,n\} \tag{5.1a}$$

$$\bar{y}_{i,j} = \frac{y_{i,j} - \mathbf{min}\{y_{i=1:N,j}\}}{\mathbf{max}\{y_{i=1:N,j}\} - \mathbf{min}\{y_{i=1:N,j}\}} \quad \forall j \in \{1,\ldots,n\} \tag{5.1b}$$

where $\overline{\mathbf{X}} = [\bar{x}_{ij}]$ and $\overline{\mathbf{Y}} = [\bar{y}_{ij}]$ are the matrices of Normalized Streamflow Features (NSFs). FCM partitions the N streams into C fuzzy clusters, such that the sum of distances for all streams $i \in \{1, \ldots, N\}$ between NSFs and cluster centroids is minimized. This is often formulated through an iterative optimization procedure, aiming at finding the cluster centroid by minimizing the generalized least-squared error function as the objective of optimization (Bezdek, 1981):

$$J(\mathbf{U}, \mathbf{V} \mid \overline{\mathbf{X}}, \overline{\mathbf{Y}}) = \sum_{c=1}^{C} \sum_{i=1}^{N} (u_{i,c})^2 d^2([\bar{x}_{i,j=1:n}\bar{y}_{i,j=1:n}], v_{c,m=1:2n}) \tag{5.2a}$$

This objective function is subject to the following two constraints:

$$\sum_{c=1}^{C} u_{i,c} = 1 \quad \forall\, i \in \{1, \ldots, N\} \tag{5.2b}$$

$$0 < \sum_{i=1}^{N} u_{i,c} < N \quad \forall\, c \in \{1, \ldots, C\} \tag{5.2c}$$

where $\mathbf{V} = v_{c=1:C,m=1:2n} = [\overline{x^*}_{c,j=1:n}, \overline{y^*}_{c,j=1:n}] = [\overline{x^*}_{c,1}, \ldots, \overline{x^*}_{c,n}, \overline{y^*}_{c,1}, \ldots, \overline{y^*}_{c,n}] \in \mathbb{R}^{2n}$ is the matrix of cluster centroids (i.e., regime types); the matrix of $\mathbf{U} = [u_{i,c}]; i \in \{1, \ldots, N\}, c \in \{1, \ldots, C\}$ is the matrix of memberships; and $d^2([\bar{x}_{i,j=1:n}, \bar{y}_{i,j=1:n}], v_{c,m=1:2n})$ is the matrix of squared Euclidian distances between NSFs of stream i and clusters' centroid c. The fuzzy membership matrix can be accordingly calculated as:

$$u_{i,c} = \frac{\left(\dfrac{1}{d^2([\bar{x}_{i,j=1:n}\bar{y}_{i,j=1:n}], v_{c,m=1:2n})}\right)}{\displaystyle\sum_{c=1}^{C} \left(\dfrac{1}{d^2([\bar{x}_{i,j=1:n}\bar{y}_{i,j=1:n}], v_{c,m=1:2n})}\right)}; \quad i \in \{1, \ldots, N\}, c \in \{1, \ldots, C\} \tag{5.3}$$

The number of clusters C (here regime types) can be chosen as a *priori*, or empirically using validity indices (Srinivas et al., 2008). Here, we implement three validity indices of Xie-Beni index (V_{XB}; Xie and Beni, 1991), partition index (V_{SC}; Bensaid et al., 1996), and separation index (V_S; Fukuyama and Sugeno, 1989). These indices are based on two criteria, namely compactness and separation. The compactness characterizes how close members to each cluster are; whereas, the separation measures how distinct two clusters are. A good clustering result should have both small intra-cluster compactness and large inter-cluster separation. The Xie-Beni validity index is the ratio of compactness to the separation, quantified by the average of fuzzy variation of NSFs from clusters' centroids to the minimum squared distance between cluster centroids. Note that $\sum_{i=1}^{N} (u_{i,c})^2 d^2([\bar{x}_{i,j=1:n}, \bar{y}_{i,j=1:n}], v_{c,m=1:2n})$ is the compactness of fuzzy cluster c and separation of fuzzy clusters is quantified by the minimum squared Euclidean distance between cluster centroids:

$$V_{XB} = \frac{\sum_{c=1}^{C} \sum_{i=1}^{N} \left(u_{i,c}\right)^2 \boldsymbol{d}^2 \left(\left[\bar{x}_{i,j=1:n}, \bar{y}_{i,j=1:n}\right], v_{c,m=1:2n}\right)}{N \times \min\limits_{c,\ l \neq c} \left(\boldsymbol{d}^2 \left(\left[v_{l,m=1:2n}, v_{c,m=1:2n}\right]\right)\right)} \tag{5.4}$$

Partition index is quantified by the sum of *individual* fuzzy cluster variations (i.e., the compactness of fuzzy clusters) to the sum of the distances from cluster centroids (i.e., the separation of fuzzy clusters). This ratio is further normalized by fuzzy cardinality weight γ_c, defined by $\gamma_c = \sum_{i=1}^{N} u_{i,c}$, to avoid the bias made by cluster sizes.

$$V_{SC} = \sum_{c=1}^{C} \left\{ \frac{\sum_{i=1}^{N} \left(u_{i,c}\right)^2 \boldsymbol{d}^2 \left(\left[\bar{x}_{i,j=1:n}, \bar{y}_{i,j=1:n}\right], v_{c,m=1:2n}\right)}{\gamma_c \times \sum_{l=1}^{c} \boldsymbol{d}^2 \left(v_{l,m=1:2n}, v_{c,m=1:2n}\right)} \right\} \tag{5.5}$$

The separation index, also known as Fukuyama and Sugeno index, is defined based on the difference between the compactness and the separation of fuzzy clusters:

$$V_S = \left\{ \sum_{c=1}^{C} \sum_{i=1}^{N} u_{i,c}^2 \cdot \boldsymbol{d}^2 \left([\bar{x}_{i,j=1:n}, \bar{y}_{i,j=1:n}], v_{c,m=1:2n}\right) \right\}$$
$$- \left\{ \sum_{c=1}^{C} \sum_{i=1}^{N} u_{i,c}^2 \cdot \boldsymbol{d}^2 \left([v_{c,m=1:2n}, \bar{v}]\right) \right\} \tag{5.6}$$

in which $\bar{v} = \sum_{c=1}^{C} v_i / c$. We identify the optimal number of clusters using the elbow method (see Satopaa et al., 2011; Kuentz et al., 2017), which involves finding the maximum number of clusters, beyond which slopes of improvement in validity indices flatten significantly; and adding a new cluster does not justify the increased complexity.

5.2.4. Detection of change in streamflow regimes

Clustering natural streams into c regime types takes place during a baseline timeframe (i.e., the first initial years with the length of l years), in which the optimal number of clusters, cluster centroids, and initial membership degrees to each regime type are identified. For each stream, the timeframe can be moved year-by-year and the membership values can be recalculated for the new window using Eq. (3). Fig. 5.2 exemplifies this process in a hypothetical case. This results into C time series of membership degrees at each stream, showing how the association to each regime type evolves in time – see Jaramillo and Nazemi (2018). In order to quantify the gradual change in membership degrees, the Mann-Kendall trend test with the Sen's Slope is applied (Mann, 1945; Sen, 1968; Kendall, 1975). As the sum of memberships in each timeframe is 1 (see Eq. 2b), a positive trend in memberships to one cluster should coincide with a negative trend in the membership of at least one other cluster. At each stream, this transition can be identified by significant negative dependencies between membership degrees.
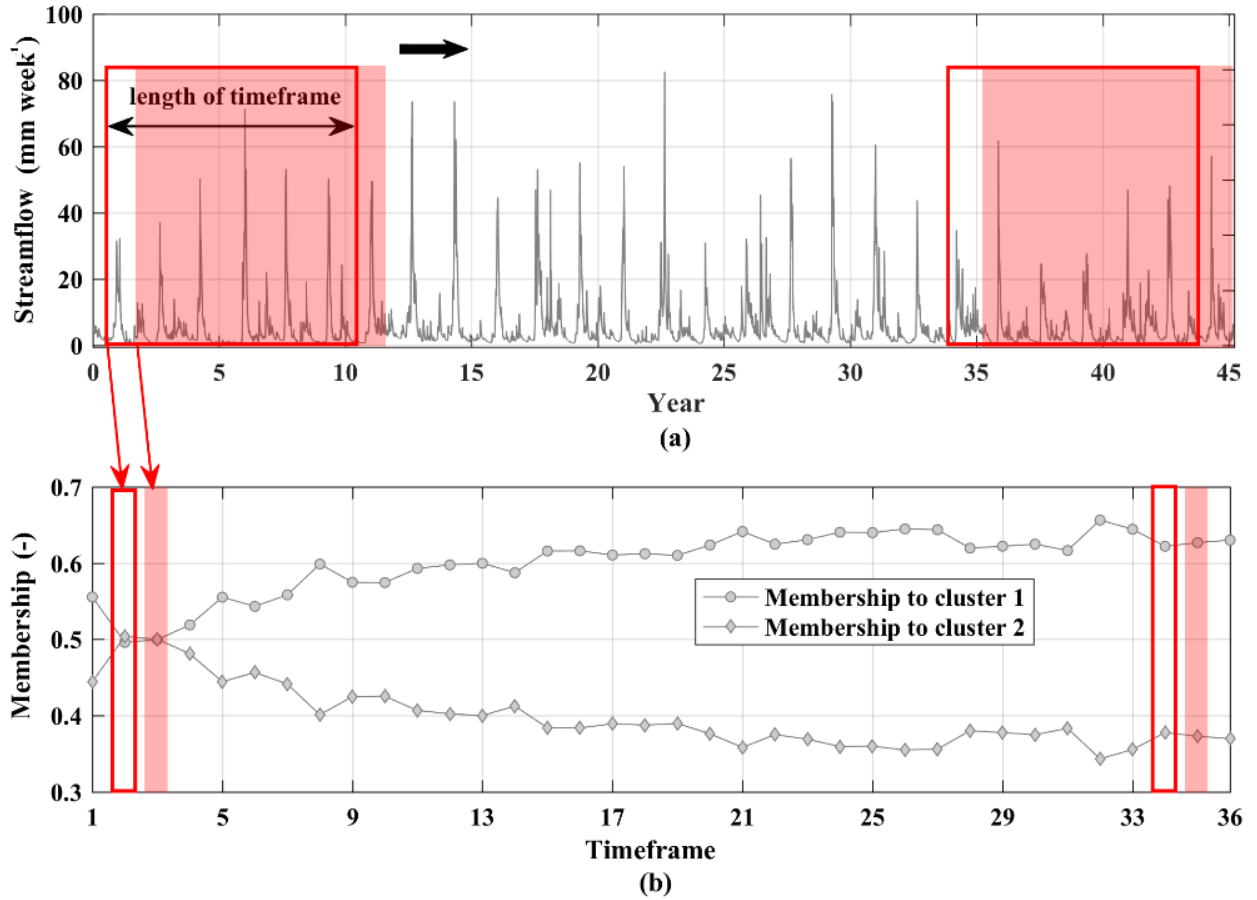
Figure 5.2. A schematic view to the procedure of identifying the evolution in membership values using a moving window; (a) a decadal timeframe slides over the streamflow time series year-by-year; (b) membership degrees are recalculated at each decadal timeframe to systematically determine the changes in association to each regime type determined in the beginning of the data period.

Given the pair of clusters p and q in the stream i, the rate of shift from p to q can be quantified using Eq. 7, where $u_{i,p}(w)$ and $u_{i,q}(w)$ are membership degrees to clusters p and q in stream i during the timeframe w; $w \in \{1, \dots, r\}$; r is the number of moving timeframes needed to cover the whole data period year-by-year; $\mathbf{E}(u_{i,p})$ and $\mathbf{E}(u_{i,q})$ are the expected memberships; and $S_{i,(p,q)}$ is the slope of the best-fitted line.

$$S_{i,(p,q)} = \left| \frac{\sum_{w=1}^{m} \left(u_{i,q}(w) - \mathbf{E}(u_{i,q}) \right) \left(u_{i,p}(w) - \mathbf{E}(u_{i,p}) \right)}{\sum_{w=1}^{m} \left(u_{i,q}(w) - \mathbf{E}(u_{i,q}) \right)^2} \right| \tag{5.7}$$

5.2.5. Attribution of change in streamflow regime to alterations in streamflow characteristics

Here, the existence of significant dependence between membership values and streamflow features is taken as the basis for attribution. Accordingly, we use Kendall's tau (Genest and Favre, 2007;

Nazemi and Elshorbagy, 2012) to detect the co-occurrence between changes in memberships and changes in NSFs. Fig. 5.3 shows the procedure of attribution. Left panels show the changes in membership degrees of two hypothetical clusters (purple lines), along with the corresponding changes in two NSFs (grey lines). Right panels show the scatter plots of membership degrees *vs.* the NSFs. We identify the significance and the direction of dependence using the Kendall's tau coefficient. To measure the linear association between changes in streamflow features $x_{i,j}$ and membership values $u_{i,c}$, the coefficient of determination (R^2; see Legates and McCabe Jr., 1999) is used. R^2 varies between [0, 1] and determines how much of the variability in the degrees of membership can be described by the variability in a given streamflow characteristic. The greater the R^2 is, the stronger the association between changes in degrees of membership and the streamflow characteristics is. The coefficient of determination can be calculated as:

$$R^2\big(u_{i,c}, x_{i,j}\big) = \frac{\left\{\sum_{w=1}^{r} \big(u_{i,c} - \mathbf{E}(u_{i,c})\big)\big(x_{i,j} - \mathbf{E}(x_{i,j})\big)\right\}^2}{\sum_{w=1}^{r} \big(u_{i,c} - \mathbf{E}(u_{i,c})\big)^2 \sum_{w=1}^{r} \big(x_{i,j} - \mathbf{E}(x_{i,j})\big)^2} \quad \forall\, i \in \{1, \dots, N\} \tag{5.8}$$

By the simultaneous use of Kendall's tau and R^2, we try to facilitate quantitative communication of the impact of changes in a specific streamflow characteristic on the transition from one regime type to another. By using the Kendall's tau, we identify the sign and significance of dependencies between changes in membership degrees and streamflow characteristics using a non-parametric approach that can handle non-linearity in the form of association. Using R^2, we quantify how much of the variability in the membership degrees can be described by the variability in the changes in streamflow characteristics. This is to provide a comprehendible measure of association between the two quantities.

As R^2 is a linear-based measure, we repeat the experiment by replacing the R^2 with squared Kendall's tau and discuss the uncertainty in our attribution. The key advantage of our proposed algorithm is in providing a workflow in which the detection of a change in streamflow regime is directly attributed to changes in streamflow characteristics. Fig. 5.4 shows this integration using a hypothetical example. The left panel demonstrates a multifaceted change in the shape of the annual hydrograph in a given stream during two separate periods, shown with grey and pink envelopes. The black and red lines are expected annual hydrographs for each envelope (i.e., the mean of annual streamflow hydrographs over the timeframe), respectively. Any shift between flow regimes is described by at least a pair of membership time series with opposite trends. The strength of the link is measured using R^2. The right panel shows the rates of shifts and the attribution to changes in streamflow characteristics. The thickness of links is proportional to rates of shift and/or R^2 values.
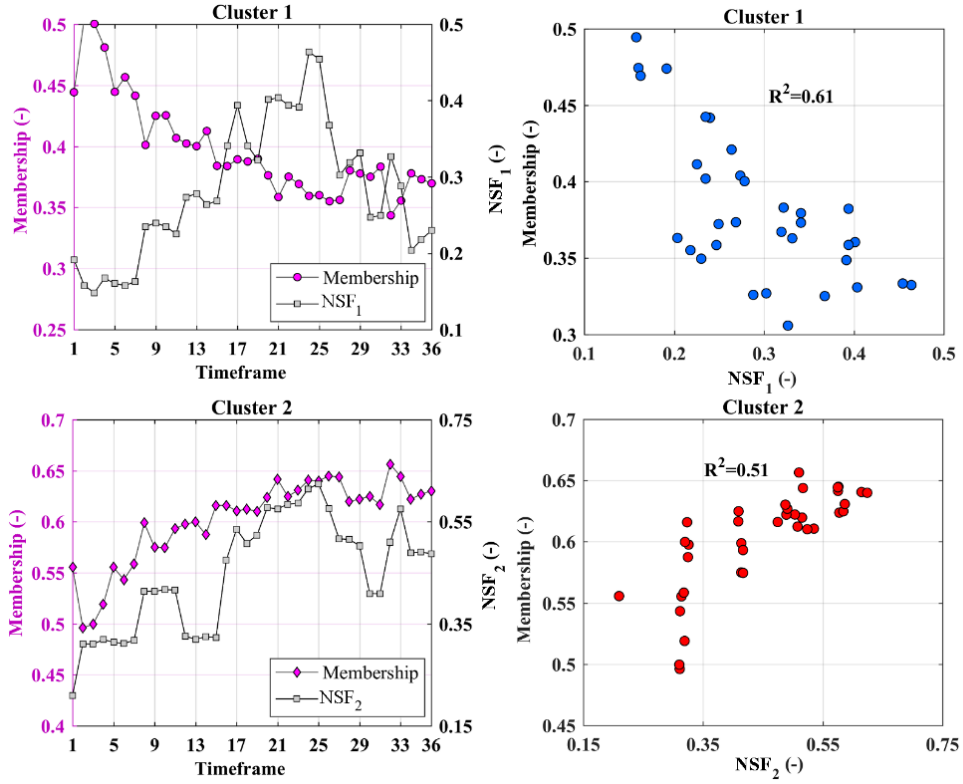
Figure 5.3. The procedure of attributing changes in membership degrees to changes in streamflow characteristics. The left column shows the co-evolution of membership degrees and Normalized Streamflow Features (i.e., NSF_1 and NSF_2). The right column measures the correspondence between changes in membership degrees and normalized streamflow features through percentage of described variance quantified using R^2. Red or blue dots show the positive or negative dependencies, respectively.
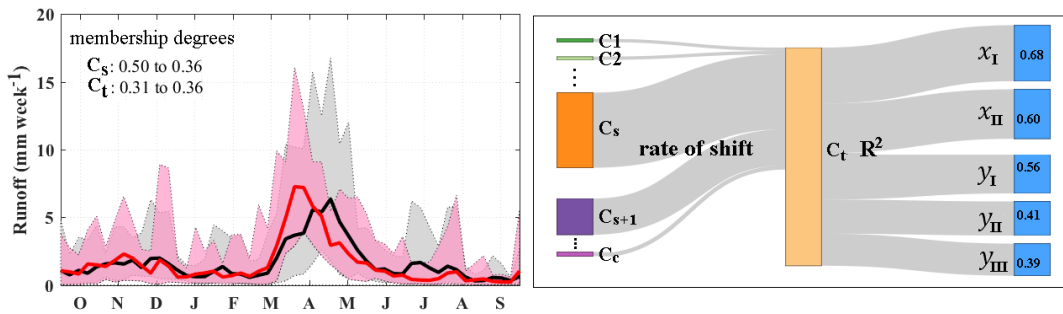
Figure 5.4. An example for transitions between regime types along with attribution of change to streamflow characteristics. The left panel shows annual hydrographs in two separate periods using grey and pink envelopes. The panel in the right shows the dominant shift in the flow regime by maximum rate of shift, and attributes this shift to changes in significantly dependent streamflow characteristics. The dominant shift is visualized by the thickest grey envelope. The strength of the association between regime shift and significantly dependent streamflow characteristics are measured and communicated by R^2.

5.3. Case study and data

With a total drainage area equivalent to 6% of the global land area, Canadian rivers support important socio-economic activities such as agriculture and hydropower production. River systems in Canada

can be divided into four major ocean-drained basins, namely Pacific, Atlantic, Arctic, and Hudson Bay that can be further divided into a number of sub-basins (Pearse et al., 1985; Natural Resources Canada, 2007). The Pacific basin, the smallest among all, spreads on the west coast from the US border to Yukon and drains around 1 million km^2. The main sub-basins in the Pacific include Fraser, Yukon, Columbia, and the Seaboard. In the east coast, the Atlantic basin drains a total area of 1.6 million km^2, and includes important water bodies such as the Great Lakes. The basin includes three sub-basins, namely the St. Lawrence River, Seaboard, and the Saint John-St. Croix. Towards the north, the Arctic basin drains over 3.5 million km^2 of northern lands and includes some of Canada's largest lakes other than the Great Lakes such as the Slave, Athabasca, and Great Bear lakes. The Mackenzie, Peace-Athabasca, and Seaboard are the main sub-basins in the Arctic basin. With an area of 3.8 million km^2, the Hudson Bay is the largest drainage basin in Canada, covering five provinces from Alberta in the west to Québec in the east. The basin includes four major sub-basins, namely Western & Northern Hudson Bay, Nelson, Northern Ontario, and Northern Québec. Nelson, Saskatchewan, and Churchill rivers are the major river systems in the Hudson Bay.

Natural streamflow regimes in Canada have undergone drastic changes in recent years, which are expected to increase under future climate change conditions (Woo et al., 2008). Observed and projected changes in streamflow regimes are not only between different regions (Kang et al., 2016; Islam et al., 2019); but also occur within the same ecological and/or hydrological regions (Whitfield, 2001, 2020). For instance, there are significant differences between forms of change in streamflow regimes between the northern and southern Pacific (Kang et al., 2016; Brahney et al., 2017). Similarly, glacier-fed rivers in northern Canada show increases in summer runoff (Fleming and Clarke, 2003); whereas other rivers show a tendency toward decreasing summer runoff (Fleming and Clarke 2003; Janowicz, 2008, 2011). To diagnose simultaneous changes in natural streamflow regimes across Canada, we use the data from Reference Hydrometric Basin Network (RHBN; Water Survey of Canada, 2017, http://www.wsc.ec.gc.ca/). RHBN includes 782 Canadian hydrometric stations that measures streamflow at unregulated tributaries and are particularly suitable to address climate change impacts on natural streamflow regimes (Brimley et al., 1999; Harvey et al., 1999). In the period of 1903 to 2015, we search for the largest subset of hydrologically unconnected stations with the longest continuous daily record during a common period and less than a month worth of missing data in a typical year. This results into selecting 105 streamflow stations during the water years of 1966 to 2010 (1 October 1965 to 30 September 2010).

Although drainage basins are often used as the spatial unit in which alteration in streamflow regime is investigated, there are substantial differences within a drainage basin in terms of climate, topography, vegetation, geology, and land use. This results into multiple forms of hydrological response within one drainage basin. In contrast to drainage basins, terrestrial ecozones are identified based on similarity in climate and land characteristics; and therefore, they can be more representative of different hydrological responses (Whitfield 2000). In brief, an ecozone is a patch of land with distinct climatic, ecologic, and aquatic characteristics (see Wiken 1986; Marshall et al., 1999; Wong et al., 2017). Canada includes 15 ecozones. Starting from the north, the Arctic Cordillera (EZ1),

covering 2% of Canada's landmass, contains the only major mountainous region in Canada other than the Rockies. The Northern Arctic (EZ2) is equivalent to 14% of Canada's landmass and covers Arctic Islands (Coops et al., 2008). The Southern Arctic (EZ3) includes the northern mainland, covering 8% of Canada. The Taiga Plains (EZ4) extends mainly on the western side of the Northwest Territories, covers 6% of Canada's landmass, and includes a large number of wetlands. Taiga Shield (EZ5) with large number of lakes, covers 13% of Canada's landmass in the south of the Southern Arctic (Marshall et al., 1999). The Boreal Shield (EZ6) is Canada's largest ecozone covering 18% of the country's landmass, extends from northern Saskatchewan toward the south into the Ontario and Québec and then northward toward eastern Newfoundland (Rowe and Sheard, 1981). The Atlantic Maritime (EZ7) includes the Appalachian mountain region, covering 2% of Canada, extends from the mouth of the St. Lawrence River and Bay of Fundy into coastlines of New Brunswick, Nova Scotia, and Prince Edward Island. The Mixedwood Plains (EZ8) is the most southerly ecozone, covering 2% of Canada, but includes the country's most populated regions in Ontario and Québec. The Boreal Plains (EZ9), covering 7% of Canada's landmass in western Canada, from British Columbia to the southeastern corner of Manitoba in the south of Boreal Shield (Ireson et al., 2015). The Prairies (EZ10) extends from south-central Alberta to southeastern Manitoba, covering 5% of Canada's landmass and the majority of Canada's agricultural lands (Nazemi et al., 2017). The Taiga Cordillera (EZ11) includes 3% of Canada with the least amount of Canada's forest and lies along the northern portion of the Rocky Mountains (Power and Gillis, 2006). The Boreal Cordillera (EZ12) covers 5% of Canada from northern British Columbia to the southern Yukon, with mountainous uplands and forested lowlands. The Pacific Maritime (EZ13) mainly includes the coastal mountains of British Columbia and lands adjacent to the Pacific Coast, having the warmest and wettest climate in the country, in an area around 2% of Canada (Wiken 1986). The Montane Cordillera (EZ14), with the most diverse climate in Canada, includes 5% of Canada in mountainous areas of southern British Columbia and southwestern Alberta and provides headwater flow to some important river systems such as Fraser, Saskatchewan, and Athabasca (Marshall et al., 1999). Finally, Hudson Plains (EZ15) includes 4% of Canada in the southern part of Hudson Bay with a large number of wetlands. Table 5.2 summarizes the selected stations within each ecozone.

Table 5.2. List of Canadian ecozones with at least one RHBN station in this study, along with their abbreviations and the number of RHBN stations considered within each ecozone.

Abbreviation	Ecozones	# of stations	Abbreviation	Ecozones	# of stations
EZ2	Northern Arctic	1	EZ8	Mixedwood Plains	5
EZ3	Southern Arctic	1	EZ9	Boreal Plains	6
EZ4	Taiga Plains	1	EZ10	Prairies	2
EZ5	Taiga Shield	4	EZ12	Boreal Cordillera	7
EZ6	Boreal Shield	25	EZ13	Pacific Maritime	9
EZ7	Atlantic Maritime	25	EZ14	Montane Cordillera	19
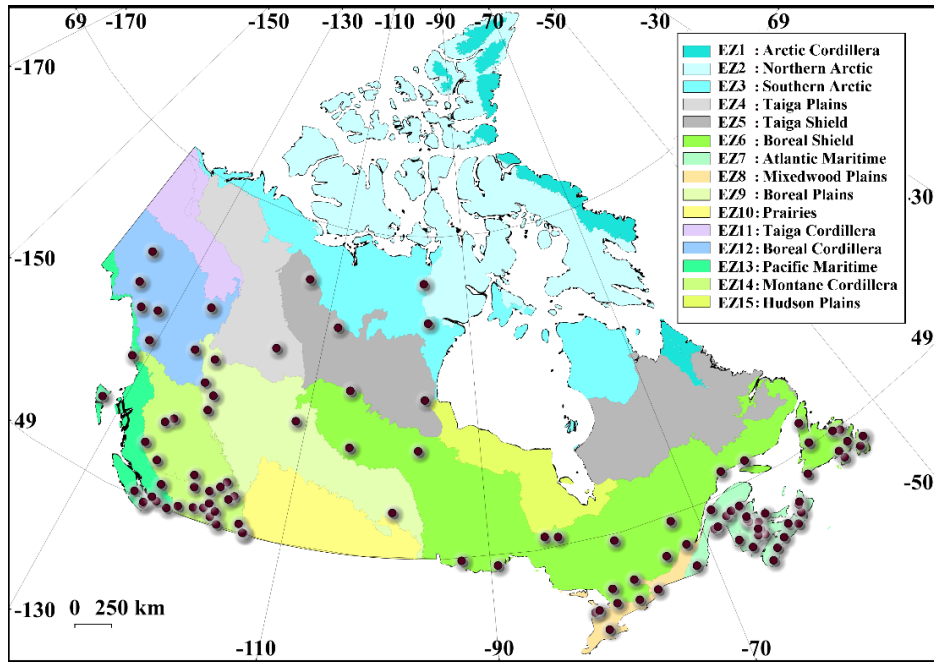
Figure 5.5. The distribution of the selected 105 RHBN streamflow stations within the Canadian ecozones.

Table D1 to D4 in the Appendix D introduce these stations across the four drainage basins in Canada. Figure 5 shows the distribution of the selected stations across the 15 ecozones. As it is clear, the density of selected stations varies greatly among ecozones. The highest numbers of stations are within Atlantic Maritime, Boreal Shield, and Montane Cordillera; while Southern and Northern Arctic as well as Taiga Plains, include only one; and there is no station in the Arctic Cordillera, Taiga Cordillera, and Hudson Plains. At the basin/sub-basin scale, the selected stations cover all 14 main Canadian sub-basins – see Table D5 and Fig. D1 in the Appendix D.

5.4. Results

We apply the framework proposed in Sect. 2 to the selected RHBN streams. At each stream, we first convert the daily discharge data into runoff depth in millimeters per week and calculate the thirty streamflow features introduced in Table 5.1. We then consider a multi-year timeframe for clustering and assigning initial membership values. The length of this timeframe should be chosen in a way that (1) provide a notion for streamflow regime, and (2) provide enough timeframes to assess evolution in membership values. As the aim is to address temporal changes in the streamflow regime, the baseline timeframe is considered at the beginning of the streamflow time series. Here, we present our result based on considering decadal timeframes and the period of 1966-1975 as the baseline. We address and discuss the sensitivity of our results to these assumptions in Sect. 5.

5.3.1. Identifying natural streamflow regimes in Canada

We attempt to find the optimal number of clusters empirically from the pool of $c = \{2, 3, \ldots, 10\}$, using the three validity indices introduced in Section 2.3. Fig. D2 in the Appendix D shows the result

of this investigation, indicating the optimal number of clusters as $c = 6$, where decreasing slopes of the three validity indices flatten. To provide a sense of these streamflow regimes and their changes in time, we visualize the shapes of annual streamflow hydrographs in the archetype streams during the baseline and the last decadal timeframe (i.e., 1966 to 1975 *vs.* 2001 to 2010) in Fig. 5.3 in the Appendix D. Archetype streams are those streams that have the highest association to the identified regime types and can represent the characteristics of a given regime better than other members of the cluster. Table 5.3 introduces these six regimes along with their notation and archetype streams. We name clusters based on two key characteristics, i.e. the form of hydrologic response (i.e. fast- *vs.* slow-response) as well as the timing of the annual peak flow (i.e., cold-season, freshet, and warm-season peak). The form of hydrologic response can be proxied by variability in the annual streamflow hydrograph. The greater the variability in the annual streamflow hydrograph is, the faster the hydrologic response is.

Table 5.3. Six identified regime clusters along with their labelled regime type and archetype stream.

Cluster	Regime type	Archetype (representative) stream
C1	slow-response/warm-season peak	Kazan River above Kazan Falls (HYDAT ID: 06LC001)
C2	fast-response/ warm-season peak	Clearwater River near Clearwater Station (HYDAT ID: 08LA001)
C3	slow-response/freshet peak	Matawin River at Saint-Michel-des-Saints (HYDAT ID: 02NF003)
C4	fast-response/freshet peak	Gander River at Big Chute (HYDAT ID: 02YQ001)
C5	slow-response/cold-season peak	Beaver Bank River near Kinsac (HYDAT ID: 01DG003)
C6	fast-response/cold-season peak	Sproat River near Alberni (HYDAT ID: 08HB008)

Fig. 5.6 shows a synoptic look at the distribution of streams belonging to each flow regime during the initial baseline timeframe. In each panel, the red star represents the archetype stream and streams with membership values of 0.1 and larger are shown with circles. The larger the size of a circle is, the greater the degree of membership to each cluster is. As Fig. 5.5 shows, the six clusters are geographically identifiable and resemble some of the already-known regime types across the country (see Whitfield, 2001; Bawden et al., 2015; Burn and Whitfield, 2016; Bush and Lemmen, 2019).

The "slow-response/warm-season peak" regime, i.e. cluster C1, includes streams with strong seasonality, high discharge in summer, and smaller variability in annual streamflow hydrograph compared to cluster C2, i.e. "fast-response/warm-season peak" regime. Cluster C1 is characterized by a gradual rise after spring snowmelt, prolonged peak discharge throughout summer, gradual recession during fall, and low runoff in winter (Déry et al., 2009). Streams belonging to C1 spread mostly in northwestern Canada and are either glacial-fed or lake-dominated streams, in which the hydrologic responses are delayed due to slow rate of glacial retreats and/or storage effects of large in-stream lakes. The Kazan River releasing into the Baker Lake in Nunavut is the archetype stream

for this regime type. C2 is very similar to C1, however with greater variability in annual streamflow hydrographs. The stream belonging to this stream are mainly concentrated in western Canada, particularly in Montane Cordillera (46% of streams), and include streams that are fed mainly through snow and glacial melts (Eaton and Moore, 2010; Moore et al., 2012; Schnorbus et al., 2014). There are, however, streams belonging to C2 that are located in Boreal Shield (23% of streams), where the streamflow generation is governed by other processes such as fill-and-spill in which segments of a basin have to be filled above their capacity before spillage (Spence and Phillips, 2015). The Clearwater River near Clearwater in southern Alberta is the representative stream for this regime type.
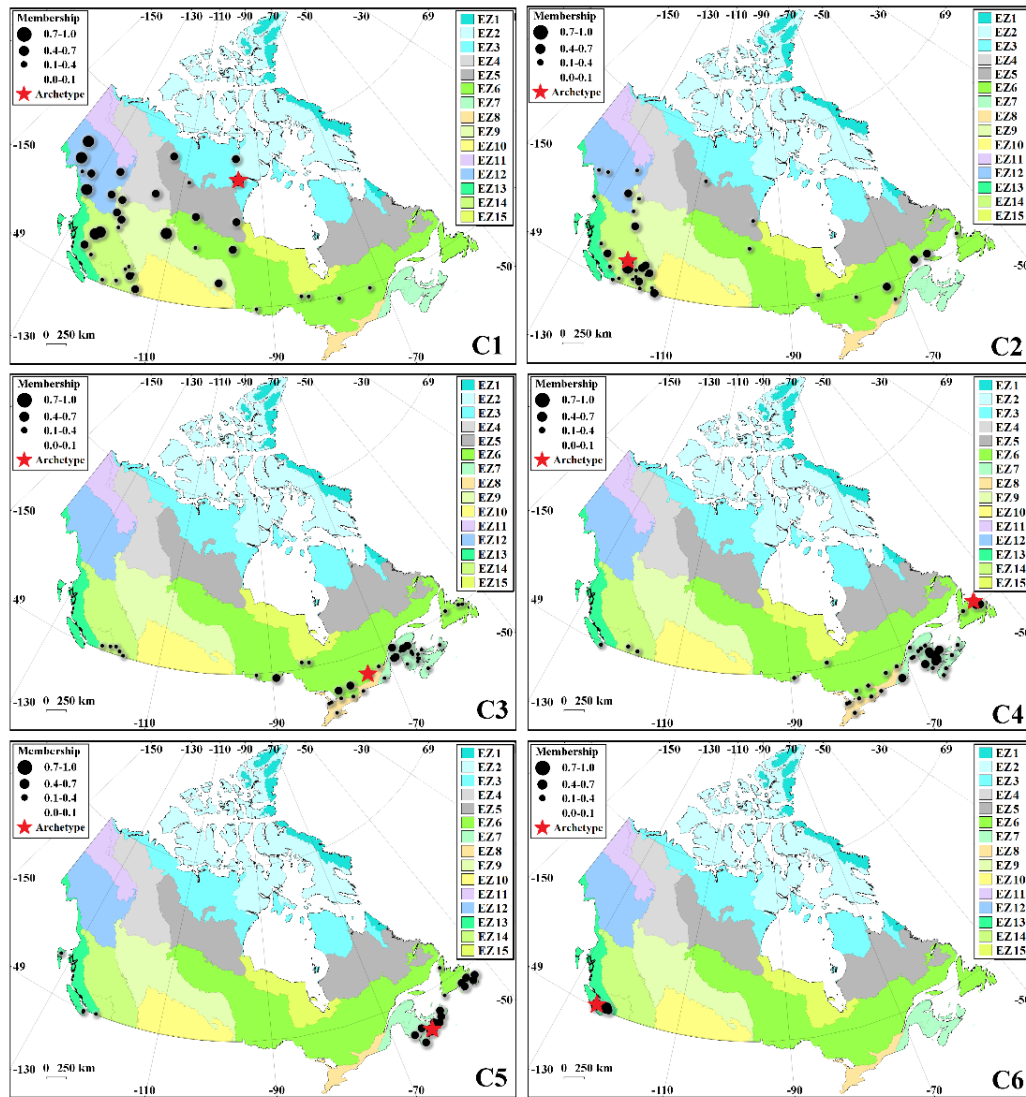
Figure 5.6. The distribution of the identified regime types across Canadian ecozones during the baseline l timeframe of 1966 to 1975. Each stream is represented by a circle with a radius proportional to a membership degree quantifying the association to a given regime type. Only RHBN stations with degrees of membership of 0.1 or larger are shown in each panel. The red stars are the archetype stations related to each regime type.

The cluster C3, i.e. the "slow-response/freshet peak" regime, includes streams in which the annual streamflow volume is mainly contributed by a short high flow period during spring snowmelt, sharp recession in summer, yet relatively smaller variations in the shape of hydrograph compared to the cluster C4, i.e. "fast-response/freshet peak" regime. Nearly 45% of the streams with this regime type are located in Atlantic Maritime. The rest are distributed in Boreal Shield (28%), Mixedwood Plains (15%), and Montane Cordillera (12%). The Matawin River originated from the lake Matawin in Québec is the archetype for the C3 regime. The streams belonging to C4 are also dominated by spring snowmelt but showing more variation in the shape of annual hydrographs compared to the C3 regime. Streams belonging to the C4 regime often have two distinct peaks, one in spring induced by snowmelt and one in fall due to high precipitation; and from that sense, they largely resemble nivo-pluvial streams (Hock et al., 2005). Almost all streams belonging to the C4 regime are located in eastern Canada (50% in Atlantic Maritime, 26% in Boreal Shield, 16% in Mixedwood Plains). Gander River at Partridgeberry Hill in Newfoundland is the archetype for this regime.

The cluster C5, i.e. "slow-response/cold-season peak" regime, comprises streams with weak seasonality and slightly more discharge in fall and winter. The annual flow for streams belonging to this regime is more influenced by rainfall around later fall, followed by a slight increase in discharge due to snowmelt; and therefore, they resemble a hybrid pluvio-nival regime (Kang et al., 2016). The concentration of streams belonging to this regime is again in the eastern Canada (48% in Atlantic Maritime; 33% in Boreal Shield), with few streams being in the Pacific Maritime. Beaver Bank River in Nova Scotia is the representative stream for this regime type. Finally, the cluster C6, i.e. "fast-response/cold season peak regime, is similar to the C5 regime and exhibits a weak seasonality, but with a greater variation in shapes of annual hydrographs. The runoff in streams belonging to this regime is dominated by heavy precipitation, especially during winter, and lower runoff during summer, resembling the pluvial regime (Wade et al., 2001; Whitfield, 2001). Streams belonging to this regime are only concentrated in the Pacific. The Sproat River near Alberni is the archetype stream of the C6 cluster.

5.3.2. Detection of changing streamflow regimes

To understand temporal shifts in streamflow regimes throughout selected RHBN streams, we calculate the decadal membership values as shown in Fig. 5.2. We accordingly apply the Mann-Kendall trend test with the Sen's Slope on the time series of decadal memberships. The detailed results including the membership time series for all streams and corresponding trend analyses are shown in Figs. D4 and D5 in the Appendix D over major drainage basins/sub-basins as well as the terrestrial ecozones in Canada, respectively. Fig. 5.7 summarizes our findings over the 15 Canadian ecozones. The color (blue *vs.* red) and the size (large *vs.* small) of triangles show decreasing *vs.* increasing trends as well as significant *vs.* insignificant trends at *p*-value ≤ 0.05. Although inconsistent patterns of change are observed in Boreal and Montane Cordillera, particularly between the southern and northern regions, there are clear downward trends in the member of regime C1 in Taiga Shield and Boreal Shield. Upward trends are observed in membership values of C2 in Boreal Cordillera and Taiga Shield, while downward trends are seen in the member of C2 in southern and

eastern parts of Montane Cordillera and Boreal Shield. The C3 regime shows intensification in Montane Cordillera and Boreal Shield. It also intensifies in southern parts of Atlantic Maritime but weakens in northern regions. The pattern of change in C4 is very similar to C3, but with fewer significant downward trends in northern parts of Atlantic Maritime. Considering the C5 regime, streams mainly show decreasing trends in the Appalachian region including eastern Boreal Shield, and southern parts of Atlantic Maritime. Mixed patterns of change in membership degree are observed in the Pacific Maritime for both C5 and C6 regimes.
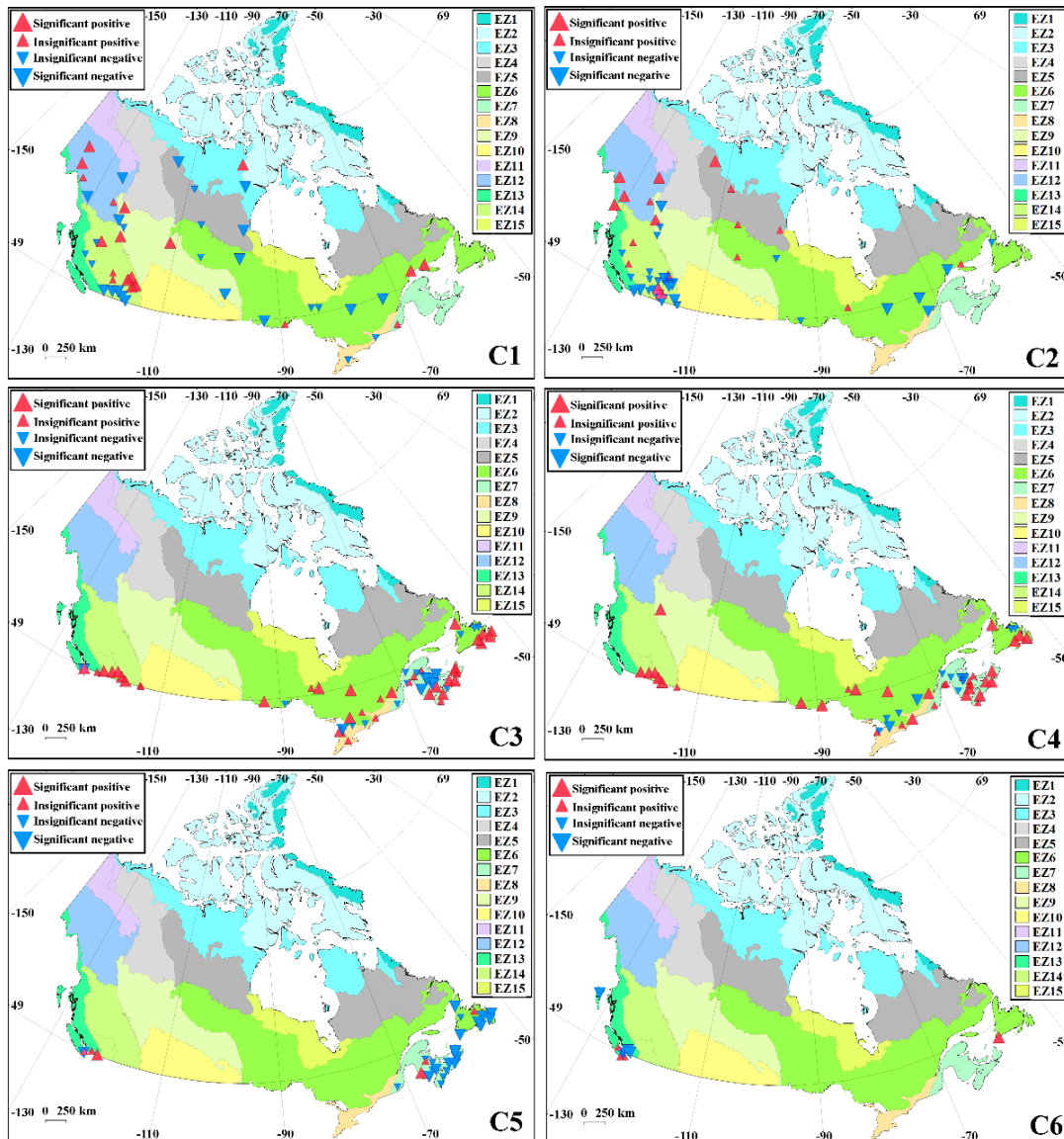
Figure 5.7. Trends in decadal memberships, quantifying the change in association of the 105 selected RHBN streams to the six regime types during 1966 to 2010.

The nature of regime shifts at each stream can be investigated by quantifying the rate of relative shift between opposing significant trends. Fig. D6 in the Appendix D summarizes the results. Overall,

the dominant modes of transition at the ecozone scale are from C1 to C2 in the northern ecozones (EZ5 and EZ12), from C2 to C1 and from C2 to C3 in the western ecozones (EZ9 and EZ14), from C2 to C3 in the two stations located in the Prairies, from C1 to C3 in the eastern ecozones (EZ6, EZ8, and EZ15), and from C5 to C4 in the Appalachian region (EZ7 and eastern part of EZ6). The variability between the regime shifts inside each ecozone can be described by elevation. To better synthesize our findings in Canada and highlight dominant regime shifts and their geographic extent across the country, Fig. 5.8 shows sankey diagrams, demonstrating how initial regime types in the considered streams. Streams are grouped by the ecozones in the left side of each panel, and transform to one particular target regime type (right side in each panel). The six natural regime types are distinguished by color codes and stations within each ecozone are sorted from the lowest to the highest elevation from top to the bottom. The width of each arrow is proportional to the rates of shift, calculated using Eq. 7. The highest rate of a shift in each stream and/or ecozone can be considered as the dominant regime shift.
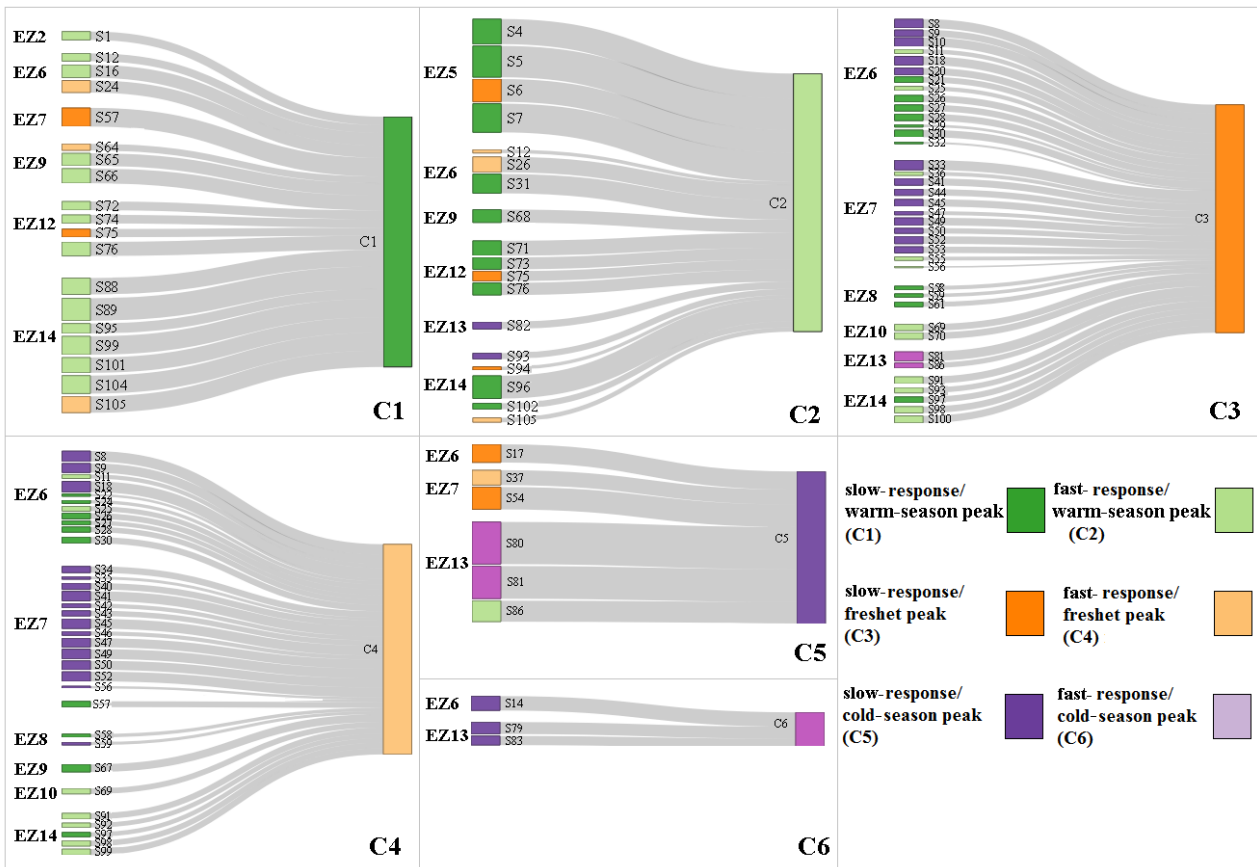
Figure 5.8. Sankey diagrams showing transitions in Canadian natural streamflow regimes described across ecozones from 1966 to 2010. Each panel presents transformation from five potential regime types to one particular target regime. Streams in the left side are grouped according to ecozones and are sorted from the lowest to highest elevations from the top to the bottom. Colors show the six regime types. The widths of arrows are proportional to the rate of shift.

101

Some important findings can be made from Fig. 5.8. While regime shifts are varied, there are some dominant regime shifts that are frequently observed across different ecozones. For example, frequent shifts are observed from C2 to C1 as well as C1 to C2 that are quite strong across Montane Cordillera and Taiga Shield, respectively. Second, it is possible that the streamflow regime in a given ecozone shifts from one regime to two or more regime types. For instance, streamflow in Atlantic Maritime shifts from C5 to C3 and C4. Also, it is possible to have opposing regime shifts in a given ecozone. As an example, the flow regime varies from C5 to C6 and vice versa across Pacific Maritime. Such variabilities in regime shift can be partially explained by latitude. More generally, it is possible to shift from two or more regime types into one or more regime types across a particular ecozone. For example, streams with C1 and C5 regimes are shifting to C3 and C4 across Boreal Shield. Such variabilities within an ecozone can be described in many cases by elevation. In Boreal Shield, for example, elevation controls the constitution of the initial streamflow regime from C5 in lowlands to C1 in highlands. Finally, the most frequent regime shifts are not necessarily the strongest ones. For instance, the streamflow regime shifts across 6 ecozones toward C3 and C4 but the rates of the shift are not strong when compared with the shift between C6 to C5 that happens in limited streams in Pacific Maritime, but quite strongly.

5.3.3. Identifying forms of transformation in streamflow regimes

The procedure presented in Sect. 2.5 attributes regime shifts to changes in streamflow characteristics using dependence analysis. Figure 5.9 summarizes the results of attribution in the 105 RHBN stations. Streams are shown in rows, grouped in each ecozone, and ordered from low to high elevations from the top to the bottom. For each stream, there are three groups of cells, with 15, 15, and 2 cells from left to right respectively. The first two groups of cells are related to the values of mean (i.e., x_1 to x_{15}) and variance (i.e., y_1 to y_{15}) of the 15 considered IHAs, respectively. In these two groups of cells, shades of blue and red show negative and positive dependencies between a given pair of streamflow characteristic and membership degree, respectively. Note that we only identify those streamflow characteristics that have significant dependencies with variations in membership degrees based on Kendall's tau (p-value ≤ 0.05) Color saturations show the values for the coefficient of determination, quantifying the fraction of variability in membership degrees that are described by the variability in streamflow characteristics. The last two cells are related to the dominant regime shift in each stream from one initial regime (left hand cell) to an altered regime (right hand cell). The color scheme, defining the regime types, is shown in the legend. The analyses over basin and sub-basin scales are presented in Figs. D7 and D8 in the Appendix D.

The most important observation is the fact that in more than 80% the considered natural streams, there are some identifiable regime shifts that are significantly dependent on the changes in the streamflow characteristics. Some dominant regime shifts are frequent within an ecozone, while some are less frequent and may depend on latitude and/or elevation. In the only considered stream in the Northern Arctic, the shift from the C2 to the C1 regime is attributed to the earlier and more variable timing of the annual low flow, and the increasing June flow. An opposing shift is observed in Taiga Shield, i.e. from C1 to C2, which can be attributed to the earlier and more variable timing of annual

high flow, and the increasing seasonal flow in fall. The regime shift from C5 to C4 in the lowlands of Boreal Shield is attributed to the decreasing mean and variance of annual flow particularly in August. In the highland of this ecozone, however, the dominant regime shift is from C1 to C3 and can be attributed to the decreasing monthly flow in August and September, and more variability in the timing of the annual low flow. In Atlantic Maritime, particularly across lowlands, decreasing mean and variation of the flow in August along with decreasing monthly flow in June and July, and decreasing mean annual and seasonal flow in the fall lead to a shift from C5 to the C4.
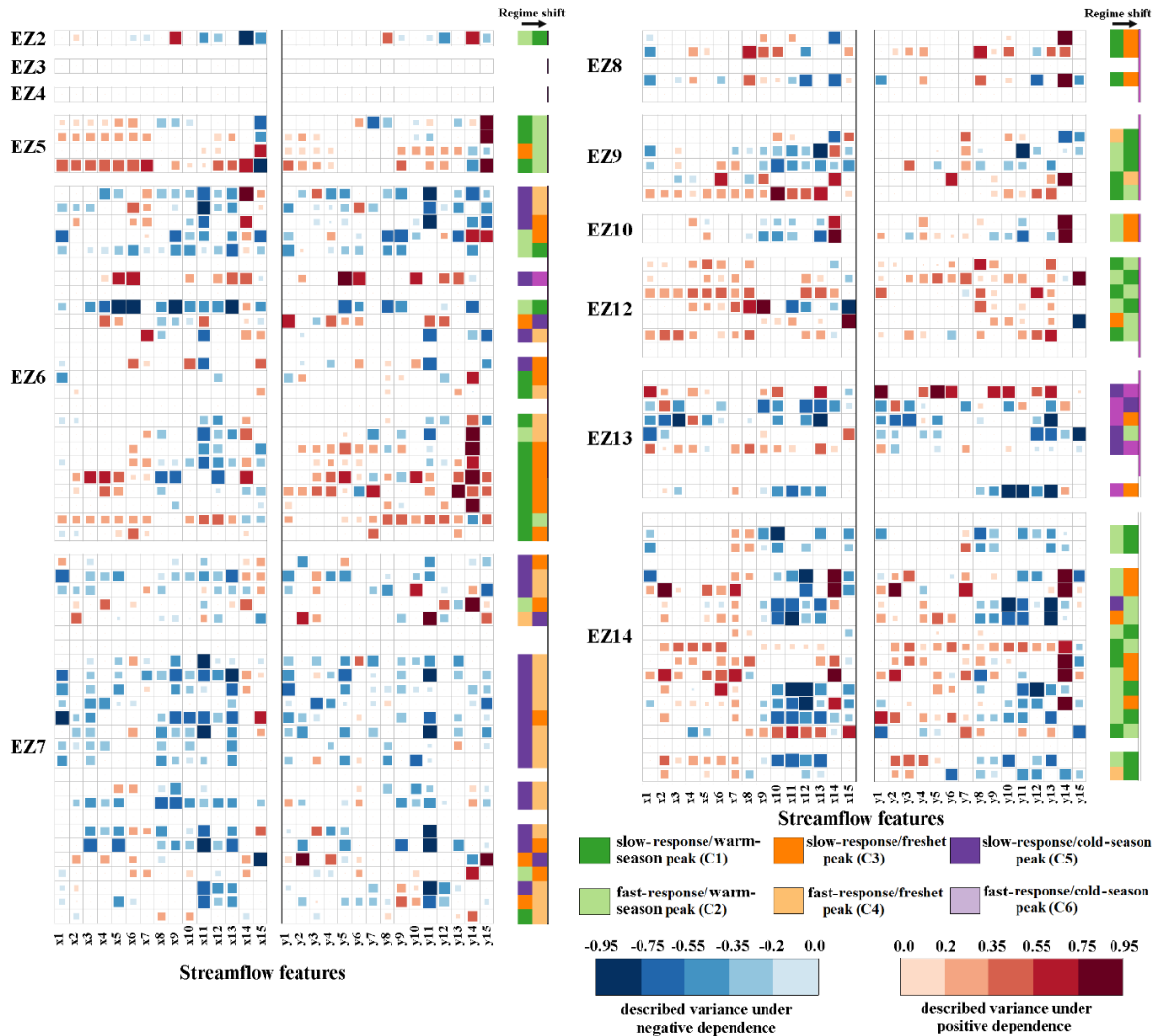
Figure 5.9. Dominant regime shifts across 105 RHBN streams in Canada attributed to the first and second moments of the 15 IHAs considered. Shades of red and blue show the positive and negative dependencies between changes in streamflow features and degrees of membership. Color saturations are proportional to the values of coefficient of determination. The dominant regime shift at each stream is identified by the color scheme described in the legend. Streams are grouped in ecozones and ordered from low (top) to the high (bottom) elevations

In Mixedwood Plains, the shift from C1 to C3 is attributed mainly to earlier and more variable timing of annual low flow. In the lowlands of Boreal Plains, the increasing variation in April's flow,

and decreasing annual and summer flows contribute to the shift from C2 to C1. Streams in the highlands of Boreal Plains, however, shift from C1 to C2 due to the increasing annual and summer flows, along with later and more variable timing of low flows. In Prairies, in the two considered streams, the shift from C2 to C3 is attributed to delayed and more variable timing of low flows and decreasing summer flows. In Boreal Cordillera, more variable annual flow and increasing mean and variation in May flow correspond to the shift from C1 to C2. Opposing shifts from C2 to C1, however, are mainly attributed to the increasing monthly flows in February, March, April, and May. The most pronounced shift in Pacific Maritime is from the C5 to C6, which mainly corresponds to increasing mean and variation of October flow, and increasing annual flows. The most pronounced shift in Montane Cordillera is from C2 to C1 for the streams in the northern part, attributed to decreasing mean and variability in July flow and increasing monthly flow in April and May. Streams in southern parts, however, shift from C2 to C3, attributed mainly to increasing monthly flow in February, March, and April, more variability in the timing of the low flow as well as decreasing September flow.

5.5. Discussion

The application of the proposed methodology in Canada identifies six distinct natural regimes across the country, address their change in time and space, attribute dominant regime shifts to changes in a range of streamflow characteristics at each stream and accordingly upscale the findings from individual streams to ecozones. Having said that, still there are some unanswered questions. First, it is still unclear how robust our proposed algorithm is particularly in light of the assumptions made with respect to the length of the timeframes and/or selecting the baseline period. Second, it is obvious that our selected streams are only a sample of available RHBN stations across Canada and it is still unclear how our findings can be extended to out-of-sample streams. Finally, there is a large body of literature, reporting shifts in streamflow regimes across different regions in Canada due to changes in temperature patterns, magnitude and form of precipitation, snowmelt and snow accumulation as well as glacier retreat and permafrost degradation. Accordingly, it is crucial to frame and position our findings with respect to earlier studies. These three tasks are pursued in this section.

5.5.1. Addressing uncertainty

The results presented in Sect. 4 are based on considering decadal timeframes and selecting the first decadal timeframe as the baseline period. Here we relax these two assumptions and monitor alterations in our findings. First, we repeat the clustering algorithm over all possible decadal timeframes throughout the study period and recalculate the cluster centers. This experiment addresses the sensitivity of our clustering algorithms to the choice of baseline period. Second, we repeat the approach implemented in Sect. 4 again with considering 15- and 20-year timeframes and address how cluster centers, as well as our specific findings would alter by increasing the length of timeframe. We do not consider timeframes less than decadal length due to the insufficiency of numbers of data points for trend analysis. We also do not consider timeframes larger than 20 year to allow at least two fully independent timeframes during the study period with a few years gap.

Figure 5.10 summarizes our findings in terms of the sensitivity of our clustering results with respect to the two assumptions made. Panel (a) shows the cluster centers when different decadal baselines are considered. Colored dots show the centers of clusters related to all possible decadal timeframes except the period of 1966-1975. The centers of clusters are scaled into two dimensions using the Multidimensional Scaling (MDS; Cox and Cox, 2008), in which the distance between the dots represents the approximate dissimilarity of centers of clusters. Dimensions 1 and 2 delineate the space, in which the original data are mapped. Black crosses show the centers of the first decadal timeframe mapped using the MDS. Colors identify regime types. The result clearly shows that despite changing the baseline timeframe, the distinction between cluster centers are maintained and the position of centers does not substantially change by changing the baseline period. Panel (b) shows the results of our sensitivity analysis with respect to changing the length of timeframe. Again, there are not notable changes in the cluster centers. These two findings highlight the robustness of our clustering analysis.
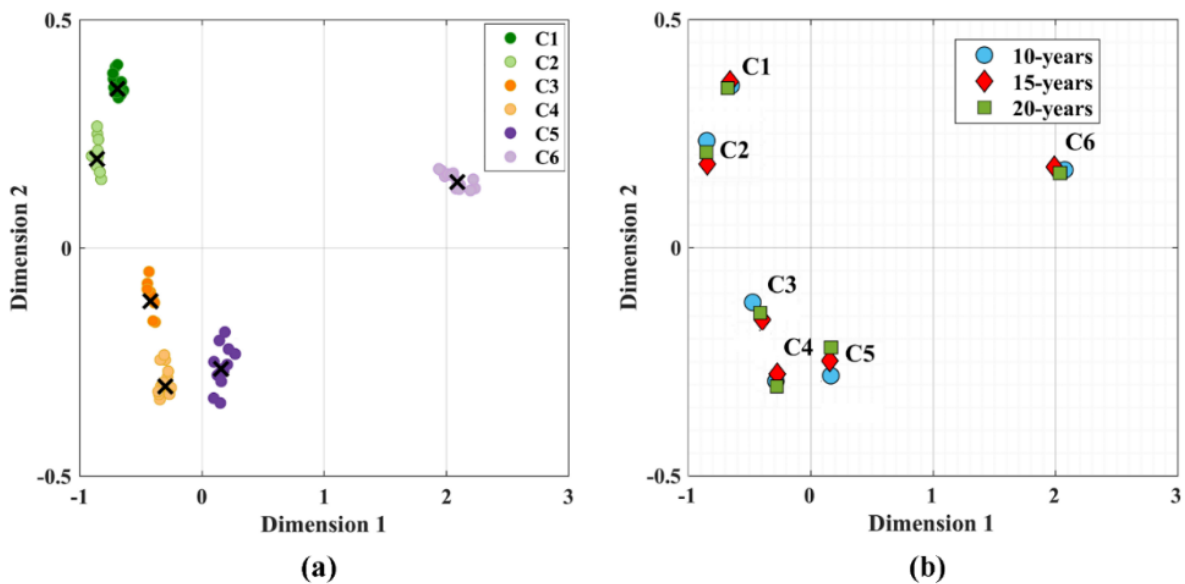
Figure 5.10. The sensitivity of the cluster centers to (a) the choice of decadal timeframe for clustering, and (b) the length of the timeframe used for analysis. In panel (a) dots show the two dimensional scaling of the cluster centers in which distances between dots represent dissimilarities between cluster centers. Black crosses show the centers identified by choosing the first decadal timeframe. Panel (b) shows the two dimensional scaling of the cluster centers considering 10-, 15- and 20-year timeframes.

We also look at possible differences in the direction of trends in membership degrees, dominant regime shifts, as well as the attribution to streamflow features at the basin scale, if the length of timeframes are changed. Fig. 5.11 (left column) intercompares the results obtained by 10-, 15- and 20-year timeframes in terms of percentages of similarities in the direction of trends during 1966 to 2010 at each basin. In brief, there are at least 80% agreements between the results obtained in the Pacific and the Arctic basins. There are more discrepancies in the direction of trends in the Atlantic and Hudson Bay basins. This is particularly the case for the C1 regime in the Hudson Bay and for the

C3 and C4 regimes in the Atlantic, for which the results are less consistent among different timeframes; yet, in the worst-case scenario (i.e., the C4 regime in Atlantic), there is still more than 60% agreement between the results of trend analysis obtained by 10-, 15- and 20-year timeframes. Dominant regime shifts are also performed with 15- and 20-year timeframes and are intercompared with corresponding results obtained by decadal timeframes. Our analysis shows that results obtained by 15- and 20-year timeframes are in large agreements with the results obtained using decadal timeframes. Even for the case with the largest discrepancy (i.e., C4 regime in the Atlantic), there is 86% agreement in terms of the direction of shift in streamflow regimes, obtained by 10- and 20-year timeframes. In terms of attribution of regime shifts to changes in streamflow characteristics, again the results obtained by different lengths are in large agreement in at least 80% of streams. Finally to investigate the sensitivity of attribution to the choice of measure, we substitute R^2 with squared Kendall's tau and repeat the experiment. The result of this experiment is summarized in Fig. D9 in the Appendix D. Comparing Fig. D9 with Fig. 5.9 shows that in general, the selected streamflow characteristics are similar with no remarkable changes in the degrees of attribution that influence our general findings. The most sensitive ecozones to the choice of measure of association are EZ5 and EZ14, demonstrating the greater values of association measured by the squared Kendall's tau. This is due to higher degree of nonlinearity between regime shifts and alterations in streamflow characteristics in these ecozones.
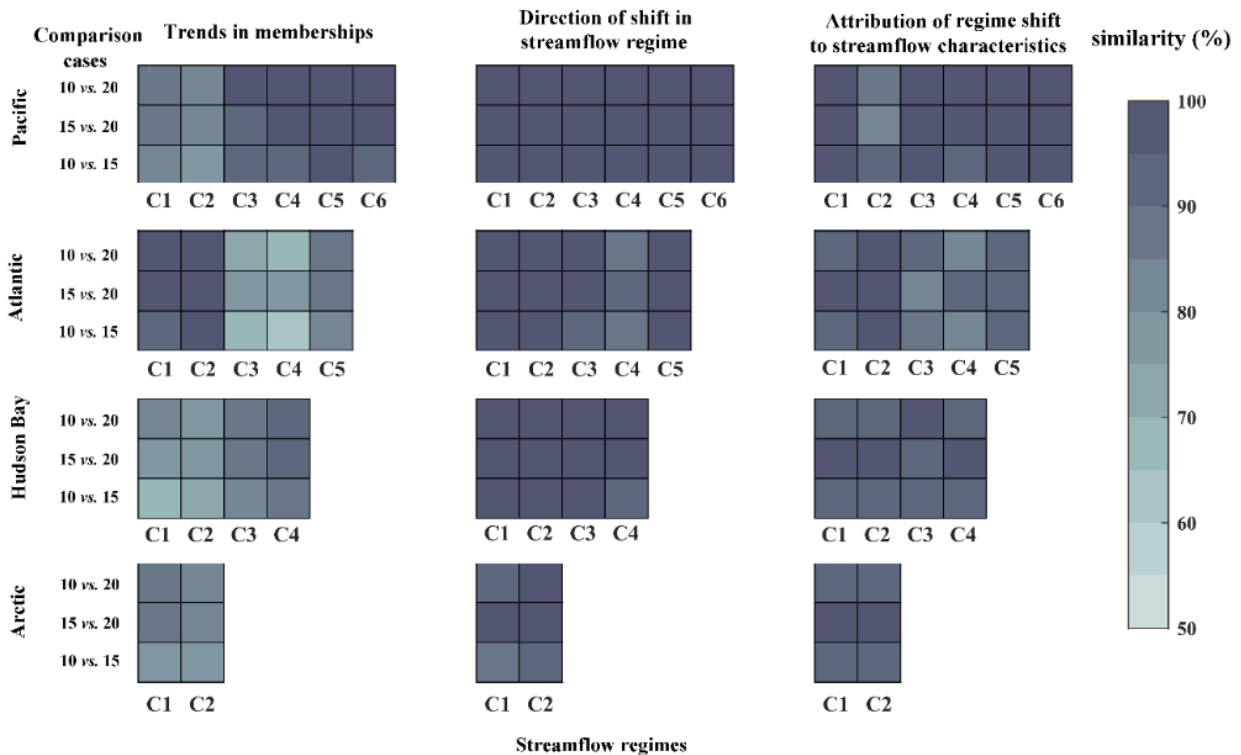
Figure 5.11. Similarities (in percentage) between the results obtained by 10-, 15- and 20-year timeframes related to trends in membership values, direction of shift in streamflow regimes, and attribution to streamflow characteristics in the four major Canadian basins.

5.5.2. Validation in out-of-sample streams

One important question remained unanswered is how the six regime types identified can be extended into out-of-sample streams. Here we investigate this in the Prairies ecozone, a region with importance for global food security. Natural streams in Prairies have been relatively overlooked in the literature (Whitfield et al., 2020), because often the streams do not have continuous streamflow records, partially due to the fact that many streams are seasonal. In addition, the majority of annual streamflow volume is contributed from mountainous headwaters outside of Prairies and the fact that at many basins large proportion of the land does not normally contribute into the streamflow (Spence et al., 2010; Shook et al., 2015; Mekonnen et al., 2015). In addition, only two stations in Prairies meet our data criteria in Sect. 3. Here, we reduce the length of data and investigate for new streams that satisfy our data criteria during 1976 to 2010. This has resulted into selection of nine new stations – see Fig. 5.12 for the location of these stations (P1 to P9).
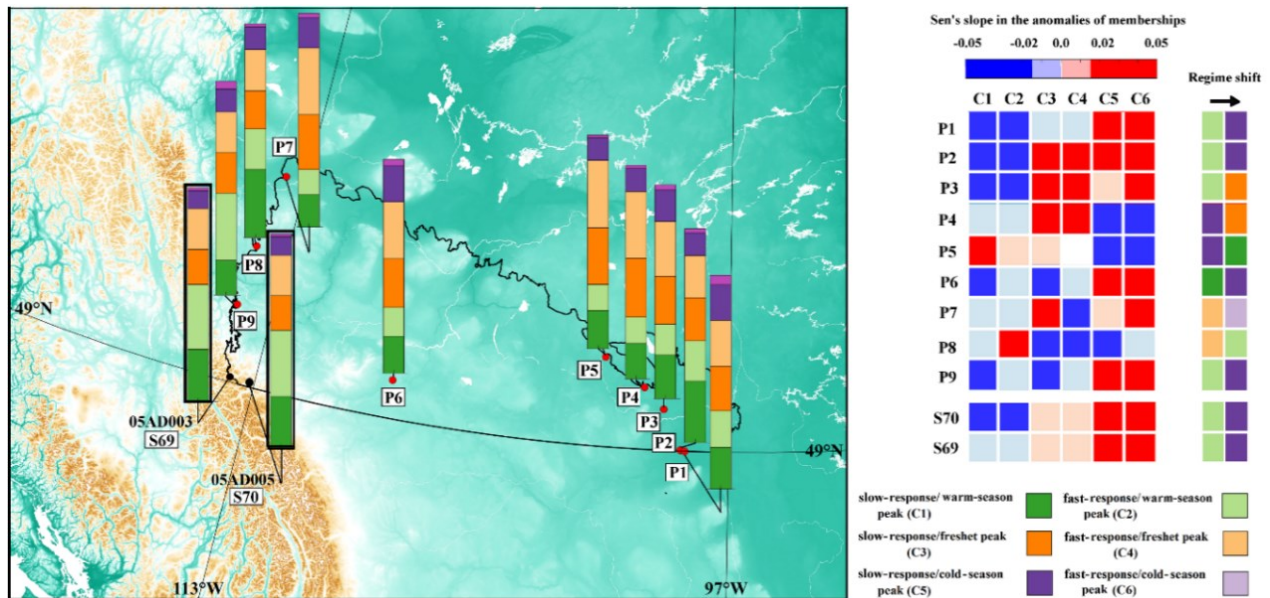
Figure 5.12. Validation of the proposed algorithm in nine out-of-sample streams during 1976 to 2010 in the Canadian Prairies. The color bars in the left map show the degrees of membership to each cluster. The right panel shows the trends in the degree of membership in the six clusters in the considered 11 stations. Positive and negative trends are shown with red and blue colors, respectively. Sharp colors show significant cases. The out-of-sample stations S1 to S9 are sorted from east to west from the top to the bottom.

The detailed information about these stations are provided in Table D6 in the Appendix D. Here we investigate how these new stations fit in previously identified regime types, check the trends in the membership degrees, and identify dominant regime shifts in these streams. We compare our findings in the nine new stations with the two previously selected stations in the Prairie region, namely, Waterton River near Waterton Park (S69; 05AD003) and Belly River near Mountain View (S70; 05AD005) during the common period of 1976-2010 for which the nine new stations are selected. The right panel shows the analysis of trends in anomalies of decadal memberships, in which stations are ordered from the east to west from the top to the bottom.

The analysis of trends in membership degrees shows mainly decreasing trends for C1 and C2 regimes and increasing trends for C5 and C6 regimes. Regarding C3 and C4 regimes, mainly upward trends are observed in the east; whereas, downward trends are observed in the west. These findings are in line with our results in S69 and S70. The two columns at the right side of right panel are related to the dominant regime shift in each stream. The legend demonstrates the six identified regime types. Although the regime shifts are vibrant, the dominant regime shift observed is from C2 to C5, which is the same in S69 and S70 during the period of 1976-2010.

We also perform an analysis of trends with focus on Quebec – see Appendix D8. We diagnose some significant changes in mean and variability of annual hydrograph in Quebec, which provides a holistic understanding of recent changes in natural streamflow regime throughout the province.

5.5.3. Summary of findings and positioning against earlier studies

Although to the best of our knowledge, our work is the first study in which a systematic algorithm is used to provide a temporally homogeneous view on recent changes in pan-Canadian streamflow regime; the literature of Canadian hydrology is rich in terms of documenting changes in streamflow characteristics across the country. Thanks to pioneering works of so many hydrologists before us, including the late iconic northern hydrologist, Richard Janowicz, to whom this paper is dedicated. Here we attempt to position our results with respect to earlier studies. Table 5.4 summarizes our findings in terms of dominant regime shifts and associated changes in streamflow characteristics at the sub-basin scale. Table 5.4 makes a clear distinction between the earlier findings, and those exclusively found in our study. Even though earlier studies have different data periods, and may include streams that are not within the RHBN streams, our study reconfirms previous findings and also discovers new changes in streamflow characteristics that have remained previously overlooked. Our study clearly shows that changes in variability of monthly, seasonal, and annual flows can be important drivers of shift in streamflow regime across the majority of sub-basins in Canada. This is another line of evidence for the complex and multifaceted nature of change in streamflow regime, and the need for a simultaneous look at alterations in both expected values and variability of streamflow characteristics to diagnose changes in natural streamflow regime.

5.6. Concluding remarks and outlook

This study presents an attempt toward providing a globally relevant algorithm for identifying changing streamflow regimes. The proposed approach is based on two fundamental considerations. First, streamflow regime is collectively formed by a large number of streamflow characteristics. Second, streamflow types are rather in the form of spectrums, not clear-cut states; and if regime shifts are caused by climate change, the transition from one regime type to another should be gradual rather than abrupt. To accommodate these two considerations, we suggest representing streamflow regime types as intersecting fuzzy sets, in a way that the belongingness of each stream to each regime type can be quantified by a membership function.

Table 5.4. Positioning our finding with respect to earlier studies across major Canadian basins and sub-basins

Basin	Sub-basin (stream location)	Dominant regime shifts	Earlier findings on changes in streamflow characteristics (reconfirmed in this study)	New findings on changes in streamflow characteristics (discovered exclusively in this study)
Pacific	Yukon	C3 to C1	Earlier timing of low and high flows; greater variability in timing of high flows (Burn 2008; Brabets and Walvoord, 2009; St. Jacques and Sauchyn, 2009)	Increasing flow in September; increasing flow variability in April and May
	Seaboard (north)	C1 to C2	Increasing winter flows (Déry et al., 2009)	Increasing monthly flow in May; earlier timing of low flow; increasing variability in March, May and annual flows
	Seaboard (south)	C1 to C3	Decreasing annual and monthly flow from April to June; decreasing flow in fall (Déry et al., 2009; Pike et al., 2010)	Delayed and more variable timing of annual low flow; increasing variability in February's monthly flow
	Fraser (north)	Case 1: C1 to C2 Case 2: C2 to C1	No earlier study in this region was found.	Case 1: Increasing mean and variance in annual and summer flows; increasing monthly flows in May and June; increasing variation in timing of low flow and the quantity of spring flows. Case 2: Decreasing mean and variance of annual flow; decreasing monthly flows in July and October; earlier timing of high flow; decreasing variability of monthly flows in May, August, September
	Fraser (south)	C2 to C5	Decreasing summer flows (Stahl and Moore, 2006); Increasing variability in monthly flows in November and April (Déry et al., 2012; Thorne and Woo, 2011)	Earlier timing of high flows; increasing mean monthly flows in November and April
	Columbia (north)	C2 to C1	Decreasing annual and summer flows (Stahl and Moore, 2006; Fleming and Weber, 2012; Forbes et al., 2019)	Decreasing variability in annual flow, and monthly flows of August and September
	Columbia (south)	C1 to C3	Increasing flow in April and decreasing flow in September (Whitfield and Cannon; 2000; Whitfield, 2001); Earlier timing of high flow (Burn and Whitfield, 2016; Burn et al., 2016)	Delayed timing and greater variability of the annual low flow; increasing mean and variance of flow in November's flow
Atlantic	Seaboard (north)	C5 to C3	increasing spring flows, corresponding to increased snow precipitation (Thistle and Caissie, 2013)	Increasing monthly flow in April; decreasing monthly flow in June; delayed and less variable timing of low flows; less variation in annual timing of high flows; decreasing mean and variation of monthly flow in August
	Seaboard (south)	Case 1: C5 to C4 Case 2: C3 to C5	Case 1: decline in the annual flow (Whitfield and Cannon, 2000; Yue et al., 2003; Thistle and Caissie 2013) Case 2: decline in winter flows, probably due to positive AMO (Whitfield and Cannon, 2000; Assani et al., 2012)	Case 1: Decreasing monthly flow in May, June and August; increasing monhly flow in March; Decreasing variability in February's monthly flow Case 2: Decreasing monthly flow in May and June; later timing of low flows
	St. Lawrence (north)	C3 to C1	smaller variations in timing of low flow (Thistle and Caissie, 2013)	Decreasing annual flow as well as seasonal flows in summer and winter; decreasing monthly flows in June, less variation in monthly flows of February, May, June
	St. Lawrence (south)	C1 to C3	No earlier study in this region was found.	Increasing mean and variation in monthly May flows; decreasing mean and variation in September flows; decreasing flow in October, increasing flow in February; increasing variance in timing of low flows; increasing variability in January's monthly flows
	Saint John- St. Croix	C5 to C4	Decreasing monthly flow in May (Kingston et al., 2011)	Decreasing annual flow; deceasing monthly flows in February and June; decreasing mean and variability of monthly flows in October and August
Arctic	Seaboard	C1 to C2	Earlier and more variable timing of high flows; increasing winter flows (Burn, 2008; Déry et al. 2016); earlier timing of high flows (Yang et al.; 2015)	increasing mean and variability of seasonal flow in fall, heightened variability in monthly flow in June
	Lower Mackenzie	C1 to C2	Increasing annual and winter flows (Smith et al., 2007; Walvoord and Striegl, 2007; St. Jacques and Sauchyn, 2009; Rood et al., 2016)	Increasing annual and seasonal flows during fall; increasing June's monthly flow; heightening variability in the timing of high flows
	Peace Athabasca	C2 to C1	Decreasing monthly flow in July (Yang et al., 2015)	earlier and less variable timing of low flows
Hudson Bay	Western & Northern Hudson Bay	C1 to C3	Increasing winter flows; decreasing summer flows; increasing variability in winter flows (Déry et al., 2011, 2018)	Delayed and more variable timing of low flows; increasing variability in February's monthly flow
	Northern Quebec & Ontario	C1 to C2	Increasing annual and winter flows, increasing variability in timing of high flows	Increasing annual and seasonal fall and summer flows; decreasing and less variable monthly flows in May; decreasing monthly flow in June
	Nelson	C1 to C3	Decreasing summer and fall flows Rood et al. (2008); Decreasing summer flows; increasing variability fall and spring flows (Déry et al., 2011)	Decreasing monthly flow in May and June; increasing variability of timing of low and high flows; increasing annual flow and seasonal flows in summer and winter

Accordingly, monitoring the trends in membership values in time and space can provide a basis to identify the regime shift from one type to another. We consider the existence of a significant trend in

membership values as an evidence for the regime shift. In addition, analyzing the covariance of membership values with streamflow characteristics can provide a basis to attribute regime shifts to alterations in certain streamflow characteristics in time and/or space. A significant dependence between a given regime shift and simultaneous alterations in streamflow characteristics highlights attribution, which can be communicated by R^2.

To apply this algorithm, we consider 45-year of daily data from 105 RHBN streamflow gauges across Canada, to provide a comprehensive and temporally homogeneous look at forms and extents of change in natural streamflow regime in Canada, coast to coast to coast. Our results show that streamflow regime in Canada can be categorized into six distinct regime types with clear physical and geographical interpretations. Analyses of trends in membership values show that alterations in natural streamflow regime are vibrant and can be different across different regions. Overall, in more than 80% of the considered stream there is a dominant regime shift that can be attributed to changes in streamflow characteristics. At the ecozone scale, the dominant regime shifts are from C1 to C2 in the northern ecozones (EZ5 and EZ12), from C2 to C1 and from C2 to C3 in the western ecozones (EZ9 and EZ14), from C2 to C3 in the two stations located in the Prairies, from C1 to C3 in the eastern ecozones (EZ6, EZ8, and EZ15), and from C5 to C4 in the Appalachian region (EZ7 and eastern part of EZ6). The variability between the regime shifts inside each ecozone can be described by elevation and/or latitude. At the basin scale, dominant modes of transition are from C3 to C1 in the northern Pacific and from C1 to C3 in the southern Pacific, between the C4 and C5 regime as well as the C3 and C5 in the Atlantic, between the C1 and C2 in the Arctic, and between C1 and C3 as well as the C2 and C3 regimes in Hudson Bay. The details of change in streamflow regime, however, are subject to a spatial variability within each drainage basin. In Atlantic and Pacific regions, there are clear divides between dominant regime shifts in northern and southern regions. For instance, In the Pacific, the association to C1 is increasing in Yukon and northern parts of Columbia and Fraser sub-basins; but it is significantly decreasing in the southern regions. This can be due to different manifestations of climate change, which are more appeared as temperature increases in the north, and growing ratios of rain over precipitation in south, shifting the streamflow more toward rain-dominated regimes (Fleming and Clarke, 2003). This reconfirms the important role of latitude in driving the streamflow response to climate change.

The proposed framework provides an opportunity to identify the changing streamflow regimes and attributes such changes to a large set of streamflow characteristics. This approach, however, do not explore the attribution of the shifts in streamflow regimes to the changes in temperature pattern, form and magnitude of precipitation, snowmelt, glacial retreat and permafrost degradation. These can be potential areas for future research. We hope our study triggers more attention to multifaceted nature of change in streamflow regime in Canada and the rest of the world during the current "*Anthropocene*".

A Generalized Approach for Synthetic Streamflow Generation under Changing Conditions[5]

The contents of this chapter are in preparation as "A Generalized Approach for Synthetic Streamflow Generation under Changing Conditions" for submission to Water Resource Research.

Synopsis

Climate change and anthropogenic interventions have drastically perturbed streamflow characteristics globally. Such changes can cause vulnerabilities in water resource systems, developed around certain characteristics of streamflow regime. Understanding the potential vulnerabilities are generally through top-down approaches, advised based on a cascade use of climate and hydrological models, and include large uncertainty. To address limitations in top-down approaches, the so-called bottom-up frameworks have been proposed. In such approaches, the response of water systems is analyzed directly as a function of potential changes in flow characteristics, requiring stochastic streamflow generation schemes. These methodologies are often developed to generate streamflow ensemble under stationarity, assuming that the characteristics of flow hydrograph will not change over time. It is, however, argued that the fundamental assumption of stationarity has been influenced by climate change and human activities, and therefore it is not applicable for synthetic generation of streamflow under changing conditions. This requires methodologies to represent changes in the streamflow hydrograph under changing conditions. Here, we propose a parsimonious framework to systematically represent shifts in the expected streamflow hydrographs and variability around it. For this purpose, we use a series of orthogonal gamma distributions, for which the properties of distributions can be perturbed, reconstructed and reproduced under changing conditions. The proposed framework is applied to a number of streams across Canada to generate large ensembles of perturbed streamflow. The results demonstrate that the proposed algorithm can implement the desired shifts quite well with relative error of less than 5% in representing the seasonal volumes in single and multisite settings. The proposed model performs well in representing the expected timing of peak, showing an absolute error of less than 0.5 week in most of cases. The best performance, however, is observed in representing the expected timing of peak and seasonal volumes of glacial regimes. The proposed algorithm is generic, providing a global scheme to analytically generate scenarios of change required for vulnerability assessment under nonstationary condition.

6.1. Introduction

Ongoing alteration of flow regime due to climate change, climate variability, and anthropogenic interventions have been witnessed in many parts of the world, affecting the freshwater availability, and subsequently both ecosystem, and socio-economic activities (Tonkin et al., 2018; Amir Jabbari and Nazemi, 2019; Ferrazzi et al., 2019; Padrón et al., 2020). Such changes have drastically perturbed streamflow characteristics throughout the world (Ma et al., 2016). In Australia, for instance, due to climate change annual streamflow in catchments on the northeast coast and east coast could change by -5 to $+15\%$ and $\pm15\%$ respectively by the year 2030, while in southeast Australia the annual

---

streamflow could decrease by up to 20% (Chiew and McMahon, 2002; Liu et al., 2019). In Europe, several studies have projected an increase in discharge in the high-latitudes and decrease in the Mediterranean and Southern Europe (Arnell and Gosling, 2013; Hagemann et al., 2013; Lobanova et al., 2018). Climate change have also led to the earlier spring timing of peak in northeastern Europe; later winter floods around the North Sea and parts of the Mediterranean coast, and earlier winter floods in Western Europe (Blöschl et al., 2017; Donnelly et al., 2017; Hall and Blöschl, 2018). In southern and western portions of United States and Canada, climate change and human interventions result in generally observed and projected decreased streamflow (Tan and Gan, 2015; Ficklin et al., 2018). Such patterns of changes in flow regimes are observed not only in the spatial scale but also across various flow regimes through a wide range of streamflow characteristics, depending on the type and the relative dominance of streamflow-generating processes (Matti et al., 2017; Curran and Biles, 2020; Zaerpour et al., 2021a). In streamflow with glacial regime, for instance, increasing annual volume is more severe, caused by glacial retreat (Stahl et al., 2008; Clarke et al., 2015; Chesnokova et al., 2020. In streams with nival regime decreasing annual volume is often accompanied by an earlier occurrence of the timing of peak caused by decrease in snow cover during winter and higher winter temperature (Vormoor et al., 2016; Matti et al., 2017; Zaerpour et al., 2021a). Flow seasonality which is another important feature of the annual hydrograph, characterizing the distribution of streamflow throughout the year is also expected to change (Matti et al., 2017; Eisner et al., 2017). The changes in flow seasonality are more likely to happen in nivo-pluvial regime caused by increase in fall flow due to rainfall, indicating a shift from snowmelt-dominated to rainfall-dominated regime (Arheimer and Lindström, 2015; Rottler et al., 2021).

Such changes in the streamflow regimes highlight just how crucial it is to secure regional water supplies for the human and environment (Villarini and Wasko, 2021). The changes in the streamflow regimes can indeed lead to significant challenges for water resource planning and management in the 21st century in coping with uncertainty from climate change, human developments, and financial factors, among others (Haddeland et al., 2014; Herman et al., 2016; Knighton et al., 2017; Borgomeo et al., 2018; Taner et al., 2019). This requires better understanding the main vulnerabilities in water resource systems under future conditions which is the key to mitigating negative impacts and exploring adaptation strategies such as expanding reservoir capacity and building desalination plant (Bhave et al., 2014; Conway et al., 2019; Fletcher et al., 2019; Herman et al., 2020; Quinn et al., 2020). The conventional approach for vulnerability assessment of water resource systems is generally through a top-down (a.k.a. scenario-led) impact assessment paradigm that uses downscaled projections of Global Climate Models (GCMs) to provide the inputs for hydrological models, with which the changes in streamflow conditions can be quantified (e.g., Gizaw et al., 2017; Krysanova et al., 2017; de Oliveira et al., 2017; Broderick et al., 2019). Although recommended by the International Panel of Climate Change (IPCC, 2014), these approaches are subject to a cascade of uncertainty (Brown and Wilby, 2012; Pielke et al., 2012; Prudhomme et al., 2014; Clark et al., 2016). For instance, the uncertainty propagates through the chain of greenhouse gas emissions, climate models and the initial conditions, making them unable to adequately reproduce major atmospheric circulation patterns (Pielke Sr., 2010; Annamalai et al., 2007), which are the main drivers of natural climate variability in many regions (e.g., Dieppois et al., 2016; Cioffi et al. 2017). These limitations and the

fact that generated scenarios are only limited to climatic conditions confine the wide applications of top-down approaches for decision-making under deep uncertainty (Herman et al., 2020; Quinn et al., 2020).

Recent work on decision making under deep uncertainty seeks to find vulnerability of water resource systems to changes in the streamflow conditions that are not only robust to scenarios of change due to climatic conditions but to possible human interventions and future socioeconomic conditions as well. These so-called bottom-up (a.k.a., scenario-neutral) approaches provide a basis to expose water resource systems to a wide range of plausible scenarios for which management options should be assessed (e.g., Prudhomme et al., 2010; Ray et al., 2019; Sauquet et al., 2019; Taner et al., 2019). Early bottom-up assessment approaches such as Robust Decision Making (Bryant and Lempert, 2010; Wilby and Dessai, 2010; Weaver et al., 2013), Info-Gap (Haim, 2006; Hall et al., 2012; Matrosov et al., 2013), and Decision Scaling (Brown et al., 2012; Poff et al., 2016), however, mainly focus on avoiding uncertainties resulted from climate projections and still implement hydrological models to translate the feasible climate envelope to projected water availability (Nazemi et al., 2020). As a result, uncertainties from hydrological models can still propagate into vulnerability assessment of water resources systems (Nazemi and Wheater, 2014a). More recent contributions, therefore, have moved towards fully bottom-up approaches to generate future water availability conditions without incorporating any climate and/or hydrological models. Accordingly, vulnerability can be directly mapped as a function of feasible changes in streamflow conditions (Nazemi et al., 2013; Borgomeo et al., 2015; Nazemi et al., 2020).

Regardless of methodological differences, these decision-centric frameworks are mainly developed to generate ensemble of synthetic streamflow series under stationarity, assuming that the characteristics of flow hydrograph will not change over time. For this purpose, stochastic modeling of streamflow has a key role in hydrology. Conventional methods typically implement autoregressive and their variants to linearly model the streamflow series (Pegram, 1980; Stedinger and Taylor 1982; Salas et al., 1985). Such approaches, however, cannot represent the marginal streamflow distribution, especially in the case of asymmetric and/or multimodal conditions (Papalexiou, 2018; Papalexiou and Serinaldi, 2020). To address these issues, non-parametric approaches have been developed as an appealing alternative (Lall and Sharma, 1996); however, they can only generate the streamflow realizations within the range of observed data and are limited in extrapolation (Papacharalampous et al., 2019; Quilty and Adamowski, 2020). More recently, copula-based models have gained lots of attention in hydrolclimatology (Nazemi and Elshorbagy, 2012; Aghakouchak, 2014) and in stochastic streamflow generation in single (Hao and Singh, 2012) and multiple sites (Pereira and Veiga, 2018; Chen et al., 2019; Nazemi et al., 2020; Zaerpour et al., 2021b). This is mainly due to flexibility of copulas in representing the nonlinear spatiotemporal dependence structures observed within streamflow (Bárdossy and Pegram, 2009; Worland et al., 2019; Wang et al., 2019).

It is, however, argued that the fundamental assumption of stationarity has been influenced by climate change and human activities (Milly et al., 2005, 2008), and therefore it is not applicable for synthetic generation of streamflow under changing conditions (Li et al., 2015; Shrestha et al., 2017;

Yang et al., 2021a, b). This requires methodologies to represent changes in the streamflow hydrograph under changing conditions capable of generating scenarios of change beyond observed data. Little attention, however, has been given on advancing the perturbation algorithms required for altering the streamflow characteristics and generate a wide range of scenarios of change (Nazemi et al., 2013; Borgomeo et al., 2015; Feng et al., 2017; Herman et al., 2020). Some studies focus on developing algorithms for perturbing only few streamflow characteristics such as annual volume or timing of annual peak (Nazemi et al. 2013; Feng et al. (2017), or the work of Herman et al. (2016) for perturbing only the frequency of low flow. The general approach for perturbing the streamflow characteristics developed by Borgomeo et al. (2015) can provide any desired shift in streamflow characteristics by rearranging the annual hydrographs to generate a set of desired properties while such characteristics are treated as a combinatorial optimization problem. Such approaches, however, are very time-consuming, and similar to other optimization techniques may converge to local optimum. Additionally, this algorithm is based on reshuffling the observed annual hydrograph, leading to the disturbance of the temporal dependence structure of streamflow series and generating the streamflow realizations limited to the observed historical hydrographs. Furthermore, for generation of streamflow realization, different characteristics of flow regime have been considered in the one objective function. Nonetheless, these characteristics are not explicitly independent of each other. The work of Nazemi et al. (2013; 2020), on the other hand, is able to generate the scenarios of change beyond the observed hydrograph by combining the conventional resampling and the simple delta-methods. This approach, however, is limited to generating scenarios of change in two main characteristics of flow regime, i.e. the expected timing of peak and annual volume. Despite some advances in such perturbation algorithms for generating scenarios of change under nonstationary conditions, none – to the best of our knowledge – are able to represent the gradual shift in the streamflow regime but they generate abrupt changes only in a few streamflow characteristics. Additionally, these approaches generally propose an ad-hoc solution by implementing a heuristic method to generate scenarios of change rather than an exact analytical solution.

Here, we propose a general approach to synthesize any plausible scenario of change by providing a large ensemble of perturbed streamflow, with which the vulnerability of water resource systems to the changes in streamflow hydrograph can be analyzed. The idea is to develop a generic stochastic algorithm to systematically generate any potential changes in the streamflow hydrographs under nonstationary conditions. The algorithm proposes an analytical solution to represent transient shifts in the streamflow hydrograph. For this purpose, we initially identify the gradual changes in the streamflow hydrographs over the historical period using a moving trend analysis, giving the opportunity to project such changes to future conditions. The proposed algorithm first decomposes the streamflow regime into an expected streamflow hydrograph and the variability around it. We then conceptualize the streamflow hydrograph as a time distribution function, mimicking all probabilistic properties of cumulative distribution function. Later, to implement the desired shifts analytically, we use a series of orthogonal generalized gamma distributions, for which the properties of distributions can be perturbed, reconstructed and reproduced under changing conditions. The algorithm is then accommodated into a copula-based stochastic streamflow generation scheme to projects the desired

shift in single- and multisite generation of streamflow at short- and long-range futures. We demonstrate the practical utility of the new perturbation algorithm in single- and multisite settings using a number of natural streams with different flow regime types across Canada. The remainder of the paper is organized as the following. Section 6.2 presents the methodologies for identifying the dominant shifts in the streamflow hydrographs and the implementation of potential shifts. Section 6.3 briefly introduces our case studies. Section 6.4 discusses the model development and experimental setup. Section 6.5 presents the results and discusses the application of the proposed algorithm. Finally, Section 6.6 concludes the study.

6.2. Methodology

6.2.1. Rationale

The streamflow regime can be defined by the shape of expected annual hydrograph and the variability around it (Zaerpour et al., 2021a). Under stationarity, it is often assumed that the probabilistic characteristics of flow regime will not change over time. Milly et al. (2005, 2008), however, argued that the fundamental assumption of stationarity has been influenced by climate change and human activities, and therefore it is not applicable for synthetic generation of streamflow under changing conditions (Chang et al., 2016). This requires methodologies to represent changes in the streamflow characteristics under changing conditions. Although some methodologies are developed to represent changes in one or few characteristics of streamflow regimes, they cannot analytically represent forms of change in different streamflow characteristics.

The responses of streamflow hydrograph to climate change and/or human intervention, however, can be observed in the form of simultaneous shifts in multiple streamflow characteristics. Here, we propose a framework, comprising a stochastic scheme to represent, perturb, and generate the streamflow hydrograph under changing condition. For this purpose, first we need to identify the changes in the main characteristics of streamflow hydrograph, i.e., the expected annual hydrograph and the first three moments of flows at the subannual timescale describing the probability distributions at each time step. We employ the concept of moving timeframe and slide it year-by-year (see Zaerpour et al., 2021a for further information on moving trend analysis). Within each timeframe we calculate the expected timing of annual peak and the values of three moments at each subannual timescale. The length of moving timeframe should be long enough to accommodate enough number of data for fitting a parametric marginal distribution (here we consider a timeframe with a length of 30-year). This leads to $52 \times 3 + 1$ time series in the case of weekly timestep. Having these timeseries, the Mann-Kendall trend test with Sen's Slope (Mann, 1945; Kendall, 1975) are applied to (1) to identify the dominant forms of change in each characteristic, (2) quantify the observed changes in these characteristics within the historical period (3) project the changes in the historical period to implement the desired shifts under future conditions. Later in section 6.4, we discuss how to obtain the desired shift under future condition.

Having the desired shifts, we first assume that the streamflow hydrograph can be described by the expected annual hydrograph and the variability around it at the subannual time steps (e.g., weekly,

monthly, or seasonal) as illustrated in Fig. 6.1a in black and gray colors, respectively. We then propose two algorithms to implement such changes to the streamflow hydrograph. First, to perturb the expected annual hydrograph, we conceptualize the annual hydrograph as a time distribution function mimicking the properties of probabilistic cumulative distribution function (CDF) – see Fig. 6.1b.
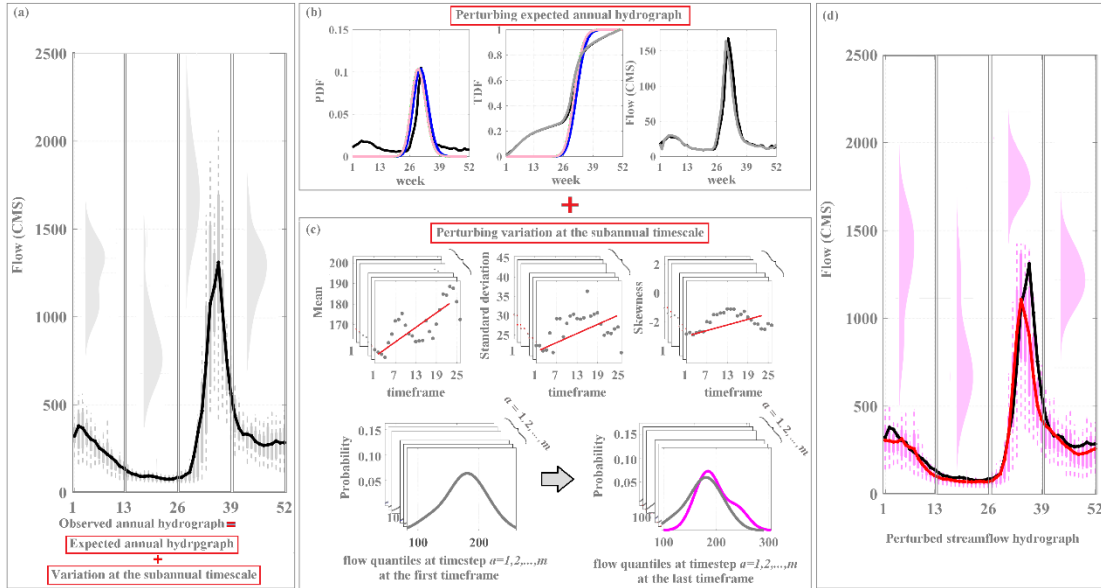
Figure 6.1. The proposed framework for shifting the streamflow annual hydrograph. The panel (a) shows the streamflow hydrograph defined by the expected annual hydrograph (black line) and the variability around it at the subannual timescale (gray boxes). The gray distributions show the seasonality defined by the changes in the seasonal volume distributions. The panels (b) and (c) illustrate the schematic procedures for perturbing the expected annual hydrograph and the variation at the subannual timescales, respectively. The panel (c) displays the shifted streamflow hydrograph composed of updated expected annual hydrograph (red line) along with updated distributions in subannual timescale (pink boxes).

We then use quantile mapping (e.g., Li et al., 2010) to systematically shift the expected annual hydrograph by assuming that the shift in the flow quantiles can be mapped by the desired shift in quantiles of a Generalized Gamma distribution (GG) with the same mode as the expected annual hydrograph (see Fig. 6.1b and section 6.2.2 for further explanation). The changes in the variability around the expected annual hydrograph can be expressed by perturbing the three moments of GG probability distributions fitted to the flows at each subannual timestep – see Fig. 6.1c and section 6.2.3 for further discussion. The changes in the expected annual hydrograph and the variability can collectively combined to represent any form of change in the streamflow regime – see the updated streamflow hydrograph in Fig. 6.1d.

6.2.2. Representing and Perturbing the Expected Annual Hydrograph

6.2.2.1. Generalized Gamma Distribution

The Generalized Gamma Distribution (GG) is one of the most common distributions. It is mainly due to its extreme flexibility and adaptability to different shape distributions, such as Levy distribution,

116

Rayleigh distribution, Weibull distribution, exponential distribution, and 2-parameter gamma distribution. Thus, it has been applied in various fields of science such as healthcare (Hill and Miller, 2010; Abadi et al., 2012; Pal et al., 2020), economics (Kleiber and Kotz, 2003; Zamani et al., 2020), and hydrology (Ashkar and Ouarda, 1998; Papalexiou and Koutsoyiannis, 2012; Chen et al., 2017; Chen and Singh, 2018).

The Generalized Gamma Distribution (GG) is one of the most common distributions. It is mainly due to its extreme flexibility and adaptability to different shape distributions, such as Levy distribution, Rayleigh distribution, Weibull distribution, exponential distribution, and 2-parameter gamma distribution. Thus, it has been applied in various fields of science such as healthcare (Hill and Miller, 2010; Abadi et al., 2012; Pal et al., 2020), economics (Kleiber and Kotz, 2003; Zamani et al., 2020), and hydrology (Ashkar and Ouarda, 1998; Papalexiou and Koutsoyiannis, 2012; Chen et al., 2017; Chen and Singh, 2018).

Historically, the generalized gamma distribution is a younger distribution than normal distribution, first introduced by Stacy (1962). The origins of the generalized gamma distribution, however, can be viewed as a special case of the Amoroso distribution which be traced back to the work of Amoroso (1925). The probability distribution function (PDF) of the 3-parameter GG distribution is given by:

$$f(x; \beta, \lambda, s) = \begin{cases} \dfrac{|s|x^{s\lambda-1}e^{-\left(\frac{x}{\beta}\right)^s}}{\beta^{s\lambda}\Gamma(\lambda)} & if \ x > 0 \\ \\ 0 & if \ x \leq 0 \end{cases} \tag{6.1}$$

where β is a scale parameter and both λ and s are shape parameters. The β and λ must be positive and s can be either positive or negative. $\Gamma(.)$ denotes the gamma function defined by $\Gamma(z) = \int_0^\infty x^{z-1}e^{-x}dx$. The cumulative distribution function (CDF) of generalized gamma distribution is given by:

$$F(x; \beta, \lambda, s) = \begin{cases} \dfrac{\gamma\left(\lambda, \left(\frac{x}{\beta}\right)^s\right)}{\Gamma(\lambda)} & if \ x > 0 \\ \\ 0 & if \ x \leq 0 \end{cases} \tag{6.2}$$

where $\gamma(.)$ is the lower incomplete gamma function defined as $\gamma(s, x) = \int_0^x t^{s-1}e^{-t}dt$.

The non-central moments of the generalized gamma distribution are defined by (Stacy, 1962):

$$\mu'_r(x) = \frac{\beta^r\Gamma(\lambda + {}^r/_s)}{\Gamma(\lambda)} \tag{6.3}$$

The moments are defined only if $\left(\lambda + \frac{r}{s}\right) > 0$. If we adopt the notation, as previously employed by Cohen and Whitten (2020), then we have $G_r(\lambda, s)$ as:

$$G_r(\lambda, s) = \frac{\Gamma(\lambda + {}^r/_s)}{\Gamma(\lambda)} \tag{6.4}$$

6.2.2.2. Representing and Perturbing the Time Distributio Function

Here, we employ GG distribution along with a quantile mapping to shift the expected annual hydrograph. For this purpose, considering n years of annual streamflow data with an expected annual hydrograph, Q^A, at any site A, first the expected annual hydrograph needs to be translated into a cumulative time distribution (TDF) as previously discussed in Nazemi et al. (2013) and later used in many applications (e.g., Hassanzadeh et al. 2016, Feng et al., 2017; Nazemi et al., 2020). TDF works similar to CDF and can be interpreted as the ratio of the total annual volume, passed prior to or at each subannual timestep. Assuming flows at the subannual timestep $t: t = 1, 2, \dots, m$ and a uniform timestep with duration of δ, the TDF can be defined at the timestep t as:

$$TDF(t) = \frac{\sum_{i=1}^{t} Q_i^A}{\sum_{j=1}^{m} Q_j^A} \tag{6.5}$$

where Q_i^A is the flow at the timestep i. The $TDFs$ have similar properties as CDF; and therefore having the total annual volume and the $TDFs$, the flow at each timestep can be estimated by:

$$Q_t^A = \left(TDF(t) - TDF(t-1)\right) \times \sum_{j=1}^{m} Q_j^A \tag{6.6}$$

Having the TDF of flows at each timestep t, to shift the timing of the annual peak, we assume that the instantaneous displacement of a GG distribution can be implemented to the expected annual hydrograph using quantile mapping. For this purpose, the TDF should have the maximum shift at the timing of the peak. This can be conceptualized using the displacement of a GG distribution for which the mode of distribution coincides with the peak of annual flow before and after desired shift. Fig. 6.1b illustrates the proposed conceptualization. The left panel of Fig. 6.1b exemplifies the concept, demonstrating a GG distribution fitted to the expected annual hydrograph shown in blue line for which the mode of distribution matches the timing of annual peak. To implement any desired shift, Δ, first we have to obtain the three parameters of the GG distribution fitted to the original annual hydrograph (the blue lines in the Fig. 6.1b) using the generalized method of moments as described by the following system of equations:

$$\mu_1'(Q^A) = E(Q^A) = \beta G_1 \tag{6.7}$$
$$\mu_2'(Q^A) = V(Q^A) = \beta^2 \left(G_2 - G_1^2\right) \tag{6.8}$$
$$Mo(Q^A) = \beta \left(\lambda - {}^1/_s\right)^{1/s}, \quad \forall \lambda s > 1 \tag{6.9}$$

118

where $G_k(\lambda, s)$ abbreviated to G_k; the left-hand side of Eqs. 6-8 are the mean, variance, and mode of original annual hydrograph. By solving this system of equations, we obtain the parameters of GG_o distribution fitted to the TDF of original annual hydrograph as shown in blue line in Fig. 6.1b. The next step is to implement the desired shift, Δ, to the timing of peak and obtain the new GG_Δ distribution containing the desired shift as shown in green line in Fig. 6.1b. For this purpose, we have to solve the above system of equations as described in Eqs. 7-9 with the same mean and variance but with a new mode of distribution shifted by $\pm\Delta$. To impose the desired shift in the timing of peak to the annual hydrograph, here we use quantile mapping to update the annual hydrograph as the following:

$$Q^A = F^{-1}(GG_o(\beta_o, \lambda_o, s_o)\{GG_\Delta^{-1}(\beta_\Delta, \lambda_\Delta, s_\Delta)(u)\}) \tag{6.10}$$

where F^{-1} is the inverse TDF of annual hydrograph. GG_o is the generalized gamma distribution fitted to the historical hydrograph. GG_Δ^{-1} is the inverse of updated generalized gamma distribution with desired shift Δ. The Q^A is the shifted annual flow hydrograph with updated flow quantiles at the nonexceedance probability u as shown in Fig. 6.1c with gray line.

6.2.3. Representing and Perturbing the Variability around Expected Hydrograph

Using the procedure explained in section 6.2.2 and illustrated in Fig. 6.1b, we are able to shift the expected annual hydrograph. The streamflow hydrograph, however, comprises the expected annual hydrograph and the variability around it at the subannual timescale (see Fig. 6.1a). This requires another algorithm to represent and perturb the variability of flows at the subannual timescale. Here, we propose an algorithm to shift the flow distributions at the subannual timestep as demonstrated in Fig. 6.1c. For this purpose, (1) we obtain the first three moments of flows at the subannual timescale $t: t = 1, 2, \ldots, m$ including mean, variance, and skewness of original flows (see the black line in bottom row of Fig. 6.1c) ; (2) we analyze the changes in the three moments using the moving timeframe and analysis of trend as demonstrated in the top row of Fig. 6.1c; (3) we impose any desired shifts, φ_t, ϕ_t , and ω_t to the three moments at the subannual timescale obtained using the concept of moving timeframes and trend analysis as explained in section 6.2.1 (see Zaerpour et al., (2021) for further discussion); (4) the method of moments are applied to the GG distributions at each timestep t to extract the updated parameters of GG^t distributions (see pink line in the bottom row of Fig. 6.1c) which can be described by solving the system of equations as follows:

$$\mu_1'(Q_t^A) \pm \varphi_t = \beta G_1 \tag{6.11}$$
$$\mu_2'(Q_t^A) \pm \phi_t = \beta^2(G_2 - G_1^2) \tag{6.12}$$
$$\mu_3'(Q_t^A) \pm \omega_t = \frac{G_3 - 3G_2G_1 + 2G_1^3}{\left(G_2 - G_1^2\right)^{3/2}} \tag{6.13}$$

where the μ_1', μ_2', and μ_3' in the left side of Eqs. 11-13 are the first three moments of the original flows at the subannual timestep t; the φ_t, ϕ_t, and ω_t are the desired shifts in the moments of

119

GG^t distribution at the subannual timestep. By solving this system of equations, we are able to impose the desired shifts and update the distributions at the subannual timestep.

6.2.4. Copula-based generation of streamflow series

6.2.4.1. Single-site Generation of Streamflow

In single site generation of streamflow, the temporal dependence structure within flows at the subannual timescale should be maintained. Here, we use bivariate copula methodology to represent the temporal dependence structure. In summary, if u and v are two continuous random – here are the flows at the two consecutive time steps $t - 1$ and t with the marginal distributions of $u = F_{t-1}(Q^A_{t-1})$ and $v = F_t(Q^A_t)$, the joint cumulative distribution $F_{U,V}(u, v)$ can be described using copula function defined by (Sklar, 1959):

$$F_{U,V}(u, v) = C(u^*, v^*) \tag{6.14}$$

where C denotes the copula function. Having the joint distribution between flows at the two consecutive time steps, the nonexceedance probability of flow at the time step t can be estimated conditionally as the following (see Salvadori and De Michele, 2007):

$$C_{u^*}(v^*) = P\{F_t(Q^A_t) \leq v | F_{t-1}(Q^A_{t-1}) = u^*\} = \frac{\partial}{\partial u}\left(C_{t,t-1}(u^*, v^*)\right) \tag{6.15a}$$

$$Q^A_t = F_t^{-1}\{C_{u^*}^{-1}(v^*)\} \tag{6.15b}$$

where Q^A_t is the flow at the time step t, Q^A_t is the flow at time step $t - 1$, F_t and F_{t-1} are the marginal $CDFs$ of flow at time steps t and $t - 1$, $C_{t,t-1}$ is the parametric copula structure describing the joint distribution between flow $CDFs$ at time steps t and $t - 1$, and P is the conditional CDF.

6.2.4.2. Multisite Generation of Streamflow

In multisite generation of streamflow, the temporal and spatial dependence structures should be preserved. Here, we use C-vine copulas to represent the dependence structure within and between streamflow series. Let Q^B_t and Q^B_{t-1} be the flows at the two consecutive time steps t and $t - 1$ at the secondary site B. Considering a 3-dimensional C-vine copula function, the joint distribution between Q^A_t, Q^B_t, and Q^B_{t-1} can be established as (Joe, 1997):

$$f(Q^A_t, Q^B_{t-1}, Q^B_t) = f_1(Q^B_{t-1})f_{2|1}(Q^A_t|Q^B_{t-1})f_{3|1,2}(Q^B_t|Q^B_{t-1}, Q^A_t) \tag{6.16}$$

where the subscripts 1, 2, and 3 correspond to Q^B_{t-1}, Q^A_t, and Q^B_t, respectively. $c(.)$ is the 3-dimensional copula PDF. Based on Joe (1997) and Bedford and Cooke (2001) the joint density in Eq. (13) can be expressed as:

$$f(Q_t^A, Q_{t-1}^B, Q_t^B)$$
$$= f_1(Q_{t-1}^B)f_2(Q_t^A)f_3(Q_t^B)c_{1,2}\big(F_1(Q_{t-1}^B), F_2(Q_t^A)\big)c_{1,3}\big(F_1(Q_{t-1}^B), F_3(Q_t^B)\big) \qquad (6.17)$$
$$c_{2,3|1}\big(F(Q_t^A|Q_{t-1}^B), F(Q_t^B|Q_{t-1}^B)\big)$$

Having the joint distribution function, the conditional distribution function of $F(Q_t^B|Q_{t-1}^B, Q_t^A)$ can be obtained as (Aas et al., 2009; Czado et al., 2012):

$$h = F(Q_t^B|Q_{t-1}^B, Q_t^A) = \frac{\partial C_{2,3|1}\big(F(Q_t^B|Q_{t-1}^B), F(Q_t^A|Q_{t-1}^B)\big)}{\partial F(Q_t^A|Q_{t-1}^B)} \qquad (6.18)$$

Note that $F(Q_t^B|Q_{t-1}^B) = h(Q_t^B|B) = \frac{\partial c_{3,1}(F(Q_t^B), F(Q_{t-1}^B))}{\partial F(Q_{t-1}^B)}$ and $F(Q_t^A|Q_{t-1}^B) = h(Q_t^A|Q_{t-1}^B) = \frac{\partial c_{2,1}\big(F(Q_t^A), F(Q_{t-1}^B)\big)}{\partial F(Q_{t-1}^B)}$. As a result, Eq. (17) can be rewritten as:

$$h = F(Q_t^B|Q_{t-1}^B, Q_t^A) = h[h(Q_t^B|Q_{t-1}^B)|h(Q_t^A|Q_{t-1}^B)] \qquad (6.19)$$

We then apply the inverse forms of h-functions given in Eq. (19) for streamflow generation at single site setting given by:

$$Q_t^B = F^{-1}\left\{h^{-1}\left[\left(h^{-1}\big(\varepsilon|h(Q_t^A|Q_{t-1}^B)\big)\right)|Q_{t-1}^B\right]\right\} \qquad (6.20)$$

The proposed streamflow generation scheme is developed to preserve the lag-1 temporal and lag-0 spatial dependencies, however, it can be extended using multidimensional C-vines to consider more than lag-1 temporal dependence in finder timescales (i.e. daily).

6.3. Case Study and Data

To showcase the performance of the proposed model in representing various forms of shift, we select six streams. These streams are derived from Canadian Reference Hydrometric Basin Network (RHBN; Brimley et al., 1999). The dataset is provided by the Water Survey of Canada (Environment Canada, HYDAT Database). RHBN stations are natural streams with relatively pristine and stable land use condition developed to identify the impact of climate change. Fig. 6.2 shows the locations of these six RHBN streams, spreading over different parts of Canada including British Columbia, Quebec, Nova Scotia, and Yukon. Table 6.1 depicts the list of six stations with their description, coordinates, and sizes of basins. The first catchment includes two streams sites G1 and G2 located in the northern part of Canada with glacial-dominated regimes and relatively large sizes of 6860 and

7050 km^2, respectively. The second catchment includes sites NG1 and NG2 located in eastern Canada with nival-glacial regimes and very large sizes of 19000 and 13000 km^2, respectively. The third catchment comprises of site N1 situated in eastern Canada with nival regime and relatively small size of 1610 km^2 compared to the two other sites. Finally, the fourth catchment includes site P1 located in southeastern part of Canada with pluvial regime and relatively small sizes of 368 km^2. All six streams are used for generation of streamflow in single site setting. The first two catchments are also used in multisite setting, since these two catchments include more than one stream. To detect the forms of changes in the six streams and making scenarios of changes in future, we extract the weekly data for the period of 1966 to 2010.

Table 6.1. Summary information of selected stations from the Canadian Hydrometric Database (Water Survey of Canada).

Name	Regime type	Description	Province	Lat.	Long.	Drainage area (Km²)	RHBN ID
G1	Glacial	Atlin River Near Atlin	BC	59.60	-133.8	6860	09AA006
G2	Glacial	Takhini River Near Whitehorse	YT	60.85	-135.7	7050	09AC001
NG1	Nival-Glacial	Moisie (Riviere) A 51 Km En Amont Du Pont Du Q.N.S.L.R.	QC	50.35	-66.2	19000	02UC002
NG2	Nival-Glacial	Romaine (Riviere) Au Pont De La Q.I.T.	QC	50.31	-63.6	13000	02VC001
N1	Nival	Rimouski (Riviere) A 3 7 Km En Amont Du Pont-Route 132	QC	48.41	-68.6	1610	02QA002
P1	Pluvial	Northeast Margaree River At Margaree Valley	NS	46.37	-61.0	368	01FB001
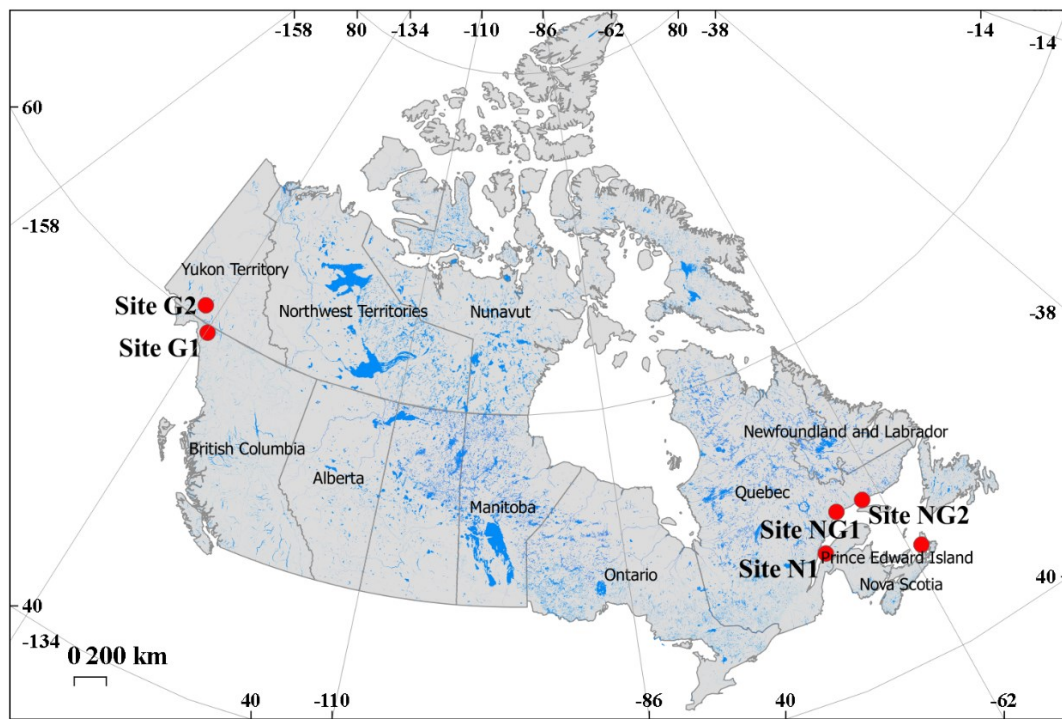
Figure 6.2. The six natural streams used as the case studies selected from canadian RHBN network.

As discussed earlier in section 6.2.1, to project the changes observed in the streamflow data and generate the plausible scenarios of changes in future, first we have to identify the dominant forms of changes under historical condition. Such changes are obtained by implementing the concept of moving timeframe and Mann-Kendall trend test. Fig. 6.3 summarizes how the streamflow hydrographs at the six streams evolve from the first timeframe (i.e., baseline period of 1966-1995; gray color) to the last timeframe (1981-2010; pink color). The black and red lines are the expected annual hydrographs at the first and last timeframes, respectively. Although, here we look at the forms of changes in the first three moments at the seasonal scale, the proposed model can easily be extended to represent the changes at the finer scale (e.g., weekly scale). In general, in the first catchment including sites G1 and G2, the dominant form of change is less variation in the spring flow. In site G2, the earlier timing of peak is also another dominant form of shift. In the second catchment which includes sites NG1 and NG2, less mean and variation in spring flows as well as earlier timing of annual peak are the most dominant forms of change observed. In site N1, the earlier timing of peak is the only dominant form of change. In site P1, a combination of various forms of change can be observed.
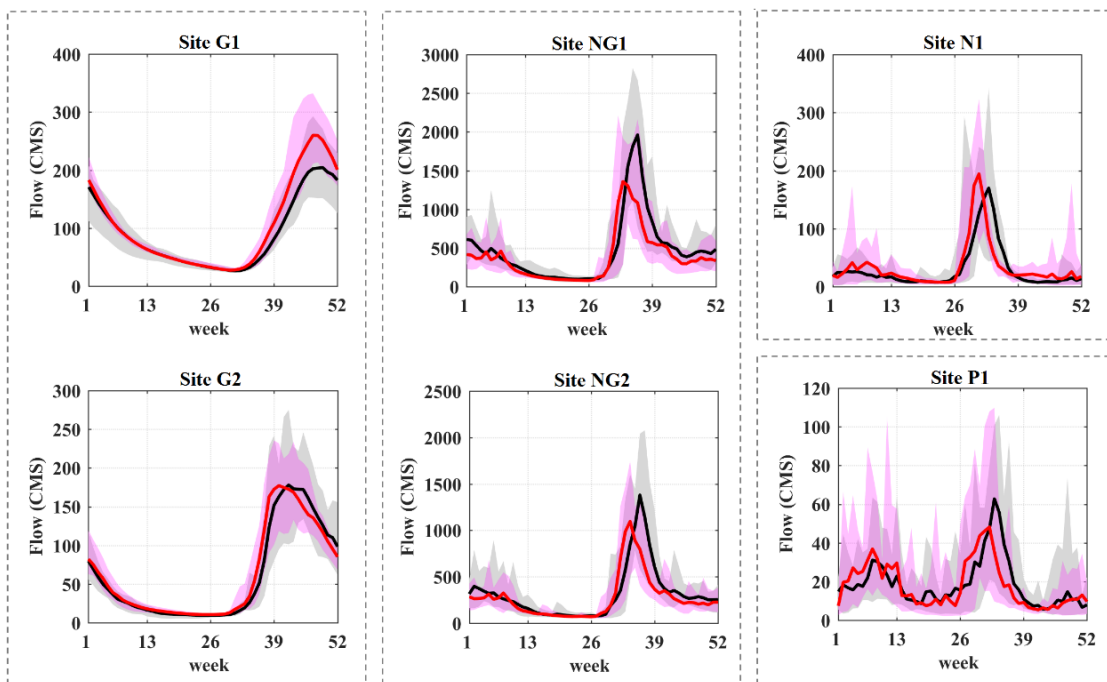
Figure 6.3. The evolution of streamflow regimes through time. The envelopes of annual hydrographs for the earliest (1966 to 1995) and the latest (1981 to 2010) episodes are shown with grey and pink colors, respectively. The expected annual hydrographs during the earliest and the latest periods are shown in solid black and red lines, respectively.

6.4. Experimental setup

To implement the desired changes, we incorporate the proposed perturbing algorithms into a copula-based stochastic streamflow generation scheme in single and multiple sites. All of six streams are considered for the single site generation of streamflow under changing condition. The first two catchments which include the two streams are additionally considered for generation of streamflow

at multisite setting. We consider a set of common parametric copula functions including Gaussian, Student t, Clayton, Gumbel, Frank, Joe, and their rotated forms for setting up bivariate and vine copulas – see Nelsen (2006) for the formulation of these copulas. The selection of copulas and parameterization are performed by applying Maximum log-Likelihood method and considering the Bayesian Information Criteria (BIC; Akaike, 1979) as the Goodness of Fit (Sadegh et al., 2017). As explained in section 6.2, the generalized gamma distribution which has been recommended for streamflow margins (e.g., Papalexiou et al., 2020) is used to establish the marginal distributions. The modelling is implemented in R platform by using the *VineCopula* (Schepsmeier et al., 2016; Nagler et al., 2019) and *gamlss* (Rigby and Stasinopoulos, 2005; Stasinopoulos et al., 2007) packages.

To showcase the application of proposed algorithms for shifting the streamflow hydrographs, we project observed changes to short-range (2025) and long-range (2055) futures. For this purpose, we calculate the Sen's slopes of the significant changes for the baseline timeframe of 1966-1995 to the last timeframe (1981-2010). This results into the $3\times52+1$ time series of expected weekly mean, standard deviation, skewness and the expected timing of annual peak for each considered stream. In order to quantify the gradual changes in such properties, the Mann-Kendall trend test with Sen's Slope is applied (Mann, 1945; Kendall, 1975). We then multiply the Sen's slopes by the 30 and 60 years to obtain the projected changes in short- and long-range futures, respectively. This leads to identification of the dominant forms of changes in the streamflow characteristics.

Table 6.2 summarizes the dominant forms of changes in expected timing of annual peak as well as changes in the three moments of seasonal flows. In site G1, the dominant forms of change are -5% (-10%) decrease in the standard deviations of fall and winter seasonal flows, 5% (10%) increase in mean seasonal flows of spring and summer under short- (long-) range futures. In site NG1, the dominant forms of change are -5% (-10%) decrease in mean seasonal flows in fall and winter, -10% (-20%) decrease in spring flow, as well as -15% (-30%) decrease in standard deviation and -5% (-10%) decrease in mean summer flow along with -1(-2) weeks earlier timing of peak in short- (long-) range futures. In site N1, -1(-2) weeks earlier timing of annual peak is the only main form of shift expected in short- (long-) range futures. In site P1, 15% (30%) increase in mean fall flow, 10% (20%) increase in winter flow, -15% (-30%) decrease in mean and -20% (-40%) decrease in standard deviation of spring flow and -2(-4) weeks earlier timing of annual peak are the main forms of change. In site G2, the standard deviation of winter flow is expected to decrease by -5%, (-10%), summer flow decreased by -10% (-20%) in short- (long-) range futures. The timing of annual peak in site G2 is expected to occur -1(-2) weeks earlier. In site NG2, the dominant modes of shift are -15% (-30%) decrease in mean and -10% (-20%) decrease in standard deviation of summer flow in short- (long-) range futures.

Having the dominant changes in the futures, we employ the proposed algorithms to implement the desired changes to the streamflow hydrographs and make various scenarios of change in futures. First, we use the algorithm developed in section 6.2.3 to implement the desired shift in expected timing of annual peak. Later, we implement the desired shift in the three moments of seasonal flows summarized in Table 6.2 using the algorithm developed in section 6.2.4. Having the perturbed

marginal distributions, we use the copula-based methodology in single and multisite settings to generate an ensemble of 1000 realizations under changing condition.

Table 6.2. The expected changes in the main streamflow characteristics including the three moments of flows at the weekly timescale as well as the expected timing of annual peak under short- (long-) range futures.

Streamflow characteristics			Site G1	Site G2	Site NG1	Site NG2	Site N1	Site P1
Changes in seasonality	OND	Mean	-	-	-5% (-10%)	-	-	+15% (+30%)
		Standard deviation	-5% (-10%)	-5% (-10%)	-	-	-	-
		Skewness	-	-	-	-	-	-
	JFM	Mean	-	-	-5% (-10%)	-	-	+10% (+20%)
		Standard deviation	-5% (-10%)	-	-	-	-	-
		Skewness	-	-	-	-	-	-
	AMJ	Mean	+5% (+10%)	-	-10% (-20%)	-	-	-15% (-30%)
		Standard deviation	-	-		-	-	-20% (-40%)
		Skewness	-	-	-	-	-	-
	JAS	Mean	+5% (+10%)	-10% (-20%)	-15% (-30%)	-15% (-30%)	-	-
		Standard deviation	-	-	-5% (-10%)	-10% (-20%)	-	-
		Skewness	-	-	-	-	-	-
Expected timing of peak	Annual	week	-	-1 (-2) week	-1 (-2) week	-1 (-2) week	-1 (-2) week	-2 (-4) week

6.5. Results

6.5.1. Performance of proposed model under historical condition

We initially analyze the performance of the proposed model in single-site setting in terms of capturing the expected annual hydrograph under historical condition. Fig. 6.4 shows the ensembles of 1000 realizations of streamflow hydrographs simulated under historical condition at the six studied sites A to F. The blue boxes are the ensemble of simulated streamflow hydrographs; and the red lines are the expected simulated streamflow hydrographs; The black lines indicate the observed values. In general, the expected simulated values often match the observed values, demonstrating that the proposed framework is able to capture the observed streamflow hydrographs very well. In sites A and E which are the glacial-dominated regime, the Relative Error (RE) in capturing the observed streamflow hydrographs is less than 1%. In sites B, C, and F which are the snow-dominated regime, the REs in capturing the observed flows are less than 2.1%. In site P1 which is rain-dominated regime, the RE in preserving the observed values are higher and reaches to $RE = 3.3\%$.

In addition to analyses of expected annual hydrographs, we assess the performance of our proposed model in representing the seasonal volumes in each site. Fig. 6.5 summarizes the findings in representing the mean and variation of seasonal volumes shown in boxplots. The gray boxes are the relative changes in the range of observed seasonal volumes with respect to the expected observed value. The blue boxes are the relative changes in the range of simulated ensemble of seasonal

volumes. The red dots are the expected values and the pink lines indicate no-change in the expected seasonal volumes. In general, the proposed model can represent the observed mean and variation of seasonal volumes quite well, demonstrating average REs of 2.9% and 8.3%, respectively. In sites A and E with glacial-dominated regime, the average REs in representing the mean and variation of seasonal volumes are 2.5% (7.4%) and 2.2% (5.4%), respectively. In sites B, C, and F, the average REs in capturing the observed mean and variation of seasonal volumes are 2.6%, 3.4%, and 1.3%, respectively. In site P1 with rain-dominated regime, however, the REs in representing the mean and variation of seasonal volumes are higher and reach to average REs of 5.4% and 11.8%, respectively. The highest RE occurs in representing mean and variation of winter seasonal volumes with average REs of 4.1% and 8.3%, respectively.
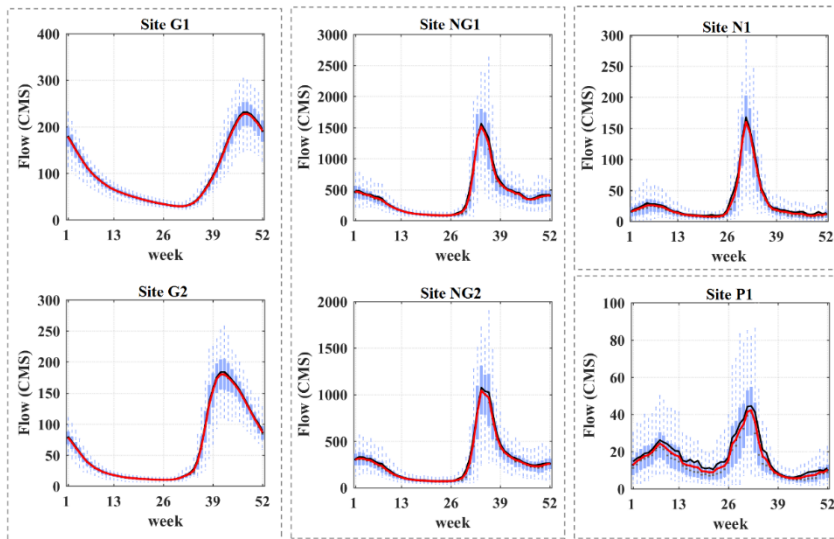
Figure 6.4. The ensemble of 1000 realizations generated by the proposed model at the six sites in single-site setting shown in blue boxplots; The red and black lines are the expected simulated and observed annual hydrographs.

We also assess the performance of the proposed model in preserving the lag-1 temporal dependencies in single-site generation of streamflow. Fig. 6.6 summarizes findings in the representation of lag-1 temporal dependencies in terms of Kendall tau. The black lines show the observed lag-1 temporal dependencies. The blue colored boxes illustrate the results of 1000 realizations obtained by the proposed model in single-site setting. In summary, the proposed model performs quite well, demonstrating a Mean Absolute Error (MAE) of less than 0.03. The best performance in capturing the observed lag-1 temporal dependence can be observed in sites A and E with glacial-dominated regime, demonstrating average MAE of 0.01. The strongest temporal dependencies can be observed in winter season, in which the proposed model performs well in representing the lag-1 temporal dependencies with average MAE of 0.02. The proposed model, however, shows slightly lower performance in site NG1 in preserving the lag-1 temporal dependencies, demonstrating average MAE of 0.03.
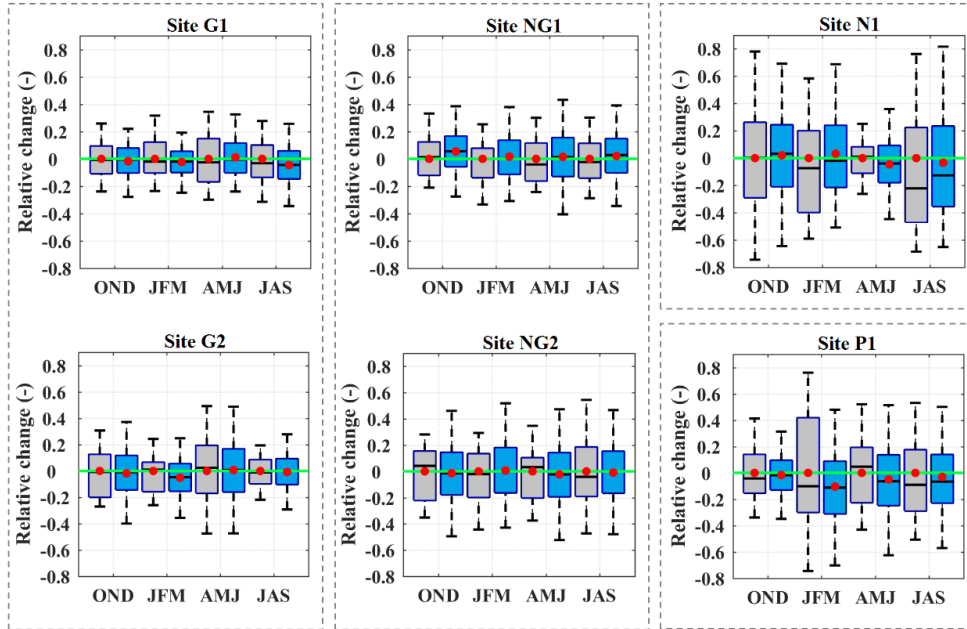
Figure 6.5. The performance of proposed model in capturing the seasonal flow volume (i.e., seasonality). The gray boxplots are the relative changes in the observed seasonal volumes with respect to the expected values. The blue boxplots show the relative changes in the simulated seasonal volumes with respect to the expected observed seasonal volume data.
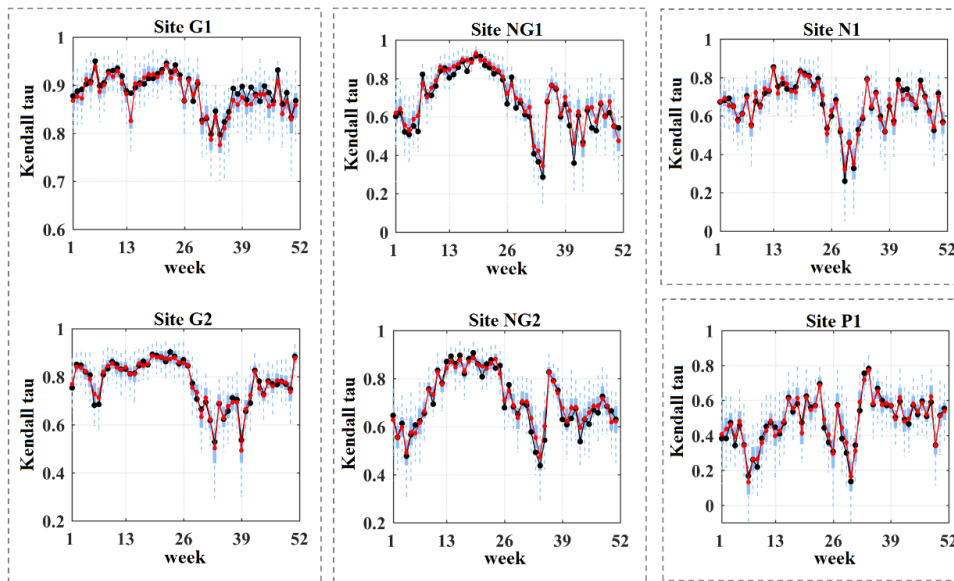
Figure 6.6. The performance of the proposed model in single-site generation of streamflow at the six sites in terms of the lag-1 temporal dependence. The black line indicate the observed lag-1 temporal dependence. The blue boxes are the ensemble of simulated values. The red line indicates the expected simulated value.

6.5.2. Scenario generation under changing conditions

The results obtained, however, are only limited to the single-site generation of streamflow under historical condition without any shift. Another experiment, therefore, is performed to investigate how the proposed model can apply the desired shifts in the expected timing of peak, update the flow

127

distributions at the subannual timescale, and consequently shift the entire streamflow hydrograph. Having the proposed model, various scenarios of change in the flow characteristics can be generated using the observed flow data, providing the opportunity to assess the vulnerability of any water resource system to different scenarios of change in the annual streamflow hydrograph. Fig. 6.7 exemplifies how the proposed algorithms can apply the desired shifts identified using the concept of moving timeframe (see Table 6.2) to the streamflow hydrographs of six studied sites.
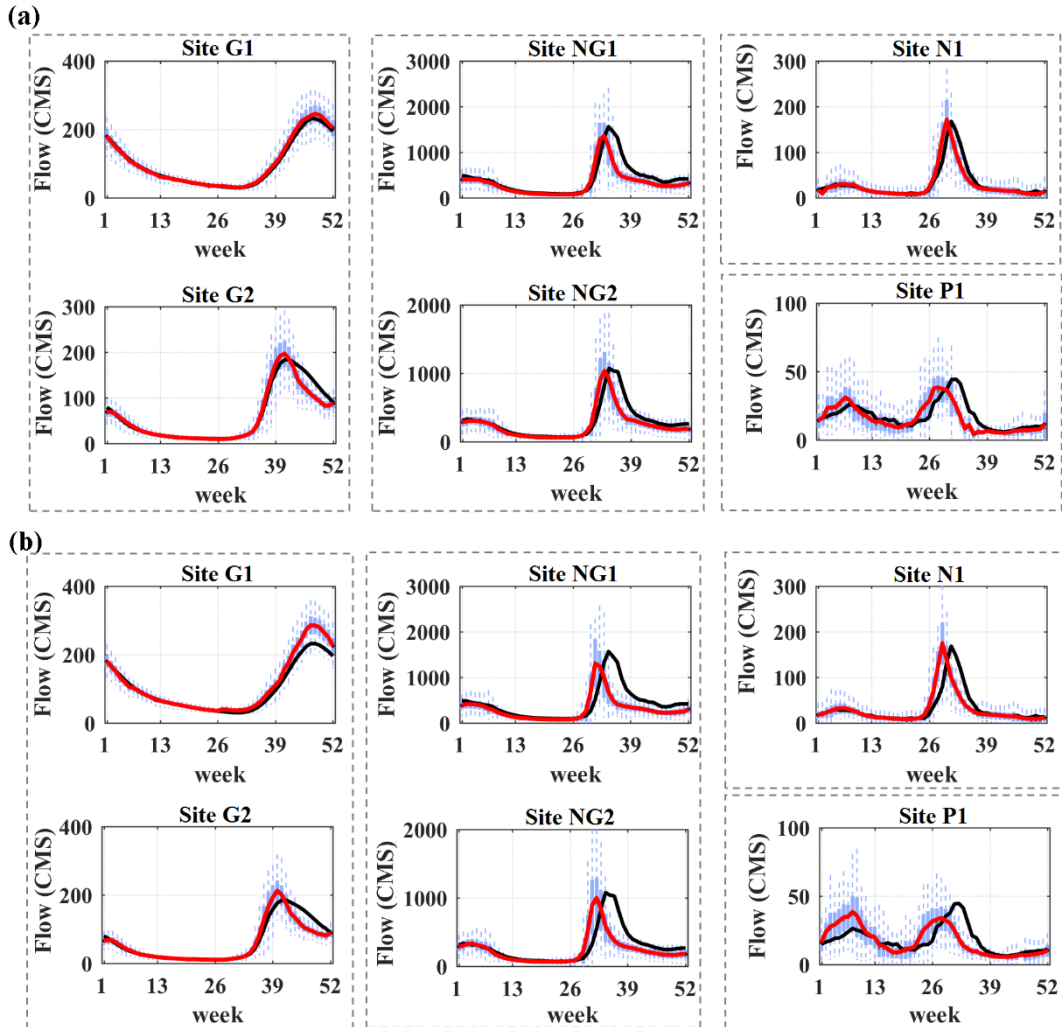
Figure 6.7. The ensemble of 1000 realizations of perturbed streamflow hydrographs generated by the proposed model at the six sites in single-site setting shown in blue boxplots; The panels (a) and (b) are related to short- and long-range futures. The red and black lines are the expected simulated and observed annual hydrographs.

The black lines show the expected observed annual hydrographs. The boxplots are the updated flow distributions at the weekly timestep and the red lines indicate the expected perturbed annual hydrographs. The panels (a) and (b) correspond to the desired shifts for the short- and long-range futures as explained in Table 6.2. Comparing the historical with the perturbed flow distributions under short and long-range futures demonstrates how the proposed algorithms can impose various forms of shifts to the weekly distributions to represent the desired shifts in the expected annual hydrographs.

The scenarios characterize various forms of changes ranging from the changes in the expected timing of peak to the changes in the seasonality or the combination of both. For each scenario, 1000 realizations are generated, each includes 45 years of weekly simulation. In site G1, for instance, the variations in low-flow seasons are decreasing while in high-flow seasons the seasonal flows are increasing without any changes in the expected timing of peak. In site NG1, however, the dominant mode of shift is related to the expected timing of peak accompanied by changes in the seasonality. In site N1, the earlier timing of peak is the dominant form of shift. In sites D, E, and F the various combination of forms of shifts in the expected timing of peak and seasonality can be observed.

To evaluate the performance of the proposed model under changing conditions, we first analyze how the desired shifts in the expected timing of peak can be represented in single-site generation of streamflow hydrographs under changing condition. For this purpose, we compare the ensemble of 1000 realizations of perturbed streamflow hydrographs with the target desired shifts as explained in Table 6.2 served as the reference points. Here, we measure the timing of annual peak using a circular statistics (Pewsey et al., 2013). The time of occurrence of annual timing of peak is defined by converting the Julian time of occurrence of annual high flow to an angular value (Burn et al., 2010). Fig. 6.8 and E1 in the Appendix E summarize the results in the short and long-range futures, respectively. The polar histogram shows the distribution of annual timing of peak happening across different time of the year. Here, the timing of annual peak is represented as an angle measured counterclockwise relative to October 1st (i.e., start date of water year). The black and blue histograms are related to the observed and simulated values, respectively. The more scattered histogram indicates the greater spread in the timing of occurrence of the annual high flows. In sites A and E with glacial-dominated regime, the timing of annual peak generally displays more regularity with the majority of annual high flows. The annual high flows often occur in summer ranging from early July to September shown in black color. As can be seen the proposed model can represent the historical values very well. As expected, there is no changes in the timing of high flows of the simulated streamflow hydrographs can be observed for in site G1 in short/long-range futures.(see Table 6.2). In sites E, however, the average *MAE* in representing the desired timing of peak in short and long-range futures are 0.1 and 0.3 weeks, respectively. In sites B, C, and F with snow-dominated regime, the timing of annual high flow often occur in the spring season, ranging from late April to early June. The average *MAE* in representing the desired shift in the timing of annual peak of sites B, C, and F in short-range future are 0.3, 0.1, and 0.2 of week, respectively. These values are 0.4, 0.2, and 0.4 of week for long-range future, respectively. In site P1 with rain-dominated regime, the more scattered observed histogram can be observed, indicating less regularity in the occurrence of timing of annual peak. As can be seen the proposed model performs well in representing the desired shift in the timing of annual peak, demonstrating MAE of 0.3 and 0.4 of week. Another high flow is expected to emerge which might be due to increasing rainfall in fall season in long-range future.
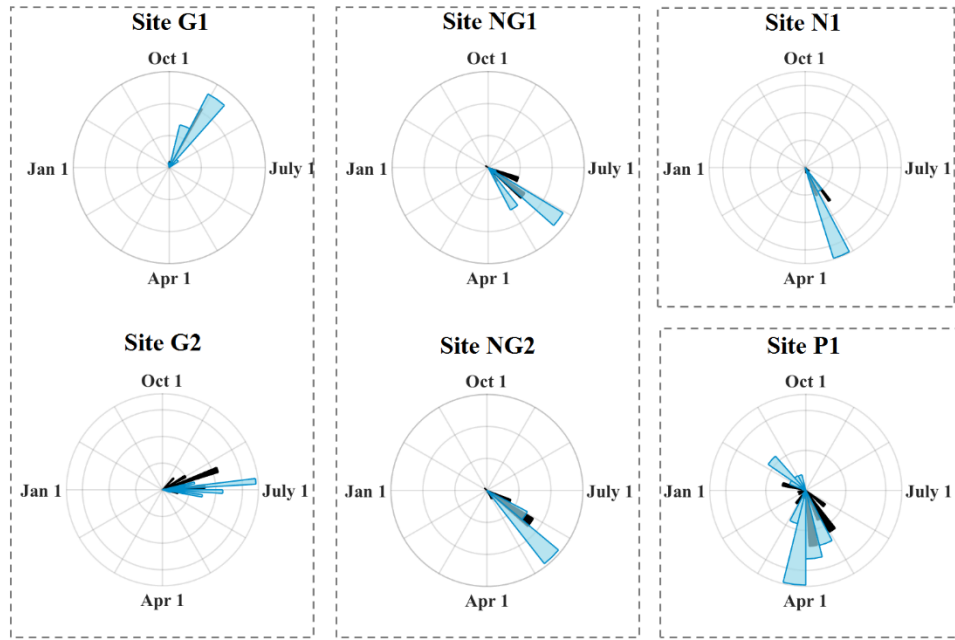
Figure 6.8. Representation of the desired shift in the expected timing of the annual peak in short range future across the six sites using the proposed approach in single-site setting. The black and blue histograms are related to the observed and generated timing of annual peak, respectively.

In addition to analyses of annual timing of peak, we assess the performance of the proposed model in representing the desired shifts in the seasonality measured by changes in the marginal distributions of seasonal volumes. Fig. 6.9 summarizes the results in representing the desired shift in distribution of seasonal volumes for short-range future in six sites sorted in rows. The columns are related to the results of four seasons. The gray distributions are related to the observed seasonal volumes; whereas, the blue ones are the simulated distributions of perturbed seasonal volumes. Fig.E2 in the Appendix E illustrate similar analysis for long-range future. In summary, the proposed model can implement the desired shifts obtained in the Table 6.2 quite well. In site G1, as explained in Table 6.2, the target desired shifts include a 5% decrease in variations of seasonal volumes in fall and winter for which the $MAEs$ are 1.3% in fall and 0.3% in winter for short-range future. These values are 3.4% and 4.1% for long-range future. In spring and summer, the $MAEs$ in representing the desired shift (5% increase in the seasonal volume) are 1.2% and 1.4%, respectively. Regarding the long-range future, these values are 1.2% and 2.8% in representing spring and summer volumes. In site NG1, the $MAEs$ in representing the target shifts in fall and winter seasons are 0.4% (1.1%) and 1.8% (3.1%) in short- (long-) range futures, respectively. In spring, the proposed model can represent the desired shift in seasonal volume with $MAEs$ of 3.9% and 2.5% in short- and long-range futures, respectively. In summer, the desired shifts are 15% (30%) and -5% (-10%) in the mean and variation of summer volumes for short- (long) range futures, respectively.
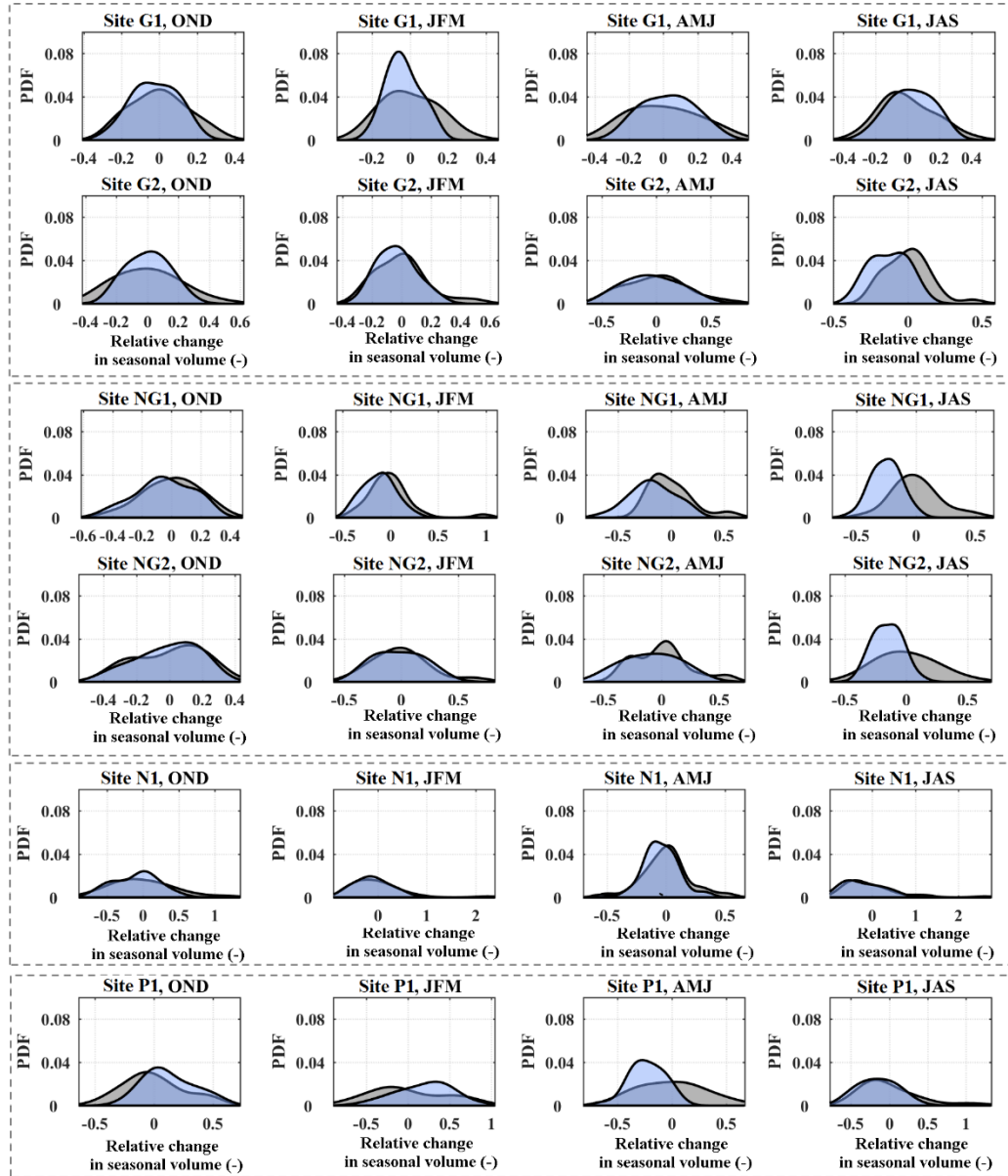
Figure 6.9. Representation of desired forms of shifts in terms of changes in the seasonal volume in six sites using the proposed approach in single-site generation of streamflow. The gray and blue colored distribution are the observed and simulated seasonal volumes. The results are related to the short-range future.

The *MAEs* in capturing the target mean and variation are 4.3% and 1.5% in short-range future; whereas, these values are 3.7% and 1.2% in long-range future. In site N1, no-significant changes in seasonal volume is expected for which the proposed model perform well in preserving the observed values with *MAEs* of less than 1.5%. In site P1, the proposed model can represent the desired shifts in seasonal volumes in fall and winter with *MAEs* of 2.3% (0.5%) and 4.3% (1.6%) in short- (long-) range futures, respectively. In spring, the *MAEs* in representing the desired shift in mean and variation of seasonal volume are 3.4% (2.3%) and 2.1% (3.6%) for short- (long-) range futures, respectively. In site G2, the proposed model performs well in representing the desired shift with *MAEs* of 2.1%

(1.3%) for short- (long-) range futures. In site NG2, the *MAEs* in representing the desired shifts in mean and variation of seasonal volume are 1.6% (3.8%) and 1.5% (4.1%) for short- (long-) range futures, respectively.

We further analyze the generalization capability of the proposed model in representing the desired shift in multisite settings. This experiment gives an insight into the performance of the proposed model in representing the desired shifts in catchments with more than one streamflow. For this purpose, we implement the desired shifts in sites E and F in both single and multisite settings and compare the results. Fig. 6.10 summarizes the results for short- and long-range futures shown in panels (a) and (b). The first and second rows in each panel are related to single and multisite settings, respectively. Similar to Fig. 6.7, the blue boxes are the simulated ensemble of perturbed streamflow hydrographs; the black and red lines are the expected observed and simulated values. In short-range future, the proposed model can represent the desired shift in the expected annual hydrographs in site G2 and F with REs of 2.8% and 3.7% in single-site setting. These values are 1.7% and 6.3% in multisite settings. Regarding the long-range future, the REs in representing the desired shift in single-site generation of sites E and F are 3.8% and 7.4%, respectively; whereas in multisite settings, these values are 3.1% and 5.6%.
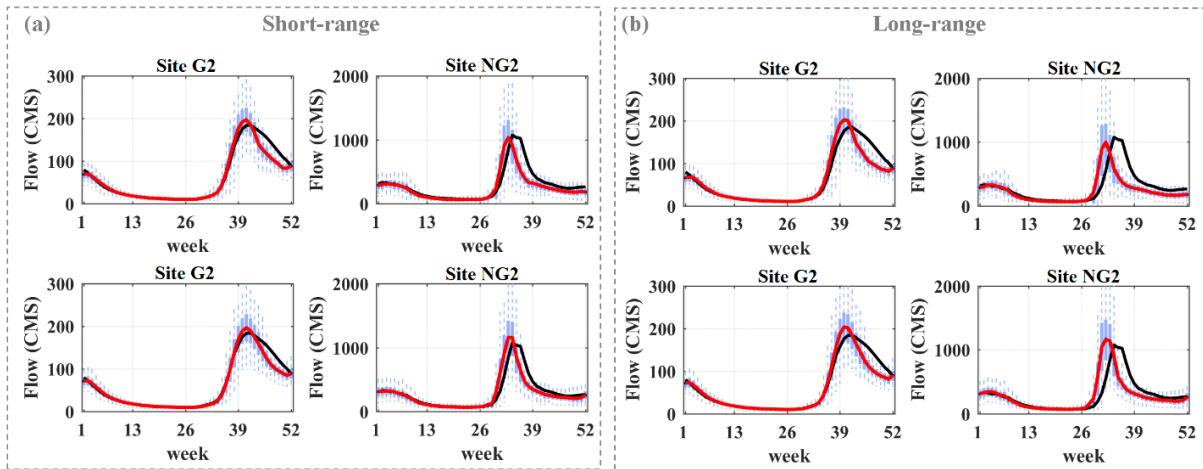
Figure 6.10. The comparison of the ensemble of 1000 realizations of perturbed streamflow hydrographs generated by the proposed model at single- and multisite settings shown in the first and second rows, respectively. The blue boxplots are the ensembles of 1000 realizations at sites E and F; The black and red lines are the expected observed and simulated annual hydrographs. The panels (a) and (b) are related to short- and long-range futures.

We further compare the performance of the proposed model in implementing the desired shift in timing of annual peak in single and multisite settings. Fig. 6.11 illustrates the results of this experiment. Similar to Fig. 6.10, the first and second rows are related to the single and multisite settings, respectively. The panels (a) and (b) correspond to the results of short and long-range futures. The black and blue polar histograms indicate the distributions of observed and simulated values, respectively. Regarding the short-range future, the proposed model can represent the desired shift in timing of peak with less than average error of 0.3 week in both single and multisite settings in site

G2. Regarding site NG2, the average errors in representing the desired shift in timing of peak are less than 0.2 of week. In long-range future, regarding site G2, the proposed model performs well in both single and multisite settings with less than average error of 0.4 of week. In site NG2, however the proposed model can better represent the desired shift in single-site setting, demonstrating average error of 0.3; whereas, this is 1.1 of week for multisite setting.

In addition to the timing of annual peak, we further compare the performance of the proposed model in single and multisite representation of the desired shift in sites E and F in terms of seasonal volume distributions. Figs. 6.12 and E3 in the Appendix E depict the results of this experiment in short and long-range futures, respectively. The lighter and darker colors are related to the single and multisite settings, respectively. Regarding the short-range future in site G2, the expected $MAEs$ in representing the desired shift in fall (i.e., -5% decrease in the standard deviation of seasonal volume) are 1.1% and 1.3% for single and multisite settings, respectively. In winter, the expected $MAEs$ in representing the observed seasonal volume are 1.3% (1.4%) for single (multisite) setting, respectively. In spring, multisite setting, however, represents less error ($MAE = 0.5\%$) in capturing the observed value compared to the single site setting with $MAE = 1.1\%$.

In summer, the proposed model can represent the desired shift with an expected MAE of less than 1.1% in both single and multisite settings. In site NG2, both single and multisite settings show similar performance in capturing the observed values in fall, winter, and spring with expected $MAEs$ of less than 1.6%, 0.5%, and 1.7%, respectively. In summer, both single and multisite settings show an expected $MAEs$ of less than 1.3% in capturing the desired shift in the mean seasonal volume; whereas, the $MAEs$ in representing the desired shift in standard deviation of seasonal volume is less than 1.5% for both single and multisite settings. Regarding the long-range future in site G2, both single and multisite settings show expected $MAEs$ of less than 1.3% in representing the desired shift in the standard deviation of seasonal volume.

In winter, the expected MAE in representing the observed mean value for both single and multisite settings are less than 1.1%. In terms of standard deviation of seasonal volume, however, single site setting show better performance with an expected MAE of 1.3% compared to an expected MAE of 3.4% for multisite setting. In spring, both settings show similar performance with $MAEs$ of less than 0.8. In summer, the expected MAE in representing the desired shift for both single and multisite settings are higher than the other seasons, reaching to an expected $MAEs$ of 3.4%. In site NG2, multisite setting with an expected MAE of 0.8% show better performance in capturing the observed seasonal volume in fall compared to single site setting with an expected MAE of 2.1%. In winter, both single and multisite settings show an expected MAE of less than 1% in capturing the observed value. In spring, similar performance for both settings can be observed. In summer, the single site setting with an expected $MAEs$ of 0.8% (1.1%) show better performance in representing the desired shifts in mean and standard deviation of seasonal volume compared to the multisite setting with expected $MAEs$ of 1.1% (2.4%).
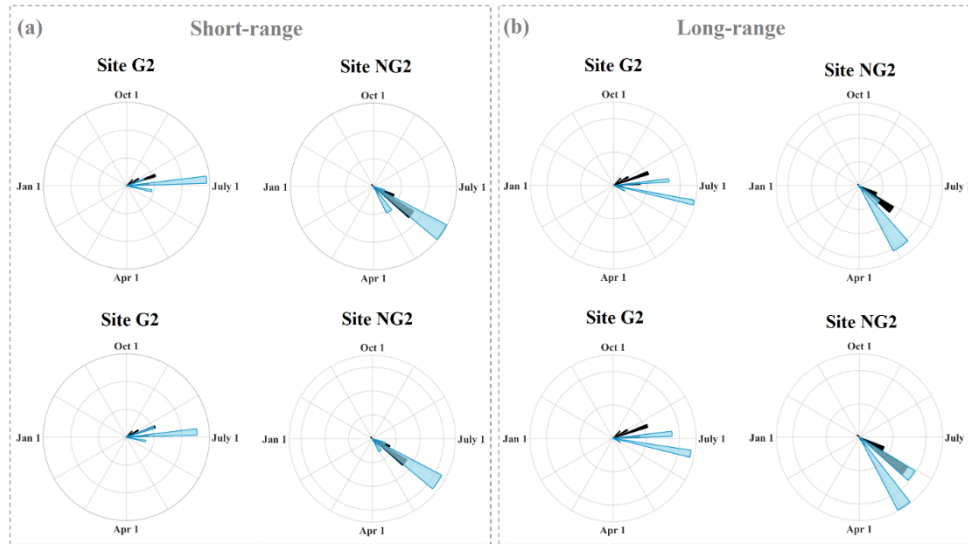
Figure 6.11. Representation of desired forms of shifts in terms of expected timing of the annual peak across the six sites using the proposed approach in single- and multisite settings shown in first and second rows, respectively. The black and blue histograms are related to the observed and generated timing of annual peak, respectively. Panels (a) and (b) are related to short- and long-range future, respectively.

In previous section it is demonstrated that the proposed model can well capture the basic statistics of streamflow hydrographs. However, the performance of the proposed model in capturing the extremes is unknown. For this purpose, we fit a Generalized Extreme Value (GEV) distribution to the annual low and high flows. Fig. 6.13 shows the uncertainty bounds of ensembles of 1000 GEV fitted to the simulated annual low and high flows in single (Fig. 6.13a) and multisite settings (Fig. 6.13b). Each panel includes two columns, showing the ensembles of fitted GEVs for the simulated annual low flows (first columns) and high flows (second columns). The dots are the observed values; the black lines are the fitted GEVs to the observed extremes. The uncertainty of the models is assessed using the indices called average width (AW) of the uncertainty bounds and percentage of coverage (POC), which is the percentage of observed data points fall within the range of uncertainty bounds. The greater the POCs indicate the better performance of the model in capturing the extremes. In general, both single and multisite settings show good performance in capturing the observed extremes in the range of uncertainty bounds. Regarding the low flows, the single-site setting can capture the observed values with POC of 100%. The AW of multisite setting in representing the low flows in sites E and F, however, 11.3% and 6.1% lower than the single-site setting. Regarding the high flows, in site G2, the POC of multisite setting in representing the observed values is 2.2% is greater than the single-site setting; whereas in terms of AW, the single-site setting performs better, demonstrating the 14.1% less AW than multisite setting. In site NG2, both single and multisite settings show similar POCs; whereas in terms of AW, the multisite setting show 5.3% less AW than single-site setting.
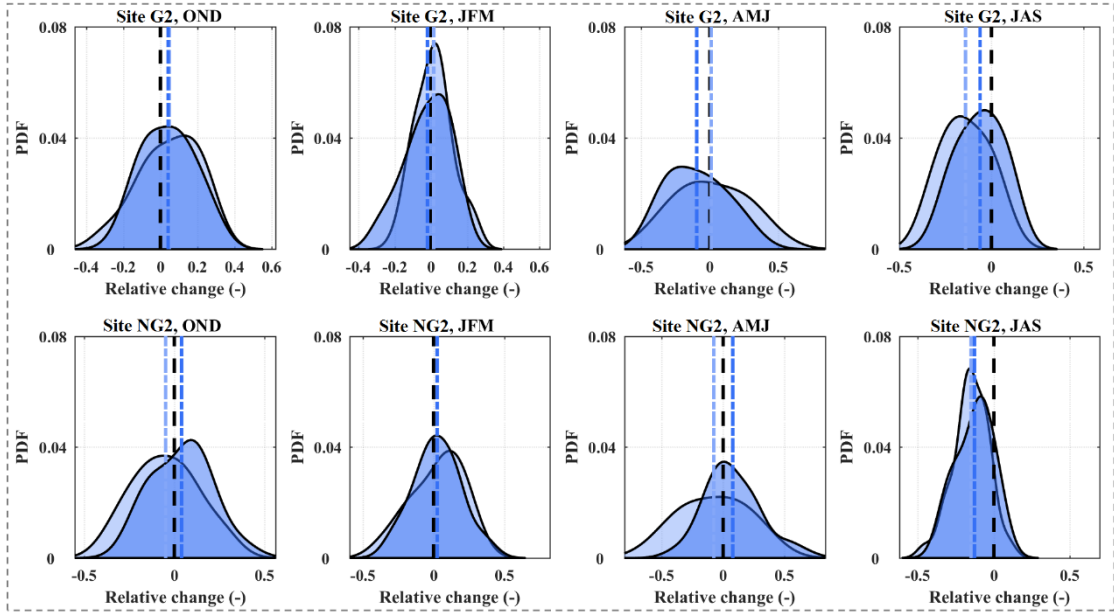
Figure 6.12. The comparison of the proposed approach in short-range generations of seasonal volumes in sites E and F. The light and dark colored distributions are the generated seasonal volume distributions generated by single and multisite settings, respectively.
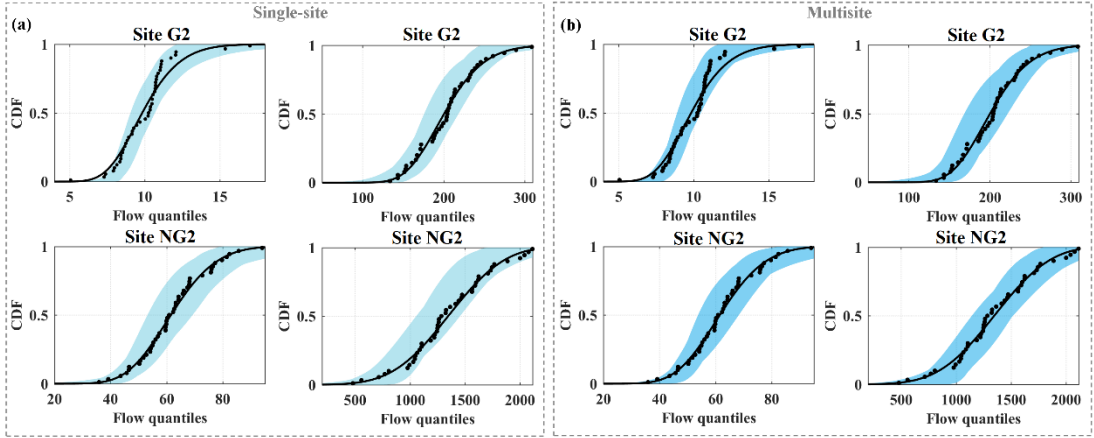
Figure 6.13. The comparison of the proposed model in single-site (panel a) and multisite (panel b) generation of streamflow in terms of capturing the annual extremes. The results of low and high flows are demonstrated in odd and even columns, respectively. The blue colors are the uncertainty bounds. The dots are the observed annual low and high flows. The solid black lines are the fitted GEV to the observed data.

6.6. Summary and Conclusion

Despite ongoing advancements in stochastic streamflow generations, little attention has been given on advancing perturbing algorithms for altering the streamflow characteristics. Such algorithms provide a generic methodology with which scenarios of changes under nonstationarity can be represented and reproduced. Here, we propose a generic and parsimonious framework, accommodating perturbing algorithms to systematically represent shifts in the characteristics of annual streamflow hydrographs and the variability around it. For this purpose, we represent the

streamflow hydrographs using a series of orthogonal generalized gamma distributions for which the distributional statistics can be analytically perturbed and further reproduced using a generic copula-based streamflow generator.

To showcase the application of the proposed framework, we use this model in single and multisite generations of scenarios of change in short- and long-range futures in six sites with different flow regime types. First, the performance of the proposed framework is rigorously evaluated under historical condition in terms of representing expected annual hydrograph, seasonal volumes and lag-1 temporal dependence. Regarding the expected annual hydrograph, the REs in capturing the observed values are less than 3.3% with the greatest errors occurring in site P1 with rain-dominated regime. In terms of seasonal volume, the proposed model performs well in capturing the observed values with expected REs of 2.9% and 8.3% in representing mean and variation of seasonal volumes. Regarding the temporal dependence, the proposed model performs quite well in capturing the observed values with expected MAE of less than 0.03 across different sites. The best performance can be observed in sites A and E with glacial-dominated regime, demonstrating average $MAEs$ of 0.01.

We also assess the performance of the proposed model in representing different scenarios of change. For this purpose, first we identify the dominant forms of change over the observed period of 1966-2010 using the concept of moving timeframe and analyses of trend. Later we project the observed trend into the short and long-range futures and make desired and plausible scenarios of change in future. Then, using the proposed framework we generate 1000 realizations of scenarios of change and assess how the model performs in representing the desired shifts in seasonal volumes and the expected timing of annual peak in single and multisite settings. In general, the more regularity in the timing of annual peak is observed in site G2 with glacial-dominated regime with the majority of annual high flows occurring in summer. The average MAEs in representing the desired shift in the timing of peak in site G2 are 0.1 and 0.3 in short and long-range futures, respectively. In site P1 with rain-dominated regime less regularity in the occurrence of timing of peak can be observed. The MAEs in representing the desired shift in timing of peak are 0.3 and 0.4 of week in short and long-range futures, respectively. Additional in terms of seasonal volume, the proposed model performs quite well, demonstrating expected MAEs of 1.5% (2%), 1.8% (2.2%), 2.2% (1.7%) and 2% (2.1%) in representing the desired shifts in seasonal volumes of fall, winter, spring, and summer in short- (long) range futures, respectively. We also compare the performance of the proposed model in single and multisite generation of desired shifts in terms of seasonal volumes and timing of peak. Regarding the timing of peak, both single and multisite settings perform well in site G2; whereas in site NG2, the single site setting shows slightly better performance with average error of 0.3 compared to 1.1 for multisite setting in long-range future. Regarding seasonal volume in site G2, the MAE in representing the desired shift in fall are 1.1% and 1.3% for single and multisite settings. These values are less than 1.3% for both settings in long-range future. The MAEs in representing seasonal volume in spring with an expected desired shift of 10% (20%) decrease in seasonal volume in short- (long-) range future are 1.1% and 0.5% for single and multisite settings, respectively. In long-range future, these

values are less than 0.8% for both settings. In site NG2 both single and multisite settings perform well in capturing the desired shift in mean and variation of seasonal volume in summer with MAEs of less than 1.5% in short-range future. Regarding the long-range, single site setting with expected MAEs of 0.8% (1.1%), however, shows better performance in representing the desired shift in mean and variation of summer seasonal volume compared to multisite setting with MAEs of 1.1% (2.4%). We also evaluate performance of the proposed model in capturing the extreme low and high flows. In general, both single and multisite settings show good performance in capturing the observed values in the range of uncertainty bounds. In terms of low flows, the multisite setting can capture the observed values in sites E and F with 11.3% and 6.1% less uncertainty bounds compared to single site setting. Regarding the high flows, multisite setting shows slightly better POC (i.e., 2.2% greater) than single site setting. The range of uncertainty bound for single site setting, however, is 14.1% better than multisite setting. In site NG2, both settings show similar POC; whereas, the multisite setting shows 5.3% less uncertainty bound compared to single site setting.

Although the model is applied to represent the desired and plausible changes in the Canadian streamflow hydrographs, the model is generic and can be applied to other basins to represent any desired shift in the streamflow hydrographs. The proposed model can be applied for vulnerability assessment of any water systems under changing condition. We hope our contribution here can inspire more efforts toward developing perturbation algorithms required for vulnerability assessment of water resource systems under nonstationary conditions.

Chapter 7.
Summary, Conclusions, Limitations, and Future Research Needs

7.1. Summary of the thesis

This thesis can be summarized into 5 main steps. First, the gaps and uncertainties in the status-quo methodologies are highlighted. For this purpose, four schemes for regional generation of streamflow are considered. These schemes are only different in representing the spatiotemporal dependence structure between streamflow series. It is shown that none of the schemes can dominate the others in representing various streamflow characteristics. The result of vulnerability assessment, however, can be substantially different between the four schemes in terms of representing expected values and coefficients of variations in long-term streamflow characteristics (and to a lesser extent in system performance) under changing conditions. The extent of such differences is more evident in terms of variability rather than the expected values of the response of the system which is dependent on the streamflow characteristic, performance measure, and the changing water availability conditions.

Second, the ability of various schemes is benchmarked in reconstructing the main long-term characteristics of streamflow (i.e., annual volume, timing, and magnitude of peak flow, 10%, 50%, and 90% quantiles). For this purpose, six catchments across southern Canada are selected with three regime types (i.e., nival, mixed, and pluvial) in catchments with large and small contributing areas and considering representing temporal and spatial dependence at daily, weekly and monthly timescales. It is shown that in the local generation of streamflow series, linear and nonlinear schemes result in a statistically similar performance in representing the majority of streamflow characteristics. At the regional scale, the linear and nonlinear schemes, however, show different performances depending on the flow regime, catchment area, as well as the modeling timescale and the long-term statistics. In nival and mixed streams, nonlinear schemes and in particular the scheme employing vine copulas outperform linear schemes. In pluvial streams, however, the linear schemes show better performance and less uncertainty in representing the main characteristics of streamflow. Regardless of regime type, the skill of various schemes in representing the expected timing of the peak is highly dependent on the size of the basin, demonstrating better performance in the catchment with smaller contributing areas. In terms of flow quantiles, nonlinear approaches dominate linear schemes in representing the extreme low and high quantiles in nival and mixed catchments, whereas, the linear scheme performs better in pluvial streams. In terms of lag-1 temporal dependence, linear schemes, as well as vine-based schemes outperform others. In terms of lag-0 spatial dependence, the vine-based scheme performs better than other schemes. When moving toward coarser time scales, differences in the skills and uncertainty of different schemes become less significant. These findings provide a practical guideline for selecting the best stochastic schemes in the right circumstance, depending on the application in hand.

Here we.

Third, the skills of stochastic streamflow generation at single and multiple sites is improved by explicit incorporation of LSCIs through a stochastic generator. The results of the study show that while simulation performances of the reference and proposed models are very similar in representing

the first three moments of monthly streamflow as well as lag-1 temporal and lag-0 spatial dependencies within and between streamflow reaches, the explicit consideration of LSCIs can significantly reduce simulation uncertainty and improve simulation skills in projection and prediction modes and in both single and multisite settings, particularly in high flow seasons. In projection mode and considering the single site setting, the expected reductions in CI in the three sites are 34.1% and 37.1% in low and high flow seasons, respectively. In multisite setting, these values are 33.6% and 34.5% in low and high flow seasons, respectively. The average improvement in the interannual variability skill score in single and multisite settings is over 10% across the three considered sites. Having said that during the high flow season, considering relevant LSCI in the multisite streamflow generation results in expected improvement in capturing the interannual variability by more than 23%. In terms of observed annual extremes, both reference and proposed models can capture the observed values within the range of CI with high POC values of greater than 90% in most cases. The proposed model, however, demonstrates less uncertainty in capturing the observed extremes, particularly regarding high flows for which the ranges of CI are decreased by 15.5% and 31.1% in single and multisite settings, respectively. In prediction mode, both reference and proposed models show slight overdispersion in PIT histograms in single and multisite settings, but with expected deviation from uniformity close to perfect reliability value $D_p = 0.0267$. The expected deviations from the uniformity of PIT histograms of the proposed model are 0.0233 and 0.0203 in single and multisite settings; whereas, these values are 0.0265 and 0.0237 for the benchmark model, indicating slightly better reliability of the proposed model. In terms of CI, the average reduction during the low flow season is 18.3% and 21.1% in single and multisite settings. Reductions in the uncertainty bounds during the high flow season, however, are much larger with expected reductions of 41.3% and 45.1% through the single and multisite settings, respectively. Within the high flow season, the largest improvements in the uncertainty bounds happen during dry conditions with average reductions of 68.3% and 64.5% in CI through single and multisite settings, respectively.

Fourth, a new methodology is developed to systematically quantify streamflow regimes and their alteration to one another using a large set of simultaneously changing streamflow characteristics. The results show that the streamflow regime in Canada can be categorized into six distinct regime types with clear physical and geographical interpretations. Analyses of trends in membership values show that alterations in the natural streamflow regime are vibrant and can be different across different regions. Overall, in more than 80% of the considered stream, there is a dominant regime shift that can be attributed to changes in streamflow characteristics. At the ecozone scale, the dominant regime shifts are from slow-response/warm-season peak to fast-response/warm-season peak regime in the northern ecozones (EZ5 and EZ12), from fast-response/warm-season peak to slow-response/warm-season peak regime, and from fast-response/warm-season peak to slow-response/freshet peak regime in the western ecozones (EZ9 and EZ14), from fast-response/warm-season peak to slow-response/freshet peak regime at the two stations located in the Prairies, from slow-response/warm-season peak to slow-response/freshet peak regime in the eastern ecozones (EZ6, EZ8, and EZ15), and from slow-response/cold-season peak to fast-response/freshet peak regime in the Appalachian region (EZ7 and eastern part of EZ6). The variability between the regime shifts inside each ecozone can be described by elevation and/or latitude. At the basin scale, dominant modes of transition are from slow-response/freshet peak regime to slow-response/warm-season peak in the northern Pacific and

from slow-response/warm-season peak regime to slow-response/freshet peak regime in the southern Pacific, between the fast-response/freshet peak regime and slow-response/cold-season peak regimes, as well as slow-response/freshet peak regime and slow-response/cold-season peak regime, in the Atlantic, between slow-response/warm-season peak and fast-response/warm-season peak in the Arctic, and between the slow-response/warm-season peak regime and slow-response/freshet peak regime, as well as fast-response/warm-season peak and slow-response/freshet peak regime, regimes in Hudson Bay. The details of the change in streamflow regime, however, are subject to spatial variability within each drainage basin. In the Atlantic and Pacific regions, there are clear divides between dominant regime shifts in northern and southern regions. For instance, In the Pacific, the association to slow-response/warm-season peak regime is increasing in Yukon and northern parts of the Columbia and Fraser subbasins, but it is significantly decreasing in the southern regions. This can be due to different manifestations of climate change, which are more apparent as temperature increases in the north and growing ratios of rain over precipitation in the south, shifting the streamflow more toward rain-dominated regimes (Fleming and Clarke, 2003). This reconfirms the important role of latitude in driving the streamflow response to climate change.

Finally, a generalized approach is proposed to systematically synthesize a large ensemble of perturbed streamflow with which the vulnerability of water resource systems to the plausible changes in the streamflow hydrograph can be analyzed. To showcase the application of the proposed framework, we use this model in single and multisite generations of scenarios of change in short- and long-range futures in six sites with different flow regime types. First, the performance of the proposed framework is rigorously evaluated under historical condition in terms of representing expected annual hydrograph, seasonal volumes and lag-1 temporal dependence. Regarding the expected annual hydrograph, the REs in capturing the observed values are less than 3.3% with the greatest errors occurring in site P1 with rain-dominated regime. In terms of seasonal volume, the proposed model performs well in capturing the observed values with expected REs of 2.9% and 8.3% in representing mean and variation of seasonal volumes. Regarding the temporal dependence, the proposed model performs quite well in capturing the observed values with expected MAE of less than 0.03 across different sites. The best performance can be observed in sites A and E with glacial-dominated regime, demonstrating average $MAEs$ of 0.01. We also assess the performance of the proposed model in representing different scenarios of change. For this purpose, we first identify the dominant forms of change over the observed period of 1966-2010 using the concept of moving timeframe and analyses of trends. Later we project the observed trend into the short and long-range futures and make desired and plausible scenarios of change in the future. Then, using the proposed framework we generate 1000 realizations of scenarios of change and assess how the model performs in representing the desired shifts in seasonal volumes and the expected timing of the annual peak in single and multisite settings. In general, more regularity in the timing of the annual peak is observed in site G2 with the glacial-dominated regime. The average MAEs in representing the desired shift in the timing of the peak in site G2 are 0.1 and 0.3 in short and long-range futures, respectively. In site P1 with a rain-dominated regime, less regularity in the occurrence of the timing of the peak can be observed. The MAEs in representing the desired shift in the timing of peak are 0.3 and 0.4 of the week in short and long-range futures, respectively. Additional in terms of seasonal volume, the proposed model performs quite well, demonstrating expected MAEs of 1.5% (2%), 1.8% (2.2%), 2.2% (1.7%), and

2% (2.1%) in representing the desired shifts in seasonal volumes of fall, winter, spring, and summer in short- (long) range futures, respectively.

7.2. Conclusion

This study sets an improved stochastic generation approach for vulnerability assessment of water resource systems under changing conditions. First, it is shown that the differences in representing the streamflow characteristics using different methodologies can introduce uncertainty in understanding the stress-response relationship under changing streamflow conditions and changing system performance. Then, various linear and nonlinear methodologies for representing spatiotemporal dependencies are considered. The performance of various schemes in representing key characteristics of streamflow regime is investigated. This leads to a set of guidelines for choosing the right spatiotemporal representation across different flow regimes, sizes of catchment, and timescales.

Later, to improve stochastic generation methods a generic approach based on vine copulas is proposed to explicitly incorporate LSCIs as exogenous covariates in stochastic streamflow generation at single and multiple sites. In particular, a sampling scheme based on using C-vine copulas is suggested, in which the structure and parameters of the model change at each time step. This is due to the variation of the influential LSCIs and the type of dependencies, which can change across different timesteps. To accommodate this, a global input selection algorithm is used to pick the most significant LSCIs from a pool of potential predictors at each month and consider the selected LSCIs as influential predictors, to which the streamflow is conditioned.

An attempt is then made toward providing a globally relevant algorithm for identifying changing streamflow regimes. The proposed approach is based on two fundamental considerations. First, a streamflow regime is collectively formed by a large number of streamflow characteristics. Second, streamflow types are rather in the form of spectrums, not clear-cut states; if regime shifts are caused by climate change, the transition from one regime type to another should be gradual rather than abrupt. To accommodate these two considerations, streamflow regime types are represented as intersecting fuzzy sets in such a way that the belongingness of each stream to each regime type can be quantified by a membership function. Accordingly, monitoring the trends in membership values in time and space can provide a basis to identify the regime shift from one type to another.

As a final step toward improving stochastic streamflow generator under changing conditions, a generic and parsimonious framework is proposed, accommodating perturbing algorithms to systematically represent shifts in the characteristics of annual streamflow hydrographs and the variability around it. For this purpose, the streamflow hydrographs isd represented using a series of orthogonal generalized gamma distributions for which the distributional statistics can be analytically perturbed and further reproduced using a generic copula-based streamflow generator. This framework provides the opportunity to generate any plausibile scenario of change under changing streamflow conditions required for vulnerability assessment of water resource systems.

7.3. Contributions of the thesis

This thesis is written in a manuscript-based format, aiming at providing an improved stochastic streamflow generation approach for bottom-up impact assessment of the water resources system to changing streamflow conditions. Chapters 2 to 6 contribute to first identifying the uncertainties in

bottom-up impact assessment of water resources systems and then improving different aspects of the stochastic streamflow generation approach. First, in chapter two through a set of experimentations, the existence of uncertainties in the bottom-up impact assessment of water resources systems using various schemes for representing the spatiotemporal dependence structure is demonstrated. Four different spatial extension schemes are used that differ from one another only in the way the spatiotemporal dependencies between regional streamflow reaches are represented. Through a rigorous intercomparison, it is shown that despite having different degrees of realism, none of the schemes can dominate others with respect to reproducing streamflow characteristics during a common historical period. As a result, they can be considered alternative hypotheses for bottom-up impact assessment under changing conditions.

The findings of analyses of the stress-response relationship in chapter two necessitate providing a set of guidelines to use the right scheme for representing the spatiotemporal dependence structure in the right circumstance. For this purpose, in chapter three various parametric schemes for representing the spatiotemporal dependence structures, ranging from the fully linear to fully nonlinear stochastic models are considered. After a brief overview of theoretical aspects of the parametric representation of dependence, a comprehensive experiment is designed to benchmark the skill and uncertainty of various representations in a range of timescales, catchments, and streamflow regimes. The proposed guideline here provides a set of recommendations on the use of the best scheme in the representation of spatiotemporal dependence structure across different circumstances without considering the effect of large-scale climate indices in the streamflow generation process.

As a further step toward improving the stochastic streamflow generation scheme, in chapter four a generic approach based on vine copulas is proposed to explicitly incorporate the LSCIs into nonlinear stochastic streamflow generation schemes. The skill of the proposed framework informed by LSCIs is then assessed for the prediction and projection of three mountainous headwaters in southern Alberta, Canada. To benchmark the performance of the proposed algorithm, the model is compared with already existing reference algorithms. At the single site, the performance of the proposed algorithm is compared with a baseline copula model, developed by (Nazemi et al., 2013) and extended into multisite mode using regression models (Nazemi and Wheater, 2014a). Both single and multisite versions of this existing copula-based algorithm were previously implemented in the same case study. These models provide a benchmark to discuss the added value of incorporating LSCIs in the process of streamflow generation.

As another step toward developing an improved stochastic model capable of generating streamflow under nonstationary conditions, in chapter five a global algorithm is proposed to detect the forms of changes in the streamflow regimes. The algorithm is based on fuzzy set theory in which the streams classify into a finite set of intersecting fuzzy clusters. Accordingly, by analyzing the changes in the degrees of membership to each cluster, the shifts from one regime to another are quantified. Such changes in the degrees of membership are then attributed to the changes in the collective changes in the streamflow characteristics by using R^2. To apply the proposed algorithm for identifying the flow regime changes, 45-year of daily data from 105 RHBN streamflow gauges are considered across Canada, to provide a comprehensive and temporally homogeneous look at forms and extents of change in natural streamflow regime in Canada, coast to coast to coast.

As the final step toward improving the stochastic streamflow generation scheme under nonstationary conditions, in chapter six an algorithm is developed to make scenarios of change under nonstationary conditions. The proposed algorithm can represent the shifts in the expected streamflow hydrograph and variability around it. This approach proposes an analytical solution to represent transient shifts in the streamflow hydrograph. For this purpose, we initially identify the gradual changes in the streamflow hydrographs over the historical period using moving trend analysis, giving the opportunity to project such changes to future conditions. For this purpose, we first decompose the streamflow regime into an expected streamflow hydrograph and the variability around it. We then conceptualize the streamflow hydrograph as a time distribution function, mimicking all probabilistic properties of the cumulative distribution function. Later, to implement the desired shifts analytically, we use a series of orthogonal generalized gamma distributions, for which the properties of distributions can be perturbed, reconstructed, and reproduced under changing conditions. To showcase the applicability of the proposed algorithm, it is then applied to a number of streams across Canada to generate large ensembles of perturbed streamflow.

The proposed approach provides a tool to assess the vulnerability assessment of water resources systems under changing streamflow conditions. The proposed approach can benefit a variety of engineering applications from operations of water resource systems to long-term planning and management of water-related infrastructures such as reservoirs. For instance, the proposed approach improves the streamflow predictions at a monthly scale, particularly at the high flow seasons required for flood management practices. The proposed approach can also benefit the long-term planning of water-related systems by providing a tool to assess the impact of a wide range of plausible scenarios of streamflow change on water resources systems.

7.3. Limitations of the proposed framework

Despite advancements in the stochastic streamflow generation under nonstationary conditions made by the proposed framework, a few points are remained and should be put in perspective. First, as it was shown in Nazemi et al. (2020), even when the skills in reconstructing long-term streamflow characteristics are similar, it does not necessarily mean that the results of stress tests made with the generated synthetic streamflow series would be similar too. This can lead to an even larger uncertainty in the stress-response under changing conditions which is more relevant to water resource planning and management. Additionally, none of the streamflow generation schemes are able to capture modes of variability inherited in streamflow series. The inclusion of LSCIs into the nonlinear copula-based approaches proposed here is a step forward to better representing interannual variability, and the low and high flow quantiles but it cannot lead to capturing all modes of variability. Moreover, the proposed algorithm is only limited to the effect of LSCIs, but it can be extended to incorporate climatic variables such as temperature and precipitation as exogenous covariates in stochastic streamflow generation, leading to more realistic scenarios of change under nonstationary conditions.

Additionally, the proposed framework provides an opportunity to identify the changing streamflow regimes and attributes such changes to a large set of streamflow characteristics. This approach, however, does not explore the attribution of the shifts in streamflow regimes to the changes in temperature pattern, form and magnitude of precipitation, snowmelt, glacial retreat, and permafrost degradation. This could help in better understanding the casual relationship required for water

resource decision-making. Moreover, the types of changes identified here in the streamflow regime are only limited to the analysis of trends in various streamflow characteristics, and other forms of changes (e.g., changes in the temporal dependence structure) were not considered.

The improved bottom-up assessment framework presented here is ideally suitable for addressing challenges in making decisions and adaptation policies under changing conditions. In fact, an evaluation of decision alternatives under a wide range of scenarios of change, rather than a priori restriction of space of uncertain factors – for instance only considering the effect of climate factors- may reveal the true vulnerabilities in the water resource system. Additionally, this approach can give more insight into the vulnerability of the system and can be useful in risk assessment, but further research is needed to link it to top-down projections to better constrain the range of possible future states. For instance, in risk quantification, although the response of the system to changes in streamflow conditions has been defined as risk, but the probability of occurrence of any plausible change is unknown. There remains the potential to better integrate the result of vulnerability mapping with scenario-led simulations to provide an informative notion of risk and understand which scenario of change is more probable than the others. This can provide more informative tools for improving the vulnerability assessment of water resource systems to changing streamflow conditions under nonstationary conditions.

7.4. Outlook and future remarks

While this thesis contributes to the methodological advancements of the bottom-up frameworks required for vulnerability assessment of water resource systems, further research can be performed to address other limitations of this framework:

First, although some aspects of uncertainties in the bottom-up framework including the uncertainties in the representation of spatiotemporal dependencies are highlighted and addressed considering four schemes, a set of comprehensive intercomparison studies can be implemented to address the pros and cons of multiple methodologies including the nonparametric streamflow generation schemes (e.g., Lall and Sharma, 1996; Sharma and O'Neill, 2002). This analysis can be performed to generate several streamflow series with various flow regimes across different timescales and sizes of basins.

Second, although the method is developed for a lead time of one month and applied in a few catchments, the proposed algorithm is generic and can be applied in other basins considering more than the lag-1 temporal dependence structure. The proposed method can be also extended by including more conditioning variables such as precipitation and/or temperature, whether observed or simulated. This can provide a versatile and comprehensive model to inform water management models for better planning under current and future conditions. I hope that the contribution here can inspire more efforts toward an improved stochastic generation of streamflow in prediction and projection modes. Moreover, the model is applied and assessed to represent the desired and plausible changes in the Canadian streamflow hydrographs, but the model is generic and can be applied to other basins to represent any desired shift in the streamflow hydrographs. The proposed model can be applied for vulnerability assessment of any water system under changing conditions. I hope this

contribution here can inspire more efforts toward developing perturbation algorithms required for vulnerability assessment of water resource systems under nonstationary conditions.

Additionally, the bottom-up framework presented here should be linked with the scenario-led approach to have a more comprehensive risk assessment through constraining the range of plausible future states of the system and obtaining the posterior likelihood of occurrence of each event (realization). This framework can play a prominent role in mapping the vulnerability of the system to climatic and/or anthropogenic changes in the face of recognized uncertainties in GCMs and HMs. It is specifically designed to facilitate vulnerability assessment of water resource systems to changes in streamflow characteristics and measure the risk of failure of the system to these changes. In fact, in risk quantification, although in a bottom-up framework, the response of the system to changes in streamflow conditions has been defined as risk, the probability of occurrence of any plausible change is unknown. There remains the potential to better integrate the result of vulnerability mapping with scenario-led simulations to provide an informative notion of risk and understand which scenario of change is more probable than the others. This can provide more informative tools for improving the vulnerability assessment of water resource systems to changing streamflow conditions under nonstationary conditions.

Moreover, the proposed framework is designed to evaluate the impact of changes in streamflow conditions on the vulnerability of water resource systems. The implication of climate change on the environment and society and in particular in making decision and policy is, however, not only depend on how the system response to streamflow changes but also on how the system will respond to changes in technology, economy, and lifestyle. Extensive uncertainties exist both in top-down approaches as the result of uncertainties in socio-economic assumptions, emission scenarios, climate, and hydrological models and in the bottom-up approaches as the result of high uncertainty inherited in hydrological models. This necessitates the use of a new bottom-up framework to explore directly the impacts of plausible changes in streamflow conditions on water resource systems. Although the proposed framework helps in better understanding of the vulnerability of water resources system to changing streamflow conditions, more efforts are needed to combine such changes with the changes in other effective factors that make the water system vulnerable including the various scenarios of human intervention (e.g., population growth, irrigation development, different policy options, etc.).

Finally, although the proposed framework helps in better assessing the vulnerability of water resource systems to changing streamflow conditions, it cannot tell us about the causes of such changes in the streamflow conditions which is an important factor in decision making under uncertainties. Further research is required to combine such framework with the process-based modeling of streamflow series, helping in making an informative decision making.

Bibliography

Aas, K., & Berg, D. (2013). Models for construction of multivariate dependence–a comparison study. In Copulae and Multivariate Probability Distributions in Finance (pp. 43-64). Routledge.

Aas, K., Czado, C., Frigessi, A., & Bakken, H. (2009). Pair-copula constructions of multiple dependence. Insurance: Mathematics and economics, 44(2), 182-198.

Abadi, A., Amanpour, F., Bajdik, C., & Yavari, P. (2012). Breast cancer survival analysis: Applying the generalized gamma distribution under different conditions of the proportional hazards and accelerated failure time assumptions. International journal of preventive medicine, 3(9), 644.

AghaKouchak, A., Mirchi A., K. Madani, Giuliano Di Baldassarre, Ali Nazemi, Aneseh Alborzi, Hassan Anjileli et al. et al. (2021). Anthropogenic drought: Definition, challenges and opportunities, Rev. Geophys.

Aghakouchak, A. (2014). Entropy–copula in hydrology and climatology. Journal of Hydrometeorology, 15(6), 2176-2189.

AghaKouchak, A., Cheng, L., Mazdiyasni, O., & Farahmand, A. (2014). Global warming and changes in risk of concurrent climate extremes: Insights from the 2014 California drought. Geophysical Research Letters, 41(24), 8847-8852.

Ahmed, K. F., Wang, G., Silander, J., Wilson, A. M., Allen, J. M., Horton, R., & Anyah, R. (2013). Statistical downscaling and bias correction of climate model outputs for climate change impact assessment in the US northeast. Global and Planetary Change, 100, 320-332.

Aires, F., Chédin, A., & Nadal, J. P. (2000). Independent component analysis of multivariate time series: Application to the tropical SST variability. Journal of Geophysical Research: Atmospheres, 105(D13), 17437-17455.

Akaike, H. (1979). A Bayesian extension of the minimum AIC procedure of autoregressive model fitting. Biometrika, 66(2), 237-242.

Aksamit, N. O., and Whitfield, P. H.: Examining the pluvial to nival river regime spectrum using nonlinear methods: Minimum delay embedding dimension. Journal of Hydrology, 572, 851-868.

Alam, M. S., & Elshorbagy, A. (2015). Quantification of the climate change-induced variations in Intensity–Duration–Frequency curves in the Canadian Prairies. Journal of Hydrology, 527, 990-1005.

Alberta Environment (2010). South Saskatchewan regional plan: Water quantity and quality modelling results. Edmonton, Canada: Government of Alberta.

Amell, N. W. (1999). Climate change and global water resources. Global Environmental Change, 9(50), 531-549.

Amir Jabbari, A., & Nazemi, A. (2019). Alterations in Canadian hydropower production potential due to continuation of historical trends in climate variables. Resources, 8(4), 163.

Amoroso, L. Ricerche intorno alla curva dei redditi. Annali di Matematica Pura ed Applicata 1925, 2, 123–159.

Annamalai, H., Hamilton, K., & Sperber, K. R. (2007). The South Asian summer monsoon and its relationship with ENSO in the IPCC AR4 simulations. Journal of Climate, 20(6), 1071-1092.

Arheimer, B., & Lindström, G. (2015). Climate impact on floods: changes in high flows in Sweden in the past and the future (1911–2100). Hydrology and Earth System Sciences, 19(2), 771-784.

Arnell, N. W., & Gosling, S. N. (2013). The impacts of climate change on river flow regimes at the global scale. Journal of Hydrology, 486, 351-364.

Arnell, N. W., & Gosling, S. N. (2016). The impacts of climate change on river flood risk at the global scale. Climatic Change, 134(3), 387-401.

Arnell, N. W., & Lloyd-Hughes, B. (2014). The global-scale impacts of climate change on water resources and flooding under new climate and socio-economic scenarios. Climatic change, 122(1), 127-140.

Ashkar, F., & Ouarda, T. B. (1998). Approximate confidence intervals for quantiles of gamma and generalized gamma distributions. Journal of Hydrologic Engineering, 3(1), 43-51.

Ashraf, S., AghaKouchak, A., Nazemi, A., Mirchi, A., Sadegh, M., Moftakhari, H. R., ... & Mallakpour, I. (2019). Compounding effects of human activities and climatic changes on surface water availability in Iran. Climatic change, 152(3), 379-391.

Asong, Z. E., Wheater, H. S., Bonsal, B., Razavi, S., & Kurkute, S. (2018). Historical drought patterns over Canada and their teleconnections with large-scale climate signals. Hydrology & Earth System Sciences, 22(6).

Assani, A. A., Landry, R., & Laurencelle, M. (2012). Comparison of interannual variability modes and trends of seasonal precipitation and streamflow in southern Quebec (Canada). River Research and Applications, 28(10), 1740-1752.

Bárdossy, A. (1998). Generating precipitation time series using simulated annealing. Water Resources Research, 34(7), 1737-1744.

Bárdossy, A., & Pegram, G. G. S. (2009). Copula based multisite model for daily precipitation simulation. Hydrology & Earth System Sciences, 13(12).

Barnett, T. P., Adam, J. C., & Lettenmaier, D. P. (2005). Potential impacts of a warming climate on water availability in snow-dominated regions. Nature, 438(7066), 303-309.

Barnston, A. G., & Ropelewski, C. F. (1992). Prediction of ENSO episodes using canonical correlation analysis. Journal of climate, 5(11), 1316-1345.

Barsugli, J. J., Guentchev, G., Horton, R. M., Wood, A., Mearns, L. O., Liang, X. Z., ... & Ammann, C. (2013). The practitioner's dilemma: How to assess the credibility of downscaled climate projections. Eos, Transactions American Geophysical Union, 94(46), 424-425.

Bartolini, P., Salas, J. D., & Obeysekera, J. T. B. (1988). Multivariate periodic ARMA (1, 1) processes. Water Resources Research, 24(8), 1237-1246.

Bawden, A. J., Burn, D. H., and Prowse, T. D.: Recent changes in patterns of western Canadian river flow and association with climatic drivers. Hydrology Research, 46(4), 551-565.

Bedford, T., & Cooke, R. M. (2001). Probability density decomposition for conditionally dependent random variables modeled by vines. Annals of Mathematics and Artificial intelligence, 32(1-4), 245-268.

Bedford, T., & Cooke, R. M. (2002). Vines--a new graphical model for dependent random variables. The Annals of Statistics, 30(4), 1031-1068.

Bennett, J. C., Wang, Q. J., Pokhrel, P., & Robertson, D. E. (2014). The challenge of forecasting high streamflow 1–3 months in advance with lagged climate indices in southeast Australia. Natural Hazards & Earth System Sciences, 14(2).

Bensaid, A. M., Hall, L. O., Bezdek, J. C., Clarke, L. P., Silbiger, M. L., Arrington, J. A., & Murtagh, R. F. (1996). Validity-guided (re) clustering with applications to image segmentation. IEEE Transactions on fuzzy systems, 4(2), 112-123.

Berg, D., & Aas, K. (2007). Models for construction of multivariate dependence. Preprint series. Statistical Research Report http://urn. nb. no/URN: NBN: no-23420.

Berg, D., & Aas, K. (2009). Models for construction of multivariate dependence: A comparison study. The European Journal of Finance, 15(7), 639-659.

Bevacqua, E. CDVineCopulaConditional: Sampling from Conditional C- and D-Vine Copulas, R package version 0.1.0, https://CRAN.R-project.org/package=CDVineCopulaConditional, 2017.

Beven, K. (2011). I believe in climate change but how precautionary do we need to be in planning for the future?. Hydrological Processes, 25(9), 1517-1520.

Beven, K. (2016). Facets of uncertainty: epistemic uncertainty, non-stationarity, likelihood, hypothesis testing, and communication. Hydrological Sciences Journal, 61(9), 1652-1665.

Bezdek, J. C. (1981). Objective function clustering. In Pattern recognition with fuzzy objective function algorithms (pp. 43-93). Springer, Boston, MA.

Bhave, A. G., Mishra, A., & Raghuwanshi, N. S. (2014). A combined bottom-up and top-down approach for assessment of climate change adaptation options. Journal of Hydrology, 518, 150-161.

Bland, J. M., & Altman, D. G. (1995). Multiple significance tests: the Bonferroni method. Bmj, 310(6973), 170.

Blöschl, G., Ardoin-Bardin, S., Bonell, M., Dorninger, M., Goodrich, D., Gutknecht, D., ... & Szolgay, J. (2007). At what scales do climate variability and land cover change impact on flooding and low flows?. Hydrological Processes, 21(9), 1241-1247.

Blöschl, G., Hall, J., Parajka, J., Perdigão, R. A., Merz, B., Arheimer, B., ... & Živković, N. (2017). Changing climate shifts timing of European floods. Science, 357(6351), 588-590.

Blöschl, G., Viglione, A., Merz, R., Parajka, J., Salinas, JL, & Schöner, W. (2011). Effects of climate change on floods and low flows (Climate impacts on floods and low flows), Österr. Water waste management , 63 , 21-30.

Bonsal, B. R., Prowse, T. D., Duguay, C. R., & Lacroix, M. P. (2006). Impacts of large-scale teleconnections on freshwater-ice break/freeze-up dates over Canada. Journal of Hydrology, 330(1-2), 340-353, https://doi.org/10.1016/j.jhydrol.2006.03.022.

Bonsal, B., & Shabbar, A. (2008). Impacts of large-scale circulation variability on low streamflows over Canada: a review. Canadian Water Resources Journal, 33(2), 137-154.

Borgomeo, E., Farmer, C. L., & Hall, J. W. (2015). Numerical rivers: A synthetic streamflow generator for water resources vulnerability assessments. Water Resources Research, 51(7), 5382-5405.

Borgomeo, E., Pflug, G., Hall, J. W., & Hochrainer-Stigler, S. (2015). Assessing water resource system vulnerability to unprecedented hydrological drought using copulas to characterize drought duration and deficit. Water resources research, 51(11), 8927-8948.

Borgomeo, E., Pflug, G., Hall, J. W., & Hochrainer-Stigler, S. (2015). Assessing water resource system vulnerability to unprecedented hydrological drought using copulas to characterize drought duration and deficit. Water Resources Research, 51(11), 8927-8948.

Bourdin, D. R., Nipen, T. N., & Stull, R. B. (2014). Reliable probabilistic forecasts from an ensemble reservoir inflow forecasting system. Water Resources Research, 50(4), 3108-3130.

Brabets, T. P., & Walvoord, M. A. (2009). Trends in streamflow in the Yukon River Basin from 1944 to 2005 and the influence of the Pacific Decadal Oscillation. Journal of Hydrology, 371(1-4), 108-119.

Brahney, J., Weber, F., Foord, V., Janmaat, J., & Curtis, P. J. (2017). Evidence for a climate-driven hydrologic regime shift in the Canadian Columbia Basin. Canadian Water Resources Journal/Revue canadienne des ressources hydriques, 42(2), 179-192.

Brechmann, E. C. and U. Schepsmeier (2013). Modeling Dependence with C- and D-Vine Copulas: The R Package CDVine. Journal of Statistical Software, 52 (3), 1-27.

Brekke, L. D. (2009a). Climate change and water resources management: A federal perspective. DIANE Publishing.

Brekke, L. D., Maurer, E. P., Anderson, J. D., Dettinger, M. D., Townsley, E. S., Harrison, A., & Pruitt, T. (2009). Assessing reservoir operations risk under climate change. Water Resources Research, 45(4).

Brimley, B., Cantin, J.F., Harvey, D., Kowalchuk, M., Marsh, P., Ouarda, T.M.B.J., Phinney, B., Pilon, P., Renouf, M., Tassone, B. and Wedel, R., (1999). Establishment of the reference hydrometric basin network (RHBN) for Canada. Environment Canada, 41.

Bröcker, J., & Smith, L. A. (2007). Increasing the reliability of reliability diagrams. Weather and forecasting, 22(3), 651-661.

Broderick, C., Murphy, C., Wilby, R. L., Matthews, T., Prudhomme, C., & Adamson, M. (2019). Using a scenario-neutral framework to avoid potential maladaptation to future flood risk. Water resources research, 55(2), 1079-1104.

Brown, C., & Wilby, R. L. (2012). An alternate approach to assessing climate risks. Eos, Transactions American Geophysical Union, 93(41), 401-402.

Brown, C., Ghile, Y., Laverty, M., & Li, K. (2012). Decision scaling: Linking bottom-up vulnerability analysis with climate projections in the water sector. Water Resources Research, 48(9).

Brown, C., Werick, W., Leger, W., & Fay, D. (2011). A Decision-Analytic approach to managing climate risks: Application to the upper great lakes 1. JAWRA Journal of the American Water Resources Association, 47(3), 524-534.

Brown, C., & Wilby, R. L. (2012). An alternate approach to assessing climate risks. Eos, Transactions American Geophysical Union, 93(41), 401-402.

Brown, G., Pocock, A., Zhao, M. J., & Luján, M. (2012). Conditional likelihood maximisation: a unifying framework for information theoretic feature selection. The journal of machine learning research, 13, 27-66.

Brunner, M. I., Bárdossy, A., & Furrer, R. (2019). Stochastic simulation of streamflow time series using phase randomization. Hydrology and Earth System Sciences, 23(8), 3175-3187.

Brunner, M. I., Farinotti, D., Zekollari, H., Huss, M., & Zappa, M. (2019). Future shifts in extreme flow regimes in Alpine regions. Hydrology and Earth System Sciences, 23(11), 4471-4489.

Brunner, M. I., Gilleland, E., Wood, A., Swain, D. L., & Clark, M. (2020). Spatial dependence of floods shaped by spatiotemporal variations in meteorological and land-surface processes. Geophysical Research Letters, 47(13), e2020GL088000.

Brunner, M. I., Melsen, L. A., Newman, A. J., Wood, A. W., & Clark, M. P. (2020). Future streamflow regime changes in the United States: assessment using functional classification. Hydrology and Earth System Sciences, 24(8), 3951-3966.

Brunner, M. I., Viviroli, D., Furrer, R., Seibert, J., & Favre, A. C. (2018). Identification of flood reactivity regions via the functional clustering of hydrographs. Water Resources Research, 54(3), 1852-1867.

Brunner, M. I., Zappa, M., & Stähli, M. (2019). Scale matters: Effects of temporal and spatial data resolution on water scarcity assessments. Advances in Water Resources, 123, 134-144.

Bryant, B. P., & Lempert, R. J. (2010). Thinking inside the box: A participatory, computer-assisted approach to scenario discovery. Technological Forecasting and Social Change, 77(1), 34-49.

Burn, D. H. (2008). Climatic influences on streamflow timing in the headwaters of the Mackenzie River Basin. Journal of Hydrology, 352(1-2), 225-238.

Burn, D. H., & Whitfield, P. H. (2016). Changes in floods and flood regimes in Canada. Canadian Water Resources Journal/Revue canadienne des ressources hydriques, 41(1-2), 139-150.

Burn, D. H., & Whitfield, P. H. (2017). Changes in cold region flood regimes inferred from long-record reference gauging stations. Water Resources Research, 53(4), 2643-2658.

Bush, E. and Lemmen, D.S., editors (2019). Canada's Changing Climate Report; Government of Canada, Ottawa, ON. 444 p.

Buttle, J. M., Allen, D. M., Caissie, D., Davison, B., Hayashi, M., Peters, D. L., ... & Whitfield, P. H. (2016). Flood processes in Canada: Regional and special aspects. Canadian Water Resources Journal/Revue canadienne des ressources hydriques, 41(1-2), 7-30.

Cayan, D. R., Dettinger, M. D., Pierce, D., Das, T., Knowles, N., Ralph, F. M., & Sumargo, E. (2016). Natural variability, anthropogenic climate change, and impacts on water availability and flood extremes in the Western United States. Water Policy and Planning in a Variable and Changing Climate, 17.

Cayan, D. R., Redmond, K. T., & Riddle, L. G. (1999). ENSO and hydrologic extremes in the western United States. Journal of Climate, 12(9), 2881-2893.

Champagne, O., Arain, M. A., Leduc, M., Coulibaly, P., & McKenzie, S. (2020). Future shift in winter streamflow modulated by the internal variability of climate in southern Ontario. Hydrology and Earth System Sciences, 24(6), 3077-3096.

Chang, J., Zhang, H., Wang, Y., & Zhu, Y. (2016). Assessing the impact of climate variability and human activities on streamflow variation. Hydrology and Earth System Sciences, 20(4), 1547-1560.

Change, C. (2007). Climate change impacts, adaptation and vulnerability. Science of the Total Environment, 326(1-3), 95-112.

Chase, T. N., Wolter, K., Pielke Sr, R. A., & Rasool, I. (2006). Was the 2003 European summer heat wave unusual in a global context?. Geophysical Research Letters, 33(23).

Chen, H. L., & Rao, A. R. (2003). Linearity analysis on stationary segments of hydrologic time series. Journal of Hydrology, 277(1-2), 89-99.

Chen, L., & Singh, V. P. (2018). Entropy-based derivation of generalized distributions for hydrometeorological frequency analysis. Journal of Hydrology, 557, 699-712.

Chen, L., Qiu, H., Zhang, J., Singh, V. P., Zhou, J., & Huang, K. (2019). Copula-based method for stochastic daily streamflow simulation considering lag-2 autocorrelation. Journal of Hydrology, 578, 123938.

Chen, L., Singh, V. P., & Guo, S. (2012). Measure of correlation between river flows using the copula-entropy method. Journal of Hydrologic Engineering, 18(12), 1591-1606.

Chen, L., Singh, V. P., & Xiong, F. (2017). An entropy-based generalized gamma distribution for flood frequency analysis. Entropy, 19(6), 239.

Chen, L., Singh, V. P., Guo, S., Zhou, J., & Zhang, J. (2015). Copula-based method for multisite monthly and daily streamflow simulation. Journal of Hydrology, 528, 369-384, https://doi.org/10.1016/j.jhydrol.2015.05.018.

Cheng, L., Hoerling, M., AghaKouchak, A., Livneh, B., Quan, X. W., & Eischeid, J. (2016). How has human-induced climate change affected California drought risk?. Journal of Climate, 29(1), 111-120.

Chesnokova, A., Baraër, M., Laperrière-Robillard, T., & Huh, K. (2020). Linking mountain glacier retreat and hydrological changes in southwestern Yukon. Water Resources Research, 56(1), e2019WR025706.

Chiew, F. H., & McMAHON, T. A. (2002). Global ENSO-streamflow teleconnection, streamflow forecasting and interannual variability. Hydrological Sciences Journal, 47(3), 505-522.

Chiew, F. H., Piechota, T. C., Dracup, J. A., & McMahon, T. A. (1998). El Nino/Southern Oscillation and Australian rainfall, streamflow and drought: Links and potential for forecasting. Journal of hydrology, 204(1-4), 138-149.

Christensen, N. S., & Lettenmaier, D. P. (2007). A multimodel ensemble approach to assessment of climate change impacts on the hydrology and water resources of the Colorado River Basin. Hydrology and Earth System Sciences, 11(4), 1417-1434.

Christensen, N. S., Wood, A. W., Voisin, N., Lettenmaier, D. P., & Palmer, R. N. (2004). The effects of climate change on the hydrology and water resources of the Colorado River basin. Climatic change, 62(1), 337-363.

Chun, K. P., Wheater, H. S., Nazemi, A., & Khaliq, M. N. (2013). Precipitation downscaling in Canadian Prairie Provinces using the LARS-WG and GLM approaches. Canadian Water Resources Journal, 38(4), 311-332.

Cioffi, F., Conticello, F., Lall, U., Marotta, L., & Telesca, V. (2017). Large scale climate and rainfall seasonality in a Mediterranean Area: Insights from a non-homogeneous Markov model applied to the Agro-Pontino plain. Hydrological Processes, 31(3), 668-686.

Clark, M. P., Wilby, R. L., Gutmann, E. D., Vano, J. A., Gangopadhyay, S., Wood, A. W., ... & Brekke, L. D. (2016). Characterizing uncertainty of the hydrologic impacts of climate change. Current Climate Change Reports, 2(2), 55-64.

Clarke, G. K., Jarosch, A. H., Anslow, F. S., Radić, V., & Menounos, B. (2015). Projected deglaciation of western Canada in the twenty-first century. Nature Geoscience, 8(5), 372-377.

Clayton, D. G. (1978). A model for association in bivariate life tables and its application in epidemiological studies of familial tendency in chronic disease incidence. Biometrika, 65(1), 141-151.

Collins, M. (2000). Understanding uncertainties in the response of ENSO to greenhouse warming. Geophysical Research Letters, 27(21), 3509-3512.

Conway, D. (1996). The impacts of climate variability and future climate change in the Nile Basin on water resources in Egypt. International Journal of Water Resources Development, 12(3), 277-296.

Conway, D., Nicholls, R. J., Brown, S., Tebboth, M. G., Adger, W. N., Ahmad, B., ... & Wester, P. (2019). The need for bottom-up assessments of climate risks and adaptation in climate-sensitive regions. Nature Climate Change, 9(7), 503-511.

Coops, N. C., Wulder, M. A., Duro, D. C., Han, T., & Berry, S. (2008). The development of a Canadian dynamic habitat index using multi-temporal satellite estimates of canopy light absorbance. Ecological Indicators, 8(5), 754-766.

Coulibaly, P., & Burn, D. H. (2004). Wavelet analysis of variability in annual Canadian streamflows. Water Resources Research, 40(3).

Coulibaly, P., & Burn, D. H. (2005). Spatial and temporal variability of Canadian seasonal streamflows. Journal of Climate, 18(1), 191-210.

Couture, R., Smith, S., Robinson, S. D., Burgess, M. M., & Solomon, S. (2003). On the hazards to infrastructure in the Canadian North associated with thawing of permafrost. Proceedings of Geohazards, 97-104.

Culley, S., Noble, S., Yates, A., Timbs, M., Westra, S., Maier, H. R., ... & Castelletti, A. (2016). A bottom-up approach to identifying the maximum operational adaptive capacity of water resource systems to a changing climate. Water Resources Research, 52(9), 6751-6768.

Cunha, M. D. C., & Sousa, J. (1999). Water distribution network design optimization: simulated annealing approach. Journal of water resources planning and management, 125(4), 215-221.

Curran, J. H., & Biles, F. E. (2021). Identification of seasonal streamflow regimes and streamflow drivers for daily and peak flows in Alaska. Water Resources Research. 57 (2): 1-21., 57(2), 1-21.

Czado, C. (2010). Pair-copula constructions of multivariate copulas. In Copula theory and its applications (pp. 93-109). Springer, Berlin, Heidelberg.

Czado, C., Brechmann, E. C., & Gruber, L. (2013). Selection of vine copulas. In Copulae in mathematical and quantitative finance (pp. 17-37). Springer, Berlin, Heidelberg.

Czado, C., Schepsmeier, U., & Min, A. (2012). Maximum likelihood estimation of mixed C-vines with application to exchange rates. Statistical Modelling, 12(3), 229-255.

Dai, A., Trenberth, K. E., & Qian, T. (2004). A global dataset of Palmer Drought Severity Index for 1870–2002: Relationship with soil moisture and effects of surface warming. Journal of Hydrometeorology, 5(6), 1117-1130.

Danner, A. G., Safeeq, M., Grant, G. E., Wickham, C., Tullos, D., & Santelmann, M. V. (2017). Scenario-based and scenario-neutral assessment of climate change impacts on operational performance of a multipurpose reservoir. JAWRA Journal of the American Water Resources Association, 53(6), 1467-1482.

Dauwalter, D. C., Fisher, W. L., & Belt, K. C. (2006). Mapping stream habitats with a global positioning system: accuracy, precision, and comparison with traditional methods. Environmental Management, 37(2), 271-280.

Davin, E. L., de Noblet-Ducoudré, N., & Friedlingstein, P. (2007). Impact of land cover change on surface climate: Relevance of the radiative forcing concept. Geophysical research letters, 34(13).

Dawid, A. P. (1984). Present position and potential developments: Some personal views statistical theory the prequential approach. Journal of the Royal Statistical Society: Series A (General), 147(2), 278-290.

De Fraiture, C., & Wichelns, D. (2010). Satisfying future water demands for agriculture. Agricultural water management, 97(4), 502-511.

De Oliveira, V. A., de Mello, C. R., Viola, M. R., & Srinivasan, R. (2017). Assessment of climate change impacts on streamflow and hydropower potential in the headwater region of the Grande river basin, Southeastern Brazil. International Journal of Climatology, 37(15), 5005-5023.

DeBeer, C. M., Wheater, H. S., Carey, S. K., & Chun, K. P. (2016). Recent climatic, cryospheric, and hydrological changes over the interior of western Canada: a review and synthesis. Hydrology and Earth System Sciences, 20(4), 1573-1598.

Defra, (2011). Climate resilient infrastructure: preparing for a changing climate. London: Department of Environment, Food, and Rural Affairs.

Déry, S. J., & Wood, E. F. (2005). Decreasing river discharge in northern Canada. Geophysical research letters, 32(10).

Déry, S. J., Hernández-Henríquez, M. A., Owens, P. N., Parkes, M. W., & Petticrew, E. L. (2012). A century of hydrological variability and trends in the Fraser River Basin. Environmental Research Letters, 7(2), 024019.

Déry, S. J., Mlynowski, T. J., Hernández-Henríquez, M. A., & Straneo, F. (2011). Interannual variability and interdecadal trends in Hudson Bay streamflow. Journal of Marine Systems, 88(3), 341-351.

Déry, S. J., Stadnyk, T. A., MacDonald, M. K., & Gauli-Sharma, B. (2016). Recent trends and variability in river discharge across northern Canada. Hydrology and Earth System Sciences, 20(12), 4801-4818.

Déry, S. J., Stadnyk, T. A., MacDonald, M. K., Koenig, K. A., & Guay, C. (2018). Flow alteration impacts on Hudson Bay river discharge. Hydrological Processes, 32(24), 3576-3587.

Déry, S. J., Stahl, K., Moore, R. D., Whitfield, P. H., Menounos, B., & Burford, J. E. (2009). Detection of runoff timing changes in pluvial, nival, and glacial rivers of western Canada. Water Resources Research, 45(4).

Deser, C., Phillips, A., Bourdette, V., & Teng, H. (2012). Uncertainty in climate change projections: the role of internal variability. Climate dynamics, 38(3), 527-546.

Dessai, S., & Hulme, M. (2007). Assessing the robustness of adaptation decisions to climate change uncertainties: A case study on water resources management in the East of England. Global environmental change, 17(1), 59-72.

Dibike, Y., Shakibaeinia, A., Eum, H. I., Prowse, T., & Droppo, I. (2018). Effects of projected climate on the hydrodynamic and sediment transport regime of the lower Athabasca River in Alberta, Canada. River Research and Applications, 34(5), 417-429.

Didovets, I., Lobanova, A., Bronstert, A., Snizhko, S., Maule, C. F., & Krysanova, V. (2017). Assessment of climate change impacts on water resources in three representative Ukrainian catchments using eco-hydrological modelling. Water, 9(3), 204.

Dieppois, B., Pohl, B., Rouault, M., New, M., Lawler, D., & Keenlyside, N. (2016). Interannual to interdecadal variability of winter and summer southern African rainfall, and their teleconnections. Journal of Geophysical Research: Atmospheres, 121(11), 6215-6239.

Dierauer, J. R., Allen, D. M., & Whitfield, P. H. (2021). Climate change impacts on snow and streamflow drought regimes in four ecoregions of British Columbia. Canadian Water Resources Journal/Revue canadienne des ressources hydriques, 1-26.

Dierauer, J. R., Whitfield, P. H., & Allen, D. M. (2018). Climate controls on runoff and low flows in mountain catchments of Western North America. Water Resources Research, 54(10), 7495-7510.

Dissmann, J., Brechmann, E. C., Czado, C., & Kurowicka, D. (2013). Selecting and estimating regular vine copulae and application to financial returns. Computational Statistics & Data Analysis, 59, 52-69.

Döll, P., Jiménez-Cisneros, B., Oki, T., Arnell, N. W., Benito, G., Cogley, J. G., ... & Nishijima, A. (2015). Integrating risks of climate change into water management. Hydrological Sciences Journal, 60(1), 4-13.

Dupuis, D. J. (2007). Using copulas in hydrology: Benefits, cautions, and issues. Journal of Hydrologic Engineering, 12(4), 381-393.

Duran-Encalada, J. A., Paucar-Caceres, A., Bandala, E. R., & Wright, G. H. (2017). The impact of global climate change on water quantity and quality: A system dynamics approach to the US–Mexican transborder region. European Journal of Operational Research, 256(2), 567-581.

Eakins, B. W., & Sharman, G. F. (2007, December). Volumes of the World's Oceans From ETOPO2v2. In AGU Fall Meeting Abstracts (Vol. 2007, pp. OS13A-0999).

Eaton, B., & Moore, R. D. (2010). Regional hydrology. Compendium of forest hydrology and geomorphology in British Columbia, 1, 85-110.

Efstratiadis, A., Dialynas, Y. G., Kozanis, S., & Koutsoyiannis, D. (2014). A multivariate stochastic model for the generation of synthetic time series at multiple time scales reproducing long-term persistence. Environmental Modelling and Software, 62(July), 139–152.

Eisner, S., Flörke, M., Chamorro, A., Daggupati, P., Donnelly, C., Huang, J., ... & Krysanova, V. (2017). An ensemble analysis of climate change impacts on streamflow seasonality across 11 large river basins. Climatic Change, 141(3), 401-417.

Elshorbagy, Amin, Alireza Nazemi, and S. Alam, , (2015). Analyzing the variations in intensity–duration–frequency (IDF) curves in the city of Saskatoon under climate change. CANSIM Series Report No. CAN-15-01, Centre for Advanced Numerical simulation (CANSIM), Department of Civil & Geological Engineering, University of Saskatchewan, Saskatoon, Canada. <http://www. hydropyramids.com/files/CAN-15-01-Final-City.pdf>.

Embrechts, P., Lindskog, F., & McNeil, A. (2001). Modelling dependence with copulas. Rapport technique, Département de mathématiques, Institut Fédéral de Technologie de Zurich, Zurich, 14.

Enfield, D. B., & Cid-Serrano, L. (2010). Secular and multidecadal warmings in the North Atlantic and their relationships with major hurricane activity. International Journal of Climatology: A Journal of the Royal Meteorological Society, 30(2), 174-184.

Enfield, D. B., Mestas-Nuñez, A. M., & Trimble, P. J. (2001). The Atlantic multidecadal oscillation and its relation to rainfall and river flows in the continental US. Geophysical Research Letters, 28(10), 2077-2080.

Farmer, W. H., & Vogel, R. M. (2016). On the deterministic and stochastic use of hydrologic models. Water Resources Research, 52(7), 5619-5633.

Fekete, B. M., Wisser, D., Kroeze, C., Mayorga, E., Bouwman, L., Wollheim, W. M., & Vörösmarty, C. (2010). Millennium ecosystem assessment scenario drivers (1970–2050): climate and hydrological alterations. Global Biogeochemical Cycles, 24(4).

Feng, M., Liu, P., Guo, S., Gui, Z., Zhang, X., Zhang, W., & Xiong, L. (2017). Identifying changing patterns of reservoir operating rules under various inflow alteration scenarios. Advances in Water Resources, 104, 23-36.

Fernandez, B., & Salas, J. D. (1986). Periodic gamma autoregressive processes for operational hydrology. Water Resources Research, 22(10), 1385-1396.

Ferrazzi, M., Vivian, R., & Botter, G. (2019). Sensitivity of regulated streamflow regimes to interannual climate variability. Earth's Future, 7(11), 1206-1219.

Fiering, M. B. (1967). Streamflow synthesis. CAMBRIDGE, HARVARD UNIVERSITY PRESS, 1967. 139 P.

Fleming, S. W., & Clarke, G. K. (2003). Glacial control of water resource and related environmental responses to climatic warming: empirical analysis using historical streamflow data from northwestern Canada. Canadian Water Resources Journal, 28(1), 69-86.

Fleming, S. W., & Sauchyn, D. J. (2013). Availability, volatility, stability, and teleconnectivity changes in prairie water supply from Canadian Rocky Mountain sources over the last millennium. Water Resources Research, 49(1), 64-74.

Fleming, S. W., & Weber, F. A. (2012). Detection of long-term change in hydroelectric reservoir inflows: Bridging theory and practise. Journal of Hydrology, 470, 36-54.

Fleming, S. W., and Dahlke, H. E. (2014). Parabolic northern-hemisphere river flow teleconnections to El Niño-Southern Oscillation and the Arctic Oscillation. Environmental Research Letters, 9(10), 104007.

Fleming, S. W., Whitfield, P. H., Moore, R. D., & Quilty, E. J. (2007). Regime-dependent streamflow sensitivities to Pacific climate modes cross the Georgia–Puget transboundary ecoregion. Hydrological Processes: An International Journal, 21(24), 3264-3287.

Forbes, W. L., Mao, J., Ricciuto, D. M., Kao, S. C., Shi, X., Tavakoly, A. A., ... & Hoffman, F. M. (2019). Streamflow in the Columbia River Basin: Quantifying changes over the period 1951-2008 and determining the drivers of those changes. Water Resources Research, 55(8), 6640-6652.

Forsythe, N., Fowler, H. J., Blenkinsop, S., Burton, A., Kilsby, C. G., Archer, D. R., ... & Hashmi, M. Z. (2014). Application of a stochastic weather generator to assess climate change impacts in a semi-arid climate: The Upper Indus Basin. Journal of Hydrology, 517, 1019-1034.

Fu, C., Jiang, Z., Guan, Z., He, J., & Xu, Z. F. (Eds.). (2008). Regional climate studies of China. Springer Science & Business Media.

Fukuyama, Y. (1989). A new method of choosing the number of clusters for the fuzzy c-mean method. In Proc. 5th Fuzzy Syst. Symp., 1989 (pp. 247-250). (in Japanese).

Genest, C. (1987). Frank's family of bivariate distributions. Biometrika, 74(3), 549-555.

Genest, C., & Favre, A. C. (2007). Everything you always wanted to know about copula modeling but were afraid to ask. Journal of hydrologic engineering, 12(4), 347-368.

Ghile, Y. B., Taner, M. Ü., Brown, C., Grijsen, J. G., & Talbi, A. (2014). Bottom-up climate risk assessment of infrastructure investment in the Niger River Basin. Climatic change, 122(1), 97-110.

Giuntoli, I., Renard, B., Vidal, J. P., & Bard, A. (2013). Low flows in France and their relationship to large-scale climate indices. Journal of Hydrology, 482, 105-118.

Gizaw, M. S., Biftu, G. F., Gan, T. Y., Moges, S. A., & Koivusalo, H. (2017). Potential impact of climate change on streamflow of major Ethiopian rivers. Climatic Change, 143(3), 371-383.

Gleick, P. H. (1993). Water in crisis (Vol. 100). New York: Oxford University Press.

Glenis, V., Pinamonti, V., Hall, J. W., & Kilsby, C. G. (2015). A transient stochastic weather generator incorporating climate model uncertainty. Advances in Water Resources, 85, 14-26.

Gneiting, T., Balabdaoui, F., & Raftery, A. E. (2007). Probabilistic forecasts, calibration and sharpness. Journal of the Royal Statistical Society: Series B (Statistical Methodology), 69(2), 243-268.

Gobena, A. K., & Gan, T. Y. (2006). Low-frequency variability in Southwestern Canadian stream flow: links with large-scale climate anomalies. International Journal of Climatology: A Journal of the Royal Meteorological Society, 26(13), 1843-1869.

Gober, P., & Kirkwood, C. W. (2010). Vulnerability assessment of climate-induced water shortage in Phoenix. Proceedings of the National Academy of Sciences, 107(50), 21295-21299.

Gober, P., & Wheater, H. S. (2014). Socio-hydrology and the science–policy interface: a case study of the Saskatchewan River basin. Hydrology and Earth System Sciences, 18(4), 1413-1422,.

Goldenberg, S. B., Landsea, C. W., Mestas-Nuñez, A. M., & Gray, W. M. (2001). The recent increase in Atlantic hurricane activity: Causes and implications. Science, 293(5529), 474-479.

Goodrich, D. C., Lane, L. J., Shillito, R. M., Miller, S. N., Syed, K. H., & Woolhiser, D. A. (1997). Linearity of basin response as a function of scale in a semiarid watershed. Water resources research, 33(12), 2951-2965.

Gosling, S. N., & Arnell, N. W. (2016). A global assessment of the impact of climate change on water scarcity. Climatic Change, 134(3), 371-385.

Grafton, R. Q., Pittock, J., Davis, R., Williams, J., Fu, G., Warburton, M., ... & Quiggin, J. (2013). Global insights into water resources, climate change and governance. Nature Climate Change, 3(4), 315-321.

Grantz, K., Rajagopalan, B., Clark, M., & Zagona, E. (2005). A technique for incorporating large-scale climate information in basin-scale ensemble streamflow forecasts. Water Resources Research, 41(10).

Griffin, R. C. (1998). The fundamental principles of cost-benefit analysis. Water resources research, 34(8), 2063-2071.

Grimaldi, S., & Serinaldi, F. (2006). Asymmetric copula in multivariate flood frequency analysis. Advances in Water Resources, 29(8), 1155-1167.

Groves, D. G., & Lempert, R. J. (2007). A new analytic method for finding policy-relevant scenarios. Global Environmental Change, 17(1), 73-85.

Groves, D. G., Yates, D., & Tebaldi, C. (2008). Developing and applying uncertain global climate change projections for regional water management planning. Water Resources Research, 44(12).

Guetter, A. K., & Georgakakos, K. P. (1993). River outflow of the conterminous United States, 1939–1988. Bulletin of the American Meteorological Society, 74(10), 1873-1892.

Guo, D., Westra, S., & Maier, H. R. (2018). An inverse approach to perturb historical rainfall data for scenario-neutral climate impact studies. Journal of hydrology, 556, 877-890.

Guo, Y., Huang, S., Huang, Q., Wang, H., Wang, L., & Fang, W. (2019). Copulas-based bivariate socioeconomic drought dynamic risk assessment in a changing environment. Journal of Hydrology, 575, 1052-1064.

Gupta, H. V., Kling, H., Yilmaz, K. K., & Martinez, G. F. (2009). Decomposition of the mean squared error and NSE performance criteria: Implications for improving hydrological modelling. Journal of hydrology, 377(1-2), 80-91.

Gutiérrez, F., & Dracup, J. A. (2001). An analysis of the feasibility of long-range streamflow forecasting for Colombia using El Nino–Southern Oscillation indicators. Journal of Hydrology, 246(1-4), 181-196.

Haddeland, I., Heinke, J., Biemans, H., Eisner, S., Flörke, M., Hanasaki, N., ... & Wisser, D. (2014). Global water resources affected by human interventions and climate change. Proceedings of the National Academy of Sciences, 111(9), 3251-3256.

Hagemann, S., Chen, C., Clark, D. B., Folwell, S., Gosling, S. N., Haddeland, I., ... & Wiltshire, A. J. (2013). Climate change impact on available water resources obtained using multiple global climate and hydrology models. Earth System Dynamics, 4(1), 129-144.

Haim, Y. B. (2006). Info-gap decision theory.

Hall, J. W., Lempert, R. J., Keller, K., Hackbarth, A., Mijere, C., & McInerney, D. J. (2012). Robust climate policies under uncertainty: A comparison of robust decision making and info-gap methods. Risk Analysis: An International Journal, 32(10), 1657-1672.

Hall, J., Arheimer, B., Borga, M., Brázdil, R., Claps, P., Kiss, A., ... & Blöschl, G. (2014). Understanding flood regime changes in Europe: a state-of-the-art assessment. Hydrology and Earth System Sciences, 18(7), 2735-2772.

Hamududu, B., & Killingtveit, A. (2017). Assessing Climate Change Impacts on Global Hydropower. In Climate Change and the Future of Sustainability (pp. 109-132). Apple Academic Press.

Hannachi, A., Unkel, S., Trendafilov, N. T., & Jolliffe, I. T. (2009). Independent component analysis of climate data: a new look at EOF rotation. Journal of Climate, 22(11), 2797-2812.

Hao, Z., & Singh, V. P. (2011). Single-site monthly streamflow simulation using entropy theory. Water Resources Research, 47(9).

Hao, Z., & Singh, V. P. (2012). Entropy-copula method for single-site monthly streamflow simulation. Water Resources Research, 48(6).

Hao, Z., & Singh, V. P. (2013). Modeling multisite streamflow dependence with maximum entropy copula. Water Resources Research, 49(10), 7139-7143.

Harder, P., Pomeroy, J. W., & Westbrook, C. J. (2015). Hydrological resilience of a Canadian Rockies headwaters basin subject to changing climate, extreme weather, and forest management. Hydrological Processes, 29(18), 3905-3924.

Harrigan, S., Prudhomme, C., Parry, S., Smith, K., & Tanguy, M. (2018). Benchmarking ensemble streamflow prediction skill in the UK. Hydrology and Earth System Sciences, 22(3), 2023-2039.

Harvey, K.D., Pilon, P.J. and Yuzyk, T.R. (1999). Canada's reference hydrometric basin network (RHBN). In Proceedings of the CWRA 51st Annual Conference, Nova Scotia.

Hashimoto, T., Stedinger, J. R., & Loucks, D. P. (1982). Reliability, resiliency, and vulnerability criteria for water resource system performance evaluation. Water resources research, 18(1), 14-20.

Hassanzadeh, E., Elshorbagy, A., Nazemi, A., Jardine, T. D., Wheater, H., & Lindenschmidt, K. E. (2017). The ecohydrological vulnerability of a large inland delta to changing regional streamflows and upstream irrigation expansion. Ecohydrology, 10(4), e1824.

Hassanzadeh, E., Elshorbagy, A., Wheater, H., & Gober, P. (2014). Managing water in complex systems: An integrated water resources model for Saskatchewan, Canada. Environmental Modelling & Software, 58, 12-26.

Hassanzadeh, E., Elshorbagy, A., Wheater, H., & Gober, P. (2016a). A risk-based framework for water resource management under changing water availability, policy options, and irrigation expansion. Advances in Water Resources, 94, 291-306.

Hassanzadeh, E., Elshorbagy, A., Wheater, H., Gober, P., & Nazemi, A. (2016b). Integrating supply uncertainties from stochastic modeling into integrated water resource management: Case study of the Saskatchewan River basin. Journal of water resources Planning and Management, 142(2), 05015006.

Hatami, S., Zandmoghaddam, S., & Nazemi, A. (2019). Statistical modeling of monthly snow depth loss in southern Canada. Journal of Hydrologic Engineering, 24(3), 04018071.

Hatami, S., & Nazemi, A. (2021). A Statistical Framework for Assessing Temperature Controls on Landscape Freeze-Thaw: Application and Implications in Québec, Canada (1979-2016). Journal of Hydrology, 126891.

Herman, J. D., Quinn, J. D., Steinschneider, S., Giuliani, M., & Fletcher, S. (2020). Climate adaptation as a control problem: Review and perspectives on dynamic water resources planning under uncertainty. Water Resources Research, 56(2), e24389.

Herman, J. D., Reed, P. M., Zeff, H. B., & Characklis, G. W. (2015). How should robustness be defined for water systems planning under change?. Journal of Water Resources Planning and Management, 141(10), 04015012.

Herman, J. D., Zeff, H. B., Lamontagne, J. R., Reed, P. M., & Characklis, G. W. (2016). Synthetic drought scenario generation to support bottom-up water supply vulnerability assessments. Journal of Water Resources Planning and Management, 142(11), 04016050.

Hill, S. C., & Miller, G. E. (2010). Health expenditure estimation and functional form: applications of the generalized gamma and extended estimating equations models. Health economics, 19(5), 608-627.

Hipel, K. W., McLeod, A. I., & Lennox, W. C. (1977). Advances in Box-Jenkins modeling: 1. Model construction. Water Resources Research, 13(3), 567-575.

Hirabayashi, Y., Mahendran, R., Koirala, S., Konoshima, L., Yamazaki, D., Watanabe, S., ... & Kanae, S. (2013). Global flood risk under climate change. Nature climate change, 3(9), 816-821.

Hisdal, H., Stahl, K., Tallaksen, L. M., & Demuth, S. (2001). Have streamflow droughts in Europe become more severe or frequent?. International Journal of Climatology, 21(3), 317-333.

Hlinka, J., Hartman, D., Vejmelka, M., Novotná, D., & Paluš, M. (2014). Non-linear dependence and teleconnections in climate data: sources, relevance, nonstationarity. Climate dynamics, 42(7-8), 1873-1886.

Hock, R., Jansson, P., & Braun, L. N. (2005). Modelling the response of mountain glacier discharge to climate warming. In Global change and mountain regions (pp. 243-252). Springer, Dordrecht.

Hodgkins, G. A., Whitfield, P. H., Burn, D. H., Hannaford, J., Renard, B., Stahl, K., ... & Wilson, D. (2017). Climate-driven variability in the occurrence of major floods across North America and Europe. Journal of Hydrology, 552, 704-717.

Hoerling, M. P., Kumar, A., and Zhong, M. (1997). El Niño, La Niña, and the nonlinearity of their teleconnections. Journal of Climate, 10(8), 1769-1786.

Hofert, M., Kojadinovic, I., Maechler, M., Yan, J., Maechler, M. M., & Suggests, M. A. S. S. (2014). Package 'copula'. URL http://ie. archive. ubuntu. com/disk1/disk1/cran. r-project. org/web/packages/copula/copula. pdf.

Huang, G. R., & Rui, X. F. (2004). Study advances in diagnosis of chaotic behaviour and its prediction for rainfall and streamflow time series in watershed. Advances in Water Science, 15(2), 255-259.

Hughes, D. A., Kapangaziwiri, E., & Sawunyama, T. (2010). Hydrological model uncertainty assessment in southern Africa. Journal of Hydrology, 387(3-4), 221-232.

Intergovernmental Panel on Climate Change. (2007). Climate change impacts, adaptation and vulnerability." Working Group II, IPCC 4th Assessment Report.

Intergovernmental Panel on Climate Change. (2014). Climate Change Impacts, Adaptation and Vulnerability: Regional Aspects. Cambridge University Press.

Ireson, A. M., Barr, A. G., Johnstone, J. F., Mamet, S. D., Van der Kamp, G., Whitfield, C. J., ... & Sagin, J. (2015). The changing water cycle: the Boreal Plains ecozone of Western Canada. Wiley Interdisciplinary Reviews: Water, 2(5), 505-521.

Islam, S. U., Curry, C. L., Déry, S. J., & Zwiers, F. W. (2019). Quantifying projected changes in runoff variability and flow regimes of the Fraser River Basin, British Columbia. Hydrology and Earth System Sciences, 23(2), 811-828.

Islam, Z., & Gan, T. Y. (2016). Water allocation challenges of south Saskatchewan River Basin under the combined impacts of climate change and El Niño Southern Oscillation. Journal of Water Resources Planning and Management, 142(10), 04016039.

Janowicz, J. R. (2008). Apparent recent trends in hydrologic response in permafrost regions of northwest Canada. Hydrology Research, 39(4), 267-275.

Janowicz, J. R. (2011). Streamflow responses and trends between permafrost and glacierized regimes in northwestern Canada. IAHS Publ, 346, 9-14.

Jaramillo, P., & Nazemi, A. (2018). Assessing urban water security under changing climate: Challenges and ways forward. Sustainable cities and society, 41, 907-918.

Jehn, F. U., Bestian, K., Breuer, L., Kraft, P., & Houska, T. (2020). Using hydrological and climatic catchment clusters to explore drivers of catchment behavior. Hydrology and Earth System Sciences, 24(3), 1081-1100.

Jenkins, G., & Lowe, J. (2003). Handling uncertainties in the UKCIP02 scenarios of climate change. Met Office.

Jeong, C., & Lee, T. (2015). Copula-based modeling and stochastic simulation of seasonal intermittent streamflows for arid regions. Journal of Hydro-Environment Research, 9(4), 604-613.

Joe, H. (1997). Multivariate models and multivariate dependence concepts. CRC Press.

Joe, H. (2014). Dependence modeling with copulas. CRC press.

Johnson, F., & Sharma, A. (2011). Accounting for interannual variability: A comparison of options for water resources climate change impact assessments. Water Resources Research, 47(4).

Johnson, T. E., and C. P. Weaver (2009). A framework for assessing climate change impacts on water and watershed systems, Environ. Manage, 43, 118–134.

Johnston, C. A., & Shmagin, B. A. (2008). Regionalization, seasonality, and trends of streamflow in the US Great Lakes Basin. Journal of Hydrology, 362(1-2), 69-88.

Jolliffe, I. T., & Stephenson, D. B. (Eds.). (2012). Forecast verification: a practitioner's guide in atmospheric science. John Wiley & Sons.

Jones, W. D. (2008). How much water does it take to make electricity. IEEE Spectrum, 23.

Kang, D. H., Gao, H., Shi, X., ul Islam, S., & Déry, S. J. (2016). Impacts of a rapidly declining mountain snowpack on streamflow timing in Canada's Fraser River basin. Scientific Reports, 6(1), 1-8.

Kashyap, S., Dibike, Y., Shakibaeinia, A., Prowse, T., & Droppo, I. (2017). Two-dimensional numerical modelling of sediment and chemical constituent transport within the lower reaches of the Athabasca River. Environmental Science and Pollution Research, 24(3), 2286-2303.

Kaune, A., Chowdhury, F., Werner, M., & Bennett, J. (2020). The benefit of using an ensemble of seasonal streamflow forecasts in water allocation decisions. Hydrology and Earth System Sciences, 24(7), 3851-3870.

Keef, C., Svensson, C., & Tawn, J. A. (2009). Spatial dependence in extreme river flows and precipitation for Great Britain. Journal of Hydrology, 378(3-4), 240-252.

Kendall, M. G. (1976). Rank Auto Correlation Methods, 4th Edn., Griffin.

Kendall, M. G., (1975). Rank Correlation Methods. Griffin & Co, London. ISBN 0-85264-199-0.

Khan, S., Ganguly, A. R., Bandyopadhyay, S., Saigal, S., Erickson III, D. J., Protopopescu, V., and Ostrouchov, G. (2006). Nonlinear statistics reveals stronger ties between ENSO and the tropical hydrological cycle. Geophysical Research Letters, 33(24).

Khatri, K. B., Strong, C., Kochanski, A. K., Burian, S., Miller, C., & Hasenyager, C. (2018). Water resources criticality due to future climate change and population growth: case of river basins in Utah, USA. Journal of Water Resources Planning and Management, 144(8), 04018041.

Kiem, A. S., Kuczera, G., Kozarovski, P., Zhang, L., & Willgoose, G. (2021). Stochastic generation of future hydroclimate using temperature as a climate change covariate. Water Resources Research, 57(2), 2020WR027331.

Kilsby, C. G., Jones, P. D., Burton, A., Ford, A. C., Fowler, H. J., Harpham, C., ... & Wilby, R. L. (2007). A daily weather generator for use in climate change studies. Environmental Modelling & Software, 22(12), 1705-1719.

Kim, T., Shin, J. Y., Kim, H., Kim, S., & Heo, J. H. (2019). The use of large-scale climate indices in monthly reservoir inflow forecasting and its application on time series and artificial intelligence models. Water, 11(2), 374.

King, L. M., McLeod, A. I., & Simonovic, S. P. (2015). Improved weather generator algorithm for multisite simulation of precipitation and temperature. JAWRA Journal of the American Water Resources Association, 51(5), 1305-1320.

Kingston, D. G., Hannah, D. M., Lawler, D. M., & McGregor, G. R. (2011). Regional classification, variability, and trends of northern North Atlantic river flow. Hydrological Processes, 25(7), 1021-1033.

Kisi, O., Choubin, B., Deo, R. C., & Yaseen, Z. M. (2019). Incorporating synoptic-scale climate signals for streamflow modelling over the Mediterranean region using machine learning models. Hydrological Sciences Journal, 64(10), 1240-1252.

Kleiber, C., & Kotz, S. (2003). Statistical size distributions in economics and actuarial sciences (Vol. 470). John Wiley & Sons.

Knight, J. R., Folland, C. K., & Scaife, A. A. (2006). Climate impacts of the Atlantic multidecadal oscillation. Geophysical Research Letters, 33(17).

Knighton, J., Steinschneider, S., & Walter, M. T. (2017). A vulnerability-based, bottom-up assessment of future riverine flood risk using a modified peaks-over-threshold approach and a physically based hydrologic model. Water Resources Research, 53(12), 10043-10064.

Knoben, W. J., Freer, J. E., & Woods, R. A. (2019). Inherent benchmark or not? Comparing Nash–Sutcliffe and Kling–Gupta efficiency scores. Hydrology and Earth System Sciences, 23(10), 4323-4331.

Knoben, W. J., Woods, R. A., & Freer, J. E. (2018). A quantitative hydrological climate classification evaluated with independent streamflow data. Water Resources Research, 54(7), 5088-5109.

Knouft, J. H., & Ficklin, D. L. (2017). The potential impacts of climate change on biodiversity in flowing freshwater systems. Annual Review of Ecology, Evolution, and Systematics, 48, 111-133.

Konapala, G., & Mishra, A. K. (2016). Three-parameter-based streamflow elasticity model: Application to MOPEX basins in the USA at annual and seasonal scales. Hydrology and Earth System Sciences, 20(6), 2545.

Konapala, G., Veettil, A. V., & Mishra, A. K. (2018). Teleconnection between low flows and large-scale climate indices in Texas River basins. Stochastic Environmental Research and Risk Assessment, 32(8), 2337-2350.

Kong, X. M., Huang, G. H., Fan, Y. R., & Li, Y. P. (2015). Maximum entropy-Gumbel-Hougaard copula method for simulation of monthly streamflow in Xiangxi river, China. Stochastic environmental research and risk assessment, 29(3), 833-846.

Koutsouris, A. J., & Lyon, S. W. (2018). Advancing understanding in data-limited conditions: estimating contributions to streamflow across Tanzania's rapidly developing Kilombero Valley. Hydrological Sciences Journal, 63(2), 197-209.

Krysanova, V., Vetter, T., Eisner, S., Huang, S., Pechlivanidis, I., Strauch, M., ... & Hattermann, F. F. (2017). Intercomparison of regional-scale hydrological models and climate change impacts projected for 12 large river basins worldwide—a synthesis. Environmental Research Letters, 12(10), 105002.

Kuentz, A., Arheimer, B., Hundecha, Y., & Wagener, T. (2017). Understanding hydrologic variability across Europe through catchment classification. Hydrology and Earth System Sciences, 21(6), 2863-2879.

Kumar, D. N., Lall, U., & Petersen, M. R. (2000). Multisite disaggregation of monthly to daily streamflow. Water Resources Research, 36(7), 1823-1833.

Kundzewicz, Z. W., Kanae, S., Seneviratne, S. I., Handmer, J., Nicholls, N., Peduzzi, P., ... & Sherstyukov, B. (2014). Flood risk and climate change: global and regional perspectives. Hydrological Sciences Journal, 59(1), 1-28.

Kundzewicz, Z. W., Krysanova, V., Dankers, R., Hirabayashi, Y., Kanae, S., Hattermann, F. F., ... & Schellnhuber, H. J. (2017). Differences in flood hazard projections in Europe–their causes and consequences for decision making. Hydrological Sciences Journal, 62(1), 1-14.

Kwon, H. H., Brown, C., & Lall, U. (2008). Climate informed flood frequency analysis and prediction in Montana using hierarchical Bayesian modeling. Geophysical Research Letters, 35(5).

Lall, U. (1995). Recent advances in nonparametric function estimation: Hydrologic applications. Reviews of Geophysics, 33(S2), 1093-1102.

Lall, U., & Sharma, A. (1996). A nearest neighbor bootstrap for resampling hydrologic time series. Water Resources Research, 32(3), 679–693.

Lall, U., Devineni, N., & Kaheil, Y. (2016). An empirical, nonparametric simulator for multivariate random variables with differing marginal densities and nonlinear dependence with hydroclimatic applications. Risk Analysis, 36(1), 57-73.

Lamontagne, J. R., & Stedinger, J. R. (2018). Generating synthetic streamflow forecasts with specified precision. Journal of Water Resources Planning and Management, 144(4), 04018007.

Landis, W. G., Markiewicz, A. J., Ayre, K. K., Johns, A. F., Harris, M. J., Stinson, J. M., & Summers, H. M. (2017). A general risk-based adaptive management scheme incorporating the Bayesian Network Relative Risk Model with the South River, Virginia, as case study. Integrated environmental assessment and management, 13(1), 115-126.

Lavers, D., Prudhomme, C., & Hannah, D. M. (2010). Large-scale climate, precipitation and British river flows: Identifying hydroclimatological connections and dynamics. Journal of Hydrology, 395(3-4), 242-255.

Lawrance, A. J., & Lewis, P. (1981). A new autoregressive time series model in exponential variables (NEAR (1)). Advances in Applied Probability, 13(4), 826-845.

Le Rest, K., Pinaud, D., Monestiez, P., Chadoeuf, J., & Bretagnolle, V. (2014). Spatial leave-one-out cross-validation for variable selection in the presence of spatial autocorrelation. Global ecology and biogeography, 23(7), 811-820.

Lee, D., Ward, P. J., & Block, P. (2018b). Identification of symmetric and asymmetric responses in seasonal streamflow globally to ENSO phase. Environmental Research Letters, 13(4), 044031, https://doi.org/10.1088/1748-9326/aab4ca.

Lee, D., Ward, P., & Block, P. (2018a). Attribution of large-scale climate patterns to seasonal peak-flow and prospects for prediction globally. Water Resources Research, 54(2), 916-938, https://doi.org/10.1002/2017WR021205.

Lee, T., & Salas, J. D. (2011). Copula-based stochastic simulation of hydrological data applied to Nile River flows. Hydrology Research, 42(4), 318-330.

Lee, T., Salas, J. D., & Prairie, J. (2010). An enhanced nonparametric streamflow disaggregation model with genetic algorithm. Water Resources Research, 46(8).

Legates, D. R., & McCabe Jr, G. J. (1999). Evaluating the use of "goodness-of-fit" measures in hydrologic and hydroclimatic model validation. Water resources research, 35(1), 233-241.

Lehner, B., Döll, P., Alcamo, J., Henrichs, T., & Kaspar, F. (2006). Estimating the impact of global change on flood and drought risks in Europe: a continental, integrated analysis. Climatic Change, 75(3), 273-299.

Lehner, F., Wood, A. W., Llewellyn, D., Blatchford, D. B., Goodbody, A. G., & Pappenberger, F. (2017). Mitigating the impacts of climate nonstationarity on seasonal streamflow predictability in the US Southwest. Geophysical Research Letters, 44(24), 12-208.

Lei, X. H., Tan, Q. F., Wang, X., Wang, H., Wen, X., Wang, C., & Zhang, J. W. (2018). Stochastic optimal operation of reservoirs based on copula functions. Journal of Hydrology, 557, 265-275.

Lempert, R. J., & Collins, M. T. (2007). Managing the risk of uncertain threshold responses: comparison of robust, optimum, and precautionary approaches. Risk Analysis: An International Journal, 27(4), 1009-1026.

Lempert, R. J., Groves, D. G., Popper, S. W., & Bankes, S. C. (2006). A general, analytic method for generating robust strategies and narrative scenarios. Management science, 52(4), 514-528.

Lempert, R., Nakicenovic, N., Sarewitz, D., & Schlesinger, M. (2004). Characterizing climate-change uncertainties for decision-makers. Climatic Change, 65(1-2), 1-9.

Leonard, M., Westra, S., Phatak, A., Lambert, M., van den Hurk, B., McInnes, K., ... & Stafford-Smith, M. (2014). A compound event framework for understanding extreme impacts. Wiley Interdisciplinary Reviews: Climate Change, 5(1), 113-128.

Li, H., Sheffield, J., & Wood, E. F. (2010). Bias correction of monthly precipitation and temperature fields from Intergovernmental Panel on Climate Change AR4 models using equidistant quantile matching. Journal of Geophysical Research: Atmospheres, 115(D10).

Liu, Z., Zhou, P., Chen, X., & Guan, Y. (2015). A multivariate conditional model for streamflow prediction and spatial precipitation refinement. Journal of Geophysical Research: Atmospheres, 120(19), 10-116.

Loucks, D. P., & Van Beek, E. (2017). Water resource systems planning and management: An introduction to methods, models, and applications. Springer.

Lownsbery, K. E. (2014). Quantifying the impacts of future uncertainties on the Apalachicola-Chattahoochee-Flint basin.

MacDonald, M. K., Stadnyk, T. A., Déry, S. J., Braun, M., Gustafsson, D., Isberg, K., & Arheimer, B. (2018). Impacts of 1.5 and 2.0° C warming on pan-Arctic river discharge into the Hudson Bay complex through 2070. Geophysical Research Letters, 45(15), 7561-7570.

Macknick, J., Newmark, R., Heath, G., & Hallett, K. C. (2012). Operational water consumption and withdrawal factors for electricity generating technologies: a review of existing literature. Environmental Research Letters, 7(4), 045802.

Madadgar, S., & Moradkhani, H. (2011). Drought analysis under climate change using copula. Journal of Hydrologic Engineering, 18(7), 746-759.

Magilligan, F. J., & Nislow, K. H. (2005). Changes in hydrologic regime by dams. Geomorphology, 71(1-2), 61-78.

Mallakpour, I., & Villarini, G. (2015). The changing nature of flooding across the central United States. Nature Climate Change, 5(3), 250-254.

Mallakpour, I., Sadegh, M., & AghaKouchak, A. (2018). A new normal for streamflow in California in a warming climate: Wetter wet seasons and drier dry seasons. Journal of hydrology, 567, 203-211.

Mann, H. B. (1945). Nonparametric tests against trend. Econometrica: Journal of the econometric society, 245-259.

Mann, M. E., & Gleick, P. H. (2015). Climate change and California drought in the 21st century. Proceedings of the National Academy of Sciences, 112(13), 3858-3859.

Mantua, N. J., Hare, S. R., Zhang, Y., Wallace, J. M., & Francis, R. C. (1997). A Pacific interdecadal climate oscillation with impacts on salmon production. Bulletin of the american Meteorological Society, 78(6), 1069-1080.

Maraun, D., Shepherd, T. G., Widmann, M., Zappa, G., Walton, D., Gutiérrez, J. M., ... & Mearns, L. O. (2017). Towards process-informed bias correction of climate change simulations. Nature Climate Change, 7(11), 764-773.

Marković, Đ., Plavšić, J., Ilich, N., & Ilić, S. (2015). Non-parametric stochastic generation of streamflow series at multiple locations. Water Resources Management, 29(13), 4787-4801.

Marshall, I. B., Schut, P., & Ballard, M. (1999). A national ecological framework for Canada: attribute data. Environmental quality branch, Ecosystems Science Directorate, Environment Canada and Research Branch. Agriculture and Agri-Food Canada, Ottawa, 1375.

Martz, L., Armstrong, R., & Pietroniro, E. (2007). The South Saskatchewan River Basin: Physical Geography. In'Climate Change and Water SSRB Final Technical Report.

Martz, L., Bruneauand, J., & Rolfe, J. T. (2007). Assessment of the vulnerability of key water use sectors in the South Saskatchewan River Basin (Alberta and Saskatchewan) to changes in water supply resulting from climate change. In SSRB Final Technical Report.

Matalas, N. C. (1967). Mathematical assessment of synthetic hydrology. Water Resources Research, 3(4), 937–945.

Mateus, M. C., & Tullos, D. (2017). Reliability, sensitivity, and vulnerability of reservoir operations under climate change. Journal of Water Resources Planning and Management, 143(4), 04016085.

Matrosov, E. S., Woods, A. M., & Harou, J. J. (2013). Robust decision making and info-gap decision theory for water resource system planning. Journal of hydrology, 494, 43-58.

Matsui, T., & Pielke Sr, R. A. (2006). Measurement-based estimation of the spatial gradient of aerosol radiative forcing. Geophysical Research Letters, 33(11).

Matti, B., Dahlke, H. E., Dieppois, B., Lawler, D. M., & Lyon, S. W. (2017). Flood seasonality across Scandinavia—Evidence of a shifting hydrograph?. Hydrological Processes, 31(24), 4354-4370.

Maurer, E. P., Lettenmaier, D. P., & Mantua, N. J. (2004). Variability and potential sources of predictability of North American runoff. Water Resources Research, 40(9).

Maurer, E. P., Stewart, I. T., Bonfils, C., Duffy, P. B., & Cayan, D. (2007). Detection, attribution, and sensitivity of trends toward earlier streamflow in the Sierra Nevada. Journal of Geophysical Research: Atmospheres, 112(D11).

May, R. J., Maier, H. R., Dandy, G. C., & Fernando, T. G. (2008). Non-linear variable selection for artificial neural networks using partial mutual information. Environmental Modelling & Software, 23(10-11), 1312-1326.

May, R., Dandy, G., & Maier, H. (2011). Review of input variable selection methods for artificial neural networks. Artificial neural networks-methodological advances and biomedical applications, 10, 16004.

Mazdiyasni, O., & AghaKouchak, A. (2015). Substantial increase in concurrent droughts and heatwaves in the United States. Proceedings of the National Academy of Sciences, 112(37), 11484-11489.

McGowan, H. A., Marx, S. K., Denholm, J., Soderholm, J., & Kamber, B. S. (2009). Reconstructing annual inflows to the headwater catchments of the Murray River, Australia, using the Pacific Decadal Oscillation. Geophysical Research Letters, 36(6).

Meehl, G. A., & Tebaldi, C. (2004). More intense, more frequent, and longer lasting heat waves in the 21st century. Science, 305(5686), 994-997.

Mekonnen, B. A., Nazemi, A., Mazurek, K. A., Elshorbagy, A., & Putz, G. (2015). Hybrid modelling approach to prairie hydrology: fusing data-driven and process-based hydrological models. Hydrological sciences journal, 60(9), 1473-1489.

Merz, B., Aerts, J. C. J. H., Arnbjerg-Nielsen, K., Baldi, M., Becker, A., Bichet, A., ... & Nied, M. (2014). Floods and climate: emerging perspectives for flood risk assessment and management. Natural Hazards and Earth System Sciences, 14(7), 1921-1942.

Meybeck, M. (2003). Global analysis of river systems: from Earth system controls to Anthropocene syndromes. Philosophical Transactions of the Royal Society of London. Series B: Biological Sciences, 358(1440), 1935-1955.

Middelkoop, H., Daamen, K., Gellens, D., Grabs, W., Kwadijk, J. C., Lang, H., ... & Wilke, K. (2001). Impact of climate change on hydrological regimes and water resources management in the Rhine basin. Climatic change, 49(1), 105-128.

Miles, E. L., Snover, A. K., Hamlet, A. F., Callahan, B., & Fluharty, D. (2000). Pacific Northwest regional assessment: The impacts of climate variability and climate change on the water resources of the columbia River basin 1. JAWRA Journal of the American Water Resources Association, 36(2), 399-420.

Milly, P. C. D., Betancourt, J., Falkenmark, M., Hirsch, R. M., Kundzewicz, Z. W., Lettenmaier, D. P., & Stouffer, R. J. (2008). Stationarity is dead: Whither water management?. Earth, 4(20).

Milly, P. C., Betancourt, J., Falkenmark, M., Hirsch, R. M., Kundzewicz, Z. W., Lettenmaier, D. P., ... & Krysanova, V. (2015). On critiques of "Stationarity is dead: Whither water management?". Water Resources Research, 51(9), 7785-7789.

Milly, P. C., Dunne, K. A., & Vecchia, A. V. (2005). Global pattern of trends in streamflow and water availability in a changing climate. Nature, 438(7066), 347-350.

Montanari, A., & Koutsoyiannis, D. (2012). A blueprint for process-based modeling of uncertain hydrological systems. Water Resources Research, 48(9).

Moody, P., & Brown, C. (2013). Robustness indicators for evaluation under climate change: Application to the upper Great Lakes. Water Resources Research, 49(6), 3576-3588.

Moore, R. D., Trubilowicz, J. W., & Buttle, J. M. (2012). Prediction of Streamflow regime and annual runoff for ungauged basins using a distributed monthly water balance model 1. JAWRA Journal of the American Water Resources Association, 48(1), 32-42.

Mote, P., Brekke, L., Duffy, P. B., & Maurer, E. (2011). Guidelines for constructing climate scenarios. Eos, Transactions American Geophysical Union, 92(31), 257-258.

Murphy, B. F., & Timbal, B. (2008). A review of recent climate variability and climate change in southeastern Australia. International Journal of Climatology: A Journal of the Royal Meteorological Society, 28(7), 859-879.

Myhre, G., & Myhre, A. (2003). Uncertainties in radiative forcing due to surface albedo changes caused by land-use changes. Journal of Climate, 16(10), 1511-1524.

Nagler, T., Schepsmeier, U., Stoeber, J., Brechmann, E.C., Graeler, B. and Erhardt, T. (2019). VineCopula: Statistical Inference of Vine Copulas. R package version 2.2.0. https://CRAN.Rproject.org/package=VineCopula

Nalley, D., Adamowski, J., Biswas, A., Gharabaghi, B., & Hu, W. (2019). A multiscale and multivariate analysis of precipitation and streamflow variability in relation to ENSO, NAO and PDO. Journal of Hydrology, 574, 288-307.

Nalley, D., Adamowski, J., Khalil, B., & Biswas, A. (2016). Inter-annual to inter-decadal streamflow variability in Quebec and Ontario in relation to dominant large-scale climate indices. Journal of hydrology, 536, 426-446.

Natural Resources Canada. The Atlas of Canada: Lakes, Rivers and Names of Canada, online at https://open.canada.ca/data/en/dataset/e625c0b0-2d5f-50d8-9e0c-a6e0fd5876ee, 2007.

Nazemi, A. A., & Wheater, H. S. (2014a). Assessing the vulnerability of water supply to changing streamflow conditions. Eos, Transactions American Geophysical Union, 95(32), 288-288.

Nazemi, A. R., Akbarzadeh, M. R., & Hosseini, S. M. (2002, June). Fuzzy-stochastic linear programming in water resources engineering. In 2002 Annual Meeting of the North American Fuzzy Information Processing Society Proceedings. NAFIPS-FLINT 2002 (Cat. No. 02TH8622) (pp. 227-232). IEEE.

Nazemi, A., & Elshorbagy, A. (2012). Application of copula modelling to the performance assessment of reconstructed watersheds. Stochastic environmental research and risk assessment, 26(2), 189-205.

Nazemi, A., & Wheater, H. S. (2014b). How can the uncertainty in the natural inflow regime propagate into the assessment of water resource systems?. Advances in water resources, 63, 131-142.

Nazemi, A., & Wheater, H. S. (2015a). On inclusion of water resource management in Earth system models–Part 1: Problem definition and representation of water demand. Hydrology and Earth System Sciences, 19(1), 33-61.

Nazemi, A., & Wheater, H. S. (2015b). On inclusion of water resource management in Earth system models–Part 2: Representation of water supply and allocation and opportunities for improved modeling. Hydrology and Earth System Sciences, 19(1), 63-90.

Nazemi, A., Wheater, H. S., Chun, K. P., & Elshorbagy, A. (2013). A stochastic reconstruction framework for analysis of water resource system vulnerability to climate-induced changes in river flow regime. Water Resources Research, 49(1), 291-305.

Nazemi, A., Wheater, H. S., Chun, K. P., Bonsal, B., & Mekonnen, M. (2017). Forms and drivers of annual streamflow variability in the headwaters of Canadian Prairies during the 20th century. Hydrological Processes, 31(1), 221-239.

Nazemi, A., Zaerpour, M., & Hassanzadeh, E. (2020). Uncertainty in Bottom-Up Vulnerability Assessments of Water Supply Systems due to Regional Streamflow Generation under Changing Conditions. Journal of Water Resources Planning and Management, 146(2), 04019071.

Nelsen, R. B. (2006.) An introduction to copulas. New York: Springer. Nowak, K. C., B.

Nelsen, R. B. (2007). An introduction to copulas. Springer Science & Business Media.

New, M., & Hulme, M. (2000). Representing uncertainty in climate change scenarios: a Monte-Carlo approach. Integrated assessment, 1(3), 203-213.

Nguyen-Huy, T., Deo, R. C., Yaseen, Z. M., Prasad, R., & Mushtaq, S. (2020). Bayesian Markov Chain Monte Carlo-based copulas: factoring the role of large-scale climate indices in monthly flood prediction. In Intelligent Data Analytics for Decision-Support Systems in Hazard Mitigation (pp. 29-47). Springer, Singapore.

Nijssen, B., O'Donnell, G. M., Hamlet, A. F., & Lettenmaier, D. P. (2001). Hydrologic sensitivity of global rivers to climate change. Climatic change, 50(1), 143-175.

Nipen, T., & Stull, R. (2011). Calibrating probabilistic forecasts from an NWP ensemble. Tellus A: Dynamic Meteorology and Oceanography, 63(5), 858-875.

Nowak, K. C., Rajagopalan, B., & Zagona, E. (2011). Wavelet Auto-Regressive Method (WARM) for multi-site streamflow simulation of data with non-stationary spectra. Journal of hydrology, 410(1-2), 1-12.

Olden, J. D., & Poff, N. L. (2003). Redundancy and the choice of hydrologic indices for characterizing streamflow regimes. River research and applications, 19(2), 101-121.

Olden, J. D., Kennard, M. J., & Pusey, B. J. (2012). A framework for hydrologic classification with a review of methodologies and applications in ecohydrology. Ecohydrology, 5(4), 503-518.

O'Neil, H. C. L., Prowse, T. D., Bonsal, B. R., & Dibike, Y. B. (2017). Spatial and temporal characteristics in streamflow-related hydroclimatic variables over western Canada. Part 1: 1950–2010. Hydrology Research, 48(4), 915-931.

Otterman, J., Atlas, R., Chou, S. H., Jusem, J. C., Pielke Sr, R. A., Chase, T. N., ... & Terry, J. (2002). Are stronger North-Atlantic southwesterlies the forcing to the late-winter warming in Europe?. International Journal of Climatology: A Journal of the Royal Meteorological Society, 22(6), 743-750.

Overland, J. E., & Preisendorfer, R. W. (1982). A significance test for principal components applied to a cyclone climatology. Monthly Weather Review, 110(1), 1-4.

Padrón, R. S., Gudmundsson, L., Decharme, B., Ducharne, A., Lawrence, D. M., Mao, J., ... & Seneviratne, S. I. (2020). Observed changes in dry-season water availability attributed to human-induced climate change. Nature geoscience, 13(7), 477-481.

Pal, S., Yu, H., Loucks, Z. D., & Harris, I. M. (2020). Illustration of the Flexibility of Generalized Gamma Distribution in Modeling Right Censored Survival Data: Analysis of Two Cancer Datasets. Annals of Data Science, 7(1), 77-90.

Panofsky, H. A., Brier, G. W., & Best, W. H. (1958). Some application of statistics to meteorology.

Papacharalampous, G., Tyralis, H., & Koutsoyiannis, D. (2019). Comparison of stochastic and machine learning methods for multi-step ahead forecasting of hydrological processes. Stochastic Environmental Research and Risk Assessment, 33(2), 481-514.

Papalexiou, S. M. (2018). Unified theory for stochastic modelling of hydroclimatic processes: Preserving marginal distributions, correlation structures, and intermittency. Advances in water resources, 115, 234-252.

Papalexiou, S. M., & Koutsoyiannis, D. (2012). Entropy based derivation of probability distributions: A case study to daily rainfall. Advances in Water Resources, 45, 51-57.

Papalexiou, S. M., & Serinaldi, F. (2020). Random Fields Simplified: Preserving Marginal Distributions, Correlations, and Intermittency, with applications from rainfall to humidity. Water Resources Research, 56(2), e2019WR026331.

Pearse, P. H., Bertrand, F., & MacLaren, J. W. (1985). Currents of change: final report, inquiry on federal water policy. The Inquiry.

Pegram, G. G. S. (1980). A continuous streamflow model. Journal of Hydrology, 47(1-2), 65-89.

Peñuelas, J., Lloret, F., & Montoya, R. (2001). Severe drought effects on Mediterranean woody flora in Spain. Forest Science, 47(2), 214-218.

Pereira, G. A., Veiga, Á., Erhardt, T., & Czado, C. (2017). A periodic spatial vine copula model for multi-site streamflow simulation. Electric Power Systems Research, 152, 9-17.

Pereira, G., & Veiga, A. (2018). PAR (p)-vine copula based model for stochastic streamflow scenario generation. Stochastic environmental research and risk assessment, 32(3), 833-842.

Pewsey, A., Neuhäuser, M., & Ruxton, G. D. (2013). Circular statistics in R. Oxford University Press.

Piani, C., Weedon, G. P., Best, M., Gomes, S. M., Viterbo, P., Hagemann, S., & Haerter, J. O. (2010). Statistical bias correction of global simulated daily precipitation and temperature for the application of hydrological models. Journal of hydrology, 395(3-4), 199-215.

Pielke Sr, R. A., Wilby, R., Niyogi, D., Hossain, F., Dairuku, K., Adegoke, J., ... & Suding, K. (2012). Dealing with complexity and extreme events using a bottom-up, resource-based vulnerability perspective. Extreme events and natural hazards: The complexity perspective, 196, 345-359.

Pielke, R. A. (2010). Comments on "A Unified Modeling Approach to Climate System Prediction". Bulletin of the American Meteorological Society, 91(12), 1699-1701.

Pike, R. G., Redding, T. E., Moore, R. D., Winker, R. D., & Bladon, K. D. (2010). Compendium of forest hydrology and geomorphology in British Columbia. BC Min. For. Range. In For. Sci. Prog., Victoria, BC and FORREX Forum for Research and Extension in Natural Resources, Kamloops, BC Land Manag. Handb (Vol. 66).

Pilgrim, D. H. (1976). Travel times and nonlinearity of flood runoff from tracer measurements on a small watershed. Water Resources Research, 12(3), 487-496.

Pina, J., Tilmant, A., & Anctil, F. (2017). Horizontal approach to assess the impact of climate change on water resources systems. Journal of Water Resources Planning and Management, 143(4), 04016081.

Pinson, P., McSharry, P., & Madsen, H. (2010). Reliability diagrams for non-parametric density forecasts of continuous variables: Accounting for serial correlation. Quarterly Journal of the Royal Meteorological Society: A journal of the atmospheric sciences, applied meteorology and physical oceanography, 136(646), 77-90.

Plackett, R. L. (1965). A class of bivariate distributions. Journal of the American Statistical Association, 60(310), 516-522.

Poff, N. L., Allan, J. D., Bain, M. B., Karr, J. R., Prestegaard, K. L., Richter, B. D., ... & Stromberg, J. C. (1997). The natural flow regime. BioScience, 47(11), 769-784.

Poff, N. L., Brown, C. M., Grantham, T. E., Matthews, J. H., Palmer, M. A., Spence, C. M., ... & Baeza, A. (2016). Sustainable water management under future uncertainty with eco-engineering decision scaling. Nature Climate Change, 6(1), 25-34.

Poff, N. L., Richter, B. D., Arthington, A. H., Bunn, S. E., Naiman, R. J., Kendy, E., ... & Warner, A. (2010). The ecological limits of hydrologic alteration (ELOHA): a new framework for developing regional environmental flow standards. Freshwater biology, 55(1), 147-170.

Pomeroy, J. W., D. D. Boer, and L. W. Martz. (2005). Hydrology and water resources of Saskatchewan. Saskatoon, Canada: Univ. of Saskatchewan.

Pomeroy, J. W., X. Fang, and B. Williams. (2009). Impacts of climate change on Saskatchewan's water resources. Saskatoon, Saskatchewan: Univ. of Saskatchewan.

Power, K., and Gillis, M. D., (2006). Canada's forest inventory 2001 (Vol. 408). Pacific Forestry Centre.

Prairie, J. R., B. Rajagopalan, T. J. Fulp, and E. A. Zagona (2005). Statistical nonparametric model for natural salt estimation, J. Environ. Eng., 131(1), 130–138.

Prairie, J. R., Rajagopalan, B., Fulp, T. J., & Zagona, E. A. (2006). Modified K-NN model for stochastic streamflow simulation. Journal of Hydrologic Engineering, 11(4), 371-378.

Prairie, J., Nowak, K., Rajagopalan, B., Lall, U., & Fulp, T. (2008). A stochastic nonparametric approach for streamflow generation combining observational and paleoreconstructed data. Water Resources Research, 44(6).

Prairie, J., Rajagopalan, B., Lall, U., & Fulp, T. (2007). A stochastic nonparametric technique for space-time disaggregation of streamflows. Water Resources Research, 43(3).

Prowse, T. D., Beltaos, S., Gardner, J. T., Gibson, J. J., Granger, R. J., Leconte, R., ... & Toth, B. (2006). Climate change, flow regulation and land-use effects on the hydrology of the Peace-Athabasca-Slave system; Findings from the Northern Rivers Ecosystem Initiative. Environmental Monitoring and Assessment, 113(1), 167-197.

Prudhomme, C., Giuntoli, I., Robinson, E. L., Clark, D. B., Arnell, N. W., Dankers, R., ... & Wisser, D. (2014). Hydrological droughts in the 21st century, hotspots and uncertainties from a global multimodel ensemble experiment. Proceedings of the National Academy of Sciences, 111(9), 3262-3267.

Prudhomme, C., Wilby, R. L., Crooks, S., Kay, A. L., & Reynard, N. S. (2010). Scenario-neutral approach to climate change impact studies: application to flood risk. Journal of Hydrology, 390(3-4), 198-209.

Pui, A., Lal, A., & Sharma, A. (2011). How does the Interdecadal Pacific Oscillation affect design floods in Australia?. Water Resources Research, 47(5).

Pui, A., Sharma, A., Santoso, A., & Westra, S. (2012). Impact of the El Niño–Southern Oscillation, Indian Ocean dipole, and southern annular mode on daily to subdaily rainfall characteristics in east Australia. Monthly Weather Review, 140(5), 1665-1682.

Quilty, J., & Adamowski, J. (2020). A stochastic wavelet-based data-driven framework for forecasting uncertain multiscale hydrological and water resources processes. Environmental Modelling & Software, 130, 104718.

Quilty, J., Adamowski, J., & Boucher, M. A. (2019). A stochastic data-driven ensemble forecasting framework for water resources: A case study using ensemble members derived from a database of deterministic wavelet-based models. Water Resources Research, 55(1), 175-202.

Quilty, J., Adamowski, J., Khalil, B., & Rathinasamy, M. (2016). Bootstrap rank-ordered conditional mutual information (broCMI): A nonlinear input variable selection method for water resources modeling. Water Resources Research, 52(3), 2299-2326.

Quinn, N., Bates, P. D., Neal, J., Smith, A., Wing, O., Sampson, C., ... & Heffernan, J. (2019). The spatial dependence of flood hazard and risk in the United States. Water Resources Research, 55(3), 1890-1911.

Rajagopalan, B., & Lall, U. (1999). A k-nearest-neighbor simulator for daily precipitation and other weather variables. Water resources research, 35(10), 3089-3101.

Rajagopalan, B., Cook, E., Lall, U., & Ray, B. K. (2000). Spatiotemporal variability of ENSO and SST teleconnections to summer drought over the United States during the twentieth century. Journal of Climate, 13(24), 4244-4255.

Rajagopalan, B., Erkyihun, S. T., Lall, U., Zagona, E., & Nowak, K. (2019). A nonlinear dynamical systems-based modeling approach for stochastic simulation of streamflow and understanding predictability. Water Resources Research, 55(7), 6268-6284.

Rajagopalan, B., Salas, J. D., & Lall, U. (2010). Stochastic methods for modeling precipitation and streamflow. In Advances in data-based approaches for hydrologic modeling and forecasting (pp. 17-52).

Rao, A. R., & Yu, G. H. (1990). Gaussianity and linearity tests of hydrologic time series. Stochastic Hydrology and Hydraulics, 4(2), 121-134.

Rasmusson, E. M., & Wallace, J. M. (1983). Meteorological aspects of the El Nino/southern oscillation. Science, 222(4629), 1195-1202.

Rasouli, K., Scharold, K., Mahmood, T. H., Glenn, N. F., & Marks, D. (2020). Linking hydrological variations at local scales to regional climate teleconnection patterns. Hydrological Processes, 34(26), 5624-5641.

Ray, P. A., Bonzanigo, L., Wi, S., Yang, Y. C. E., Karki, P., Garcia, L. E., ... & Brown, C. M. (2018). Multidimensional stress test for hydropower investments facing climate, geophysical and financial uncertainty. Global Environmental Change, 48, 168-181.

Ray, P. A., Taner, M. Ü., Schlef, K. E., Wi, S., Khan, H. F., Freeman, S. S. G., & Brown, C. M. (2019). Growth of the Decision Tree: Advances in Bottom-Up Climate Change Risk Management. JAWRA Journal of the American Water Resources Association, 55(4), 920-937.

Ray, Patrick Alexander, et al. "Growth of the Decision Tree: Advances in Bottom-Up Climate Change Risk Management." JAWRA Journal of the American Water Resources Association 55.4 (2019): 920-937.

Regonda, S. K., Rajagopalan, B., Clark, M., & Pitlick, J. (2005). Seasonal cycle shifts in hydroclimatology over the western United States. Journal of climate, 18(2), 372-384.

Renard, B., & Lang, M. (2007). Use of a Gaussian copula for multivariate extreme value analysis: some case studies in hydrology. Advances in Water Resources, 30(4), 897-912.

Richards, R., Sanó, M., Roiko, A., Carter, R. W., Bussey, M., Matthews, J., & Smith, T. F. (2013). Bayesian belief modeling of climate change impacts for informing regional adaptation options. Environmental modelling & software, 44, 113-121.

Richter, B. D., Baumgartner, J. V., Powell, J., & Braun, D. P. (1996). A method for assessing hydrologic alteration within ecosystems. Conservation biology, 10(4), 1163-1174.

Rigby, R. A., & Stasinopoulos, D. M. (2005). Generalized additive models for location, scale and shape. Journal of the Royal Statistical Society: Series C (Applied Statistics), 54(3), 507-554.

Roach, T., Kapelan, Z., Ledbetter, R., & Ledbetter, M. (2016). Comparison of robust optimization and info-gap methods for water resource management under deep uncertainty. Journal of Water Resources Planning and Management, 142(9), 04016028.

Roberts, D. R., Bahn, V., Ciuti, S., Boyce, M. S., Elith, J., Guillera-Arroita, G., ... & Dormann, C. F. (2017). Cross-validation strategies for data with temporal, spatial, hierarchical, or phylogenetic structure. Ecography, 40(8), 913-929.

Robertson, D. E., & Wang, Q. J. (2012). A Bayesian approach to predictor selection for seasonal streamflow forecasting. Journal of Hydrometeorology, 13(1), 155-171.

Robinson, J. S., Sivapalan, M., & Snell, J. D. (1995). On the relative roles of hillslope processes, channel routing, and network geomorphology in the hydrologic response of natural catchments. Water Resources Research, 31(12), 3089-3101.

Rood, S. B., Foster, S. G., Hillman, E. J., Luek, A., & Zanewich, K. P. (2016). Flood moderation: Declining peak flows along some Rocky Mountain rivers and the underlying mechanism. Journal of Hydrology, 536, 174-182.

Rood, S. B., Pan, J., Gill, K. M., Franks, C. G., Samuelson, G. M., & Shepherd, A. (2008). Declining summer flows of Rocky Mountain rivers: Changing seasonal hydrology and probable impacts on floodplain forests. Journal of Hydrology, 349(3-4), 397-410.

Rottler, E., Bronstert, A., Bürger, G., & Rakovec, O. (2021). Projected changes in Rhine River flood seasonality under global warming. Hydrology and Earth System Sciences, 25(5), 2353-2371.

Rottler, E., Francke, T., Bürger, G., & Bronstert, A. (2020). Long-term changes in central European river discharge for 1869–2016: impact of changing snow covers, reservoir constructions and an intensified hydrological cycle. Hydrology and Earth System Sciences, 24(4), 1721-1740.

Rowe, J. S., & Sheard, J. W. (1981). Ecological land classification: a survey approach. Environmental management, 5(5), 451-464.

Roy, T., & Gupta, H. (2021). How certain are our uncertainty bounds? Accounting for sample variability in Monte Carlo-based uncertainty estimates. Environmental Modelling & Software, 136, 104931.

Sadegh, M., Ragno, E., & AghaKouchak, A. (2017). Multivariate Copula Analysis Toolbox (MvCAT): describing dependence and underlying uncertainty using a Bayesian framework. Water Resources Research, 53(6), 5166-5183.

Sagin, J., Sizo, A., Wheater, H., Jardine, T. D., & Lindenschmidt, K. E. (2015). A water coverage extraction approach to track inundation in the Saskatchewan River Delta, Canada. International Journal of Remote Sensing, 36(3), 764-781.

Salas, J. D. (1980). Applied modeling of hydrologic time series. Water Resources Publication.

Salas, J. D., & Obeysekera, J. T. B. (1982). ARMA model identification of hydrologic time series. Water Resources Research, 18(4), 1011-1021.

Salas, J. D., & Pegram, G. G. S. (1977). A seasonal multivariate multilag autoregressive model in hydrology. In Proc. Third Int. Symp. on Theoretical and Applied Hydrology, Colorado State Univ., Fort Collins, CO, USA.

Salas, J. D., Rajagopalan, B., Saito, L., & Brown, C. (2012). Special section on climate change and water resources: Climate nonstationarity and water resources management.

Salas, J. D., Tabios III, G. Q., & Bartolini, P. (1985). Approaches to multivariate modeling of water resources time series 1. JAWRA Journal of the American Water Resources Association, 21(4), 683-708.

Salathé Jr, E. P. (2005). Downscaling simulations of future global climate with application to hydrologic modelling. International Journal of Climatology: A Journal of the Royal Meteorological Society, 25(4), 419-436.

Salvadori, G., & De Michele, C. (2004). Frequency analysis via copulas: Theoretical aspects and applications to hydrological events. Water resources research, 40(12).

Salvadori, G., & De Michele, C. (2007). On the use of copulas in hydrology: theory and practice. Journal of Hydrologic Engineering, 12(4), 369-380.

Sapin, J., Rajagopalan, B., Saito, L., & Caldwell, R. J. (2017). A K-Nearest neighbor based stochastic multisite flow and stream temperature generation technique. Environmental Modelling & Software, 91, 87-94.

Satopaa, V., Albrecht, J., Irwin, D., & Raghavan, B. (2011, June). Finding a" kneedle" in a haystack: Detecting knee points in system behavior. In 2011 31st international conference on distributed computing systems workshops (pp. 166-171). IEEE.

Sauquet, E., Richard, B., Devers, A., & Prudhomme, C. (2019). Water restrictions under climate change: a Rhône–Mediterranean perspective combining bottom-up and top-down approaches. Hydrology and Earth System Sciences, 23(9), 3683-3710.

Savu, C., & Trede, M. (2006). Hierarchical Archimedean Copulas: International Conference on High Frequency Finance. Konstanz, Germany, 27.

Scanlon, B. R., Jolly, I., Sophocleous, M., & Zhang, L. (2007). Global impacts of conversions from natural to agricultural ecosystems on water resources: Quantity versus quality. Water resources research, 43(3).

Schellnhuber, H. J., Frieler, K., & Kabat, P. (2014). The elephant, the blind, and the intersectoral intercomparison of climate impacts. Proceedings of the National Academy of Sciences, 111(9), 3225-3227.

Schepsmeier, U., Stoeber, J., Brechmann, E. C., Graeler, B., Nagler, T., and Erhardt, T. (2016). VineCopula: Statistical Inference of Vine Copulas, R package version 2.0.5, https://CRAN.R-project.org/package=VineCopula (last access: 1 June 2017).

Schiermeier, Q. (2014). Water risk as world warms. Nature News, 505(7481), 10.

Schnorbus, M., Werner, A., & Bennett, K. (2014). Impacts of climate change in three hydrologic regimes in British Columbia, Canada. Hydrological Processes, 28(3), 1170-1189.

Seiller, G., & Anctil, F. (2014). Climate change impacts on the hydrologic regime of a Canadian river: comparing uncertainties arising from climate natural variability and lumped hydrological model structures. Hydrology and Earth System Sciences, 18(6), 2033-2047.

Sen, P. K. (1968). Estimates of the regression coefficient based on Kendall's tau. Journal of the American statistical association, 63(324), 1379-1389.

Serinaldi, F., & Kilsby, C. G. (2017). A blueprint for full collective flood risk estimation: demonstration for European river flooding. Risk Analysis, 37(10), 1958-1976.

Shabbar, A., Bonsal, B., & Khandekar, M. (1997). Canadian precipitation patterns associated with the Southern Oscillation. Journal of Climate, 10(12), 3016-3027.

Shakibaeinia, A., Kashyap, S., Dibike, Y. B., & Prowse, T. D. (2016). An integrated numerical framework for water quality modelling in cold-region rivers: A case of the lower Athabasca River. Science of the Total Environment, 569, 634-646.

Sharma, A. (2000). Seasonal to interannual rainfall probabilistic forecasts for improved water supply management: Part 1—A strategy for system predictor identification. Journal of Hydrology, 239(1-4), 232-239.

Sharma, A., & O'Neill, R. (2002). A nonparametric approach for representing interannual dependence in monthly streamflow sequences. Water resources research, 38(7), 5-1.

Sharma, A., Tarboton, D. G., & Lall, U. (1997). Streamflow simulation: A nonparametric approach. Water resources research, 33(2), 291-308.

Shaw, J., Taylor, R. B., Solomon, S., Christian, H. A., & Forbes, D. L. (1998). Potential impacts of global sea-level rise on Canadian coasts. Canadian Geographer/Le Géographe canadien, 42(4), 365-379.

Sheffield, J., Andreadis, K. M., Wood, E. F., & Lettenmaier, D. P. (2009). Global and continental drought in the second half of the twentieth century: Severity–area–duration analysis and temporal variability of large-scale events. Journal of Climate, 22(8), 1962-1981.

Shiklomanov, I. A., & Rodda, J. C. (Eds.). (2004). World water resources at the beginning of the twenty-first century. Cambridge University Press.

Shoda, M. E., Gorbach, K. R., Benbow, M. E., & Burky, A. J. (2012). Cascade macroinvertebrate assemblages for in-stream flow criteria and biomonitoring of tropical mountain streams. River research and applications, 28(3), 326-337.

Shojaeezadeh, S. A., Nikoo, M. R., McNamara, J. P., AghaKouchak, A., & Sadegh, M. (2018). Stochastic modeling of suspended sediment load in alluvial rivers. Advances in Water Resources, 119, 188-196.

Shook, K., & Pomeroy, J. (2012). Changes in the hydrological character of rainfall on the Canadian prairies. Hydrological Processes, 26(12), 1752-1766.

Shook, K., Pomeroy, J., & van der Kamp, G. (2015). The transformation of frequency distributions of winter precipitation to spring streamflow probabilities in cold regions; case studies from the Canadian Prairies. Journal of Hydrology, 521, 395-409.

Shortridge, J. E., & Zaitchik, B. F. (2018). Characterizing climate change risks by linking robust decision frameworks and uncertain probabilistic projections. Climatic Change, 151(3), 525-539.

Shrestha, D. L., Robertson, D. E., Wang, Q. J., Pagano, T. C., & Hapuarachchi, H. A. P. (2013). Evaluation of numerical weather prediction model precipitation forecasts for short-term streamflow forecasting purpose. Hydrology and Earth System Sciences, 17(5), 1913.

Sikorska, A. E., Viviroli, D., & Seibert, J. (2015). Flood-type classification in mountainous catchments using crisp and fuzzy decision trees. Water Resources Research, 51(10), 7959-7976.

Simonovic, S. P. (2017). Bringing future climatic change into water resources management practice today. Water Resources Management, 31(10), 2933-2950.

Singh, R., Wagener, T., Crane, R., Mann, M. E., & Ning, L. (2014). A vulnerability driven approach to identify adverse climate and land use change combinations for critical hydrologic indicator thresholds: Application to a watershed in Pennsylvania, USA. Water Resources Research, 50(4), 3409-3427.

Sklar, M. (1959). Fonctions de repartition an dimensions et leurs marges. Publ. inst. statist. univ. Paris, 8, 229-231.

Slater, L. J., & Villarini, G. (2018). Enhancing the predictability of seasonal streamflow with a statistical-dynamical approach. Geophysical Research Letters, 45(13), 6504-6513.

Smith, L. C., Pavelsky, T. M., MacDonald, G. M., Shiklomanov, A. I., & Lammers, R. B. (2007). Rising minimum daily flows in northern Eurasian rivers: A growing influence of groundwater in the high-latitude hydrologic cycle. Journal of Geophysical Research: Biogeosciences, 112(G4).

Smith, R. L., Tebaldi, C., Nychka, D., & Mearns, L. O. (2009). Bayesian modeling of uncertainty in ensembles of climate models. Journal of the American Statistical Association, 104(485), 97-116.

Souza Filho, F. A., & Lall, U. (2003). Seasonal to interannual ensemble streamflow forecasts for Ceara, Brazil: Applications of a multivariate, semiparametric algorithm. Water Resources Research, 39(11).

Spence, C. M., & Brown, C. M. (2018). Decision analytic approach to resolving divergent climate assumptions in water resources planning. Journal of Water Resources Planning and Management, 144(9), 04018054.

Spence, C., & Phillips, R. W. (2015). Refining understanding of hydrological connectivity in a boreal catchment. Hydrological Processes, 29(16), 3491-3503.

Spence, C., Guan, X. J., Phillips, R., Hedstrom, N., Granger, R., & Reid, B. (2010). Storage dynamics and streamflow in a catchment with a variable contributing area. Hydrological Processes, 24(16), 2209-2221.

Sperotto, A., Molina, J. L., Torresan, S., Critto, A., & Marcomini, A. (2017). Reviewing Bayesian Networks potentials for climate change impacts assessment and management: A multi-risk perspective. Journal of environmental management, 202, 320-331.

Srinivas, V. V., & Srinivasan, K. (2001). Post-blackening approach for modeling periodic streamflows. Journal of Hydrology, 241(3-4), 221-269.

Srinivas, V. V., & Srinivasan, K. (2005). Hybrid moving block bootstrap for stochastic simulation of multi-site multi-season streamflows. Journal of Hydrology, 302(1-4), 307-330.

Srinivas, V. V., Tripathi, S., Rao, A. R., & Govindaraju, R. S. (2008). Regional flood frequency analysis by combining self-organizing feature map and fuzzy clustering. Journal of Hydrology, 348(1-2), 148-166.

St. Jacques, J. M., & Sauchyn, D. J. (2009). Increasing winter baseflow and mean annual streamflow from possible permafrost thawing in the Northwest Territories, Canada. Geophysical Research Letters, 36(1).

Stacy, E. W. (1962). A generalization of the gamma distribution. The Annals of mathematical statistics, 1187-1192.

Stahl, K., Hisdal, H., Hannaford, J., Tallaksen, L. M., Van Lanen, H. A. J., Sauquet, E., ... & Jódar, J. (2010). Streamflow trends in Europe: evidence from a dataset of near-natural catchments. Hydrology and Earth System Sciences, 14(12), 2367-2382.

Stahl, K., Moore, R. D., Shea, J. M., Hutchinson, D., & Cannon, A. J. (2008). Coupled modelling of glacier and streamflow response to future climate scenarios. Water Resources Research, 44(2).

Stainforth, D. A., Aina, T., Christensen, C., Collins, M., Faull, N., Frame, D. J., ... & Allen, M. R. (2005). Uncertainty in predictions of the climate response to rising levels of greenhouse gases. Nature, 433(7024), 403-406.

Stainforth, D. A., Downing, T. E., Washington, R., Lopez, A., & New, M. (2007). Issues in the interpretation of climate model ensembles to inform decisions. Philosophical Transactions of the Royal Society A: Mathematical, Physical and Engineering Sciences, 365(1857), 2163-2177.

Stakhiv, E. Z. (2011). Pragmatic approaches for water management under climate change uncertainty 1. JAWRA Journal of the American Water Resources Association, 47(6), 1183-1196.

Stasinopoulos, D. M., & Rigby, R. A. (2007). Generalized additive models for location scale and shape (GAMLSS) in R. Journal of Statistical Software, 23(7), 1-46.

Stedinger, J. R., & Taylor, M. R. (1982). Synthetic streamflow generation: 1. Model verification and validation. Water resources research, 18(4), 909-918.

Stedinger, J. R., Lettenmaier, D. P., & Vogel, R. M. (1985). Multisite ARMA (1,1) and disaggregation models for annual streamflow generation. Water Resources Research, 21(4), 497-509.

Steinschneider, S., & Brown, C. (2013). A semiparametric multivariate, multisite weather generator with low-frequency variability for use in climate risk assessments. Water resources research, 49(11), 7205-7220.

Steinschneider, S., McCrary, R., Wi, S., Mulligan, K., Mearns, L. O., & Brown, C. (2015). Expanded decision-scaling framework to select robust long-term water-system plans under hydroclimatic uncertainties. Journal of Water Resources Planning and Management, 141(11), 04015023.

Steinschneider, S., Ray, P., Rahat, S. H., & Kucharski, J. (2019). A weather-regime-based stochastic weather generator for climate vulnerability assessments of water systems in the western United States. Water Resources Research, 55(8), 6923-6945.

Steirou, E., Gerlitz, L., Apel, H., & Merz, B. (2017). Links between large-scale circulation patterns and streamflow in Central Europe: A review. Journal of Hydrology, 549, 484-500.

Stewart, I. T., Cayan, D. R., & Dettinger, M. D. (2005). Changes toward earlier streamflow timing across western North America. Journal of climate, 18(8), 1136-1155.

Stoutenborough, J. W., & Vedlitz, A. (2014). Public attitudes toward water management and drought in the United States. Water Resources Management, 28(3), 697-714.

Stuart, I. G., & Jones, M. J. (2006). Movement of common carp, Cyprinus carpio, in a regulated lowland Australian river: implications for management. Fisheries Management and Ecology, 13(4), 213-219.

Su, B., Huang, J., Zeng, X., Gao, C., & Jiang, T. (2017). Impacts of climate change on streamflow in the upper Yangtze River basin. Climatic change, 141(3), 533-546.

Sunde, M. G., He, H. S., Hubbart, J. A., & Urban, M. A. (2017). Integrating downscaled CMIP5 data with a physically based hydrologic model to estimate potential climate change impacts on streamflow processes in a mixed-use watershed. Hydrological Processes, 31(9), 1790-1803.

Sutton, R. T., & Hodson, D. L. (2005). Atlantic Ocean forcing of North American and European summer climate. science, 309(5731), 115-118.

Tamaddun, K. A., Kalra, A., & Ahmad, S. (2017). Wavelet analyses of western US streamflow with ENSO and PDO. Journal of Water and Climate Change, 8(1), 26-39.

Tamaddun, K. A., Kalra, A., & Ahmad, S. (2019). Spatiotemporal variation in the continental US streamflow in association with large-scale climate signals across multiple spectral bands. Water Resources Management, 33(6), 1947-1968.

Tan, X., Gan, T. Y., & Shao, D. (2017). Effects of persistence and large-scale climate anomalies on trends and change points in extreme precipitation of Canada. Journal of Hydrology, 550, 453-465.

Taner, M. Ü., Ray, P., & Brown, C. (2019). Incorporating multidimensional probabilistic information into robustness-based water systems planning. Water Resources Research, 55(5), 3659-3679.

Tarasova, L., Merz, R., Kiss, A., Basso, S., Blöschl, G., Merz, B., ... & Wietzke, L. (2019). Causative classification of river flood events. Wiley Interdisciplinary Reviews: Water, 6(4), e1353.

Tarboton, D. G., Sharma, A., & Lall, U. (1998). Disaggregation procedures for stochastic hydrology based on nonparametric density estimation. Water resources research, 34(1), 107-119.

Taylor, K. E. (2001). Summarizing multiple aspects of model performance in a single diagram. Journal of Geophysical Research: Atmospheres, 106(D7), 7183-7192.

Ternynck, C., Ben Alaya, M. A., Chebana, F., Dabo-Niang, S., & Ouarda, T. B. (2016). Streamflow hydrograph classification using functional data analysis. Journal of hydrometeorology, 17(1), 327-344.

Teutschbein, C., & Seibert, J. (2012). Bias correction of regional climate model simulations for hydrological climate-change impact studies: Review and evaluation of different methods. Journal of hydrology, 456, 12-29.

Thieken, A. H., Apel, H., & Merz, B. (2015). Assessing the probability of large-scale flood loss events: a case study for the river R hine, G ermany. Journal of Flood Risk Management, 8(3), 247-262.

Thistle, M. E., & Caissie, D. (2013). Trends in air temperature, total precipitation, and streamflow characteristics in eastern Canada. Fisheries and Oceans Canada.

Thomas, J. A., & Fiering, M. B. (2013). 12. Mathematical Synthesis of Streamflow Sequences for the Analysis of River Basins by Simulation. In Design of water-resource systems (pp. 459-493). Harvard University Press.

Thompson, D. W., & Wallace, J. M. (1998). The Arctic Oscillation signature in the wintertime geopotential height and temperature fields. Geophysical research letters, 25(9), 1297-1300.

Thorne, R., & Woo, M. K. (2011). Streamflow response to climatic variability in a complex mountainous environment: Fraser River Basin, British Columbia, Canada. Hydrological Processes, 25(19), 3076-3085.

Timmermann, A., Oberhuber, J., Bacher, A., Esch, M., Latif, M., & Roeckner, E. (1999). Increased El Niño frequency in a climate model forced by future greenhouse warming. Nature, 398(6729), 694-697.

Tonkin, J. D., Merritt, D. M., Olden, J. D., Reynolds, L. V., & Lytle, D. A. (2018). Flow regime alteration degrades ecological networks in riparian ecosystems. Nature ecology & evolution, 2(1), 86-93.

Toth, Z., Talagrand, O., Candille, G., & Zhu, Y. (2003). Probability and ensemble forecasts. Forecast verification: A practitioner's guide in atmospheric science, 137-163.

Tran, H. D., Muttil, N., & Perera, B. J. C. (2016). Enhancing accuracy of autoregressive time series forecasting with input selection and wavelet transformation. Journal of Hydroinformatics, 18(5), 791-802.

Trenberth, K. E. (1997). The definition of el-nino. Bulletin of the American Meteorological Society, 78(12), 2771-2778.

Trenberth, K. E., & Shea, D. J. (2006). Atlantic hurricanes and natural variability in 2005. Geophysical research letters, 33(12).

Trunk, G. V. (1979). A problem of dimensionality: A simple example. IEEE Transactions on pattern analysis and machine intelligence, (3), 306-307.

Tsoukalas, I., Efstratiadis, A., & Makropoulos, C. (2018a). Stochastic periodic autoregressive to anything (SPARTA): Modeling and simulation of cyclostationary processes with arbitrary marginal distributions. Water Resources Research, 54(1), 161-185.

Tsoukalas, I., Papalexiou, S. M., Efstratiadis, A., & Makropoulos, C. (2018). A cautionary note on the reproduction of dependencies through linear stochastic models with non-Gaussian white noise. Water, 10(6), 771.

Turner, S. W., Marlow, D., Ekström, M., Rhodes, B. G., Kularathna, U., & Jeffrey, P. J. (2014). Linking climate projections to performance: A yield-based decision scaling assessment of a large urban water resources system. Water Resources Research, 50(4), 3553-3567.

Van Tra, T., Thinh, N. X., & Greiving, S. (2018). Combined top-down and bottom-up climate change impact assessment for the hydrological system in the Vu Gia-Thu Bon River Basin. Science of the Total Environment, 630, 718-727.

Vano, J. A., Scott, M. J., Voisin, N., Stöckle, C. O., Hamlet, A. F., Mickelson, K. E., ... & Lettenmaier, D. P. (2010). Climate change impacts on water management and irrigated agriculture in the Yakima River Basin, Washington, USA. Climatic Change, 102(1), 287-317.

Vicuna, S., Dracup, J. A., Lund, J. R., Dale, L. L., & Maurer, E. P. (2010). Basin-scale water system operations with uncertain future climate conditions: Methodology and case studies. Water Resources Research, 46(4).

Viles, H. A., & Goudie, A. S. (2003). Interannual, decadal and multidecadal scale climatic variability and geomorphology. Earth-Science Reviews, 61(1-2), 105-131.

Viviroli, D., Archer, D. R., Buytaert, W., Fowler, H. J., Greenwood, G. B., Hamlet, A. F., ... & Woods, R. (2011). Climate change and mountain water resources: overview and recommendations for research, management and policy. Hydrology and Earth System Sciences, 15(2), 471-504.

Vogel, R. M., & Shallcross, A. L. (1996). The moving blocks bootstrap versus parametric time series models. Water Resources Research, 32(6), 1875-1882.

Vormoor, K., Lawrence, D., Heistermann, M., & Bronstert, A. (2015). Climate change impacts on the seasonality and generation processes of floods–projections and uncertainties for catchments with mixed snowmelt/rainfall regimes. Hydrology and Earth System Sciences, 19(2), 913-931.

Vörösmarty, C. J., Green, P., Salisbury, J., & Lammers, R. B. (2000). Global water resources: vulnerability from climate change and population growth. science, 289(5477), 284-288.

Vörösmarty, C. J., Léveque, C., Revenga, C., Bos, R., Caudill, C., Chilton, J., ... & Reidy, C. A. (2005). Fresh water. Millennium ecosystem assessment, 1, 165-207.

Vörösmarty, C. J., McIntyre, P. B., Gessner, M. O., Dudgeon, D., Prusevich, A., Green, P., ... & Davies, P. M. (2010). Global threats to human water security and river biodiversity. nature, 467(7315), 555-561.

Wade, NL, Martin, J., & Whitfield, PH (2001). Hydrologic and climatic zonation of Georgia basin, British Columbia. Canadian Water Resources Journal , 26 (1), 43-70.

Walvoord, M. A., & Striegl, R. G. (2007). Increased groundwater to stream discharge from permafrost thawing in the Yukon River basin: Potential impacts on lateral export of carbon and nitrogen. Geophysical Research Letters, 34(12).

Wang, C. T., Gupta, V. K., & Waymire, E. D. (1981). A geomorphologic synthesis of nonlinearity in surface runoff. Water Resources Research, 17(3), 545-554.

Wang, C., Chang, N. B., & Yeh, G. T. (2009). Copula-based flood frequency (COFF) analysis at the confluences of river systems. Hydrological Processes: An International Journal, 23(10), 1471-1486.

Wang, J., Nathan, R., & Horne, A. (2018). Assessing the impact of climate change on environmental outcomes in the context of natural climate variability. Journal of Water Resources Planning and Management, 144(12), 05018016.

Wang, Q. J., & Robertson, D. E. (2011). Multisite probabilistic forecasting of seasonal flows for streams with zero value occurrences. Water Resources Research, 47(2).

Wang, Q. J., Robertson, D. E., & Chiew, F. H. S. (2009). A Bayesian joint probability modeling approach for seasonal forecasting of streamflows at multiple sites. Water Resources Research, 45(5).

Wang, W., Dong, Z., Lall, U., Dong, N., & Yang, M. (2019). Monthly streamflow simulation for the headwater catchment of the Yellow River basin with a hybrid statistical-dynamical model. Water Resources Research, 55(9), 7606-7621.

Wang, W., Vrijling, J. K., Van Gelder, P. H., & Ma, J. (2006). Testing for nonlinearity of streamflow processes at different timescales. Journal of Hydrology, 322(1-4), 247-268.

Wang, X., Yang, T., Yong, B., Krysanova, V., Shi, P., Li, Z., & Zhou, X. (2018). Impacts of climate change on flow regime and sequential threats to riverine ecosystem in the source region of the Yellow River. Environmental Earth Sciences, 77(12), 1-14.

Ward, P. J., Eisner, S., Flörke, M., Dettinger, M. D., & Kummu, M. (2014). Annual flood sensitivities to El Niño–Southern Oscillation at the global scale. Hydrology and Earth System Sciences, 18(1), 47-66.

Wasko, C., & Sharma, A. (2017). Global assessment of flood and storm extremes with increased temperatures. Scientific reports, 7(1), 1-8.

Watson, R. T., Zinyowera, M. C., & Moss, R. H. (1996). Climate change 1995. Impacts, adaptations and mitigation of climate change: scientific-technical analyses.

Weaver, C. P., Lempert, R. J., Brown, C., Hall, J. A., Revell, D., & Sarewitz, D. (2013). Improving the contribution of climate model information to decision making: the value and demands of robust decision frameworks. Wiley Interdisciplinary Reviews: Climate Change, 4(1), 39-60.

Webster, M. D., Babiker, M., Mayer, M., Reilly, J. M., Harnisch, J., Hyman, R., ... & Wang, C. (2002). Uncertainty in emissions projections for climate models. Atmospheric environment, 36(22), 3659-3670.

Whateley, S., Steinschneider, S., & Brown, C. (2014). A climate change range-based method for estimating robustness for water resources supply. Water Resources Research, 50(11), 8944-8961.

Whateley, S., Steinschneider, S., & Brown, C. (2016). Selecting stochastic climate realizations to efficiently explore a wide range of climate risk to water resource systems. Journal of Water Resources Planning and Management, 142(6), 06016002.

Wheater, H. S., & Gober, P. (2015). Water security and the science agenda. Water Resources Research, 51(7), 5406-5424.

Wheater, H., & Gober, P. (2013). Water security in the Canadian Prairies: science and management challenges. Philosophical Transactions of the Royal Society A: Mathematical, Physical and Engineering Sciences, 371(2002), 20120409.

Whelan, N. (2004). Sampling from Archimedean copulas. Quantitative finance, 4(3), 339.

Whitfield, P. H. (2001). Linked hydrologic and climate variations in British Columbia and Yukon. Environmental Monitoring and Assessment, 67(1), 217-238.

Whitfield, P. H., & Cannon, A. J. (2000). Recent variations in climate and hydrology in Canada. Canadian water resources journal, 25(1), 19-65.

Whitfield, P. H., & Pomeroy, J. W. (2016). Changes to flood peaks of a mountain river: implications for analysis of the 2013 flood in the Upper Bow River, Canada. Hydrological Processes, 30(25), 4657-4673.

Whitfield, P. H., Moore, R. D., Fleming, S. W., & Zawadzki, A. (2010). Pacific decadal oscillation and the hydroclimatology of western Canada—Review and prospects. Canadian Water Resources Journal, 35(1), 1-28.

Whitfield, P. H., Shook, K. R., & Pomeroy, J. W. (2020). Spatial patterns of temporal changes in Canadian prairie streamflow using an alternative trend assessment approach. Journal of Hydrology, 582, 124541.

Wiken, E. B. (1986). Terrestrial ecozones of Canada. Environment Canada, Lands Directorate.

Wilby, R. L., & Dessai, S. (2010). Robust adaptation to climate change. Weather, 65(7), 180-185.

Wilby, R. L., & Harris, I. (2006). A framework for assessing uncertainties in climate change impacts: Low-flow scenarios for the River Thames, UK. Water resources research, 42(2).

Wilby, R. L., & Wigley, T. M. (1997). Downscaling general circulation model output: a review of methods and limitations. Progress in physical geography, 21(4), 530-548.

Wilby, R. L., Dawson, C. W., & Barrow, E. M. (2002). SDSM—a decision support tool for the assessment of regional climate change impacts. Environmental Modelling & Software, 17(2), 145-157.

Wilby, R. L., Dawson, C. W., Murphy, C., Connor, P. O., & Hawkins, E. (2014). The statistical downscaling model-decision centric (SDSM-DC): conceptual basis and applications. Climate Research, 61(3), 259-276.

Wilby, R. L., Hay, L. E., & Leavesley, G. H. (1999). A comparison of downscaled and raw GCM output: implications for climate change scenarios in the San Juan River basin, Colorado. Journal of Hydrology, 225(1-2), 67-91.

Wilby, R. L., Wigley, T. M. L., Conway, D., Jones, P. D., Hewitson, B. C., Main, J., & Wilks, D. S. (1998). Statistical downscaling of general circulation model output: A comparison of methods. Water resources research, 34(11), 2995-3008.

Wiley, M. W., & Palmer, R. N. (2008). Estimating the impacts and uncertainty of climate change on a municipal water supply system. Journal of Water Resources Planning and Management, 134(3), 239-246.

Wing, O. E., Quinn, N., Bates, P. D., Neal, J. C., Smith, A. M., Sampson, C. C., ... & Alfieri, L. (2020). Toward Global Stochastic River Flood Modeling. Water Resources Research, 56(8), e2020WR027692.

Wolfe, J. D., Shook, K. R., Spence, C., & Whitfield, C. J. (2019). A watershed classification approach that looks beyond hydrology: application to a semi-arid, agricultural region in Canada. Hydrology and Earth System Sciences, 23(9), 3945-3967.

Wong, J. S., Razavi, S., Bonsal, B. R., Wheater, H. S., & Asong, Z. E. (2017). Inter-comparison of daily precipitation products for large-scale hydro-climatic applications over Canada. Hydrology and Earth System Sciences, 21(4), 2163-2185.

Woo, M. K., Thorne, R., Szeto, K., & Yang, D. (2008). Streamflow hydrology in the boreal region under the influences of climate and human interference. Philosophical Transactions of the Royal Society B: Biological Sciences, 363(1501), 2249-2258.

Wood, A. W., Maurer, E. P., Kumar, A., & Lettenmaier, D. P. (2002). Long-range experimental hydrologic forecasting for the eastern United States. Journal of Geophysical Research: Atmospheres, 107(D20), ACL-6.

Worland, S. C., Steinschneider, S., Farmer, W., Asquith, W., & Knight, R. (2019). Copula theory as a generalized framework for flow-duration curve based streamflow estimates in ungaged and partially gaged catchments. Water Resources Research, 55(11), 9378-9397.

Wu, Y., Gan, T. Y., She, Y., Xu, C., & Yan, H. (2020). Five centuries of reconstructed streamflow in Athabasca River Basin, Canada: Non-stationarity and teleconnection to climate patterns. Science of The Total Environment, 746, 141330.

Xie, X. L., & Beni, G. (1991). A validity measure for fuzzy clustering. IEEE Transactions on pattern analysis and machine intelligence, 13(8), 841-847.

Yang, D., Shi, X., & Marsh, P. (2015). Variability and extreme of Mackenzie River daily discharge during 1973–2011. Quaternary international, 380, 159-168.

Ye, B., Yang, D., & Kane, D. L. (2003). Changes in Lena River streamflow hydrology: Human impacts versus natural variations. Water resources research, 39(7).

Yu, M., Li, Q., Hayes, M. J., Svoboda, M. D., & Heim, R. R. (2014). Are droughts becoming more frequent or severe in China based on the standardized precipitation evapotranspiration index: 1951–2010?. International Journal of Climatology, 34(3), 545-558.

Yue, S., Pilon, P., & Phinney, B. O. B. (2003). Canadian streamflow trend detection: impacts of serial and cross-correlation. Hydrological Sciences Journal, 48(1), 51-63.

Zadeh, L. A., (1965). Fuzzy sets. Information and control, 8(3), 338-353.

Zaerpour, M., Hatami, S., Sadri, J., & Nazemi, A. (2019). A fuzzy clustering approach to diagnosis of change in a natural streamflow regime.

Zaerpour, M., Hatami, S., Sadri, J., & Nazemi, A. (2021a). A global algorithm for identifying changing streamflow regimes: application to Canadian natural streams (1966–2010). Hydrology and Earth System Sciences, 25(9), 5193-5217.

Zaerpour, M., Papalexiou, S. M., & Nazemi, A. (2021b). Informing Stochastic Streamflow Generation by Large-Scale Climate Indices at Single and Multiple Sites. Advances in Water Resources, 104037.

Zaerpour, M., Hatami, S., Sadri, J., & Nazemi, A. (2019). A FUZZY CLUSTERING APPROACH TO DIAGNOSIS OF CHANGE IN NATURAL STREAMFLOW REGIME.

Zamani, H., Shekari, M., & Pakdaman, Z. (2020). Modeling insurance data using generalized gamma regression. Journal of Statistical Modelling: Theory and Applications, 1(1), 169-177.

Zandmoghaddam, S., Nazemi, A., Hassanzadeh, E., & Hatami, S. (2019). Representing local dynamics of water resource systems through a data-driven emulation approach. Water Resources Management, 33(10), 3579-3594.

Zhang, L., & Singh, V. P. (2019). Copulas and their applications in water resources engineering. Cambridge University Press.

Zscheischler, J., & Seneviratne, S. I. (2017). Dependence of drivers affects risks associated with compound events. Science advances, 3(6), e1700263.

Additional materials for "Uncertainty in Bottom-Up Vulnerability Assessments of Water Supply Systems due to Regional Streamflow Generation under Changing Conditions"
 Appendix A1. Single-site streamflow generation using temporal copulas

The sampling strategy in single-site streamflow reconstruction is based on the use of lag-1 temporal copula functions. The temporal lag-1 copula function can be defined as:

$$F_{U,V}(u,v) = C(u^*, v^*) \ \ Where \ u, w \ \in R \ and \ u^* = F_U(u), \ w^* = F_V(v) \tag{A.1}$$

where C is the copula function, u and v are two random variables – here consecutive streamflow values at a sub-annual time scale; and F_X and F_Y are the corresponding empirical Cumulative Distribution Functions ($CDFs$). Knowing the empirical CDF of the streamflow value at the previous timestep $j-1$ and the joint copula function representing the dependence between timestep j and $j-1$, the non-exceedance probability of the streamflow at the timestep j can be estimated conditionally as the following (see Salvadori and De Michele 2007):

$$C_{u^*}(v^*) = P\{F_{p,j}(Flow_{p,j} \leq v | F_{p,j-1}(Flow^*_{p,j-1}) = u^*)\} = \frac{\partial}{\partial u} C_{j,j-1}(u^*, v^*) \tag{A.2}$$

and accordingly:

$$Flow^*_{P,j} = F^{-1}_{P,j}\{C^{-1}_{u^*}(v^*)\} \tag{A.3}$$

where $Flow^*_{p,j}$ is the sampled flow at timestep j in the streamflow reach p; $Flow^*_{p,j-1}$ is the sampled flow at timestep $j-1$; $C_{j,j-1}$ is the parametric bivariate copula function between consecutive $CDFs$ at timesteps j and $j-1$; and P is the conditional CDF.
 Appendix A2. Multi-site streamflow extension using spatial copula functions

Copulas can also provide an alternative approach to spatial extension. Similar to temporal resampling, this is done by bivariate parametric copulas that represent the spatial dependencies between primary and secondary reaches at the same timestep. Considering observed streamflow values at primary and secondary tributaries in an identical sub-annual timestep, the spatial copula function can be defined as:

$$F_{U,W}(u,w) = C'(u^*, w^*) \ \ Where \ u, w \ \in R \ and \ u^* = F_U(u), \ w^* = F_W(w) \tag{A.4}$$

where u and w are two random variables (here corresponding streamflow quantiles in primary and secondary streamflow reaches), and F_U and F_W are the corresponding $CDFs$, respectively. Knowing the marginal CDF of the streamflow at the primary site and the spatial copula function $C'(u^*, w^*)$, the flow quantile at secondary site can be sampled conditionally as:

$$C'_{u^*}(w^*) = P\{F_{s,j}(Flow_{s,j} \leq w | F_{p,j}(Flow^*_{p,j}) = u^*)\} = \frac{\partial}{\partial u} C'_{j,j}(u^*, w^*) \tag{A.5}$$

and accordingly:

$$Flow_{s,j}^* = F_{s,j}^{-1}\{C'^{-1}_{u^*}(w^*)\} \tag{A.6}$$

where $Flow_{s,j}^*$ is the sampled flow at timestep j in the secondary stream; $Flow_{p,j}^*$ is the sampled flow at timestep j in the primary reach; $C'_{j,j}$ is the parametric bivariate copula function between corresponding flow $CDFs$ at the primary and secondary reaches during the timestep j; and P is the conditional CDF.

Appendix A3. Multi-site streamflow extension using spatiotemporal copula functions

Although spatial copulas are able to represent the dependence between two streamflow reaches at unique time steps, they do not explicitly represent the temporal dependence at the secondary site. To tackle this problem, a trivariate copula is required to fully represent the spatiotemporal dependence by linking the lag-0 spatial dependence at primary and secondary sites with the lag-1 temporal dependence at the secondary site. Chen et al. (2015) showed that using conditional copula functions, such trivariate copulas can be decomposed into three bivariate copulas, in which parameters of each bivariate model can be estimated independently. In the context of streamflow generation, having the flow u at the primary site and time t as well as the flow v and w at the secondary site during time $t-1$ and t respectively, the trivariate copula $F(u,v,w)$ can be described as:

$$F_{U,V,W}(u,v,w) = \int_{-\infty}^{w} F_{U,V}(u,v|w)dF_W(w) \tag{A.7}$$

According to Sklar's theorem, $F_{U,V}(u,v|w)$ can be described as:

$$F_{U,V}(u,v|w) = C_{U,V}\left((F_{U|W}(u|w),F_{V|W}(v|w)\right) \tag{A.8}$$

and accordingly Equation 7 can be decomposed into 3 bivariate copulas as the following:

$$F_{U,V,W}(u,v,w) = \int_{-\infty}^{w} C_{U,V}\left((F_{U|W}(u|w),F_{V|W}(v|w)\right)dF_W(w) \tag{A.9}$$

In addition, $F_{U|W}(u|w)$ and $F_{V|W}(v|w)$ can be described as:

$$F_{U|W}(u|w) = \frac{\partial\left(C_{U,W}(u,w)\right)}{\partial w}; F_{U|W}(u|w) = \frac{\partial\left(C_{V,W}(v,w)\right)}{\partial w} \tag{A.10}$$

Equations 9 and 10 together provide a theoretical basis for sampling the streamflow at the secondary stream by representing short-term spatiotemporal dependence between the reaches using three mutually independent copula functions. Refer to original article of Chen et al. (2015) for the step-by-step simulation procedure.

Appendix A4. The choice of parametric copula functions

Temporal copula functions should maintain the lag-1 dependence structure at each tributary. Fig. A.1 compares the observed lag-1 Kendall's taus with the corresponding expected values, obtained using the three copulas at the NSR (top row) and the SSR (bottom row). Observed dependencies between consecutive weekly timesteps are shown in solid black lines whereas expected values obtained by copula functions are displayed using dashed, dotted and dash-dotted lines for Frank, Clayton and Gaussian copulas, respectively. In general, the SSR shows stronger lag-1 temporal dependence compared to the NSR, particularly during the cold periods of January and February. This is due to intensive regulation in southern Alberta that amplifies the temporal dependencies in the weekly flow. For both tributaries, the Frank copula outperforms the other copulas. The RMSE measures for the Frank, Clayton and Gaussian copulas for the NSR are 0.019, 0.087, 0.039, respectively. These measures for SSR are 0.019, 0.099, 0.047, respectively.
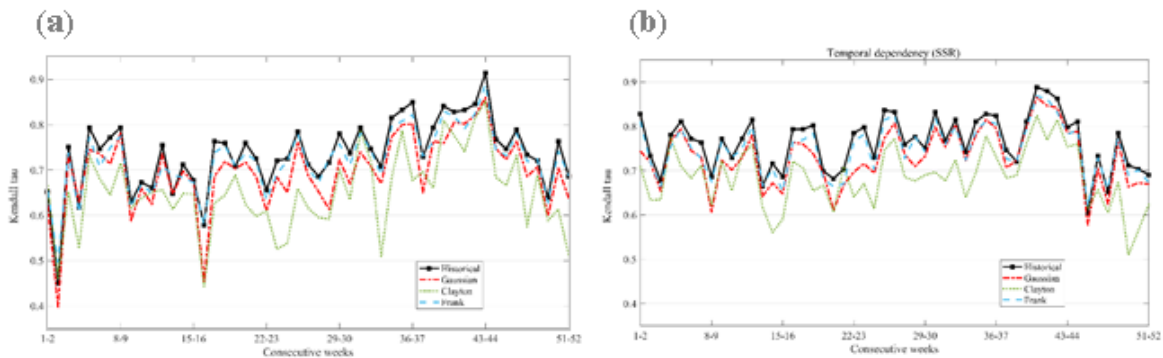

Figure A1. Representation of the lag-1 temporal dependency within synthesized weekly flows at NSR (first row) and SSR (second row) using Gaussian, Clayton and Frank copulas.

Similarly, we compare the performance of the three copula functions in preserving the lag-0 dependence structure between the two tributaries – see Fig. A2 below. In general, lag-0 spatial dependencies between NSR and SSR are stronger during the warm seasons, which can be better captured by the Frank copula. The *RMSE* for Frank copula is 0.02 whereas it is 0.03 and 0.07 for Gaussian and Clayton copulas, respectively. Accordingly, we build up the M3 and M4 using Frank copulas for representing both lag-1 dependencies at the primary reach and lag-0 spatial dependencies between primary and secondary tributaries.
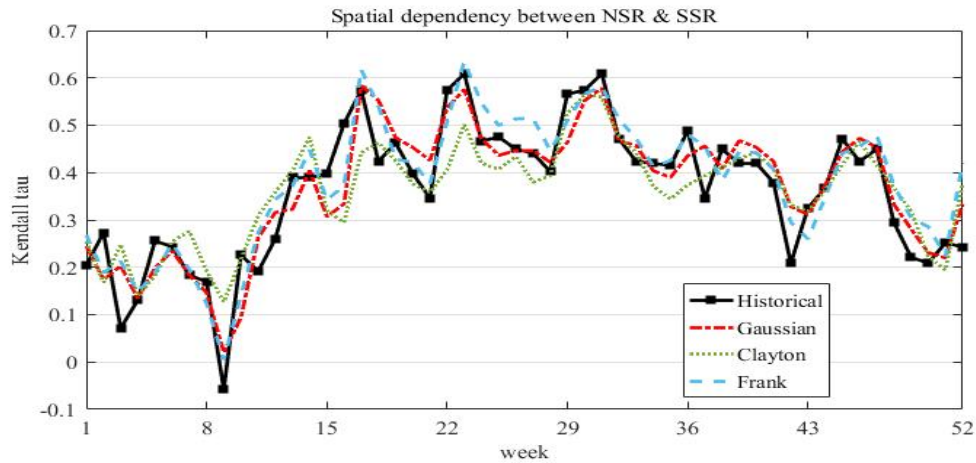
Figure A2. Representation of lag-0 spatial dependencies between synthesized weekly SSR and NSR flows using Gaussian, Clayton and Frank copulas

Appendix A5. Supporting materials for skills in reconstructing historical streamflow characteristics

Table A1. Differences among representative ensemble skills of the four spatial extension schemes in terms of reconstructing ten long-term streamflow characteristics at the NSR and SSR during the baseline period of 1980 to 2010. The differences are characterized by *p*-values of single-factor ANOVA with Bonferroni correction for multiple pairwise comparisons.

Timing of the annual peak		NSR				Annual volume		NSR			
		M1	M2	M3	M4			M1	M2	M3	M4
	M1	-	0.00	0.00	0.00		M1	-	**0.68**	0.00	0.00
SSR	M2	0.00	-	0.00	0.00	SSR	M2	0.00	-	0.00	0.00
	M3	0.00	0.00	-	0.00		M3	0.00	0.01	-	0.00
	M4	0.00	0.00	0.00	-		M4	0.00	0.00	0.00	-
Annual peak		NSR				Q10		NSR			
		M1	M2	M3	M4			M1	M2	M3	M4
	M1	-	0.00	0.00	0.00		M1	-	0.00	0.00	0.00
SSR	M2	0.00	-	0.00	0.00	SSR	M2	0.00	-	0.00	0.00
	M3	0.00	0.00	-	0.00		M3	0.00	0.00	-	0.00
	M4	0.00	0.00	0.00	-		M4	0.00	0.00	0.00	-

Table A1. Continued

Q50		NSR			
		M1	**M2**	**M3**	**M4**
SSR	M1	-	0.00	**1.00**	**1.00**
	M2	0.00	-	0.00	0.00
	M3	0.00	0.00	-	**1.00**
	M4	0.00	0.00	0.00	-

Q90		NSR			
		M1	**M2**	**M3**	**M4**
SSR	M1	-	0.00	0.00	0.00
	M2	0.00	-	0.00	0.00
	M3	0.00	0.00	-	0.00
	M4	0.00	0.00	0.00	-

Expected lag-1 temporal dependence		NSR			
		M1	**M2**	**M3**	**M4**
SSR	M1	-	**0.63**	0.00	0.00
	M2	0.00	-	0.00	0.00
	M3	0.00	0.00	-	0.00
	M4	0.00	0.00	0.00	-

Expected annual temporal dependence		NSR			
		M1	**M2**	**M3**	**M4**
SSR	M1	-	0.00	0.00	0.00
	M2	0.00	-	0.00	0.00
	M3	0.00	0.00	-	0.00
	M4	**1.00**	0.00	0.00	-

Expected lag-0 spatial dependence		NSR			
		M1	**M2**	**M3**	**M4**
SSR	M1	-	0.00	0.00	0.00
	M2	0.00	-	0.00	0.00
	M3	0.00	0.00	-	0.00
	M4	0.00	0.00	0.00	-

| Expected annual spatial dependence		NSR			
		M1	**M2**	**M3**	**M4**
SSR	M1	-	0.00	0.00	0.00
	M2	0.00	-	0.00	0.00
	M3	0.00	0.00	-	0.00
	M4	0.00	0.00	0.00	-

Figure A3. Relative expected errors for four streamflow generation schemes in reproducing values for annual volume, annual peak as well as annual Q10, Q50, Q90, respectively shown from left to right. Top and bottom rows are related to NSR→SSR and SSR→NSR generation paths.
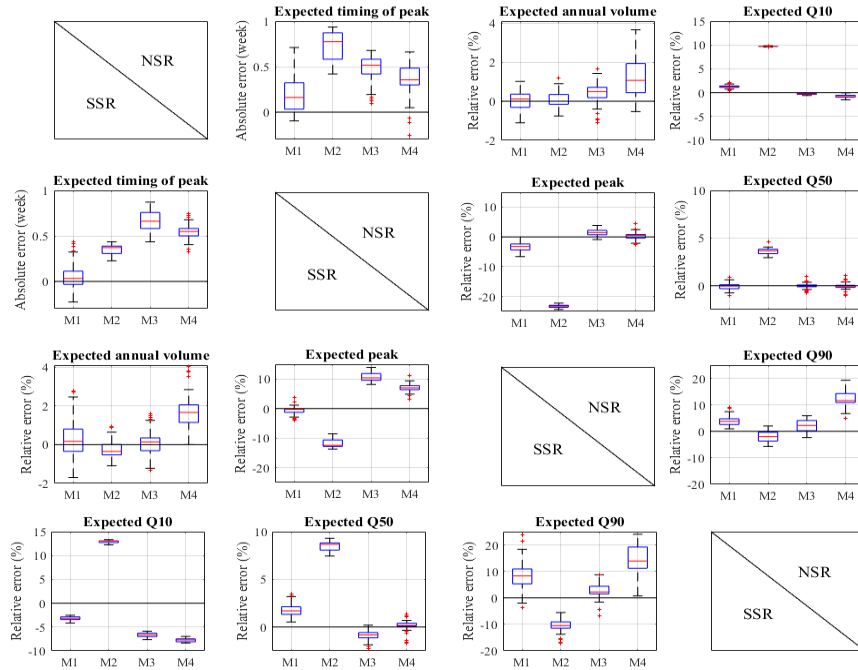
Figure A4. Representative ensemble errors in representing the expected long-term streamflow characteristics at the secondary reach under no-change condition compared between the four regional streamflow extension schemes; panels in upper and lower triangles relates to NSR and SSR as the secondary reach, respectively
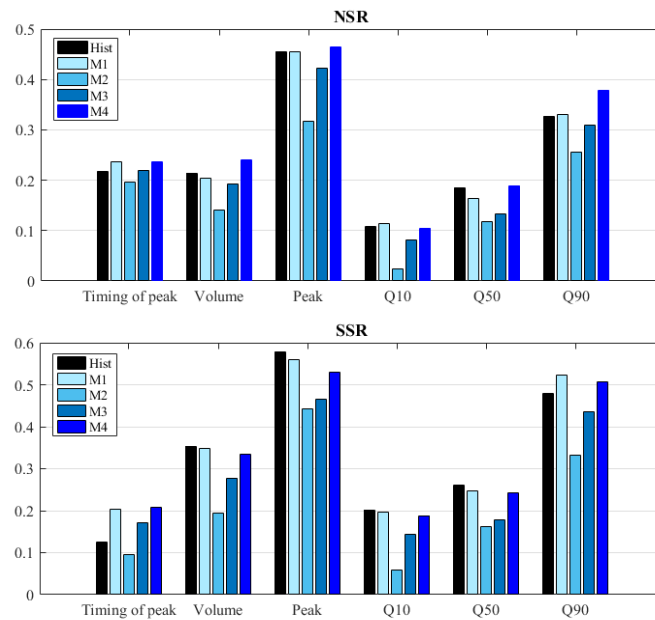

Figure A5. Observed *vs.* expected coefficients of variation for timing of the annual peak as well as the annual volume, peak, Q10, Q50 and Q90, reproduced by the four schemes at the primary (NSR; top row) and secondary (SSR; bottom row) reaches.
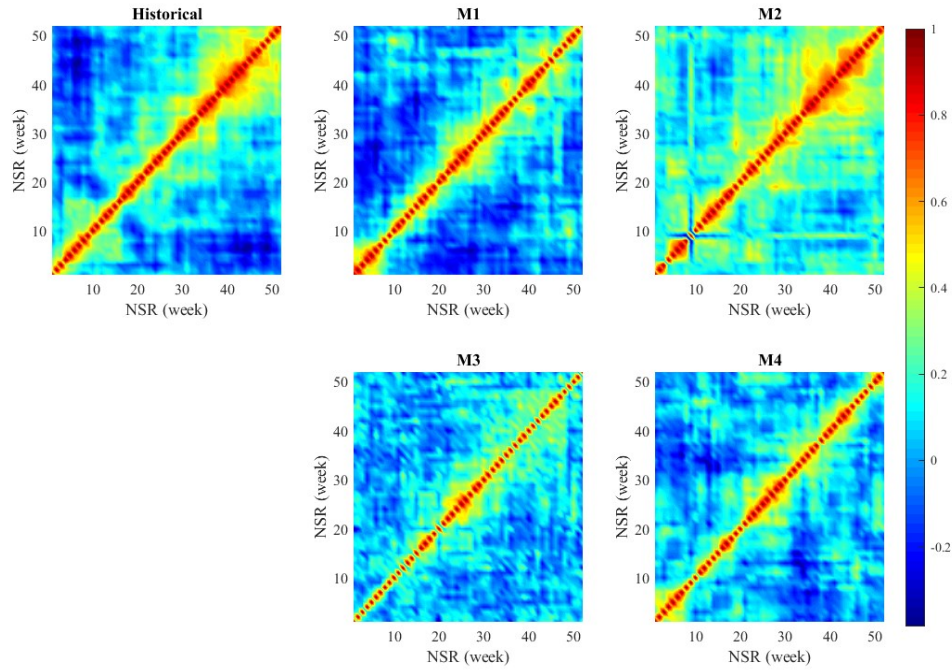
Figure A6. Expected annual temporal dependence matrices, characterized by Kendall's tau, at the NSR through four regional streamflow schemes compared with the corresponding observed matrix.
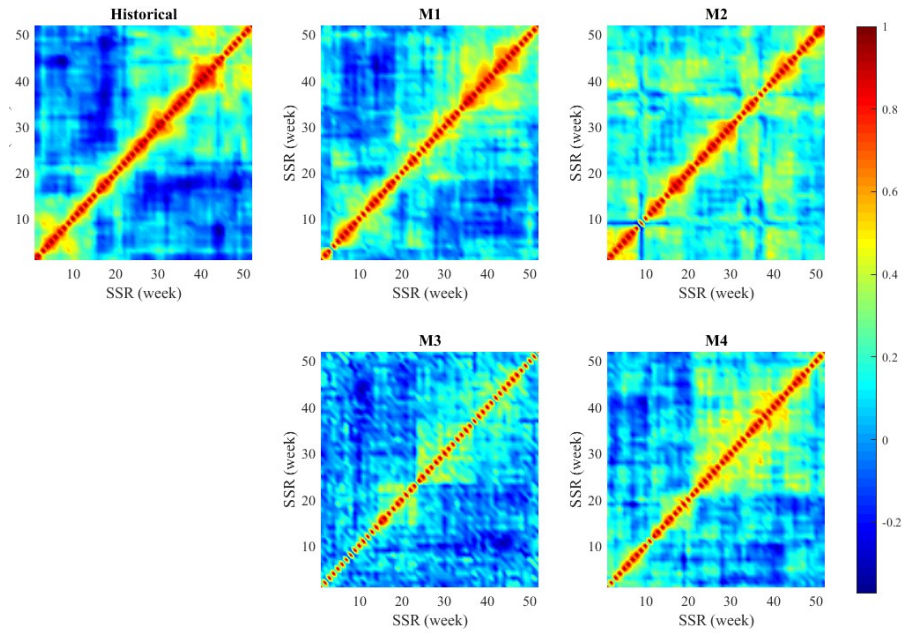

Figure A7. Expected annual temporal dependence matrices, characterized by Kendall's tau, at the SSR through four regional streamflow schemes compared with the corresponding observed matrix.
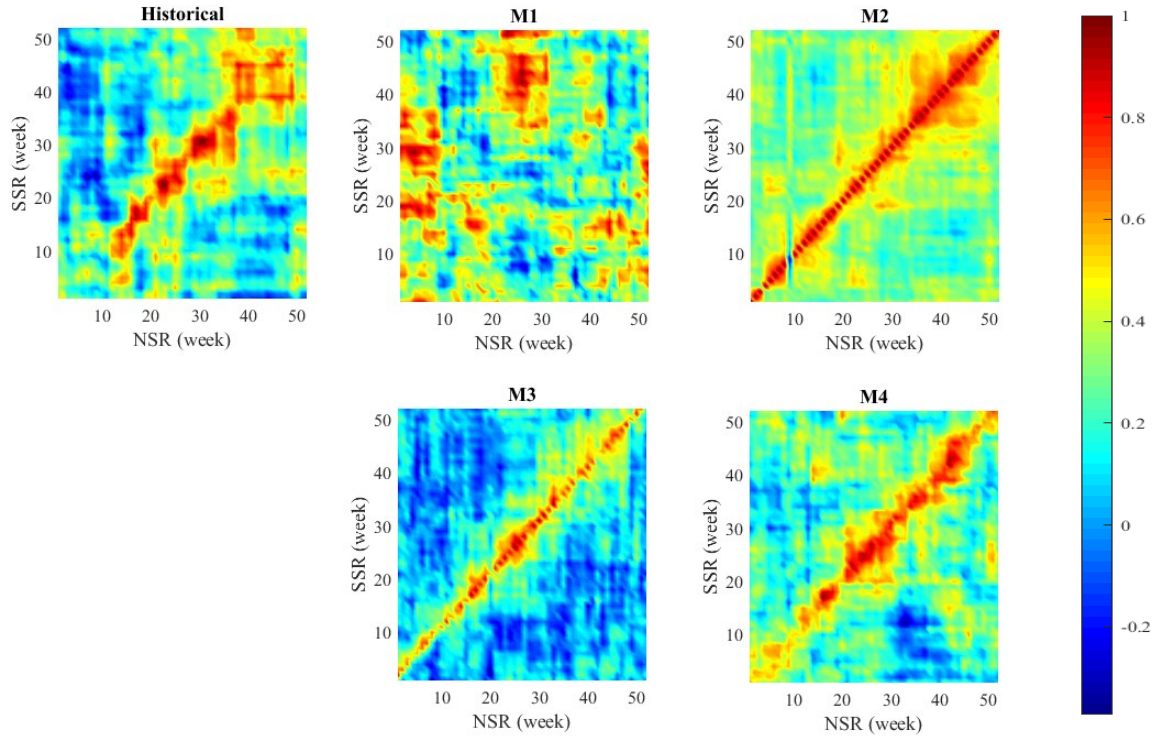
Figure A8. Expected annual spatial dependence matrices, characterized by Kendall's tau, obtained through four regional streamflow schemes compared with the historical matrix
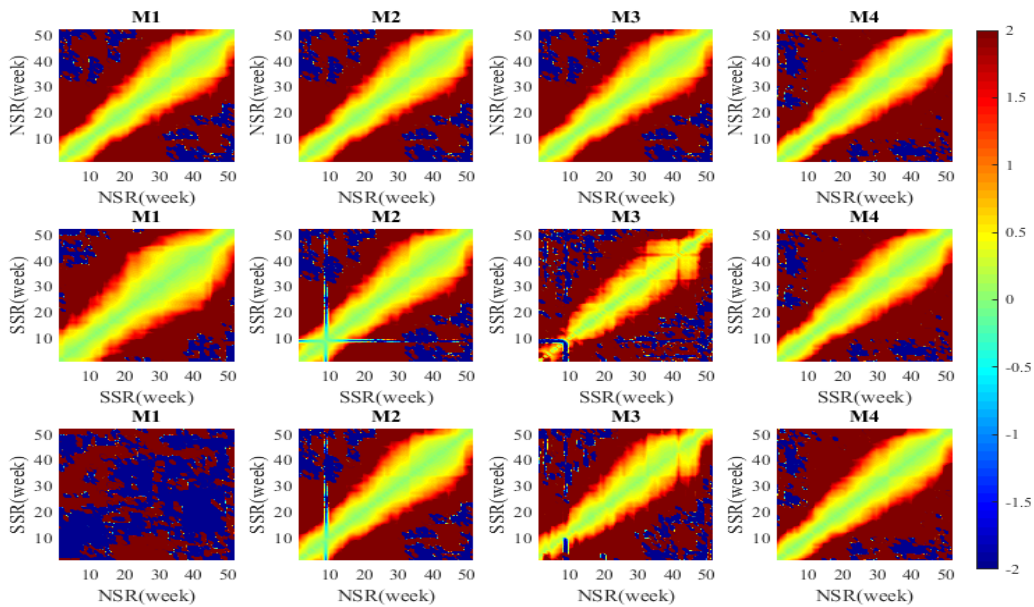

Figure A9. Coefficients of variations in representing the temporal and spatial dependence structures. Top and middle rows are related to temporal dependence matrices at primary and secondary reaches and the bottom row is related to the spatial dependence matrix

Appendix A6. Supporting materials for differences among generated streamflow ensembles and corresponding impact assessment under changing conditions

Table A2. Frequencies of having significantly different ensemble mean for local streamflow characteristic under 154 changing condition (in percentages) generated using the four spatial extension schemes at the SSR. The differences among corresponding streamflow ensembles under a unique scenario of change are characterized by *p*-values of single-factor ANOVA with Bonferroni correction for multiple pairwise comparisons (corrected *p*-value ≤ 0.0083 shows significant difference).

		Annual streamflow volume							Q10			
		M1	M2	M3	M4			M1	M2	M3	M4
Timing	M1	-	27.9	46.1	47.4	Annual peak flow	M1	-	98.7	99.4	53.9
of the	M2	91.6	-	44.2	42.2		M2	29.2	-	100.0	99.4
annual	M3	57.8	90.3	-	0.0		M3	21.4	57.8	-	100.0
peak	M4	61.7	90.3	69.5	-		M4	1.3	22.7	30.5	-

Table A3. Frequencies of having significantly different ensemble mean for system performance (in percentages) obtained by regional streamflow realizations of M1, M2, M3 and M4 under 154 changing condition. The differences among corresponding system performances under a unique scenario of change are characterized by *p*-values of single-factor ANOVA with Bonferroni correction for multiple pairwise comparisons (corrected *p*-value ≤ 0.0083 shows significant difference).

		SWC						M1	M2	M3	M4
		M1	M2	M3	M4						
	M1	-	85.1	82.5	60.4		M1	-			
PNB	M2	33.1	-	59.1	46.1	APP	M2	69.5	-		
	M3	51.3	69.5	-	42.2		M3	99.4	61.7	-	
	M4	56.5	78.6	1.3	-		M4	73.4	85.7	21.4	-

Appendix A7. Supporting materials for ambiguity in understanding stress-response relationship
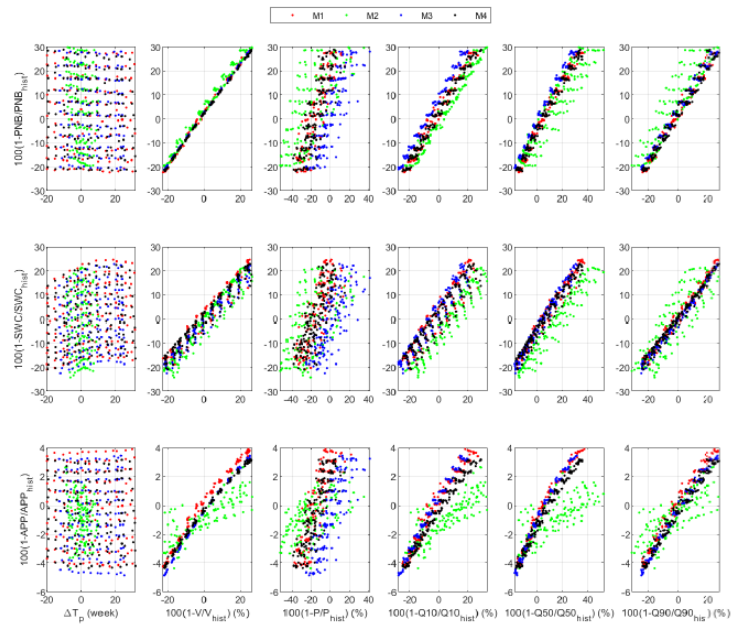

Figure A10. The relationship between changes in the expected long-term streamflow characteristics (x-axis) and changes in the expected long-term performance (y-axis) in the Sask-SRB under 154 feasible scenarios of change.
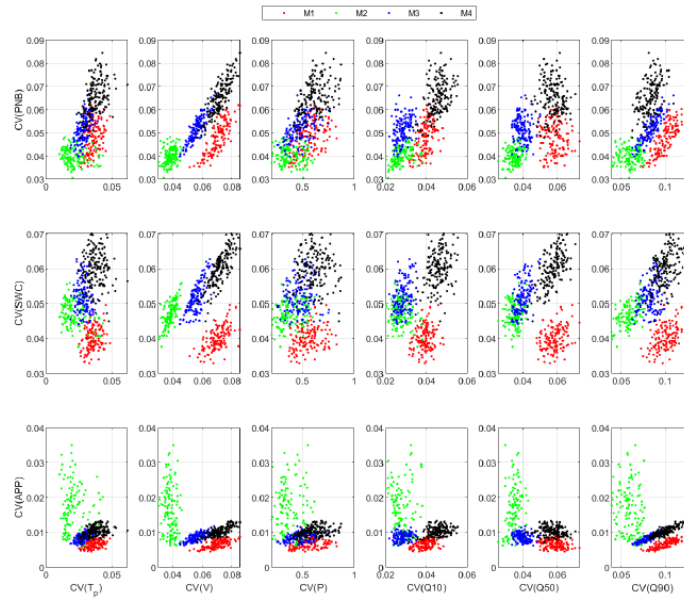

Figure A11. The relationship between the variability in long-term streamflow characteristics (x-axis) and variability in long-term performance measures (y-axis) in the Sask-SRB under 154 feasible scenarios of change.

Additional materials for "On Parametric Representations of Spatiotemporal Dependencies in Stochastic Streamflow Generation across Catchments, Timescales, and Flow Regimes"

Appendix B1. The performance of the seven considered schemes in reconstructing the long-term streamflow characteristics in coarser (monthly) and finer (daily) scales
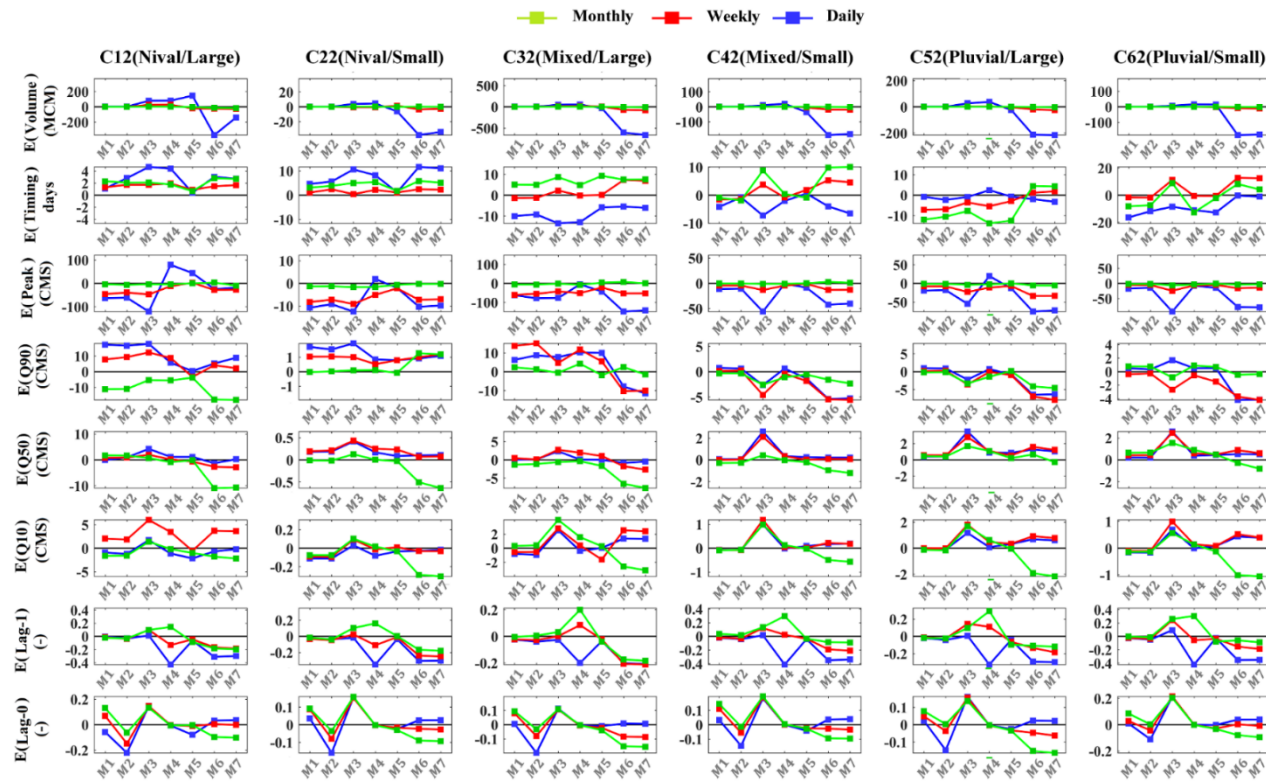

Figure B1. The estimated mean expected errors in reconstructing the key characteristics of secondary site across the six catchments considered. The statistics are derived from 100 ensembles, each with 100 realizations using M1 to M7. The green, red and blue lines show the error statistics at the monthly, weekly and daily timescales, respectively
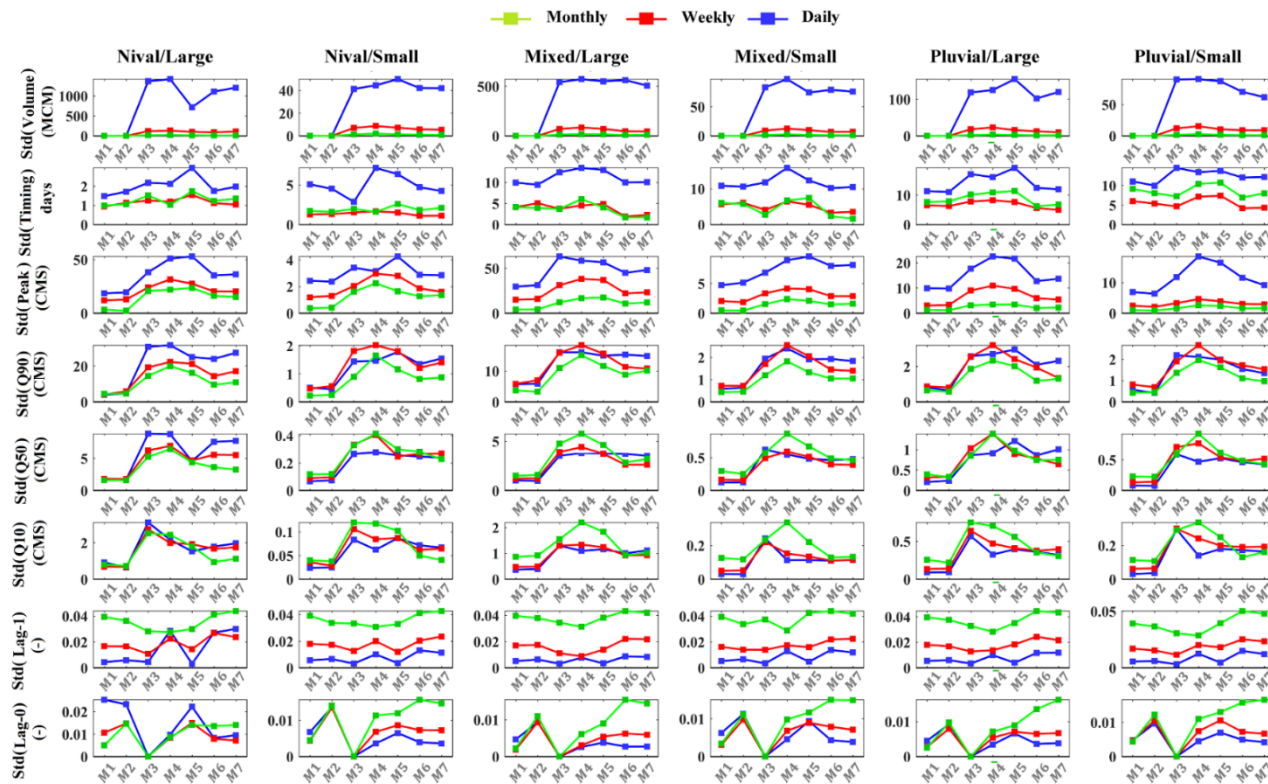
Figure B2. The estimated standard deviation of expected errors in reconstructing the key characteristics of secondary site across the six catchments considered. The statistics are derived from 100 ensembles, each with 100 realizations using M1 to M7. The green, red and blue lines show the error statistics at the monthly, weekly and daily timescales, respectivel

Additional materials for "Informing Stochastic Streamflow Generation by Large-Scale Climate Indices at Single and Multiple Sites"

Appendix C1. Selecting large-scale climate indices to inform streamflow generation using PMI algorithm
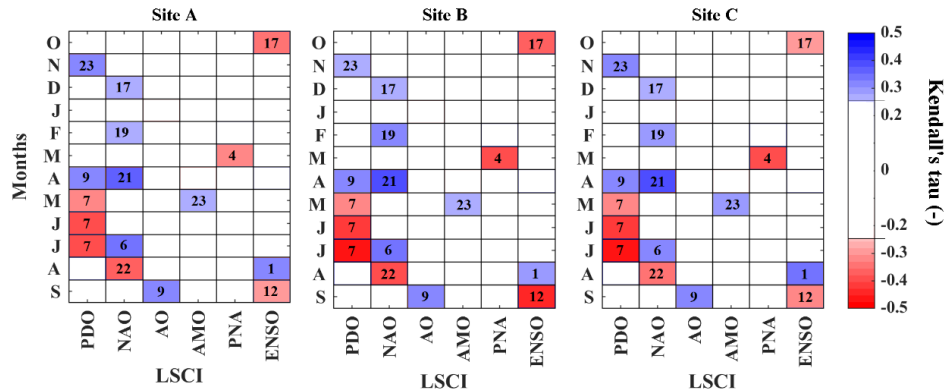

Figure C1. Influential LSCIs with their respective monthly lags, chosen collectively at sites A, B, and C using PMI algorithm. Shades of blue and red in the first row show positive and negative dependencies between lagged LSCIs and streamflow at the monthly scale, which are significant at p-value< 0.05. Numbers inside significant cells identify relevant lags in month between LSCIs and monthly flows.

Appendix C2. Streamflow projection at single and multisite
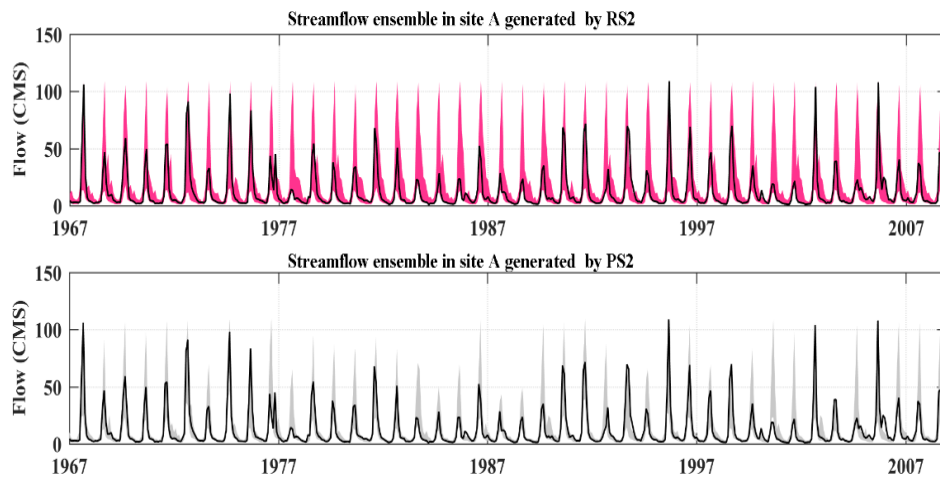
Figure C2. Streamflow ensembles generated by the reference (top row) and proposed (bottom row) algorithms at the site A in single-site setting. The pink and gray colors are the 95% confidence interval obtained by 10,000 realizations of the reference and proposed schemes, respectively. The black lines are the observed streamflow.
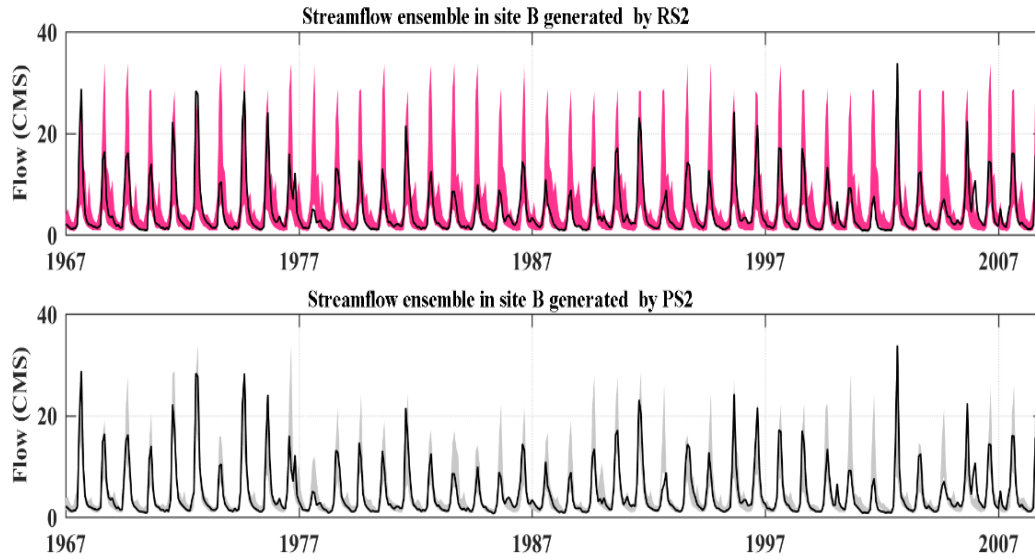
Figure C3. Streamflow ensembles generated by the reference (top row) and proposed (bottom row) algorithms at the site B in single-site setting. The pink and gray colors are the 95% confidence interval obtained by 10,000 realizations of the reference and proposed schemes, respectively. The black lines are the observed streamflow.
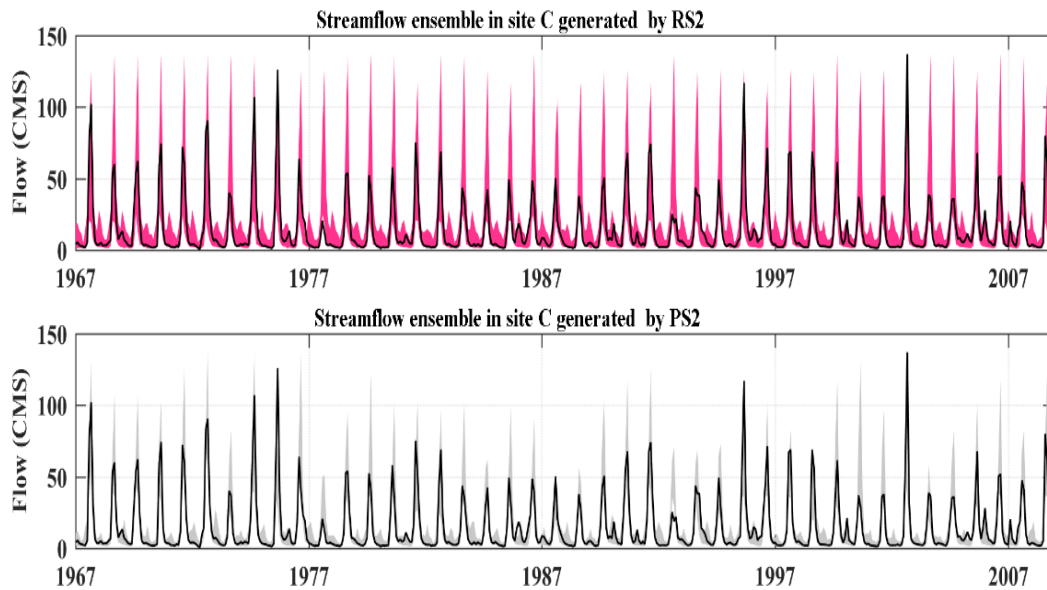

Figure C4. Streamflow ensembles generated by the reference (top row) and proposed (bottom row) algorithms at the site C in single-site setting. The pink and gray colors are the 95% confidence interval obtained by 10,000 realizations of the reference and proposed schemes, respectively. The black lines are the observed streamflow.
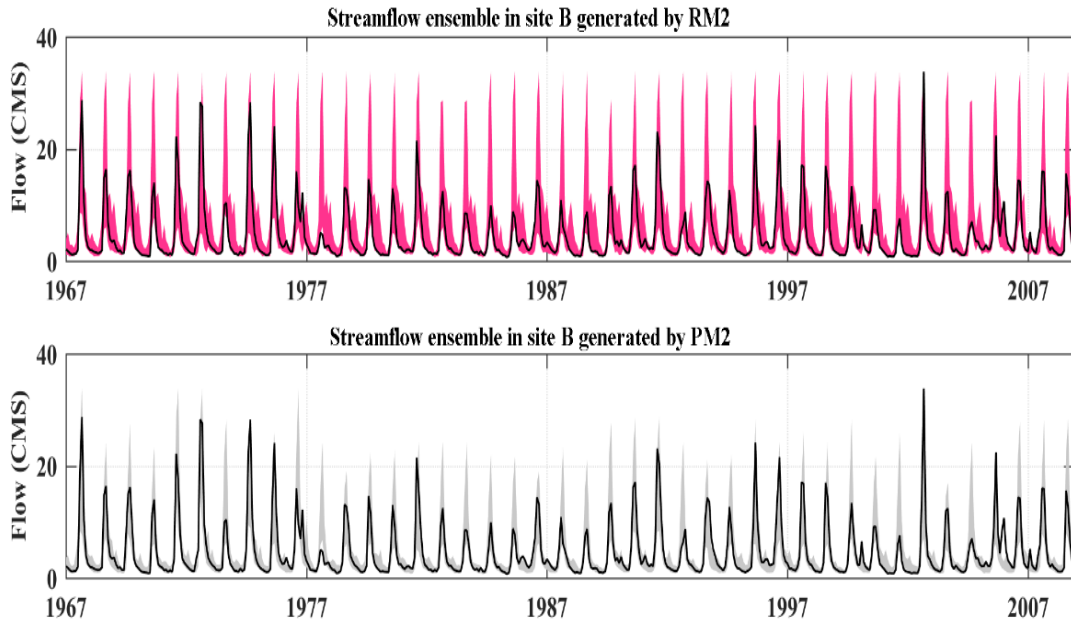
Figure C5. Streamflow ensembles generated by the reference (top row) and proposed (bottom row) algorithms at the site B in multisite setting. The pink and gray colors are the 95% confidence interval obtained by 10,000 realizations of the reference and proposed schemes, respectively. The black lines are the observed streamflow.
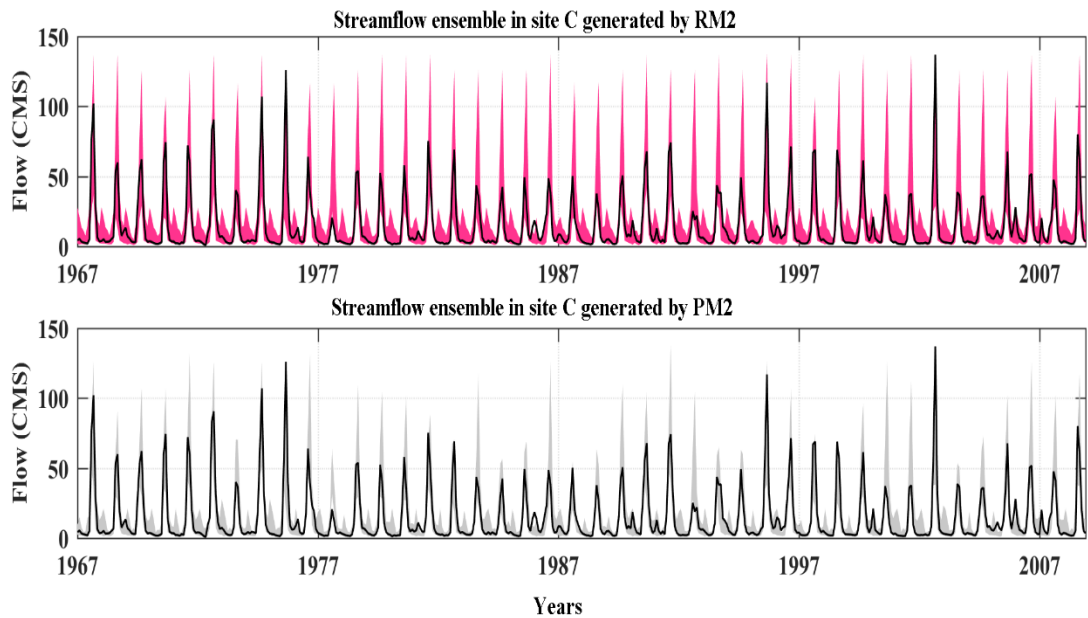

Figure C6. Streamflow ensembles generated by the reference (top row) and proposed (bottom row) algorithms at the site B in multisite setting. The pink and gray colors are the 95% confidence interval obtained by 10,000 realizations of the reference and proposed schemes, respectively. The black lines are the observed streamflow.

Additional materials for "A Global Algorithm for Identifying Changing Streamflow Regimes: Application to Canadian Natural Streams (1966-2010)"
Appendix D1. The detailed description of selected RHBN stations used in this study

Table D1. Summary information for the selected RHBN stations in the Pacific Basin.

RHBN ID	Station ID	Station Name	Province	Lat.	Long.	Basin area (km^2)	Sub-basin	Basin
09BC001	S72	Pelly River at Pelly Crossing	YT	62.8	-136.6	48900	Yukon	Pacific Ocean
09AC001	S74	Takhini River Near Whitehorse	YT	60.9	-135.7	7050	Yukon	Pacific Ocean
09AE003	S77	Swift River Near Swift River	BC	59.9	-131.8	3390	Yukon	Pacific Ocean
09AA006	S75	Atlin River Near Atlin	BC	59.6	-133.8	6860	Yukon	Pacific Ocean
08CD001	S71	Tuya River Near Telegraph Creek	BC	58.1	-130.8	3550	Seaboard	Pacific Ocean
08CG001	S82	Iskut River Below Johnson River	BC	56.7	-131.7	9500	Seaboard	Pacific Ocean
08FB006	S87	Atnarko River Near The Mouth	BC	52.4	-126.0	2550	Seaboard	Pacific Ocean
08OA002	S78	Yakoun River Near Port Clements	BC	53.6	-132.2	480	Seaboard	Pacific Ocean
08HB008	S83	Sproat River Near Alberni	BC	49.3	-124.9	351	Seaboard	Pacific Ocean
08GA010	S84	Capilano River Above Intake	BC	49.4	-123.1	173	Seaboard	Pacific Ocean
08HA001	S81	Chemainus River Near Westholme	BC	48.9	-123.7	355	Seaboard	Pacific Ocean
08HA003	S79	Koksilah River at Cowichan Station	BC	48.7	-123.7	209	Seaboard	Pacific Ocean
08JE001	S95	Stuart River Near Fort St. James	BC	54.4	-124.3	14200	Fraser	Pacific Ocean
08JB002	S96	Stellako River At Glenannan	BC	54.0	-125.0	3600	Fraser	Pacific Ocean
08LA001	S89	Clearwater River Near Clearwater Station	BC	51.6	-120.1	10300	Fraser	Pacific Ocean
08LD001	S88	Adams River Near Squilax	BC	50.9	-119.7	3210	Fraser	Pacific Ocean
08MA002	S102	Chilko River At Outlet Of Chilko Lake	BC	51.6	-124.1	2130	Fraser	Pacific Ocean
08MG005	S85	Lillooet River Near Pemberton	BC	50.3	-122.8	2100	Fraser	Pacific Ocean
08MH006	S80	North Alouette River 232nd Street Maple Ridge	BC	49.2	-122.6	37.3	Fraser	Pacific Ocean
08MH016	S86	Chilliwack River At Outlet Of Chilliwack Lake	BC	49.1	-121.5	335	Fraser	Pacific Ocean
08NB005	S99	Columbia River At Donald	BC	51.5	-117.2	9700	Columbia	Pacific Ocean
08NF001	S101	Kootenay River At Kootenay Crossing	BC	50.9	-116.0	416	Columbia	Pacific Ocean
08ND013	S90	Illecillewaet River At Greeley	BC	51.0	-118.1	1150	Columbia	Pacific Ocean
08NE006	S93	Kuskanax Creek Near Nakusp	BC	50.3	-117.7	330	Columbia	Pacific Ocean

Table D1. Continued.

RHBN ID	Station ID	Station Name	Province	Lat.	Long.	Basin area (km^2)	Sub-basin	Basin
08NE077	S91	Barnes Creek Near Needles	BC	49.9	-118.1	204	Columbia	Pacific Ocean
08NH005	S94	Kaslo River Below Kemp Creek	BC	49.9	-117.0	442	Columbia	Pacific Ocean
08NH084	S98	Arrow Creek Near Erickson	BC	49.2	-116.5	78.3	Columbia	Pacific Ocean
08NJ130	S97	Anderson Creek Near Nelson	BC	49.5	-117.3	9.07	Columbia	Pacific Ocean
08NN015	S100	West Kettle River Near Mcculloch	BC	49.7	-119.1	233	Columbia	Pacific Ocean
08NL007	S92	Similkameen River At Princeton	BC	49.5	-120.5	1810	Columbia	Pacific Ocean

Table D2. Summary information for the selected RHBN stations in the Atlantic Basin.

RHBN ID	Station ID	Station Name	Province	Lat.	Long	Basin area (km^2)	Sub-basin	Basin
02YC001	S11	Torrent River At Bristols Pool	NL	50.6	-57.2	624	Seaboard	Atlantic Ocean
02YL001	S13	Upper Humber River Near Reidville	NL	49.2	-57.4	2110	Seaboard	Atlantic Ocean
02YQ001	S17	Gander River At Big Chute	NL	49.0	-54.9	4450	Seaboard	Atlantic Ocean
02YR001	S15	Middle Brook Near Gambo	NL	48.8	-54.2	275	Seaboard	Atlantic Ocean
02ZB001	S14	Isle Aux Morts River Below Highway Bridge	NL	47.6	-59.0	205	Seaboard	Atlantic Ocean
02ZF001	S8	Bay Du Nord River At Big Falls	NL	47.7	-55.4	1170	Seaboard	Atlantic Ocean
02ZG001	S10	Garnish River Near Garnish	NL	47.2	-55.3	205	Seaboard	Atlantic Ocean
02ZH001	S18	Pipers Hole River At Mothers Brook	NL	47.9	-54.3	764	Seaboard	Atlantic Ocean
02ZK001	S9	Rocky River Near Colinet	NL	47.2	-53.6	301	Seaboard	Atlantic Ocean
02ZM006	S20	Northeast Pond River At Northeast Pond	NL	47.6	-52.8	3.63	Seaboard	Atlantic Ocean

Table D2. Continued.

RHBN ID	Station ID	Station Name	Province	Lat.	Long	Basin area (km²)	Sub-basin	Basin
01FB001	S53	Northeast Margaree River At Margaree Valley	NS	46.4	-61.0	368	Seaboard	Atlantic Ocean
01FB003	S50	Southwest Margaree River Near Upper Margaree	NS	46.2	-61.1	357	Seaboard	Atlantic Ocean
01FA001	S33	River Inhabitants At Glenora	NS	45.7	-61.3	193	Seaboard	Atlantic Ocean
01EO001	S45	St. Marys River At Stillwater	NS	45.2	-62.0	1350	Seaboard	Atlantic Ocean
01DP004	S52	Middle River Of Pictou At Rocklin	NS	45.5	-62.8	92.2	Seaboard	Atlantic Ocean
01DG003	S51	Beaverbank River Near Kinsac	NS	44.9	-63.7	96.9	Seaboard	Atlantic Ocean
01EF001	S47	Lahave River At West Northfield	NS	44.4	-64.6	1250	Seaboard	Atlantic Ocean
01EC001	S49	Roseway River At Lower Ohio	NS	43.8	-65.4	495	Seaboard	Atlantic Ocean
01BV006	S44	Point Wolfe River At Fundy National Park	NB	45.6	-65.0	130	Seaboard	Atlantic Ocean
01BU002	S46	Petitcodiac River Near Petitcodiac	NB	45.9	-65.2	391	Seaboard	Atlantic Ocean
01BS001	S40	Coal Branch River At Beersville	NB	46.4	-65.1	166	Seaboard	Atlantic Ocean
01CA003	S35	Carruthers Brook Near St. Anthony	PE	46.7	-64.2	46.8	Seaboard	Atlantic Ocean
02NF003	S32	Matawin (Riviere) A Saint-Michel-Des-Saints	QC	46.7	-73.9	1390	St. Lawrence	Atlantic Ocean
02LB007	S58	South Nation River At Spencerville	ON	44.8	-75.5	246	St. Lawrence	Atlantic Ocean
02KB001	S21	Petawawa River Near Petawawa	ON	45.9	-77.3	4122.32	St. Lawrence	Atlantic Ocean
02HL004	S22	Skootamatta River Near Actinolite	ON	44.5	-77.3	677.65	St. Lawrence	Atlantic Ocean
02EA005	S29	North Magnetawan River Near Burks Falls	ON	45.7	-79.4	328.84	St. Lawrence	Atlantic Ocean

Table D2. Continued.

RHBN ID	Station ID	Station Name	Province	Lat.	Long	Basin area (km²)	Sub-basin	Basin
02EC002	S60	Black River Near Washago	ON	44.7	-79.3	1510.27	St. Lawrence	Atlantic Ocean
02FB007	S62	Sydenham River Near Owen Sound	ON	44.5	-80.9	182.97	St. Lawrence	Atlantic Ocean
02FC001	S59	Saugeen River Near Port Elgin	ON	44.5	-81.3	3953.52	St. Lawrence	Atlantic Ocean
02GA010	S61	Nith River Near Canning	ON	43.2	-80.5	1034.28	St. Lawrence	Atlantic Ocean
02AB008	S24	Neebing River Near Thunder Bay	ON	48.4	-89.3	187	St. Lawrence	Atlantic Ocean
01AQ001	S41	Lepreau River At Lepre	NB	45.2	-66.5	239	Saint John- St. Croix	Atlantic Ocean
01AP004	S34	Kennebecasis River At Apohaqui	NB	45.7	-65.6	1100	Saint John- St. Croix	Atlantic Ocean
01AP002	S42	Canaan River At East Canaan	NB	46.1	-65.4	668	Saint John- St. Croix	Atlantic Ocean
01AK001	S54	Shogomoc Stream Near Trans-Canada Highway	NB	45.9	-67.3	234	Saint John- St. Croix	Atlantic Ocean
01AD002	S56	Saint John River At Fort Kent	NB	47.3	-68.6	14700	Saint John- St. Croix	Atlantic Ocean

Table D3. Summary information for the selected RHBN stations in the Arctic Basin.

RHBN ID	Station ID	Station Name	Province	Lat.	Long.	Basin area (km²)	Sub-basin	Basin
10PB001	S7	Coppermine River At Outlet Of Point Lake	NT	65.4	-114.0	19200	Seaboard	Arctic Ocean
10RC001	S1	Back River Above Hermann River	NU	66.1	-96.5	93900	Seaboard	Arctic Ocean
10CB001	S68	Sikanni Chief River Near Fort Nelson	BC	57.2	-122.7	2180	Lower Mackenzie	Arctic Ocean
10BE004	S76	Toad River Above Nonda Creek	BC	58.9	-125.4	2540	Lower Mackenzie	Arctic Ocean
10CD001	S65	Muskwa River Near Fort Nelson	BC	58.8	-122.7	20300	Lower Mackenzie	Arctic Ocean
07LE002	S5	Fond Du Lac River At Outlet Of Black Lake	SK	59.2	-105.5	50700	Lower Mackenzie	Arctic Ocean
07OB001	S3	Hay River Near Hay River	NT	60.7	-115.9	51700	Lower Mackenzie	Arctic Ocean
10EB001	S73	South Nahanni River Above Virginia Falls	NT	61.6	-125.8	14500	Lower Mackenzie	Arctic Ocean
07RD001	S6	Lockhart River At Outlet Of Artillery Lake	NT	62.9	-108.5	26600	Lower Mackenzie	Arctic Ocean
07FB001	S66	Pine River At East Pine	BC	55.7	-121.2	12100	Peace Athabasca	Arctic Ocean
07CD001	S64	Clearwater River At Draper	AB	56.7	-111.3	30799.4	Peace Athabasca	Arctic Ocean
07FC003	S67	Blueberry River Below Aitken Creek	BC	56.7	-121.2	1770	Peace Athabasca	Arctic Ocean

Table D4. Summary information for the selected RHBN stations in the Hudson Bay Basin.

RHBN ID	Station ID	Station Name	Province	Lat.	Long.	Basin area (km²)	Sub-basin	Basin
04NA001	S28	Harricana (Riviere) 3 1 Km En Aval Du Pont-Route 111 A Amos	QC	48.6	-78.1	3680	Western & Northern HB	Hudson Bay
04LJ001	S27	Missinaibi River At Mattice	ON	49.6	-83.3	8574.38	Western & Northern HB	Hudson Bay
04JC002	S26	Nagagami River At Highway No. 11	ON	49.8	-84.5	2178.36	Western & Northern HB	Hudson Bay
06CD002	S31	Churchill River Above Otter Rapids	SK	55.6	-104.7	119000	Northern Quebec & Ontario	Hudson Bay
06GD001	S4	Seal River Below Great Island	MB	58.9	-96.3	48100	Northern Quebec & Ontario	Hudson Bay
06LC001	S2	Kazan River Above Kazan Falls	NU	63.7	-95.9	70000	Northern Quebec & Ontario	Hudson Bay
05PB014	S30	Turtle River Near Mine Centre	ON	48.9	-92.7	4767.74	Nelson	Hudson Bay
05TD001	S23	Grass River Above Standing Stone Falls	MB	55.7	-97.0	15400	Nelson	Hudson Bay
05LH005	S63	Waterhen River Near Waterhen	MB	51.8	-99.5	55100	Nelson	Hudson Bay
05AD005	S70	Belly River Near Mountain View	AB	49.1	-113.7	319.2	Nelson	Hudson Bay
05AD003	S69	Waterton River Near Waterton Park	AB	49.1	-113.8	612.7	Nelson	Hudson Bay
05AA008	S103	Crowsnest River At Frank	AB	49.6	-114.4	402.7	Nelson	Hudson Bay
05BB001	S104	Bow River At Banff	AB	51.2	-115.6	2209.6	Nelson	Hudson Bay
05DA007	S105	Mistaya River Near Saskatchewan Crossing	AB	51.9	-116.7	248	Nelson	Hudson Bay

Appendix D2. The distribution of selected RHBN stations in major Canadian drainage basins and sub-basins

Table D5. Main sub-basins of the four Canadian major drainage basins along with their drainage areas, abbreviations and the number of RHBN stations within their territory used in this study.

| Major Basin	Sub-basin	Area (1000 km²)	# of stations	Abbreviation
Pacific	Yukon	330.4	4	P1
	Seaboard	334.2	8	P2
	Fraser	232.5	8	P3
	Columbia	102.8	10	P4
Atlantic	Seaboard	499.7	28	At1
	St. Lawrence	860.1	16	At2
	Saint John- St. Croix	41.9	5	At3
Arctic	Seaboard	1,739.3	2	Ar1
	Lower Mackenzie	1,321.1	7	Ar2
	Peace Athabasca	482.7	3	Ar3
Hudson Bay	Western & Northern HB	1,243.9	3	H1
	Northern Quebec & Ontario	1,889.2	3	H2
	Nelson	1,138.5	8	H3
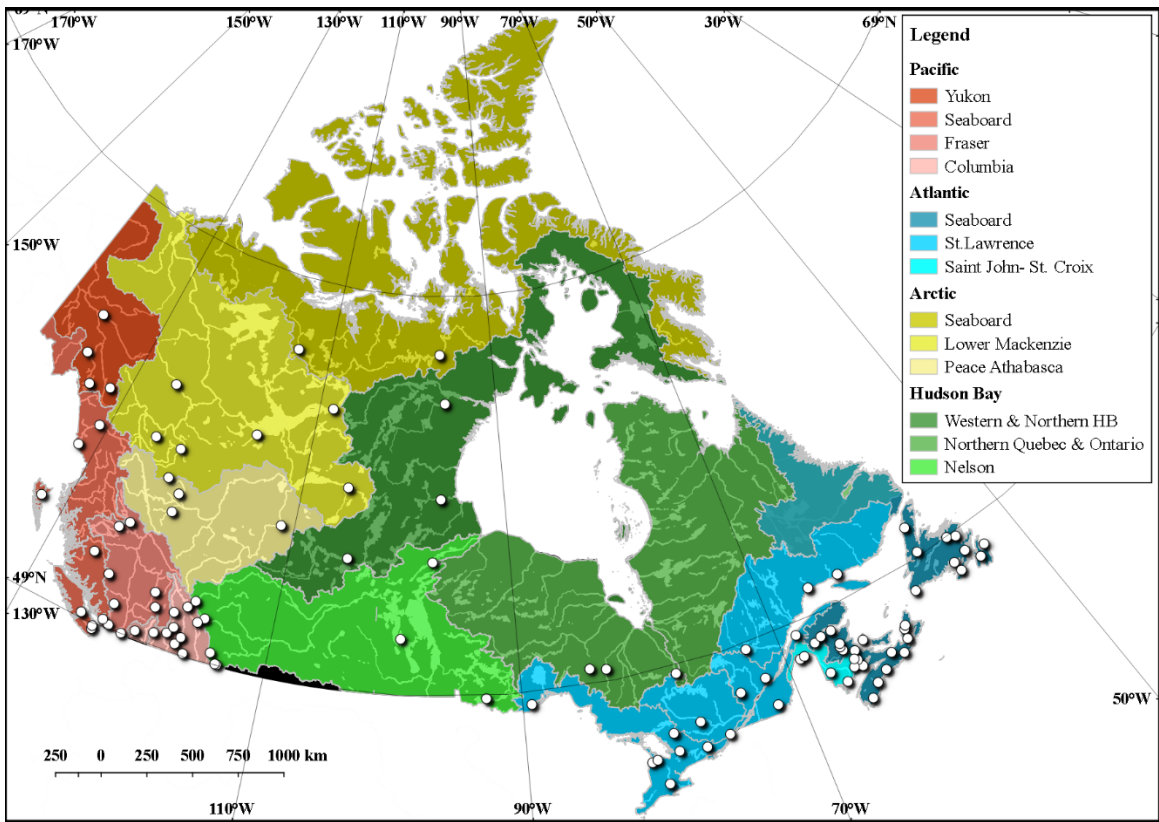
Figure D1. The distribution of the selected 105 RHBN streamflow stations across the major Canadian drainage basins and sub-basins.

## Appendix D3. Assigning the optimal number of streamflow regimes in Canada and their archetype streams
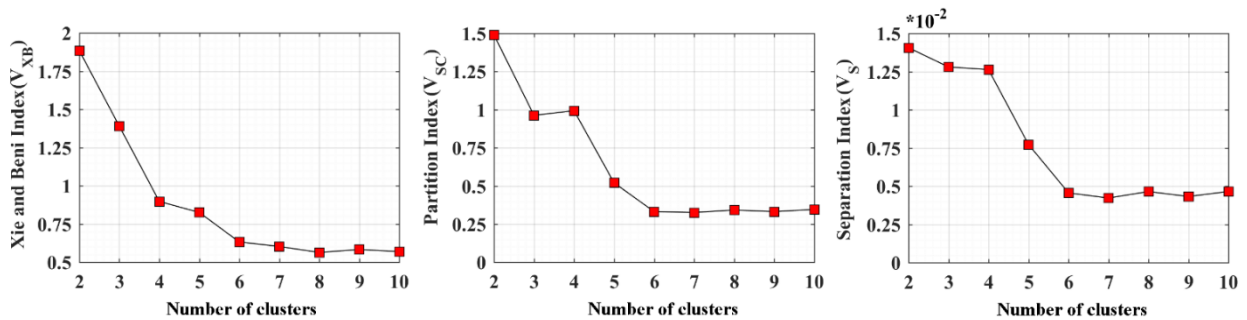
Figure D2. Variation in the Xie and Beni, Partition, and Separation indices by altering the numbers of clusters.
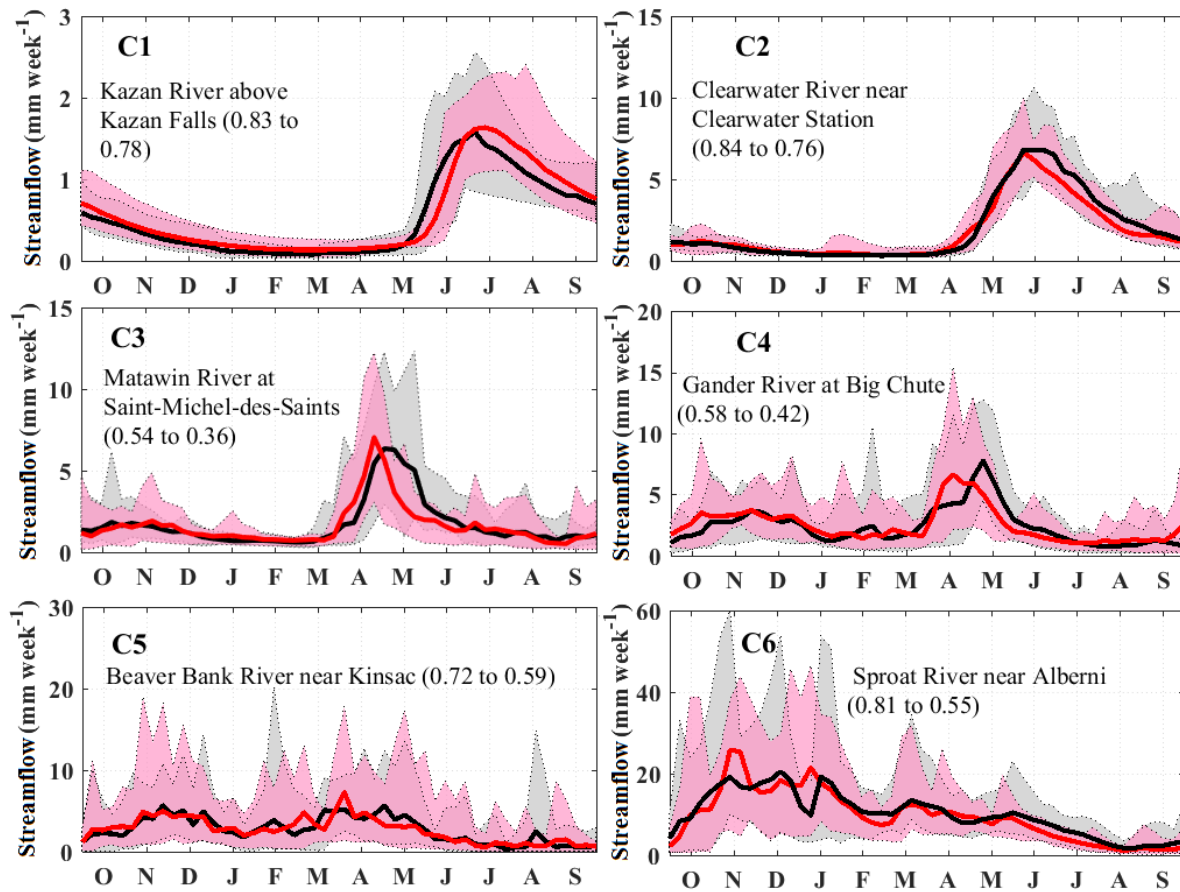
Figure D3. Alterations in the decadal streamflow regimes at the archetype streams through time. The envelopes of annual hydrographs for the earliest (1966 to 1975) and the latest (2001 to 2010) decadal episodes in archetype streams are shown with grey and pink colors, respectively. The expected annual hydrographs during the earliest and the latest decadal periods are shown in solid black and solid red lines. The change in the membership degree of each archetype stream is shown within parentheses.

Appendix D4. The detailed analysis of trend and evolution of decadal memberships
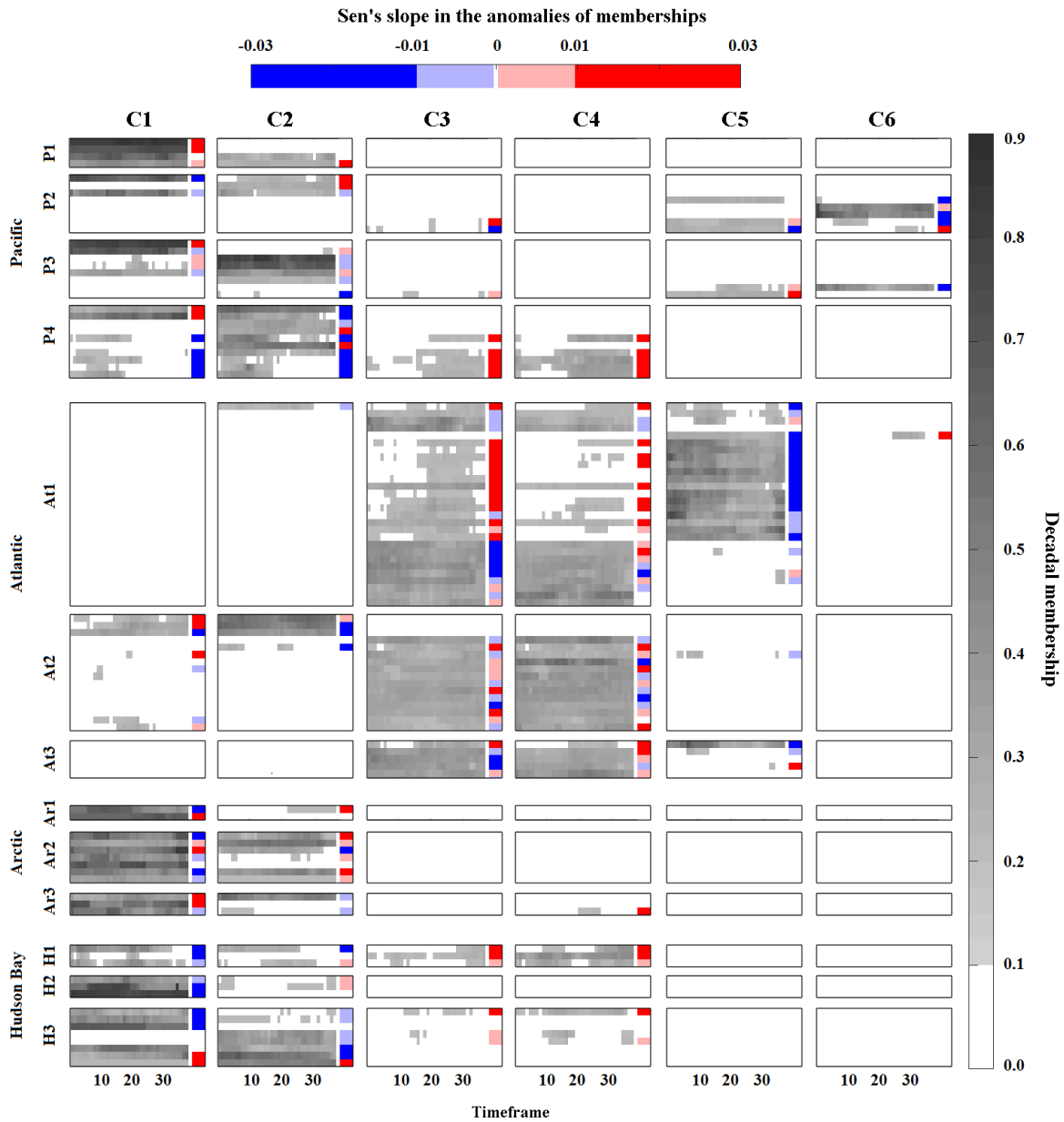
Figure D4. Evolutions in the degrees of membership to each regime type in 105 considered RHBN streams grouped in major basins/sub-basins, along with the corresponding Sen's slope. For each stream, the shades of grey show decadal memberships over the period of 1966 to 2010. The color bar shows the direction and significance of the Sen's slope of the trend in the anomalies of memberships. Positive and negative trends are shown with red and blue colors, respectively. Sharper colors show significant cases. In each sub-basin, stations are sorted from north to south from the top to the bottom.
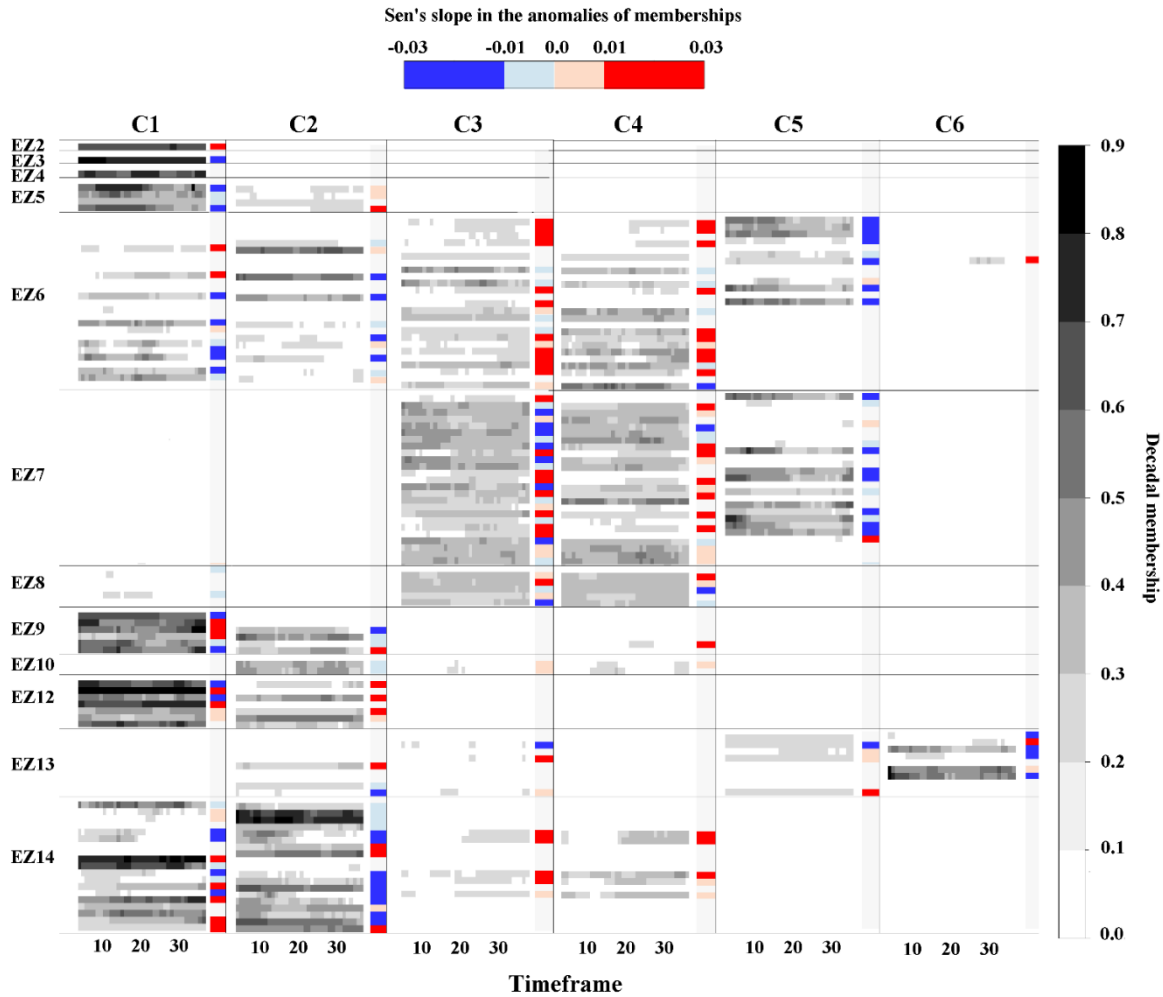
Figure D5. Evolution in degrees of membership to each regime type in the 105 considered RHBN streams grouped according to ecozones, along with the corresponding Sen's slopes. For each stream, shades of grey show decadal memberships over the period of 1966 to 2010. The color bar shows the direction and significance of the Sen's slope of the trend in the anomalies of memberships. Positive and negative trends are shown with red and blue colors, respectively. Sharper colors show significant trends. The RHBN stations at each ecozone are sorted from the lowest to the highest elevations from the top to the bottom.

Appendix D5. Mapping the dominant shifts in natural streamflow regime in Canada
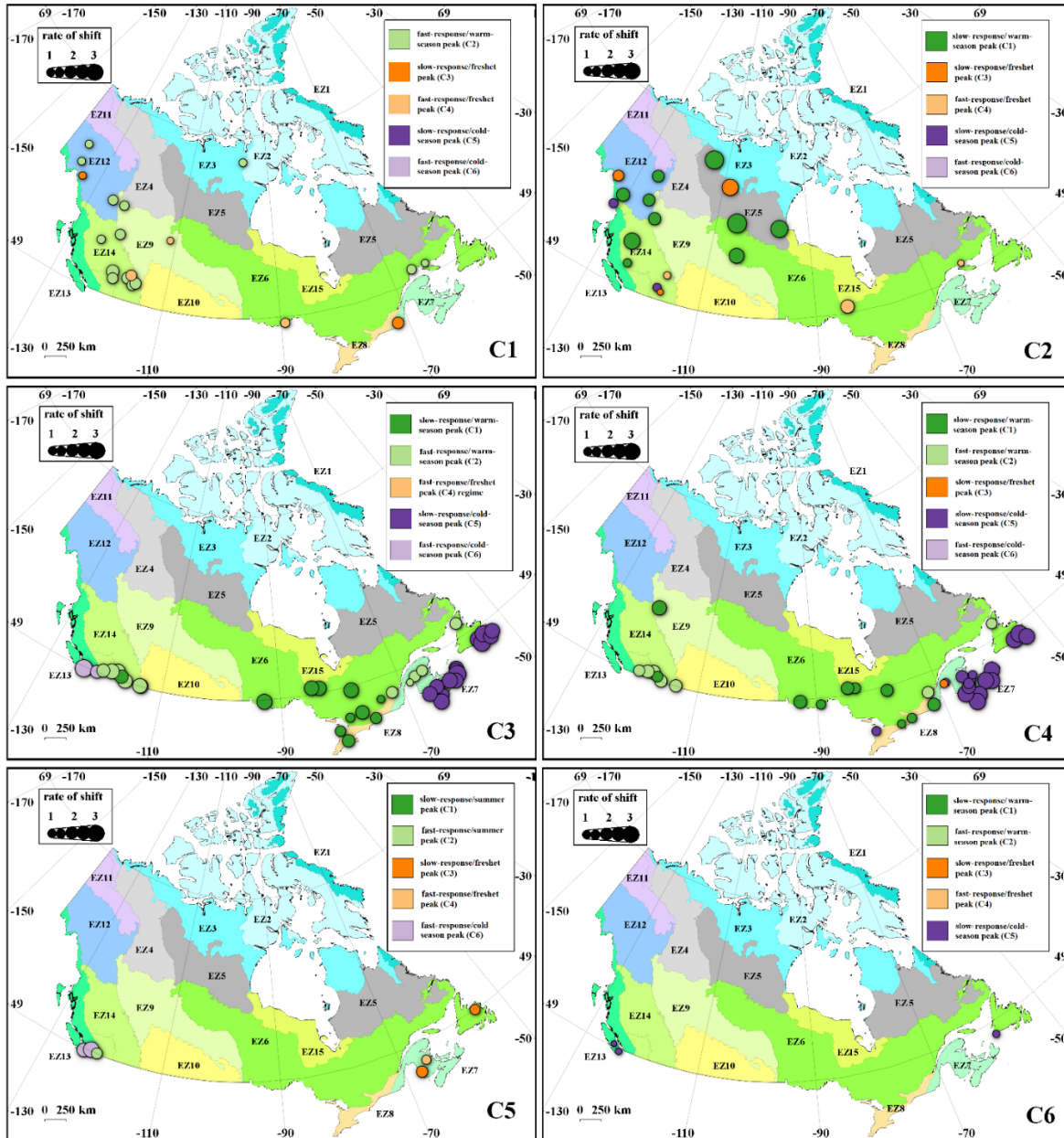
Figure D6. Mapping shifts in natural streamflow regime throughout Canada from 1966 to 2010. In each panel, circles identify the streams in which the regime is shifted. Colors show the initial regime type from which the streamflow is departed toward the reference cluster, which is given in each panel. Rates of the shifts between regime types in each stream are proportional to the size of each circle.

Appendix D6. Attribution of regime shift to changes in streamflow characteristics over basin/sub-basin scale
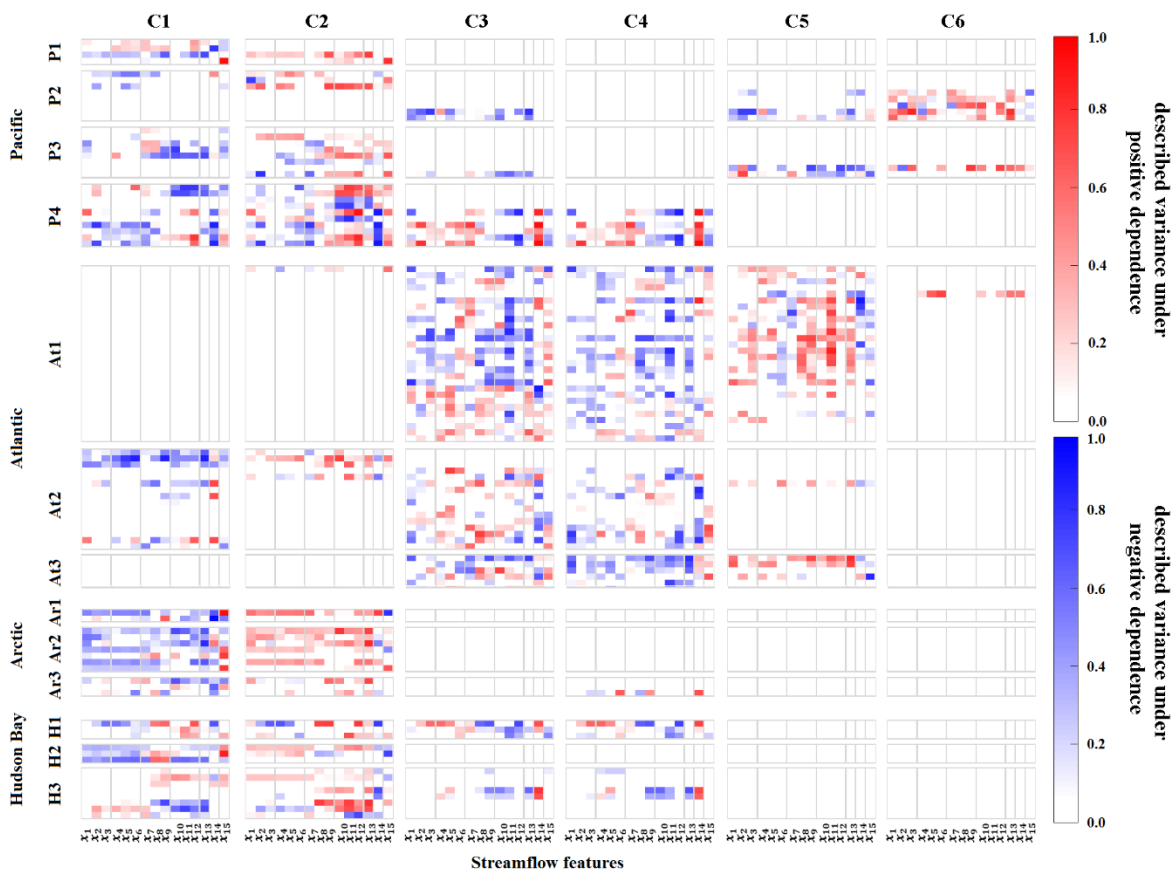
Figure D7. The alterations in regime types for 105 RHBN streams attributed to the first moments of the 15 IHA considered. Shades of red and blue show the positive and negative dependencies between changes in streamflow features and the degrees of membership, respectively. Color saturation shows the coefficient of determination between changes in the streamflow features and the degrees of membership representing the percentage of described variance in changes of streamflow regime by changes in streamflow features.
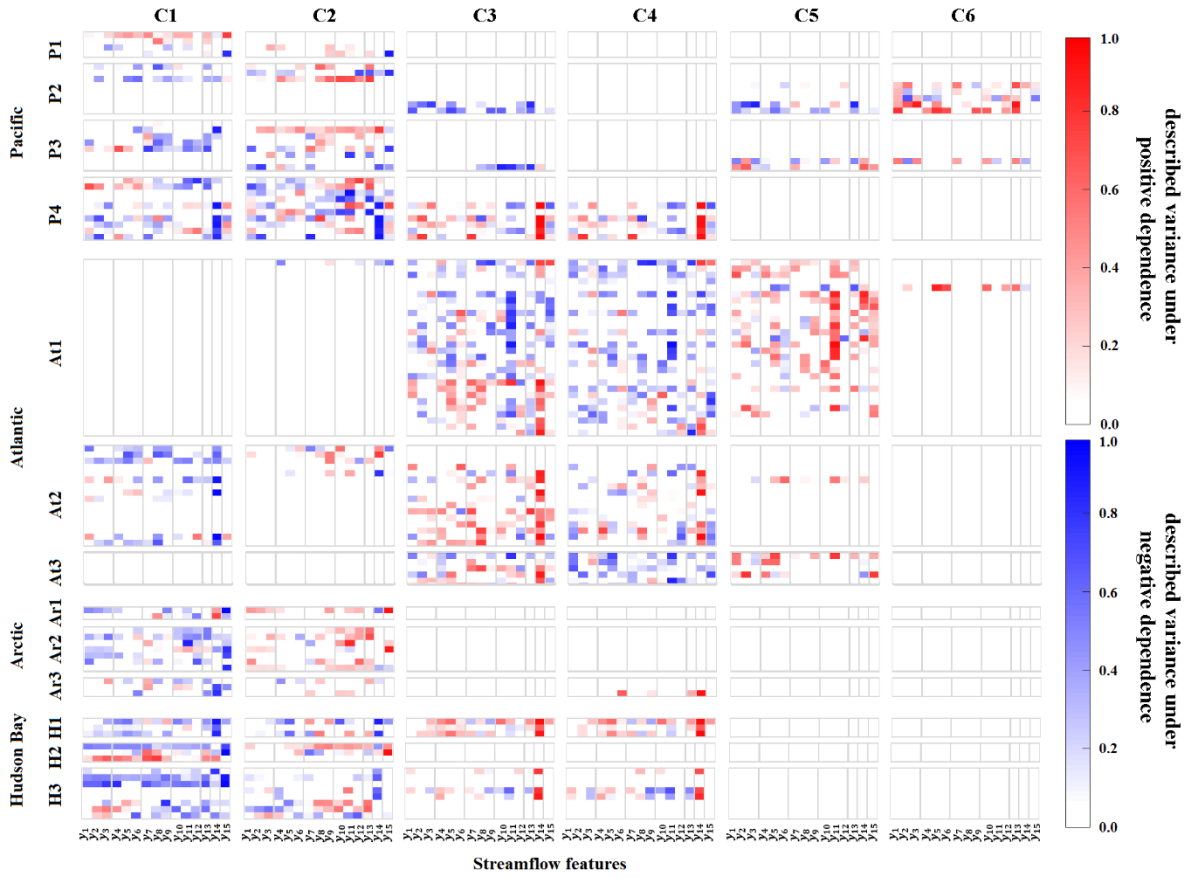
Figure D8. The alterations in regime types for 105 RHBN streams attributed to the second moments of the 15 IHA considered. Shades of red and blue show the positive and negative dependencies between changes in streamflow features and the degrees of membership, respectively. Color saturation shows the coefficient of determination between changes in the streamflow features and the degrees of membership representing the percentage of described variance in changes of streamflow regime by changes in streamflow features.
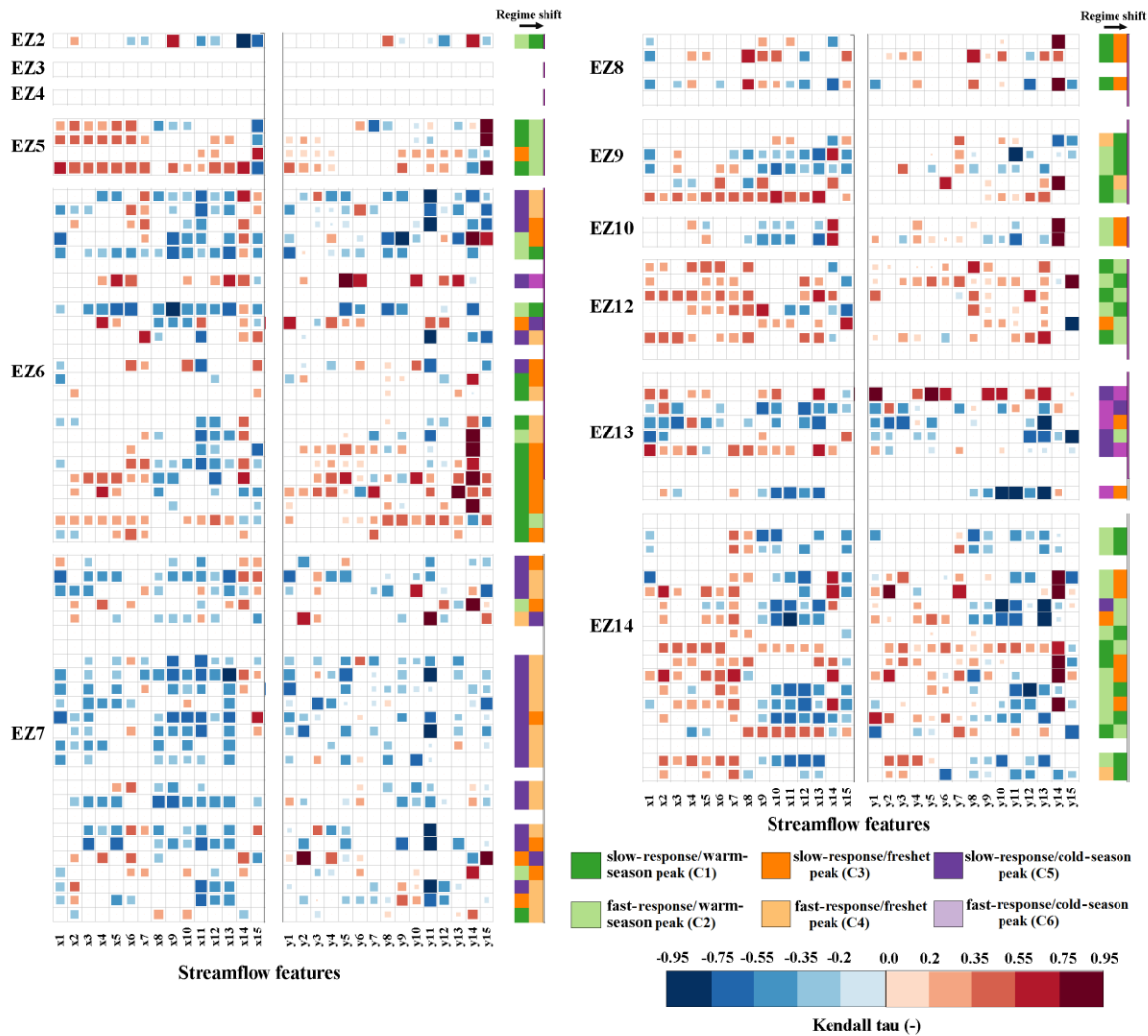
Figure D9. Dominant regime shifts across 105 RHBN streams in Canada attributed to the first and second moments of the 15 IHAs considered. Shades of red and blue show the values of squared of Kendall's tau between changes in streamflow features and degrees of membership. The dominant regime shift at each stream is identified by the color scheme described in the legend. Streams are grouped in ecozones and ordered from low (top) to the high (bottom) elevations.

Appendix D7. Additional streams in the Prairies

Table D6. Summary information for the nine unseen stations in the Prairies ecozone.

Station	Station ID	Station Name	Province	Lat.	Long.	Basin area (km2)	Sub-basin	Basin
05OB021	P1	Mowbray Creek Near Mowbray	MB	49.0	-98.4	263	Nelson	Hudson Bay
05OB016	P2	Snowflake Creek Near Snowflake	MB	49.0	-98.6	975	Nelson	Hudson Bay
05LL014	P3	Pine Creek Near Melbourne	MB	49.9	-99.2	225	Nelson	Hudson Bay
05MF001	P4	Little Saskatchewan River Near Minnedosa	MB	50.4	-99.9	2610	Nelson	Hudson Bay
05MD005	P5	Shell River Near Inglis	MB	51.0	-101.3	1970	Nelson	Hudson Bay
05HD036	P6	Swift Current Creek Below Rock Creek	SK	49.8	-108.5	1430	Nelson	Hudson Bay
05EA005	P7	Sturgeon River Near Villeneuve	AB	53.6	-113.7	1890	Nelson	Hudson Bay
05CB001	P8	Little Red Deer River Near The Mouth	AB	52.	-114.1	2580	Nelson	Hudson Bay
05BL014	P9	Sheep River At Black Diamond	AB	50.7	-114.2	592	Nelson	Hudson Bay

Additional materials for "A Generalized Approach for Synthetic Streamflow Generation under Changing Conditions"
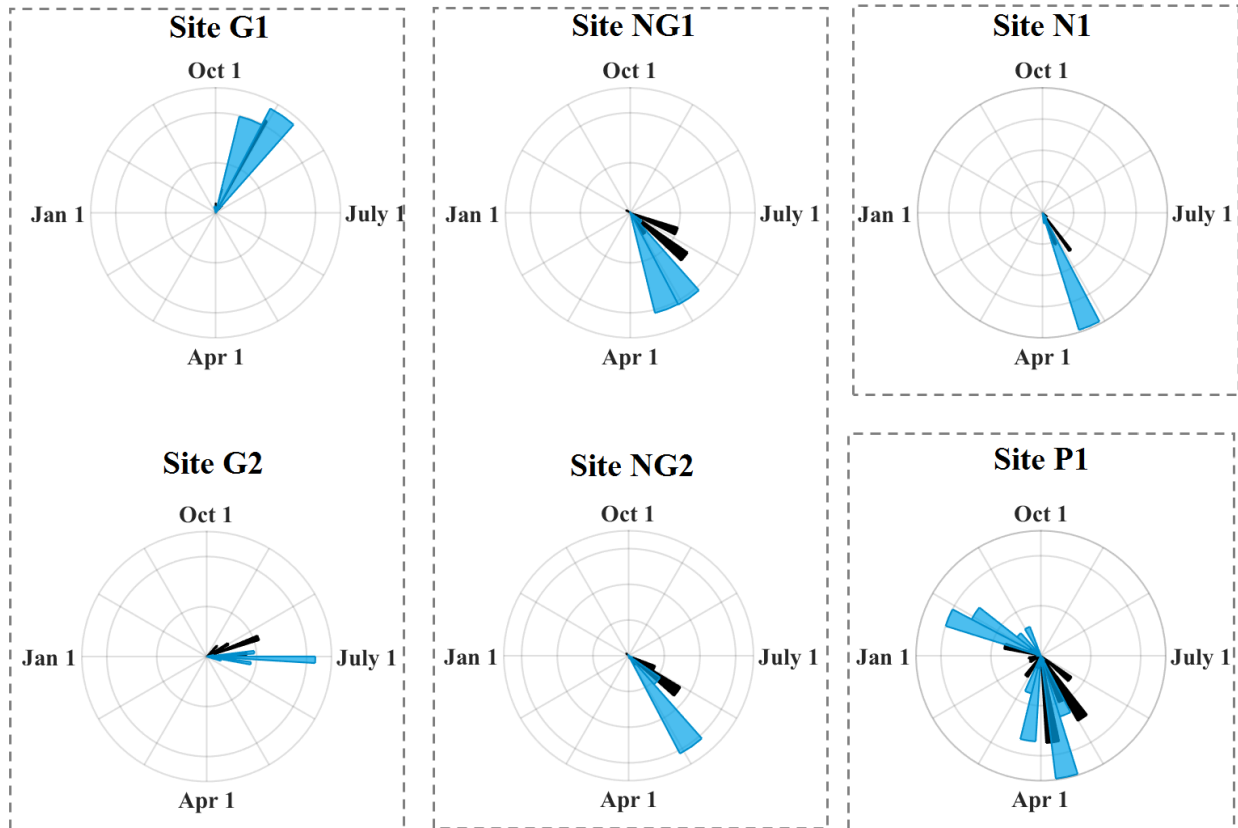

Figure E1. Representation of the desired shift in the expected timing of the annual peak in long-range future across the six sites using the proposed approach in single-site setting. The black and blue histograms are related to the observed and generated timing of annual peak, respectively.
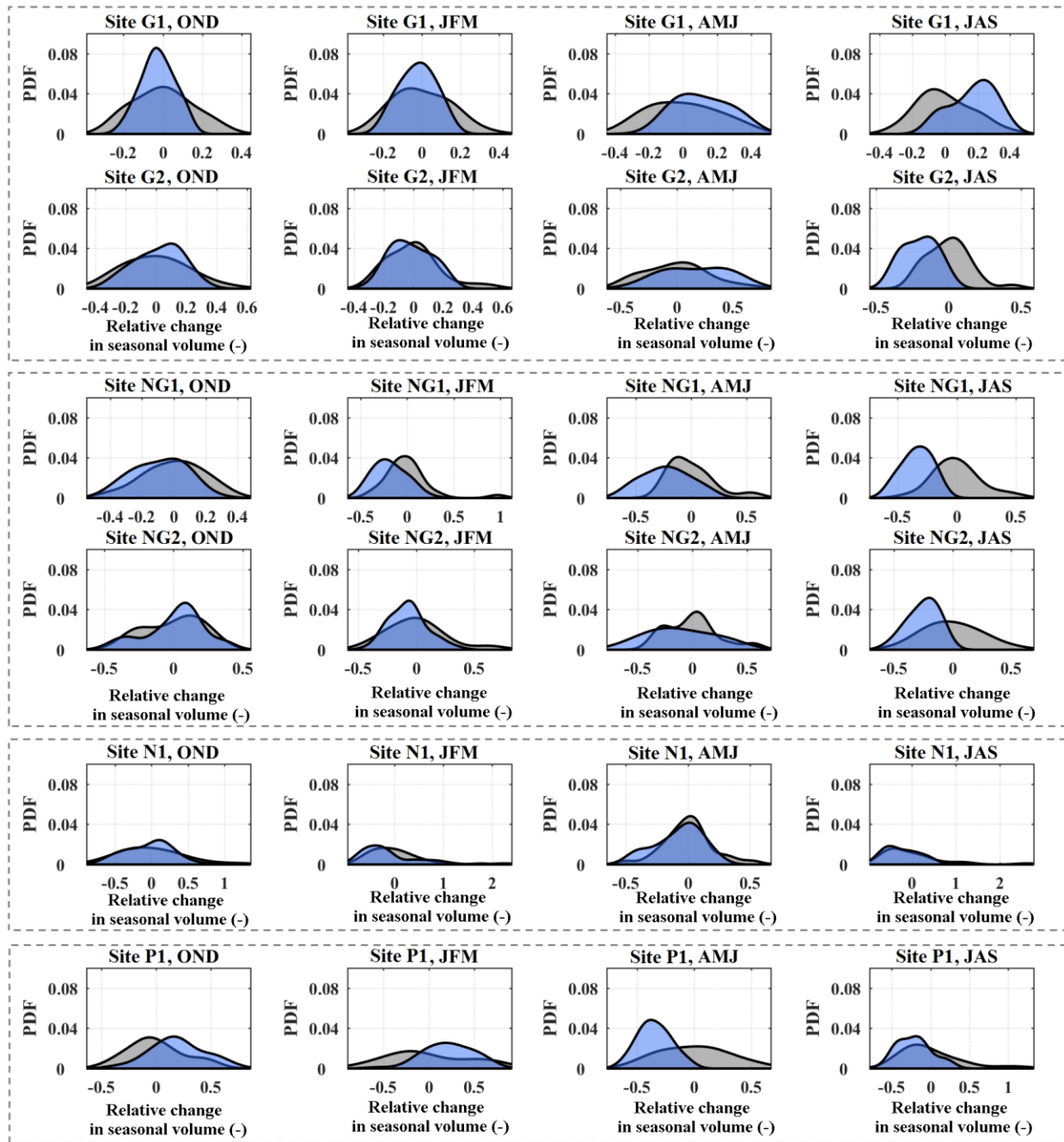
Figure E2. Representation of desired forms of shifts in terms of changes in the seasonal volume in six sites using the proposed approach in single-site generation of streamflow. The gray and blue colored distribution are the observed and simulated seasonal volumes. The results are related to the long-range future.
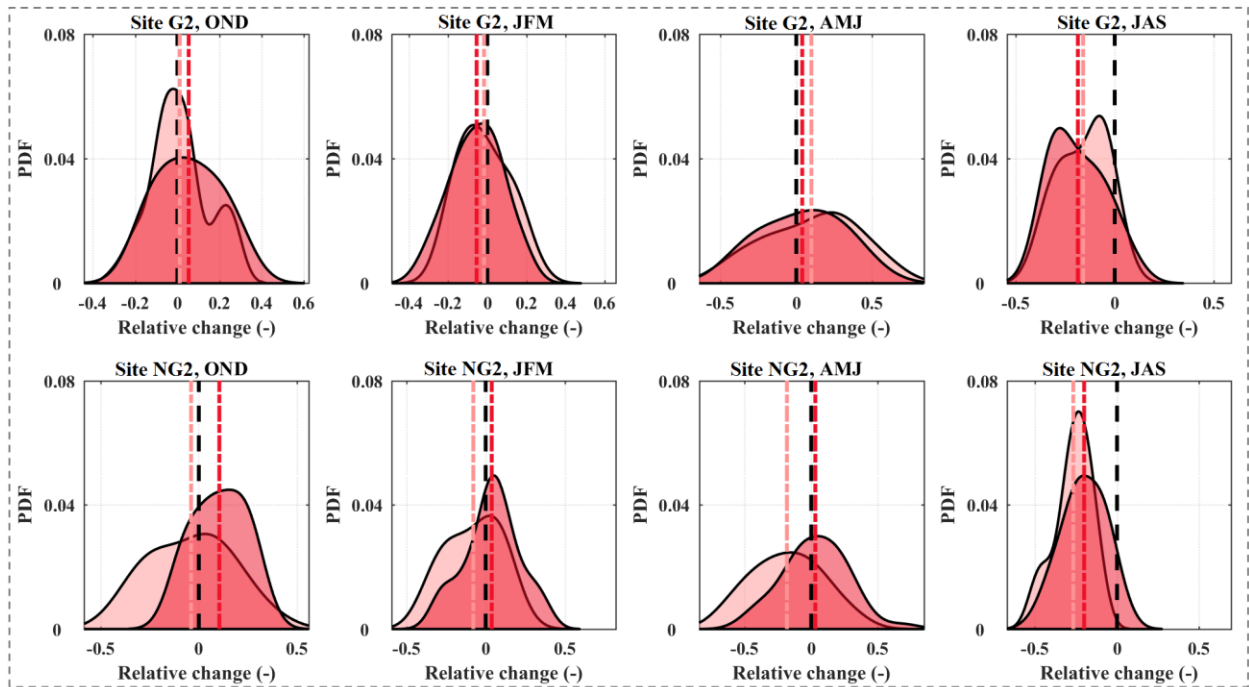
Figure E3. The comparison of the proposed approach in long-range generations of seasonal volumes in sites G2 and NG2. The light and dark colored distributions are the generated seasonal volume distributions generated by single and multisite settings, respectively.